# Determination of the Transverse Horizontal Axis and Interocclusal Registration Using a Novel Optical Technique

Andrew James Keeling BDS BSc MFGDP

Doctorate of Philosophy

The University of Leeds
School of Dentistry

February, 2016

The candidate confirms that the work submitted is his own and that appropriate credit has been given where reference has been made to the work of others.

# Acknowledgements

I would like to thank my supervisors, Professor Paul Brunton (Restorative Dentistry), Dr Raymond Holt (Mechanical Engineering), Professor David Wood (Director of Research and Innovation) and Mr Paul Franklin (Restorative Dentistry). All have added valued comment and insight throughout the project, in addition to the practicalities of completing the work.

In addition I would like to thank the statisticians at Leeds School of Dentistry, Dr Jing Kang and Dr Jianhua Wu for their guidance throughout the various statistical analyses.

Completing a PhD whilst working full time is a busy occupation. Many evenings and weekends have been spent on this thesis, and I would like to acknowledge the wholehearted support of my partner, Emma, who has never once complained of my prolonged absences in the office or late nights at work.

## Disclaimer

Some aspects of this work have been adapted and commercialised for the purpose of digitising dental study models. I confirm that the work reported herein does not directly disclose any commercially sensitive information. The software supplied with this thesis is done so in source code format, and free for use under the GNU General Public License.

# Abstract

**Motivation:** Dental treatments sometimes require the recording and reproduction of the patient's transverse horizontal axis (THA). This is the axis about which the mandible will rotate, when the condyles are fully seated in their glenoid fossae. However, methods for recording this axis are rarely used in general practice, due to expense and perceived lack of efficacy.
**Problem Statement:** A simplified method for accurately recording the THA, and interocclusal records (IORs), is needed for general dentistry.
**Approach:** An optical 3D scanning method is proposed to kinematically record the THA. A simulation determines the required hardware specifications to build the scanner at minimal cost. The ability to record the hinge axis of a dental articulator is explored. High quality interocclusal optical records are essential, and these are investigated in subsequent experiments. Areas for improvements are identified and efforts are made to enhance the system speed and calibration.
**Results:** Simulation results indicated that all 6 upper and lower anterior teeth, including 2mm of gingivae should be captured, with an accuracy of 50µm.

The THA on a dental articulator could be located with a radial accuracy of 2.65±1.01mm.

The repeatability (precision) of IORs showed a standard deviation of 22µm anteriorly, and a mean of 43µm posteriorly *in vitro*.

The accuracy (trueness and precision) of the IORs was -15±22µm anteriorly, and up to -93±121µm posteriorly *in vitro*.

A faster scanning protocol enabled *in vivo* testing. 29 IORs of a single subject took <2s to perform. The registrations showed a repeatability of 31µm anteriorly and 70µm posteriorly.

A novel calibration process produced significantly reduced stereo reprojection errors compared to traditional methods (0.22 vs 0.27 pixels), offering a potential future system enhancement.

**Conclusions:** The proposed method shows potential to improve the speed, accuracy and simplicity with which the THA, and interocclusal registration, can be recorded. Further developments have been suggested prior to embarking on clinical trials.

# Table of Contents

# List of Tables

# List of Figures

# Preface

This thesis was borne from ideas formulated whilst the author was a full time general dental practitioner. These ideas were shaped by the desire for a solution to problems faced every day by a primary care dentist. The thinking that '*there must be a better way'* occurs to many clinicians – our daily job is one of problem-solving. It is hoped this document illustrates the journey from an idea, through to its implementation and evaluation. The aim is to investigate whether the idea has the potential to be of benefit to clinicians and patients alike.

# 1 Introduction

Dentists aspire to maintain and improve the oral health of their patients. This is broadly achieved using a combination of diagnosis, prevention and operative intervention. Diagnosing pathology at an early stage can often simplify treatment and improve outcomes. Preventive treatments generally incur a lower biological cost than more significant operative interventions. If the latter are required, they should be performed to the highest clinical standards.

A correctly functioning masticatory system can be considered as one facet defining oral health. One factor contributing towards this system is a healthy 'functional occlusion'. This term has been defined as :

'*the occlusal contacts of the maxillary and mandibular teeth during function, i.e. during speech, mastication, and swallowing.*' (Clark & Evans 2001)

This functional occlusion - or articulation - is determined anteriorly by the dentition, and posteriorly by skeletal factors (the temporomandibular joints and their surrounding structures).

The importance of harmony between these anterior and posterior guiding factors has long been acknowledged by the dental profession, although the ideal nature of this harmony has been under constant review (Keshvad & Winstanley 2000).

Indeed, the precise nature of the ideal occlusion, whether 'static' or 'functional', is unclear. For more than a century, workers have been suggesting rules for the 'ideal' (McCollum & Stuart 1955; Türp et al. 2008; Carlsson 2010; Bonwill 1885). Much expert opinion exists, but there is little evidence relating to many of these dogmas. (Carlsson 2010; Shodadai et al. 2001; Türp et al. 2008; Gámez et al. 2013)

This is, perhaps, unsurprising when one considers the complexities of analysing the dynamic movements of, and forces applied to, the undulating occlusal surfaces of the dentition. In other medical fields, attempts at biomechanically modelling relatively simple structures, such as the hip joint, are still an active area of research (Taylor & Prendergast 2015). Cast in this light, the scale of the challenge facing the dental profession in determining the ideal dental arrangement, for each individual patient, becomes clear.

The clinical need to accurately model a patient's articulation arises in many situations. There is an increasing prevalence of patients presenting with worn dentitions (Van't Spijker et al. 2009), as well as many patients who have lost most,

or all, of their teeth (Steele & O'Sullivan 2011). In these groups, treatment often involves restoring the dentition at an increased degree of jaw-opening, or more properly, an increased occlusal vertical dimension (OVD). A new occlusal scheme is designed and implemented from scratch, and it is incumbent on the profession to ensure simple and accurate methods for implementing such schemes are available to every clinician (and by association, every patient).

In fact the construction of all dental prostheses would benefit from being fabricated with the patient's articulation in mind. The ideal clinical scenario is one in which such a prosthesis (eg a crown, bridge or denture) will fit in perfect harmony with the patient's stomatognathic system, without the need for any adjustment.

Perhaps less obviously, a high quality model of a patient's articulation might be useful in the prevention of tooth fractures. It seems that the field of occlusion, relative to other dental fields such as cariology or periodontology, is very *reactive* rather than *proactive*. For example, the data (backed up by common experience) shows that a typical general dentist might expect to see one or two non-carious cusp fractures *every week*, from their population of well-maintained patients (Bader et al. 2001; Fennis et al. 2002). As a profession, whilst we fight hard to preserve the smallest amounts of enamel and dentine in terms of caries treatment, we generally wait until perhaps twenty-five percent of a patient's tooth (for example a lingual molar cusp) has fractured clean off, before reactively treating the gross damage. Perversely, the treatment may involve removal of even more of the healthy tooth structure. Occlusion is only partly to blame for these fractures. They are almost certainly multi-factorial, with contributions from habits such as bruxism, and from previous restorative treatments. The latter is particularly true where marginal ridges have been removed, or endodontic access has necessitated significant removal of dentine (Reeh et al. 1989).

We are not well equipped to identify such at-risk teeth in advance. A 'blind' approach of covering any potentially weakened cusps (using direct or indirect restorations) could lead to over-treatment and unnecessary loss of healthy tooth structure.

In a recent review exploring several poorly evidenced dogmas in dentistry, one author commented:

> *'…it appears necessary to find new ways to define, diagnose and analyse occlusal features…'* (Carlsson 2010)

In fact, in consideration of the commonly taught techniques for occlusal diagnosis using articulated study models, Carlsson was not the first to question common wisdom:

*'Whereas articulators are useful in tooth setting and in designing of occlusal schemes for fixed prostheses, their use in diagnosis and the ultimate refinement of occlusion may introduce errors rather than facilitate their removal, since they cannot mimic the crucial three-dimensional movements required.'* (McMillan & McMillan 1986)

One could hypothesise of an ideal where a general dentist is able to give their patient a probability of each particular cusp fracturing, the consequences thereof, and allow the patient a truly informed choice on treatment. This would require the integration of knowledge concerning the functional occlusion, patient habits and past restorative treatments on individual teeth. Clearly, the profession is a long way from this ideal, but these are the goals to which we should aspire.

To achieve this ideal, from an occlusal perspective, the following would logically be required:

a) An accurate method to non-invasively record the patient's functional occlusion. This should be sufficiently simple, cost-effective and rapid that it would be possible to achieve during a typical general dental examination, and accessible to general dentists.
b) A simulation method (physical or virtual) which is adaptable enough to allow full and accurate reproduction of the recorded articulation.
c) A method by which all the dynamic tooth-to-tooth contacts can be analysed, to produce meaningful conclusions on the relative advantageous or deleterious effects of each contact.

One intuitive starting point for creating a dynamic model to reproduce a patient's functional occlusion is to record the arc of closure of the mandible. This will show how the teeth meet upon 'first contact', and may be useful in predicting how the subsequent tooth-guided phase of articulation might proceed.

In addition, when the condyles are fully seated in their fossae, this skeletal position (termed 'centric relation' or CR) is relatively repeatable. This is useful if anterior guiding factors (the teeth) have been lost or compromised (through wear or simply tooth loss). In such cases, this retruded arc of closure - the transverse horizontal axis (THA) - is a reasonable and repeatable position from which to start to plan rehabilitation.

## 1.1 The Transverse Horizontal Axis

### 1.1.1 Definition

The transverse horizontal axis (THA) is defined as:

'*an imaginary line around which the mandible may rotate within the sagittal plane*' (Academy of Denture Prosthetics 2005) (p.78).

However, this definition will only make sense when qualified with additional information. It must be appreciated that the human temporomandibular joint is a highly mobile joint, and not simply a hinge. The presence of the fibrocartilaginous articular disc between the two bony surfaces, imparts the ability for the joint to translate (ie to partially dislocate) in addition to rotating. In fact the condylar heads are rarely, if ever, fully seated within the glenoid fossae during normal function, implying a pure rotation about a fixed axis does not generally occur (McMillan et al. 1989). The fully seated position is called centric relation (CR), and is more formally defined as:

*'the maxillo-mandibular relationship in which the condyles articulate with the avascular portion of their respective disks with the complex in the anterior-superior position against the shapes of the articular eminencies…… It is restricted to a purely rotary movement about the transverse horizontal axis.' (Academy of Denture Prosthetics 2005)*

The THA is therefore more fully defined as the imaginary axis about which the mandible rotates, when the mandible is positioned in centric relation.

### 1.1.2 The Existence of a Pure Hinge Axis and its Physiology

The existence of a pure rotational mandibular movement (with no translational component) has been the subject of intense debate (Posselt 1956; Weinberg 1959; Ferrario et al. 2005; Ferrario et al. 1996; Lindauer et al. 1995; Jinbao et al. 1988; McMillan & McMillan 1986; McMillan et al. 1989). Early workers seemed to show the existence of an axis, although some of this research would be considered less rigorous in modern times. For example, Posselt's 'envelope of border movements' – much quoted in modern texts – was the result of the recording of just one subject, and was quite different from the recordings of many of the other subjects in the experiment (Posselt 1956). It seems Posselt favoured this result to confirm his theories of border movements and rotations of the mandible.

More recently some workers appear to have shown the lack of existence of such a pure rotation (Ferrario et al. 1996). However, it is unclear how well controlled the hinge movements were in this experiment, since the subjects appear to have been free to move their jaws as they wish, after being initially positioned in CR by the operator. This is inconsistent with clinical practice, where any recording of CR would entail full operator manipulation, or patient controlled positioning using some type of aid such as an anterior deprogrammer.

Other workers have only investigated habitual movements, in which one might not expect a pure rotation to occur (Lindauer et al. 1995). Furthermore, these workers appear to confuse an 'opening' motion (as their paper title suggests) with 'closing' (which is what they actually investigate because the patients were biting on acrylic blocks of varying thickness). This is important since the muscles controlling jaw closing are different from those controlling opening, and the superior head of the lateral pterygoid muscle is likely to be important in stabilising the TMJ in CR during closing (McNamara 1973).

When considering the anatomy of the TMJ, it seems unlikely that a perfect rotation can be accomplished. The condylar heads are neither perfectly cylindrical, nor perfectly aligned. Furthermore, such a hinge movement could be considered un-physiological. As early as 1908, Norman Bennett (Bennett 1908) demonstrated how his own freely moving mandible never rotated around a hinge axis, but rather, the movement could be described using a sequence of finite helical axes. His brother, and co-worker, was a Cambridge Fellow in Mathematics. The work was perhaps, a little too technical for the dental audience of the day, and it seems that the profession simply remembers the last page, where there were some nice tracings of Bennett's condylar movements during lateral mandibular excursions. This was an

afterthought for Bennett, not the reason for his paper. However, it is interesting to note that Bennett will forever be remembered for his lateral condylar movements, and the angle the non-working side condyle creates (viewed in the horizontal plane[1]), with the sagittal plane.

Since the time of Bennett, many workers have confirmed that physiological functional movements of the mandible tend to combine simultaneous rotation and translation of the condyle (Lindauer et al. 1995; Tokiwa et al. 2010; Fang & Kuo 2008; Ferrario et al. 1996; McMillan et al. 1989).

Further indirect evidence that this is probably the physiological norm comes from biomechanical analysis of the effectiveness of different muscles during different stages of mandibular closure. One can contrast their efficacy as a lever about an axis located in the centre of the condyle, with their effect as a lever acting about the position of the instantaneous centre of rotation (ICR). When the axis is confined to a pure rotation centred near the condyles, the *effect* of a muscle such as masseter is significantly reduced, compared to its effect if the mandible is rotating around the ICR (Grant 1973; Gal et al. 2004). Put simply, the evidence suggests that Nature maximises the chewing power and efficiency of the stomatognathic system by allowing a simultaneous sliding and rotating motion of the mandible. For clarity, these findings are illustrated in Figure 1 and Figure 2.

[1] The misinterpretation of information is further propagated when one considers that Bennett's work was reported in the frontal plane, not the horizontal. He also never mentioned, or quantified, any angle.

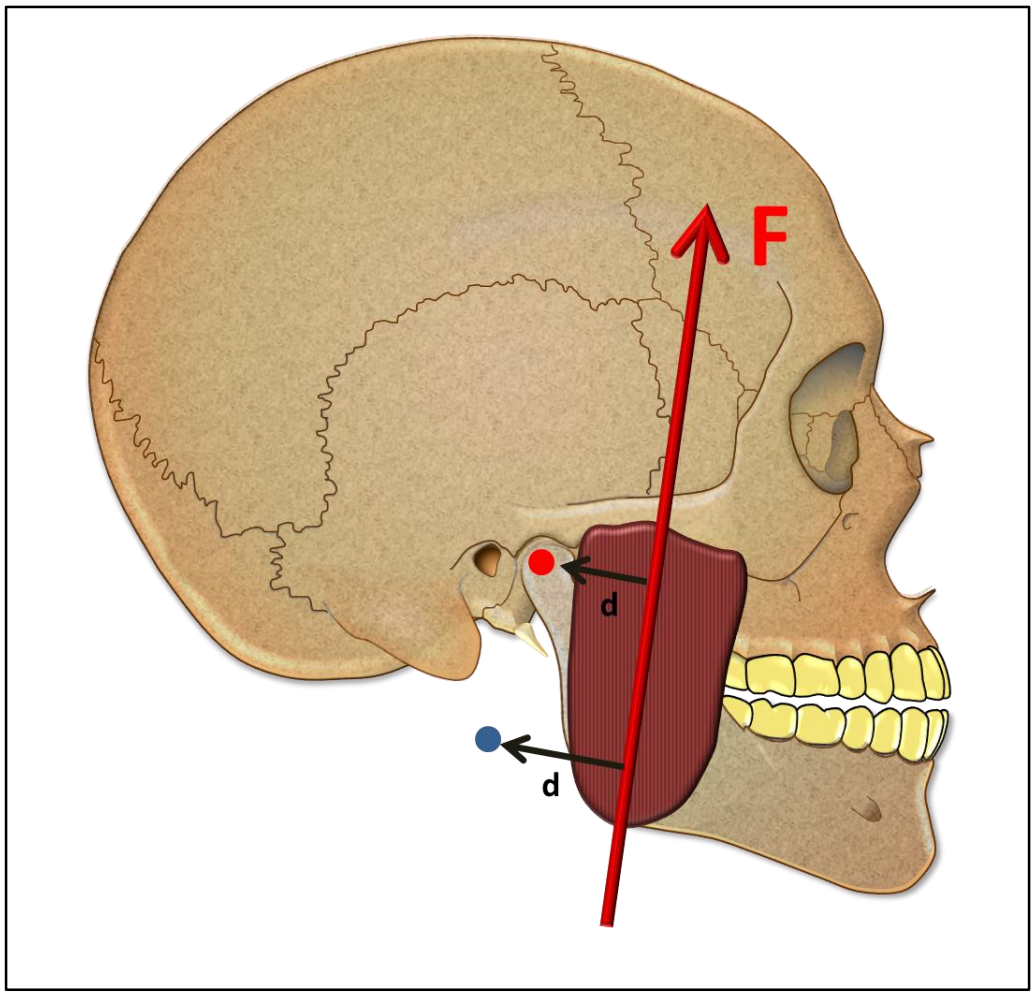


**Figure 1 Example of the Biomechanical Advantage of the Instantaneous Centre of Rotation.** A subject has their teeth almost together and is, for example, trying to bite through a hard nut. The masseter muscle is shown, and is the major closing muscle during this late stage of jaw closure. If the masseter applies its moment through the condylar head (red circle) the mechanical advantage is lower than if it applies its moment through the ICR (blue circle).

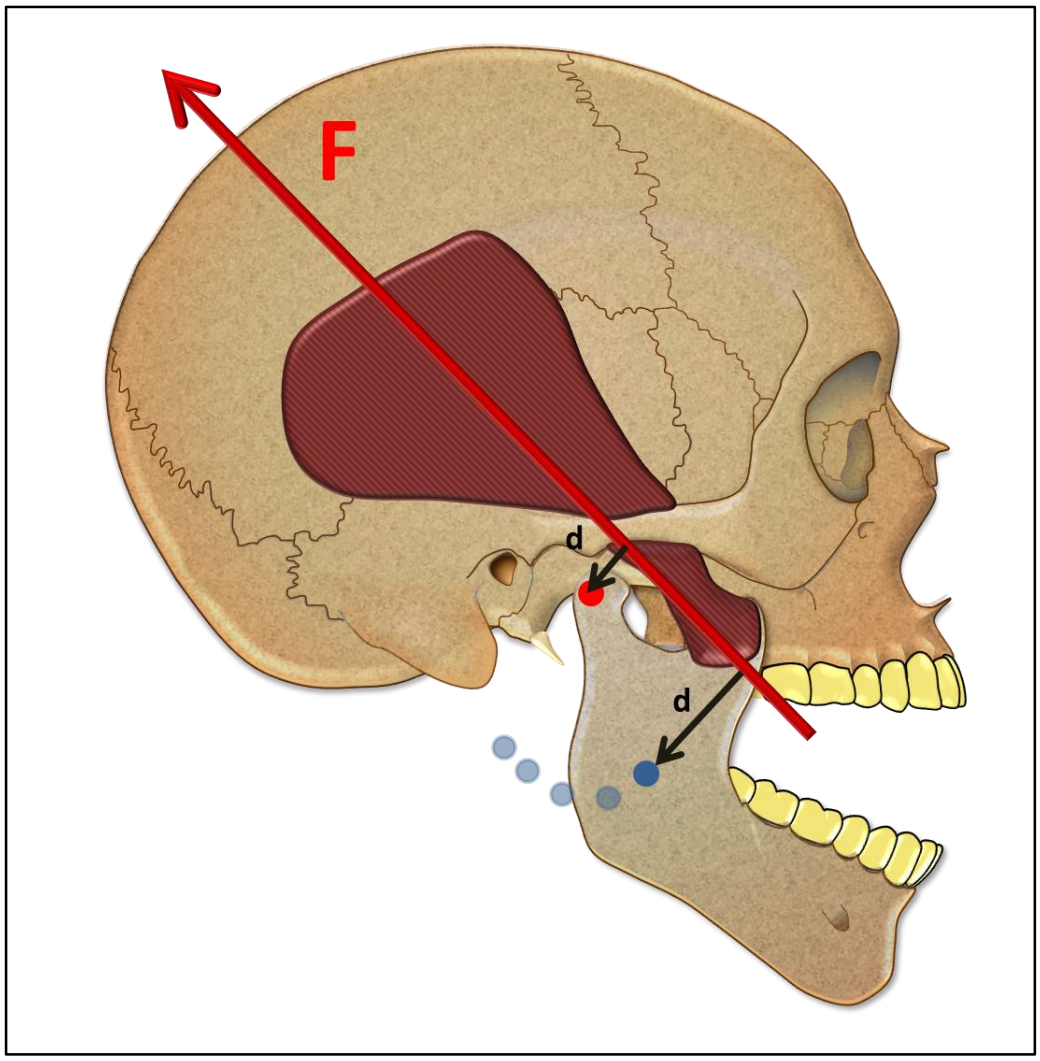


**Figure 2 The Instantaneous Centre of Rotation When Closing From a Wide Jaw Gape.** The muscle shown is the posterior belly of temporalis, which is particularly active during the initial phase of jaw closure from a wide gape. The position of the ICR at this gape is shown in dark blue (the faint blue circles show the path this ICR will take during jaw closure). Similarly to Figure 1, the mechanical advantage of the temporalis acting around the ICR, rather than the condyle (red circle), is apparent.

This goes against some expert opinion, which contests that restoring a patient in their CR position actually *increases* masticatory efficiency (Ramfjord & Ash 1983). However, the observation that most patients who are restored in CR remodel their condyles over the subsequent years to enable a non-hinge closure of the mandible (Celenza 1973), would seem to further refute such experts. Why would such remodelling occur if it was not biologically advantageous? More work is certainly needed in this area.

This CR position itself occurs briefly (and naturally) during swallowing, a fact that some clinicians have taken advantage of to help in the positioning of their patient's mandible (Campos et al. 1996; Millet et al. 2003). One might conclude therefore,

that the ability of the mandible to transiently position itself into CR is indeed, physiological. However, the ability of the mandible to perform a pure hinge movement during the last 20mm or so of jaw closure (with the condyles remaining in CR throughout) is a non-physiological phenomenon.

On balance, it is probable that the mandible can perform a motion *approximating* a pure rotation, *if* the condyles remain seated in CR. Mechanical, or graphical methods for determining the location of the THA are probably too insensitive to detect its non-existence within the limited degree of jaw opening available to the clinician (Lauritzen & Wolford 1961; Hatzi et al. 2001; Posselt 1956).

Despite these uncertainties the THA remains important in clinical dentistry as it forms a repeatable position in which the mandible may swing, and represents a posterior border movement. It provides a starting point from which relationships between the posterior and anterior guiding factors may be analysed by a clinician or technician. It seems likely that, if the THA is used as a starting point for restorative treatment, the adaptive capacity of most patients is sufficient, turning the resultant prosthetic work into a biomechanically efficient dentition.

### 1.1.3 Locating the THA

Locating the location of the THA relative to both upper and lower dental arches is the first task for the clinician. Once found, this position can then be recorded and reproduced *in vitro.*

The methods by which this axis may be found and recorded can be broadly categorised as average value, arbitrary-anatomical and kinematic. A few other methods have been suggested, though are not in general use.

#### 1.1.3.1 Average Value Methods

The first attempts at locating the THA relied on an average value method. In the mid-nineteenth century, William Bonwill claimed to have measured '*4000 dead jaws and 6000 living*' and his reports were formalised towards the end of that century (Bonwill 1896; Bonwill 1885; Bonwill 1864). He concluded that a relationship existed between the position of the point of contact between the lower central incisors, and the mandibular condyles. He stated that they always formed an equilateral triangle, and that this typically measured 4" along each side (though it could be as much as 5" in some ethnic populations). Meanwhile, a British dentist, Frances Balkwill, was making many observations of his own (Balkwill 1866), including relating the angle between the plane formed by Bonwill's triangle, to the plane formed by the lower incisors and disto-buccal cusps of the lower second molars (the occlusal plane).

These two pieces of information gave the dental profession a method by which the lower teeth could be positioned on an articulator, relative to the hinge of that articulator. Furthermore, the upper teeth could now be positioned on the articulator by relating them to the lower teeth (for example, using an interocclusal record). In this way, both the lower and upper dental arches could be fully related to the hinge axis of the articulator, and this axis was assumed to be, on average, equivalent to that of the patient.

This technique is clinically simple but potentially flawed by the observation that average values very rarely apply to individual patients. Indeed, even these average values have been subject to dispute, with later workers generally finding that the inter-condylar distance averages more than four inches (Mandilaris et al. 1992; Lazic et al. 2006), and the Balkwill angle displays large variations and is, on average, lower than the 26° originally proposed by Balkwill himself (Ohm & Silness 1982).

In fact, a simple trigonometrical calculation reveals that, even if one assumes the Balkwill angle were perfectly constant, the radius of error in locating the THA in the sagittal plane could be expected to exceed 10mm, when the variation in the size of Bonwill's triangle is considered. With the addition of a varied Balkwill angle the error could be further increased.

### 1.1.3.2 Arbitrary-Anatomical Methods

Given the potential inaccuracies of using population averages to locate the hinge axis in individuals, facebow (commonly earbow) methods can be employed. Here, an attempt is made to identify anatomical landmarks for that specific patient (for example the external auditory meatus, and the infra-orbital notch). An assumption is then made regarding the location of the THA, based on these landmarks. An example is the Bergstrom point, located 10mm anterior to the external auditory meatus, and 7mm below the Frankfort plane (Bergstrom 1950). A Denar® Slidematic facebow (Whip Mix, Louisville, USA) is shown in Figure 3.

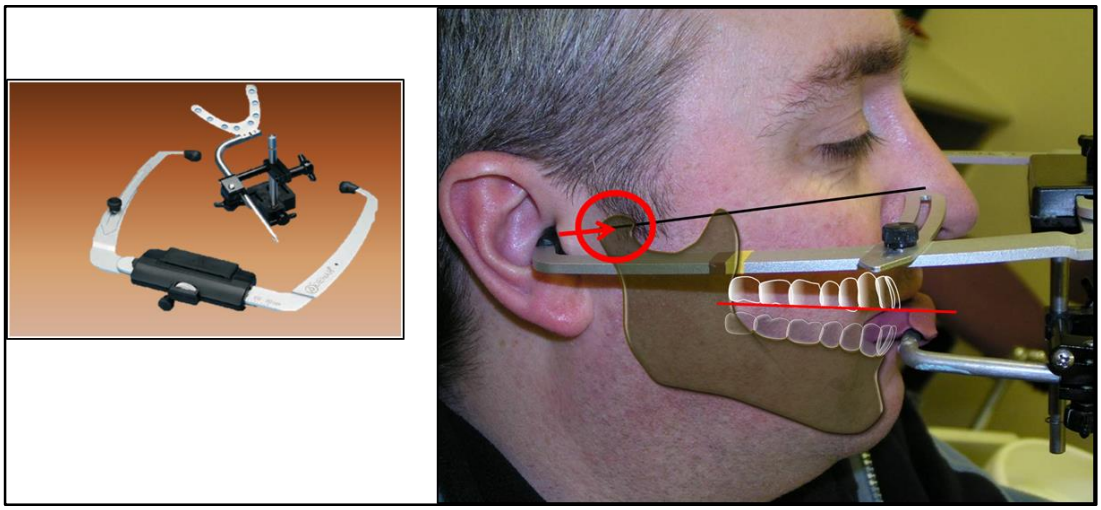

**Figure 3 Example of an Earbow.** The earbow and bite fork are shown separately on the left, and positioned on a patient (right). Anatomical reference points are used to find the condyle (and THA), on the assumption that this lies a fixed distance from the reference points.

It can be seen that this method combines some of the patient's real anatomy, with some average values. There is also an assumption that the kinematic axis of rotation of any given mandible is consistently located with reference to the anatomy.

The accuracy of this method varies slightly, depending on the reference points. Typical errors in axis location range from around 5mm or more (Lauritzen & Bodner 1961; Morneburg & Pröschel 2002; Piehslinger et al. 1995), to a reported 2 mm

(Nagy et al. 2002), the latter when using a point 10 mm anterior to the axis-orbital plane.

The most recent published work compared the use of a simplified ‘facebow’ (the Kois dentofacial analyser), and a standard facebow, using 15 dried skulls as the subjects (Lux et al. 2015). The work showed that both methods were comparable and recommended the Kois can be used as an alternative to a facebow. However, it also stated that both methods located the upper incisor in a significantly different position to true (typically with a 5mm error), and the 3-dimensional position of the maxillary cast relative to the THA, typically varied by around 10mm. One might conclude from these results that both methods are equally poor at relating the maxillary cast relative to the THA.

It must be remembered that much of the work cited above only considers the effectiveness of the earbow to locate the THA *on the patient.* Earbows are mechanical and subject to some variability during use, and during transfer to an articulator. This repeatability has been shown to be ±1.2 mm, for 95% of cases (Choi et al. 1999). This error is additional to the error incurred by the anatomically incorrect arbitrary point.

As before, only the maxillary teeth are related to the THA using this method. An interocclusal record is required to relate the lower dentition to the upper, and so indirectly, to the THA.

The facebow method remains a stalwart of undergraduate teaching (Hindle & Craddock 2006), although its adoption in general practice remains poor (Clark et al. 2001; Storey & Coward 2014). A lack or perceived clinical benefit is often cited (Carlsson 2010; Gámez et al. 2013; Shodadai et al. 2001), and so it would seem that the average value method remains the predominant pragmatic clinical standard.

#### 1.1.3.3 Kinematic Methods

Chronologically, these methods were precursors to arbitrary-anatomic methods. The first method for kinematically locating the hinge axis was described by Beverley McCollum in 1921 (see McCollum & Stuart 1955). The axis is simultaneously related to both the upper, and lower, dentition using facebows and clutches attached to both dental arches. The upper component forms a stable base from which to measure the position of the axis using the lower component.

The devices were originally fully mechanical pantographs. They would usually employ flags or slides, attached to the upper member in the region of the condyles. The lower part would contain an adjustable rod, ending in a pin or other marking device. The clinician positioned the patient into their terminal arc of closure and adjusted the location of the mandibular pins (left and right) until they were not moving, only rotating, as the patient was guided in performing a terminal hinge movement of the mandible. This position was then marked on the upper flags.

This method, the Lauritzen Method (Lauritzen & Wolford 1961), has been shown to be highly accurate *in vitro*, with a repeatability of 0.2mm. A caveat with this impressive result is that the experiment only tested the ability of a person to co-align the pins on a benchtop facsimile of a clinical pantograph. The apparatus was not a true pantograph, as would be used clinically, and lacked some of the complexities therein. Even so, clinical application of this method has been shown to locate the axis with a repeatability of around 1-2mm (Beard & Clayton 1981).

Work using an electronic pantograph (Tuppy et al. 1994) would suggest (from the title of the paper) that the THA can be located clinically with a reproducibility of 0.2mm. However, this is simply the reproducibility of the slide from CR to ICP. Since this is predominantly a translation (not rotation), the authors methodology will not identify *where* the THA is, only that the bodily shift from CR to ICP is reproducible.

More recently, further *in vitro* work using modern pantographs (one opto-electronic and one mechano-electronic) found inaccuracies with both systems such that the authors suggested some occlusal adjustment would still be necessary (Balch 2012).

As with the earbow methods, many of the repeatability studies cited above do not account for the transfer and mounting onto an articulator. The usual methodology is to measure the variation in axis location directly on the flags on the patient. Since the maxillary and mandibular arms of the pantograph are similar mechanical constructs to the earbow, one might expect similar errors in their transfer to the articulator. Previously cited reports of ±1.2mm (Choi et al. 1999), might imply the ‘real’ error is almost doubled, and any theoretical benefits of using such pantographic techniques may become swamped by practical errors in their application.

Regardless, the largest problem with kinematic methods relates to their complexity, time-consumption and cost. This has limited their use in general clinical practice.

#### 1.1.3.4 Other Methods

Various other methods for locating the THA have been suggested. Simply palpating the condyles and marking these on the skin has been shown to be relatively accurate, somewhere between the kinematic method, and earbow method (Razek 1981). Radiographic (lateral cephalometric) techniques have also been described, though much of this work was in conjunction with temporomandibular disorders (Weinberg 1972), and would not be clinically justifiable in modern times. Both methods would still require a protocol to transfer the measured axis position onto the articulator.

There has been one documented attempt at intra-oral location of the THA (Long 1970). This involved recording two wax interocclusal records (in CR), one 6mm 'thick' (using five tongue blades) and one 'thin' (using just one tongue blade). The author recorded the hinge axis on the articulator using an instrument he designed called a 'Buhnergraph' – essentially a precursor to the Denar Vericheck (Denar Corp, Anaheim, CA). Using graph paper at the articulator condyles, Long attempted to bisect the movement of a point, as the thick and thin interocclusal records were placed between the models. He then constructed a chord at right angles to this line. Repeating the process for a second point, the true axis will be the intersection of these two chords. No error analysis was performed but the author found the procedure highly variable, with multiple attempts needed to find the correct axis. This is unsurprising as the distance between point pairs was less than 1mm, and he was attempting to bisect this (with a pencil) and draw an accurate perpendicular – not an easy task. To compound matters, errors also arose from material distortions, particularly from the thick wax records. The author concluded that the method was simply not sensitive enough, and it disappeared from the literature as quickly as it came.

### 1.1.4 How Accurately Should the THA be Located?

The previous sections reveal a trend in the accuracy with which a clinician may locate the THA. Purely average values might be accurate to about 5-10 mm, arbitrary earbow methods might expect to be about 2-5 mm in error, whilst kinematic methods could be within 1-2 mm. Meanwhile, the clinical effort, cost and time increases with the complexity of method. This has led academic clinicians to explore the question – 'How accurately do I need to find the THA in my patients?'.

Mathematical modelling is a popular way to explore this question (Kois et al. 2013; Morneburg & Pröschel 2011; Gordon et al. 1984; Adrien & Schouver 1997; Fox

1967; Morneburg & Pröschel 2002), as this negates other clinical issues such as loose screws on facebows, inaccurate dental models, distortion of bite registrations etc.

Most recently, Kois and co-workers analysed the expected antero-posterior error in the position of the central incisal edges, if an average THA was used in place of the actual THA (Kois et al. 2013). They simulated axis location errors of up to 20mm in the horizontal plane, using up to 3mm thick (hypothetical) bite registrations.

It has been shown in the preceding section that these errors are certainly towards the upper end of that which might be expected to occur clinically, even with the simplest techniques. Incredibly, they found that the *maximum* error in incisal edge position, given these unfavourable parameters, was 11.26µm (micrometres). The threshold of human dental tactile perception is about 12µm (Reveredo et al. 2013), so one might hope such an the error would pass unnoticed by the patient.

Surprisingly, the authors make no comment regarding the diminutive size of these errors, accepting them on face value. If they are correct, William Bonwill's average value method was correct 150 years ago, and there has never been any clinical benefit to locating the THA with any greater accuracy than 2 centimetres. Common clinical experience of the frequent need to perform occlusal adjustments to prostheses sits at odds with this statement. This dichotomy will now be explored.

Unfortunately, whilst the authors mathematics is correct, their application of it is in error. They calculate the hinge error along a horizontal axis, level with the incisal edges. This is incorrect, since the true axis is known to lie somewhere above the level of the incisal edges, in the region of the condyle. This is a crucial point, since the *direction* of any error in THA location has a large effect on the expected error at the level of the dentition (Adrien & Schouver 1997; Morneburg & Pröschel 2002; Piehslinger et al. 1995; Gordon et al. 1984). In fact, the combined errors in the methodology of Kois *et al* happen to produce the most favourable outcome in terms of predicted occlusal errors.

Since this concept is still being misunderstood by some workers, in peer reviewed journals, a simplified pictorial explanation will now be given (Figure 4 to Figure 8).

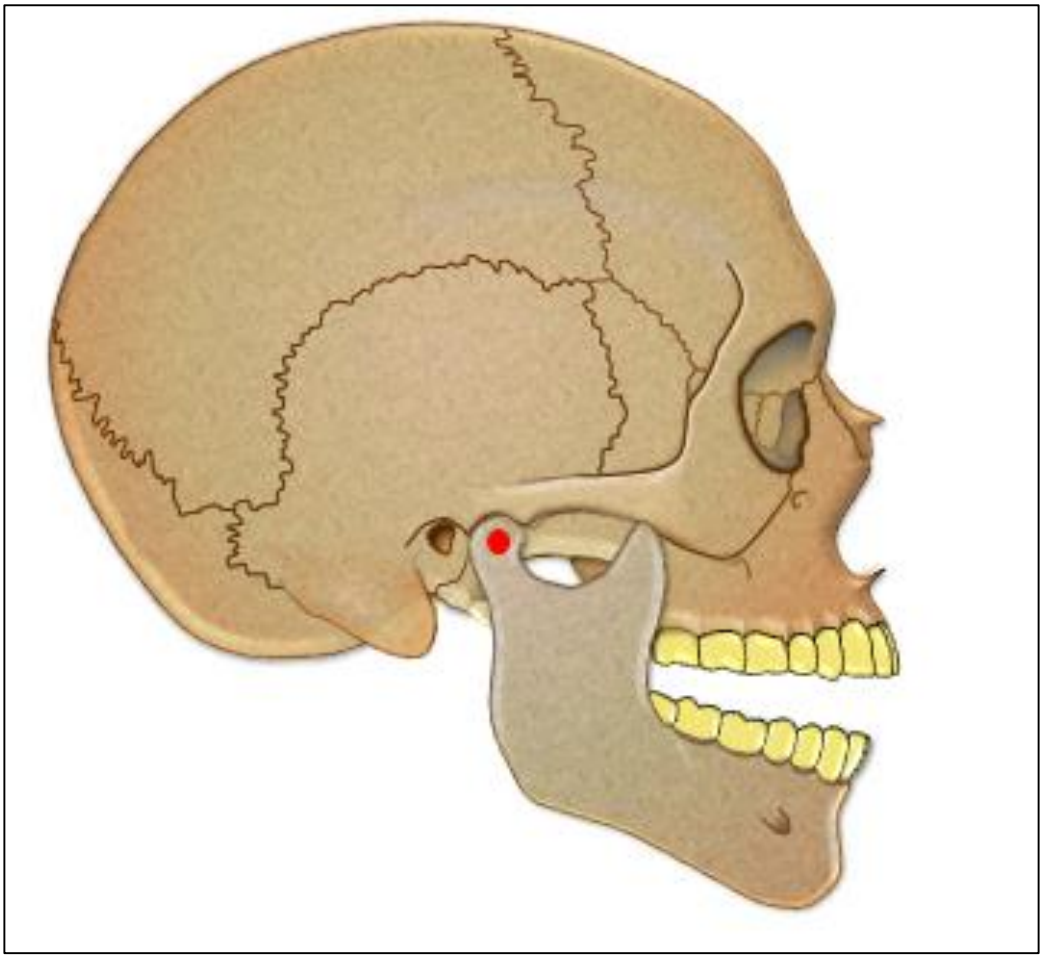

**Figure 4 The Clinical Situation Following an Interocclusal Registration.** The relationship between the upper and lower dentition has been recorded with the teeth slightly apart. This ensures the registration was not influenced by dental factors. The patient's real THA is shown as a red circle.

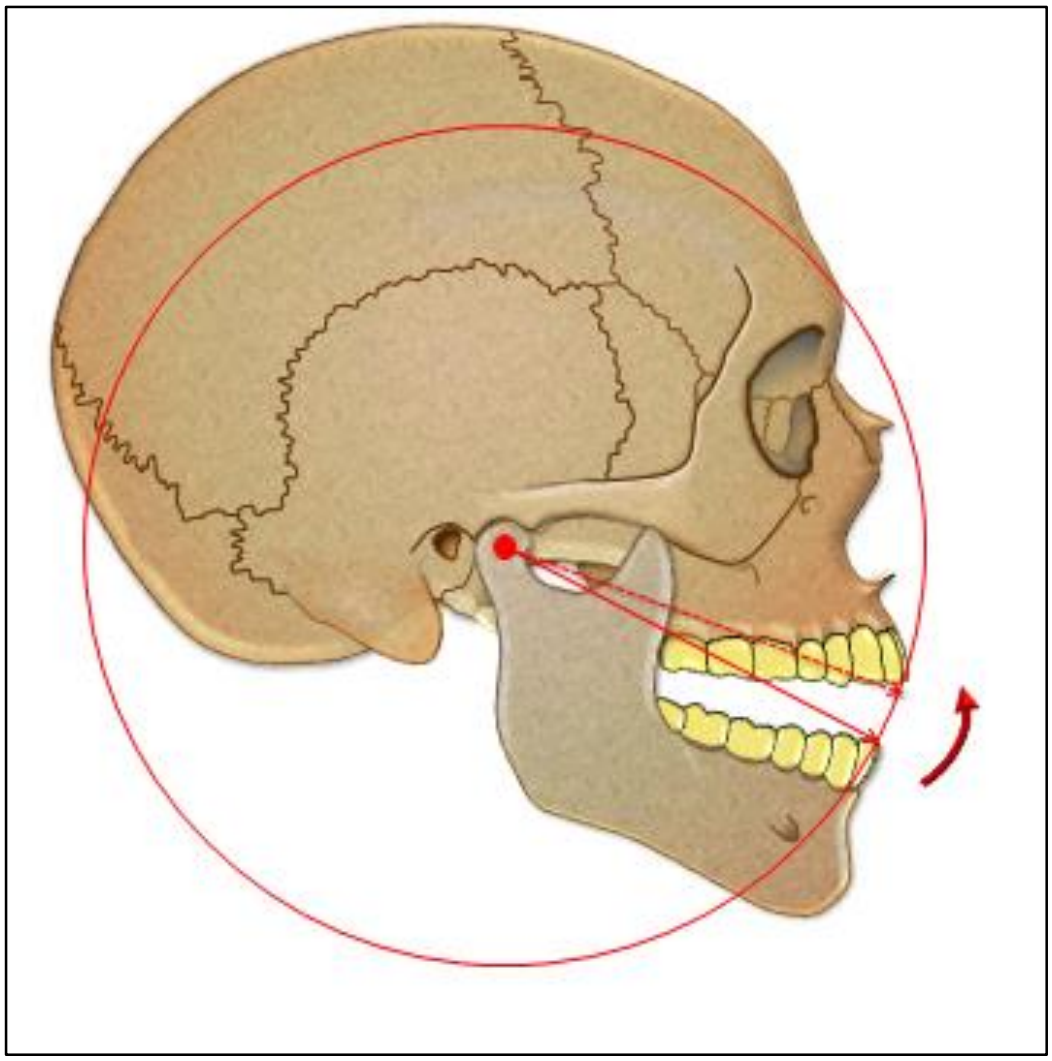

**Figure 5 Mandibular Closure Around the Hinge Axis.** When the mandible is closed around this hinge axis, the lower teeth will eventually meet the uppers, at their retruded contact position (RCP). The start and end points of the lower incisor are illustrated as solid red and dotted red arrows respectively. The direction of mandibular motion is also shown (curved arrow).

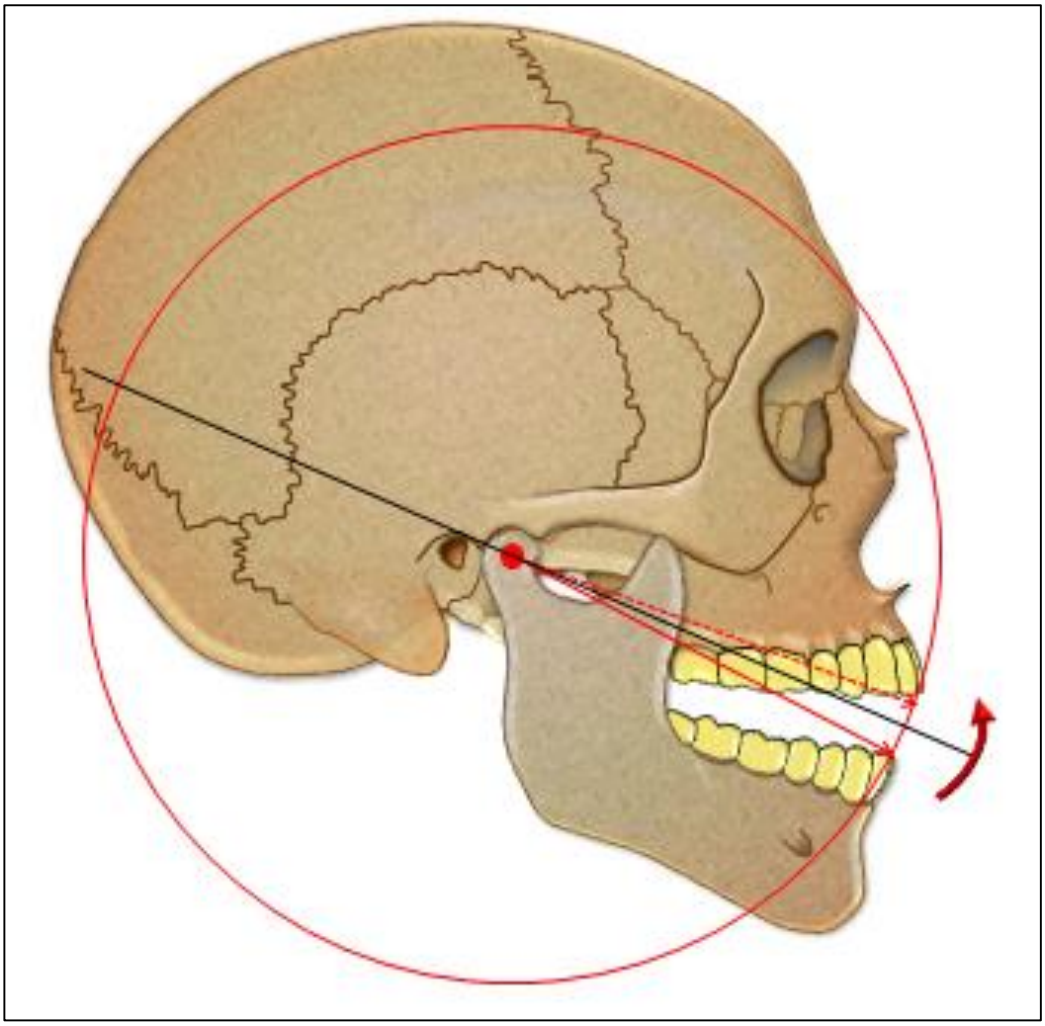

**Figure 6 A Line Bisecting the Complete Movement is Constructed.** If the THA is incorrectly recorded, but lies along this line (shown in black), the introduced occlusal error will be minimal (see Figure 7).

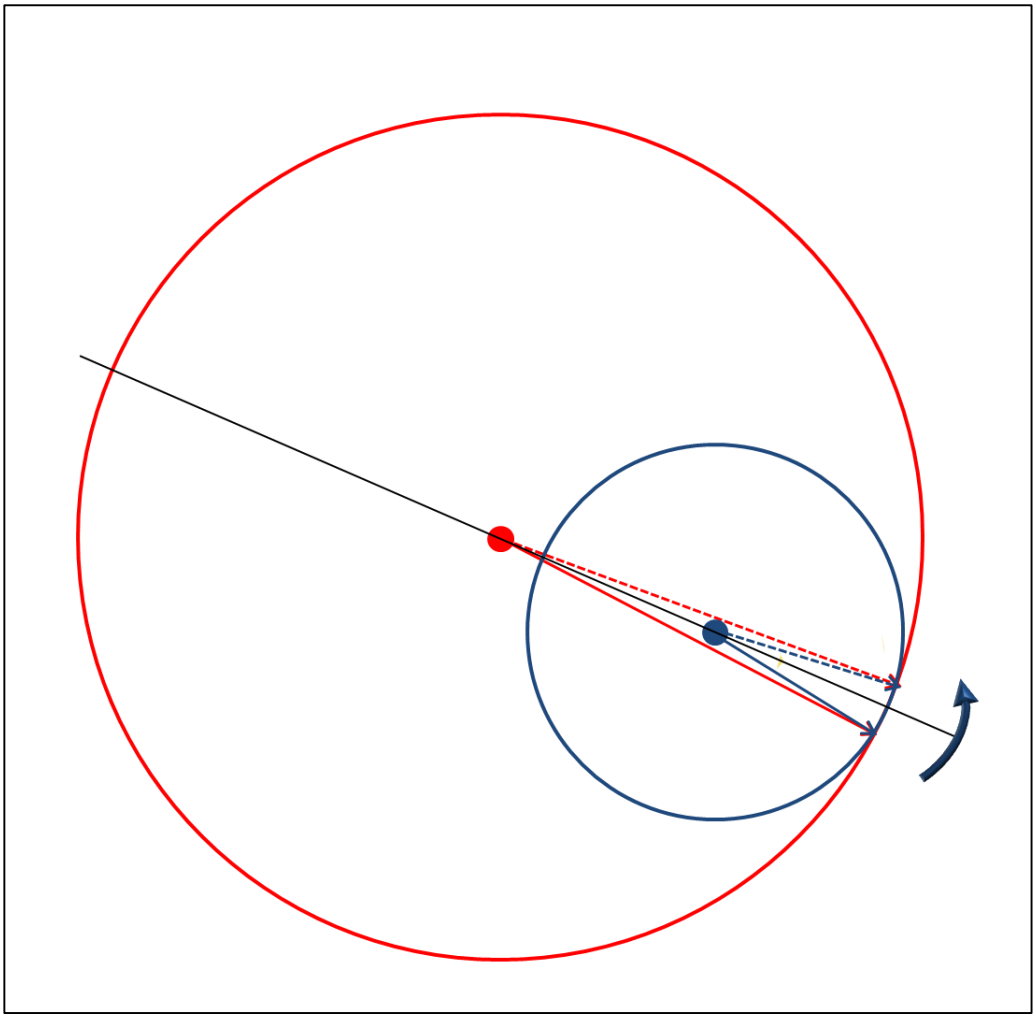

**Figure 7 An Example of a Grossly Misplaced THA.** The misplaced axis (shown in blue) is shown compared to the true THA (in red). The axis lies along the bisecting line described in Figure 6. Despite the much smaller radius arc of closure, the lower incisor point will still finish in approximately the correct position (dotted blue arrow), after rotation around the blue axis. Therefore, very little occlusal error will be introduced.

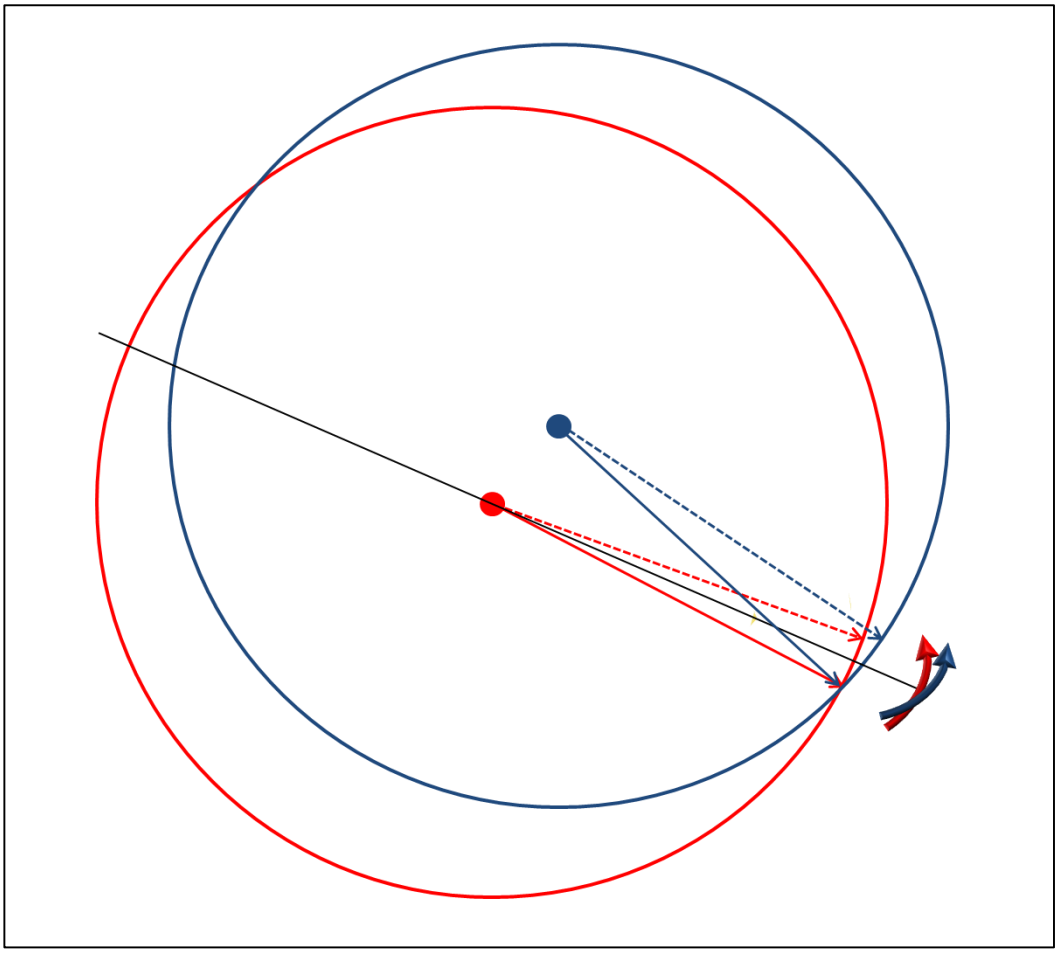

**Figure 8 An Example of an Unfavourably Misplaced Axis.** The absolute displacement from the true THA (red) is smaller than that shown in Figure 7 and the radius arc of closure is very similar to the true radius. Despite this, the occlusal error induced at the incisors after rotation around the incorrect axis (shown in blue), will be significant (dotted blue arrow).

The situation is further complicated because the direction of the bisecting line (ie the line along which an error in THA location will have minimal clinical effect) will vary, depending upon the point of measurement of the occlusal error. For example, when considering occlusal errors at the cusp tips of the lower second molars, any THA misplacement would preferably lie along a different bisecting line to that when considering the incisors. Regardless, there will still be more favourable positions to erroneously locate the THA, and less favourable ones.

The potential occlusal errors when using an earbow method to locate the THA, have been investigated (Morneburg & Pröschel 2002). The direction of the THA error was shown to be randomly distributed and so the authors provided a probability of inducing a particular occlusal error. For example, if a 2mm arc of closure is performed on the articulator, about 35% of cases will induce an occlusal error of 200µm or more at the level of the second molars. The authors comment

that other technical errors, for example in impression taking, pouring and mounting models, will further increase the error.

In later work by the same group, a comparison of expected occlusal errors when using average value mounting vs arbitrary earbow mounting, was made (Morneburg & Pröschel 2011). They showed that the Balkwill angle can have a significant effect on occlusal errors, and should be set no higher than 17° for average transfer methods.

They commented that such an angle is not possible for average value techniques, using the positioning aids currently on the market (range 18-25°). With the Balkwill angle set as favourably as possible (18°), they describe a 10% probability of inducing occlusal errors ≥ 430µm (although their graph seems to report a 20% probability). This rises to well over 1mm if the Balkwill angle is set at 25°, as recommended by some manufacturers. These figures are all based on a 2mm degree of opening.

By comparison, the authors found that when using an arbitrary facebow, there was a 10% probability of inducing occlusal errors ≥ 340µm. Again, their text differs from how one might read their graph (which seems to show a 20% probability of inducing an error of ≥ 340µm).

Curiously, they conclude that for increased openings of ≤ 2mm, an arbitrary facebow transfer is preferred to an average value transfer. Given the reticence of general dentists to use facebows (Clark et al. 2001; Carlsson 2010), another conclusion might have been that, for the sake of a theoretical difference in occlusal error of ≤ 90µm, going to the expense and trouble of using a facebow does not seem justified. At least, not in respect of modelling the patient's THA. It has been shown that other 'real world' issues, such as the repeatability of a physical facebow transfer (Choi et al. 1999) potentially induce errors, perhaps negating the small benefit a facebow might confer.

Regardless, all of these errors are an order of magnitude greater than the patient's perception threshold. This is, perhaps, in line with common clinical experience relating to the need for occlusal adjustment when fitting dental prostheses. The exact degree of occlusal precision required (which could be different to the threshold of patient sensitivity) is not known. The impact of established occlusal interferences on temporomandibular diseases (TMDs) is in doubt (De Boever et al. 2000), but other consequences of 'intolerable' contacts seem likely (Davies & Gray 2001; Davies et al. 2001) and remain unpredictable. Artificially induced acute occlusal interferences have recently been shown to cause increased occlusal

discomfort in a cohort of TMD females, though no exacerbation of muscular pain was found (Cioffi et al. 2015).

Perhaps, until there is a better understanding of the physiology of occlusion, clinicians should endeavour to be as precise as is reasonably possible within the constraints of time and cost. A simple and accurate method of locating the THA would help towards this counsel of perfection.

## 1.2 Centric Relation and the THA

Since centric relation comprises any position in which the mandible is rotating around the THA, the theoretical problem of locating the hinge axis becomes the clinical problem of positioning the mandible into CR. In addition most techniques for mounting dental models on an articulator rely on mounting at least one of the models by relating it to the other, via an interocclusal record. The accuracy with which CR can be located *and* recorded is therefore paramount.

### 1.2.1 Redefinitions

The first caveat in any search of the literature in this field is that the definition of the term 'centric relation' (CR) has progressively changed from a maxillo-mandibular relationship with the condyles positioned *posteriorly* and superiorly in the glenoid fossae, to one where the condyles articulate superiorly and *anteriorly* with the thinnest, avascular portion of the disc (Academy of Denture Prosthetics 2005).

Interestingly, throughout these redefinitions of CR, its relationship to the THA has remained unchanged – the THA lies within CR. This is perhaps a telling illustration of the uncertainty of the existence of a true hinge axis since it would seem that the clinically acceptable THA has surreptitiously crept forwards over the past few decades, to keep pace with centric relation.

Further confusions arise when considering the seemingly interchangeable 'retruded contact position' (RCP) and 'retruded contact' (RC). The former is defined as:

*'that guided occlusal relationship occurring at the most retruded position of the condyles in the joint cavities. A position that may be more retruded than the centric relation position'* (Academy of Denture Prosthetics 2005)

whilst RC is defined as :

*'contact of a tooth or teeth along the retruded path of closure. Initial contact of a tooth or teeth during closure around a transverse horizontal axis'* (Academy of Denture Prosthetics 2005)

So, it can be deduced that RCP requires operator guidance to push the mandible into, perhaps, a non-physiological posterior position, '*more retruded than CR'*. Meanwhile, RC would appear to be related to the THA and, by association, CR.

This confusion in terminology is an academic point, but it is illustrative and ironic that an expert article published in the British Dental Journal (Wilson & Banerjee 2004), whilst making the exact same point on terminology, then proceeded to reproduce the RCP definition shown above, and use it interchangeably with RC.

It is likely that the definition of RCP is ultimately at fault and out-dated. Whilst CR has moved forwards, and the THA and RC have followed by association, it seems RCP did not follow along too. Or perhaps, it deliberately remains as a super-retruded position (possibly ligamentous), which is unrelated to CR, the THA, or any physiologically achievable position of the mandible. This would cast its clinical usefulness in doubt. Even if RCP turned out to be easier to reproduce than RC, why would anyone want to restore their patient into such a position? Sadly, this confusion is not new, and these 'super-retruded' positions were the subject of scrutiny in Posselt's work, more than 60 years ago (Posselt 1952).

Finally, the idea that CR represents an area, rather than a point (Campos et al. 1996; Keshvad & Winstanley 2000) implies some play in the system is physiologically normal. Clinical variation has been shown to dominate the variability of mounted study casts (Eriksson et al. 2002). Furthermore, diurnal variation in the location of this CR area has previously been shown (Shafagh et al. 1975). Does this mean the mandible can perform a terminal hinge closure from multiple positions within the CR area?

### 1.2.2 Clinically Positioning the Mandible into CR

The techniques of clinical manipulation of the mandible into CR can broadly be divided into operator-guided and patient-guided. Examples of the former include bimanual manipulation (Dawson 1989), chin point guidance (Lucia 1960) and perhaps myocentric techniques (Jankelson 1969).

By contrast, patient-guided techniques rely on patient musculature and include the Schuyler technique (placing the tip of ones tongue towards the vibrating line of the palate), or anterior deprogramming techniques such as the Lucia jig (Lucia 1964), tongue blades (Long 1970), leaf-gauges (Long 1973) and more recently with a '*sliding, guiding acetate gauge'* (Woelfel 1986). Sometimes a combination of the

two groups is advocated (Roth & Rolfs 1981) such as having the patient deprogrammed with a Lucia jig, then operator guidance into CR.

Repeatability has been suggested as a valuable tool for assessing the validity of any CR positioning technique (Keshvad & Winstanley 2001). The reproducibility of chin point guidance and a 'modified swallowing technique' has been investigated in upright and supine patients (Campos et al. 1996). After deprogramming for 15 minutes with a Lucia jig, CR was compared using both methods and both patient positions. Swallowing (and then instructing the patient to 'hold that position') always produced a more superior and anterior condylar position, and was less affected by the position of the subject.

A more recent pilot study investigating consistencies between two techniques, bimanual manipulation and anterior deprogramming revealed no statistical difference between the two techniques (McKee 2005). Previous work by the same author shows a lack of training of general practitioners in the methods of positioning the patient into CR (McKee 1997).

One might conclude that if a method which is entirely controlled by the patient's musculature is as reliable as dentist manipulation methods, the former ought to be preferred.

Furthermore, anterior deprogramming using a leaf gauge (Long 1973) appears to be effective and this 'tripodisation' causes a superior displacement of the condyles with little antero-posterior displacement (Fenlon & Woelfel 1993). In the latter study, the authors did show a significant distalisation of the condyles with increasing bite force (up to 100N) when a force gauge was used in place of the leaf gauge but this was rigid, and 5mm in width so it is difficult to compare this with the leaf gauge results. What is apparent is that 'firm' biting on a leaf gauge positions the condyles superiorly. This finding agrees with a previous study which showed that, using a leaf gauge, the condyle was positioned more superiorly compared to bimanual manipulation, chin point guidance or self-guidance (Park et al. 1989). Similarly, orthodontic studies have found anterior deprogramming to be a useful method for positioning the patient in CR (Karl & Foley 1999).

In summary, it would seem that over the recent decades there has been a slow shift from dentist-guided to patient-guided (or combined) techniques, and perhaps this agrees well with the redefined location of CR described earlier, since the superior head of the lateral pterygoid muscles will pull the condylar heads superiorly and anteriorly, whereas a dentist is prone to displacing the mandible posteriorly unless a very careful clinical technique is adhered to.

Ultimately, it would seem that many of the proposed techniques are capable of positioning the patient within the CR area (McKee 2005), although the use of excessive posteriorly directed force is no longer acceptable. More important would be correct training of the operator in the use of a specific procedure (McKee 1997). Perhaps advocating a patient-guided technique (to reduce discrepancies between less well trained operators) is more likely to be adopted by non-specialist general practitioners.

### 1.2.3 Recording Centric Relation

With the mandible located in CR relative to the maxilla, the next task is to record this position. Generally this can be done with an interocclusal record. The interocclusal record is usually made from wax or polyvinyl silicone and is perhaps one of the weakest links in the procedure, as Lucia noted in 1964:

*'The mechanical procedures necessary to relate the mandible to the maxilla present the problem. Our task would be simple if a magic material that would solidify at a given word could be inserted between the teeth when the lower jaw is executing a perfect terminal closure. Unfortunately, we have no such material.'*
(Lucia 1964)

This difficulty is borne out by some authorities recommending that a second method of occlusal registration, for example an occlusal sketch (Davies et al. 2001), should accompany the interocclusal record to the laboratory, to verify that the articulated models do indeed replicate the situation *in vivo.*

One should also be mindful of the regrettable possibility that the recording materials used may not be manipulated in the recommended way under the constraints of a busy general dental practice. It has been shown that defects in impressions received by commercial labs in the UK are commonplace (Winstanley et al. 1997; Storey & Coward 2013; Storey & Coward 2014) and that the main errors in accuracy of impressions and dental casts arise through inappropriate use of materials and techniques (Donovan & Chee 2004). It seems reasonable to extrapolate these findings to interocclusal records which may be even more prone to error if correct clinical technique is not adhered to.

The effect on reproducibility of jaw relation records using various recording materials has been investigated in dentate, partially dentate and edentulous patients (Eriksson et al. 2002). This study found the greatest reproducibility was in the fully dentate group when no recording medium was used, and the patient was in the maximum intercuspal position (MICP). The study concluded that MICP was the most reproducible position. However, one could draw a different conclusion, namely that the most reproducible position was when *no* recording material was used. This would seem more valid since MICP was less reproducible when recording materials *were* used, a finding that agrees with previous workers (Walls et al. 1991).

Another example of this is the finding that dual-arch quadrant impressions show more accurate occlusal contacts in MICP than casts produced from complete arch impressions (Parker et al. 1997). This technique is almost the equivalent of having no interocclusal recording material (although invariably some material will flow between the occluding surfaces). However, whilst suitable for small fixed prostheses in specific cases, the authors also state that eccentric occlusal relationships will not be reproduced with this technique. It is worth noting that they were exacting with their clinical technique. They performed an initial dual-arch impression with a rigid bite registration material, before relining with a silicone wash. This first stage will effectively ‘solidify’ the tray, making it less prone to errors from flexion. However, the technique might be considered ‘dangerous’ in that bite registration material can lock into undercuts, and be difficult or impossible to remove intact.

The problem remains that there is not a simple way to record any position other than MICP, without the use of a recording material.

To that end, workers have investigated the clinical reproducibility of centric occlusal records. The reader should be cautious when assessing such literature. Most workers measure the variation in condylar position (Wood & Elliott 1994; McKee 1997; McKee 2005; Utz et al. 2002), whilst others measure bodily movements nearer the level of the dentition (Eriksson et al. 2002), and some do both (Hellmann et al. 2013). The error at the level of the dentition might be considered more clinically relevant, particularly if the height at which the CR record is taken is as close as possible to the planned restoration height (to minimise errors induced by incorrect THA location). It might also be expected that the error at the condyles is smaller than the error at the dentition, further from the hinge.

Measured near the dentition, Eriksson (Eriksson et al. 2002) found that 5 identical CR records showed total variations of at least 300µm, with the main influence on repeatability coming from clinical variation, and not the recording material or positioning method. In the same year, other workers were drawing identical

conclusions, measuring reproducibility of the condylar position (Utz et al. 2002). They found a minimal variation of 330µm, using a simple unrefined wax wafer method (which they found to be most repeatable), which rose to 2mm in some other cases. Orthodontists have found similar results (Wood & Elliott 1994), with standard errors in condylar position of 400 – 500µm reported. Interestingly, they conclude that their CR records were ‘highly reproducible’, a reminder perhaps, that what is suitable for one dental speciality may not be acceptable for another.

It is important to remember that this CR record is usually the *only* index relating one of the two dental models (usually the lower) to the THA. This is true, regardless of which of the common methods (arbitrary earbow or average value) has been used to relate the upper model to the THA. Therefore, the accuracy of the CR record has a cumulative effect of the accuracy of the simulated THA location on the articulator.

We can conclude that there is broad agreement in the evidence base. The process of taking a physical interocclusal record, and transferring this to an articulator can be expected to incur a variability of one third to one half of a millimetre, in the relative position of the upper and lower dentition.

## 1.3 Digital Bite Registration

With the advent of 3D scanners (including intra oral scanners) there has been interest in digital methods to record the occlusion. To date, investigations have been restricted to recording maximum intercuspation (MICP). Two digital techniques have been described. The first involves taking a physical bite registration, which is then digitised and used to align virtual dental models (Delong et al. 2002; DeLong et al. 2007; Quoob et al. 2011; Tanaka & Hattori 2012). The second technique is the so-called 'buccal bite' scan (Müller 2010; Straga 2009; Iwaki et al. 2013; Ueda et al. 2014; Jaschouz & Mehl 2014). This involves a scan of the upper and lower buccal (or labial) segments with the patient closed in MICP, and a derivation of the occlusal contacts (on previously scanned full arch models) by aligning the scans.

### 1.3.1 Digitising Physical Bite Registrations

The methods involving scanning physical bite registrations offer the advantage that the clinician need not change their habits and they do not need to purchase expensive scanning equipment. However, they may suffer the problems described earlier, with incorrect manipulation of bite registration materials being common, along with distortions, and undesirable effects on the path of closure of the mandible.

However, there are reports of good reproduction of occlusal contacts (DeLong et al. 2007) although the definition used by the authors to classify an occlusal contact (≤ 350µm) seems rather insensitive.

One interesting advantage proposed for the use of digitised physical bite registrations is the possibility of compensating for the physiological tooth movements (Parfitt 1960) and mandibular arch flexions (Regli & Kelly 1967) that occur variably, depending on the degree of opening. For example, the mandibular arch width decreases on opening - the position most impressions (optical and physical) are recorded in. It has been reported that the scale of these changes in width (between the mandibular molars) can reach more than 400µm (Chen et al. 2000). The authors found mean arch width reductions of 145µm, but it should be noted that the subjects were opening as wide as they could. In any event, if the mandibular impression is recorded at *some* degree of opening, a potentially significant change in arch form may occur, when compared to a bite registration recorded at 0º of opening.

Digital manipulation has been suggested (Tanaka & Hattori 2012), to virtually reposition individual teeth (sectioned from a digitised dental model), so that they align perfectly to a digitised MICP record. This method is currently very labour intensive but may offer some promise for the future, and allow clinicians to compensate for arch width changes and tooth mobility for the first time.

### 1.3.2 Optical Bite Registration

A second method of digitally recording the occlusion is to scan the buccal segments of the teeth, whilst the patient is biting in MICP. It has been suggested that this method is so accurate as to be able to use it to measure natural variation in MICP (Jaschouz & Mehl 2014). The authors found mean deviations of 42 ± 34µm when measuring the variation in position of the mandibular teeth over 8 attempts on 15 dentate subjects. By comparison, manually positioned plaster casts exhibited variations of 135 ± 77µm over five positioning attempts. Does this provide the first evidence that optical bite registrations may exceed the current best practise for aligning dentate casts in MICP, namely, using no registration material provided that the occlusal features and arch form allow the dental casts to be held in a single, stable position (Walls et al. 1991)? The work seems corroborated by a second group, who compared contact area variation using five buccal scans of a subject, with contact area variation using five different scans of the dentition, but only one buccal scan (Ueda et al. 2014). They found greater variation when multiple buccal scans were used. This implies there may have been some clinical variation in the mandibular position during each buccal scan, perhaps equivalent to the 42µm found by Jaschouz and Mehl.

An alternative theory would be that the alignment algorithm for the buccal scan is less tolerant to noise or variation. If this is the case, the occlusal scans of the arches might be expected to be more accurate, because the multiple overlapping scans required to create the dental arch allow the software to self-correct some alignment errors, in a process called ‘loop-closing’ (Sprickerhof & Nüchter 2011). In a dental context, full arch intra oral scans have recently been found to be highly accurate (regardless of which system is used), and almost comparable to silicone in a rigid impression tray (Ender et al. 2016). This may be due to the loop-closure capabilities of modern software. By contrast, the buccal bite scan will not collect sufficient data to allow such global refining techniques. It might therefore be more prone to variation and error.

Most buccal bite studies have restricted their measurements to the region of the buccal scan and used unprepared teeth (which may contain more ‘interesting’ morphology for an alignment algorithm than, for example, an all-ceramic crown preparation). This raises two questions. If the buccal scan is recorded in the right molar area and the evidence states that the occlusion will be accurate in this area, how accurate will the occlusion be at the left molar region? This is important if the buccal scan technique is to evolve from a ‘single unit’ tool, to a full arch diagnostic and reconstructive tool. Secondly, if the accuracy is only sufficient in the region of the buccal scan, does scanning a prepared tooth affect this?

These questions have been addressed (Iwaki et al. 2013) and the authors found large mean cross-arch errors in optical bite registrations (>500µm when a single unit had been prepared, rising to >800µm for multiple preparations). It is telling that they found small errors (around 40µm) in the region of the actual buccal bite scan, a value that agrees well with the work of Jaschouz and Mehl (Jaschouz & Mehl 2014).

These findings can be explained by understanding that digital alignment algorithms are not perfect and will vary (Solaberrieta et al. 2015; Brusco et al. 2007). Whilst errors in aligning the buccal scan to the models will be small near the site of the scan, they will be magnified at sites distant to it. In addition, these same alignment issues can affect the quality of a full arch scan (Ender & Mehl 2011; Ender & Mehl 2013). Perhaps it is the combination of trying to align two warped dental arches, using a third small, and imperfectly aligned buccal scan that gives rise to the observed cross-arch occlusal errors of nearly 1mm.

It is unfortunate that the size of the buccal scan must generally be kept to a minimum (in fact, it is this authors experience that larger buccal scans fail to align at all). This is partly because the bite scan should be captured as quickly as possible, before the patient moves. The field of view of most intraoral scanners is small, limiting the size of a ‘rapid’ buccal bite scan.

Recent work has attempted to specify the ideal size and location of an optical bite registration, for archiving study models in maximum intercuspation (Solaberrieta et al. 2016). An industrial scanner was used (ATOS Compact 5M, GOM GmbH) and combinations of left, right and frontal bite scans were tested. The optimal scan height was found to be 15mm in the molar region (which just covered the gingival margins of the upper and lower teeth). The width of the scans was little more than a single tooth (12mm). The best accuracy was observed when all 3 locations were scanned, but the authors concluded that, for simplicity, scanning both buccal segments was recommended since these locations were furthest apart. The work is useful in identifying two key facts. Firstly, the height of the bite registration scan is

important. Secondly, a region not covered by the bite scan will align less accurately, unless it is book-ended by a second bite scan further around the arch. The absolute accuracy reported is less valuable, since the scanner used costs up to $50,000 and would only be suitable for bite registration scans of dental study models. A second scanner would be required to actually digitise the models, and this seems like an uneconomical laboratory workflow.

One worker has tried to investigate the possibility of a labial bite which simultaneously captures a larger number of teeth than a classic buccal bite (Straga 2009). The *in vitro* work used a commercial laser scanner with an accuracy of only 220µm. The labial segment was scanned on articulated study models, and contact points noted visually (defined as contacts or penetrations on the models). Digital contacts correlated 'moderately well' with shimstock and articulating film contacts. However, Straga found the sensitivity to be below the 0.7 value suggested by some to be the clinically acceptable cut off point (Delong et al. 2002). This may be partly related to how they assessed digital contacts. Any close contacts that were not touching would not be counted, even if they were only 1µm apart. Ultimately though, the accuracy of the scanner was also an issue. It will be shown later, that the $25,000 scanner used by Straga in 2009, with an accuracy of 220µm, can be replaced with a homemade scanner costing less than £1000, with a tenfold improvement in accuracy. This is due to the rapid expansion in open-source computer software and inexpensive electronics.

Straga's work also hinted at the possibility that where 'virtual' and 'real' articulator contacts differed, these differences could be reconciled if the virtual model was rotated around a virtual hinge axis, set to mimic the articulator. This corrective rotation was only performed on one model but a rotation of just 0.15º (equivalent to 0.2mm translation at the anterior labial segment) achieved all five correct virtual contacts, when previously there was only one virtual contact. This was not investigated further, but illustrates the effect a small rotation around a correctly identified hinge axis can have.

Continuing this work is one of the aims of this thesis alongside expanding the technique to actually derive the location of the hinge axis.

### 1.3.3 Electronic Jaw Tracking

To date, intra-oral optical scanners have only been used to record the static ICP position via a buccal bite, or indirectly to record functional occlusion using a chew-in technique with a bite registration silicone, which is later scanned. These techniques

do not replace the facebow since they will not work in, for example, occlusal re-organisation cases, and suffer the disadvantage of relying on a distortable recording medium.

To overcome this, electronic jaw tracking devices (axiographs) are available. Some use optical technology, for example Jaws-3D (Gallo et al. 1997) whilst others use electromagnetics (eg Cadiax Compact, Gamma Dental, Austria) or ultrasonic transmission and transducers (JMA System, Zebris Medical GmbH, Germany). These replace the recording stylus of the previous generations of pantographs with a digital recording of the patient's movements.

However, all have the disadvantage of being expensive and time-consuming. They all involve attaching a mechanical framework to the patient, a potentially cumbersome process which may act as a further barrier preventing their widespread use. It is also unclear whether wearing such apparatus will alter the patients jaw movements due to unnatural neuromuscular feedback.

One advantage of these jaw tracking systems is the ability to model mandibular movements via a series rotations about a sequence of finite helical axes (or instantaneous axes of rotation, IARs). By breaking down a movement, such as jaw opening, into multiple small steps (much like video frames) an approximation to the IAR can be calculated for each discrete displacement. It is important to note this is an approximation since theoretically the gaps between frames need to be infinitely small to calculate a true IAR. If the movement was particularly erratic, the size of the gap between frames would need to be reduced. In the case of mandibular movements, it has been shown that the movement is smooth enough (even in the presence of temporomandibular dysfunction) to successfully model the IARs at gaps of 0.7º of opening (Gallo et al. 2006; Fang & Kuo 2008; DeLong et al. 2002; Gallo et al. 1997), which equates to approximately 1mm of incisal opening. During natural function, these IARs are not fixed and are generally not located within the condylar head. They are useful for calculating the action of muscles by considering the moments created around these axes (Gal et al. 2004; Grant 1973).

Most research with electronic jaw tracking devices has been devoted to natural jaw movements in dentate subjects (Chen 1998; Ferrario et al. 2005; Fang & Kuo 2008; Gallo et al. 1997). Very little work has been carried out with the patients positioned in CR. In one example (Ferrario et al. 1996) 28 subjects had their natural jaw movements recorded (using a magnetic device). CR movements were then investigated but the initial placement into CR was operator-guided (apparently with no anterior deprogramming), and the actual open-close movement was entirely patient guided. The conclusion was that a pure rotation did not exist, even in the early stages of opening. However, this protocol is not analogous to clinical

recording of CR, in which the mandible is static, with no tooth to tooth contact, and is operator-guided or guided by the patient biting on a deprogrammer.

A better way to reproduce the clinical technique would be to take a series of static CR recordings with the patient at different degrees of opening (eg biting on different thicknesses of leaf gauge, with or without operator guidance as well). This would allow a more controlled positioning of the mandible at each degree of opening, and would be determined consistently by the jaw closing muscles.

### 1.3.4 Virtual Articulation

Traditional dental workflows often involve mounting stone study casts on an articulator. The degree to which articulators can be customised varies, but any that accept a facebow transfer will at least attempt to relate the upper and lower models to the THA and the horizontal plane. All articulators are designed assuming the existence of a fixed axis of rotation. Since this is in dispute it is likely that they simply replicate approximations of the patient's own movements, but within clinically acceptable bounds (Morneburg & Pröschel 2002; Pröschel et al. 2000; Adrien & Schouver 1997).

As digital dental workflows develop, there is increasing interest in being able to 'virtually' articulate digital dental models (Maestre-ferrín et al. 2012; Koralakunte & Aljanakh 2014). The aim remains the same as for the mechanical counterpart. We wish to reproduce the patient's dynamic tooth-to-tooth contacts as accurately as possible.

Commercially available software generally attempts to reverse engineer articulators into the virtual environment, an example being 3Shape CAD Design Software (3Shape, Denmark).

It has been suggested that these simulations may be better utilised by allowing a moveable axis of rotation more akin to the clinical situation, something that is difficult to reproduce in a mechanical device (Maestre-ferrín et al. 2012).

Conversely, an interesting mechanical technique to relate the patient to the articulator (rather than relating the articulator to the patient), has been shown to allow a mechanical articulator to be programmed with enhanced precision (Pröschel et al. 2002). This might imply a mechanical articulator, or virtual facsimile, may be sufficient to reproduce a patients tooth contacts *if* it can be adjusted (programmed) with sufficient precision.

Unfortunately, the aforementioned study required an extra appointment, and the use of an electronic jaw tracking system. Such equipment is generally only used in research environments or specialist private dental practice.

In fact, a drawback common to all virtual simulations is that they will all require a facebow or axiograph  record. As previously noted, the use of facebows in general practice is limited (Clark et al. 2001), whilst axiographic techniques are almost, never used.

It would seem, therefore, that virtual articulation holds the promise of being more accurate than mechanical articulation, but suffers the same disadvantage of only being as good as the data it is fed. Until the *clinical* methods for acquiring this data change and improve, a dramatic improvement in articulator accuracy should not be expected.

## 1.4 Summary

The methods for modelling a patient's true tooth-to-tooth contacts have remained essentially unchanged for over 100 years. Invariably they do not precisely replicate the clinical situation.

Inaccuracies in the methods by which both the THA and CR are recorded, contribute to these differences.

If the *accuracy* of recording the THA and CR can be improved, one might expect to improve the precision with which one can reproduce an individual's articulation *in vitro*.

If the of recording the THA and CR can be *simplified*, one might expect to improve the uptake in use by general dentists, minimise human errors, and facilitate the development of virtual articulation in digital workflows.

# 2 Aim, Objectives and Programme of Work

## 2.1 Aims

- To develop a simple optical method for recording the mandibular transverse horizontal axis
- To assess the validity of this method *in vitro* and *in vivo*

## 2.2 Objectives

- To design a protocol for recording the mandibular transverse horizontal axis
- To develop scanning hardware and software to apply this protocol
- To measure the trueness and precision with which a known axis is found using articulated dental models
- To measure the trueness and precision of optical interocclusal records
- To address areas for improvement in the process to allow for clinical implementation

## 2.3 Summary of the Programme of Work

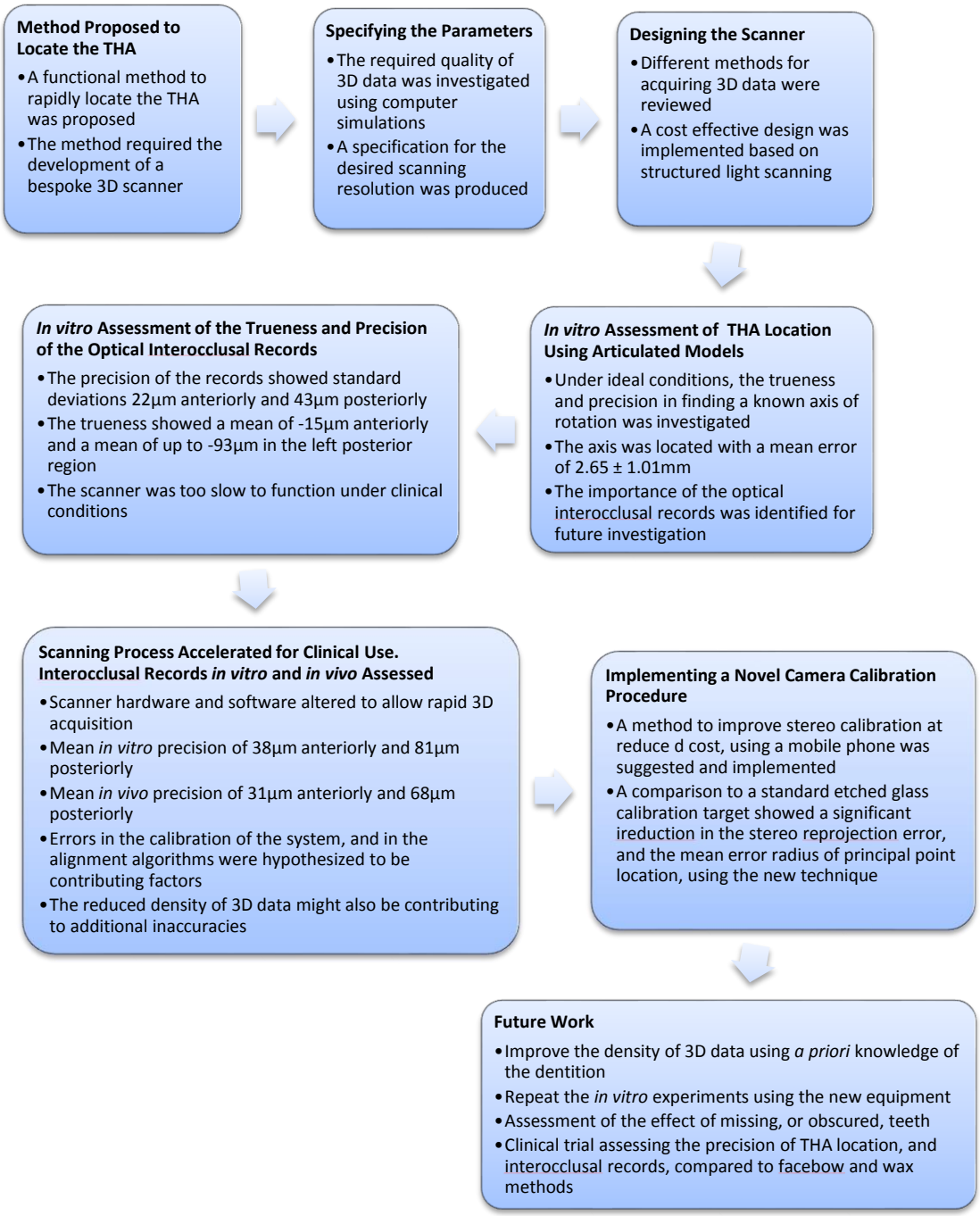


**Figure 9 Outline of the Programme of Work.** The flow chart summarises, retrospectively, the main body of work carried out during this thesis.

# 3 Proposal of a New Method to Locate and Record the THA

## 3.1 Locating the Axis by Intra-Oral Means

An intra-oral method for locating the THA using modern 3D optical scanning techniques is proposed. In fact, the axis that will be found by this method is a finite version of the instantaneous axis of rotation (see Section 3.2), and this negates any controversy over the existence of a true hinge axis. In either event, the method should locate the functional axis about which a small portion of mandibular opening can be modelled.

The method entails recording two 3D images of the labial segment, with the mandible positioned in CR, but at two different degrees of opening. From these images, the axis of rotation about which that movement has taken place can be calculated (Figure 10 and Figure 11).

This calculation can be performed by first digitally aligning models of the patient's full dentition to both labial scans in turn (Figure 12). Subsequently, a common coordinate system is created, aligned to the upper dentition (Figure 13). Finally, the relative motion of the lower dentition between the two scans is calculated (Figure 14). This motion can be decomposed to derive the instantaneous axis of rotation (see Section 3.2). This axis will be precisely equivalent to the THA, *if* such a pure rotation of the mandible actually exists clinically. In the event that only an approximate rotation exists clinically, the calculated axis will provide the mathematically optimal approximation.

One challenge is to produce scanning equipment of sufficient accuracy, yet at an affordable price. This latter point is hard to quantify, but is approached from the perspective of 'how little can be spent to achieve a scanner with sufficient accuracy?'. This will only be known once 'sufficient accuracy' has been defined. In the next section, the mechanical theory of the instantaneous axis of rotation, or screw axis, (upon which the method relies), will be explored. An attempt to define some constraints on the accuracy of the system as a whole will then be made.

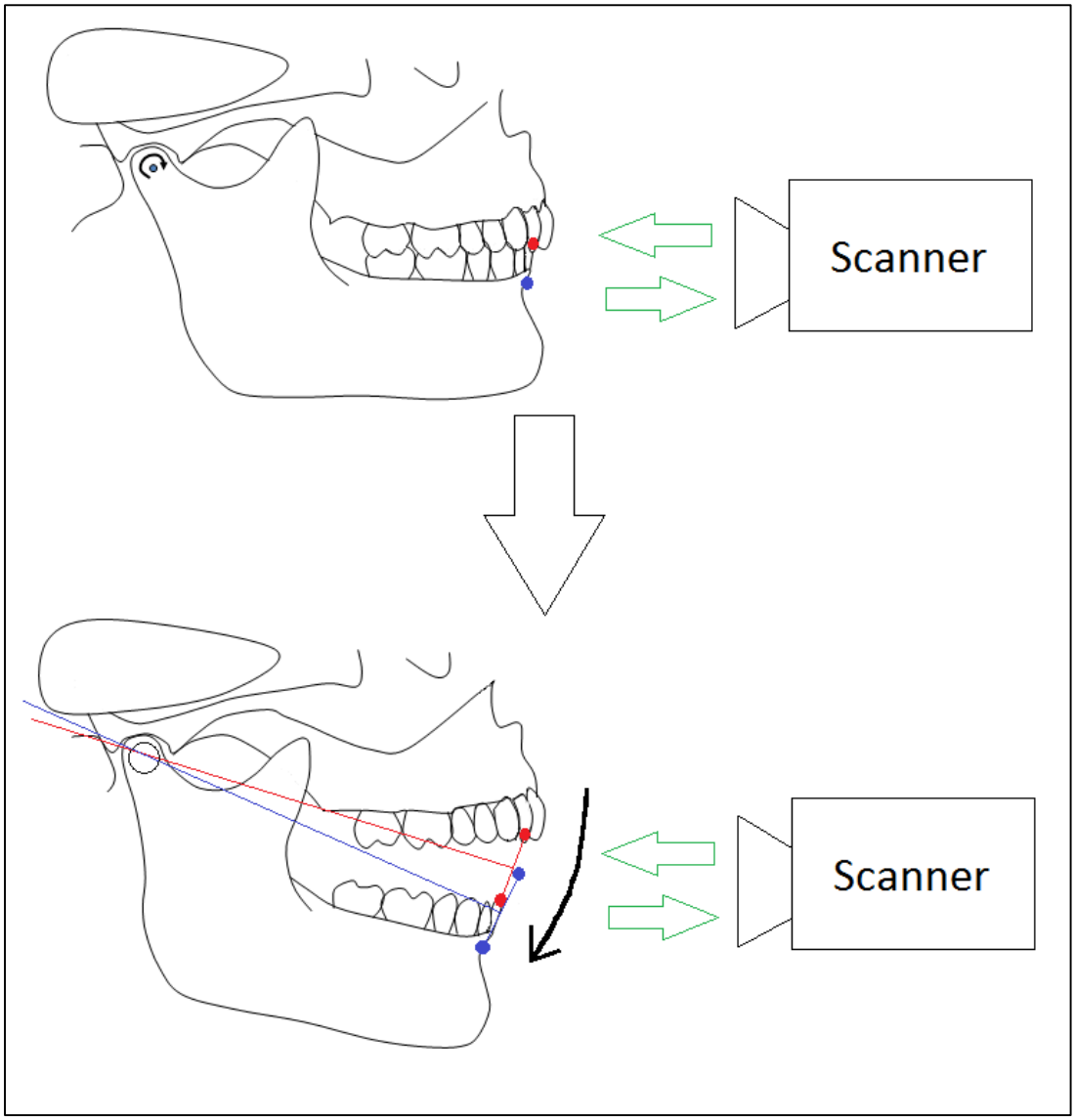


**Figure 10 Deriving the THA from Two Labial Scans.** Two points (eg lower incisal edge and cervical margin) are identified in both scans and their displacements calculated. The THA is calculated from the intersection of perpendicular lines constructed from the midpoint of both starting and ending points. The picture is 2-dimensional and simplistic compared to the actual method of calculating the 3-dimensional screw axis, but the principle remains. In addition, only two points are tracked here for clarity, but in reality thousands of points can be tracked.

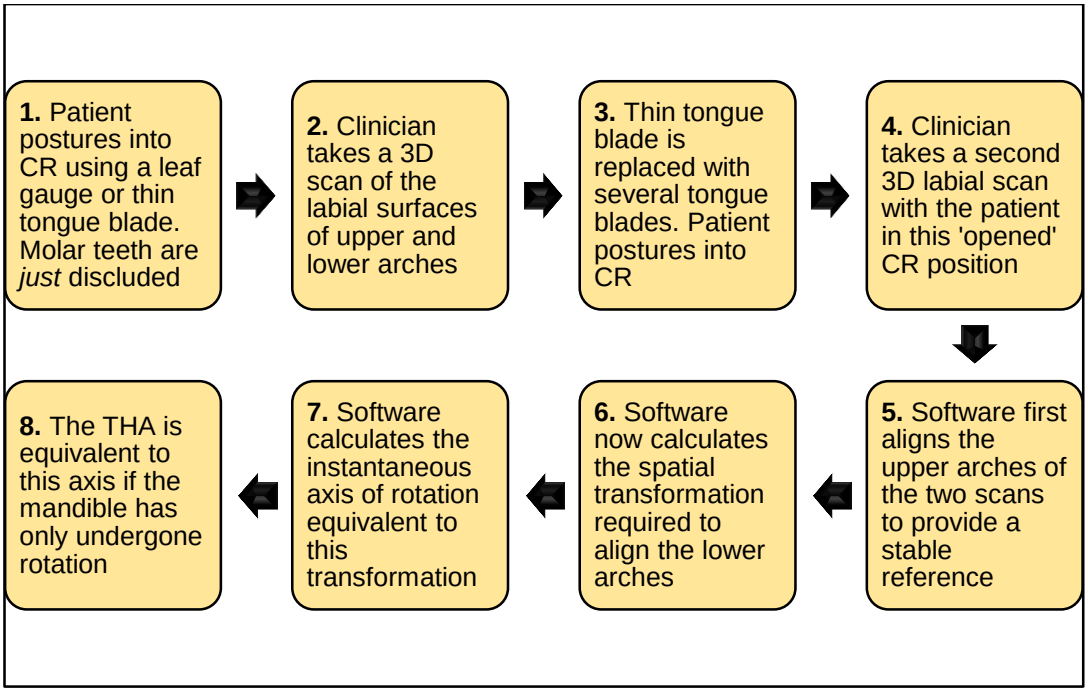


**Figure 11 Flow Chart of the Proposed Clinical Method**

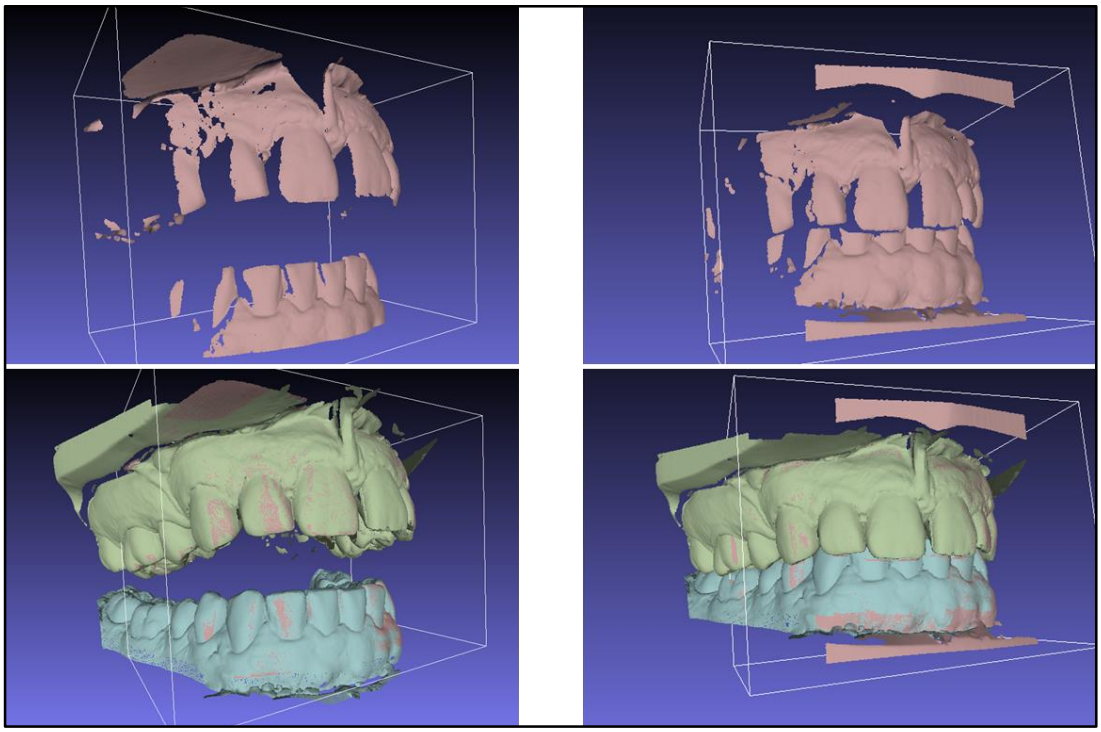

**Figure 12 Stage 1 of the Proposed Workflow.** Two labial 3D scans are recorded, with the mandible in CR during both scans, but at two different degrees of jaw opening (top pictures). Previously scanned digital models of the patient's dentition are then aligned to both bite scans in turn.

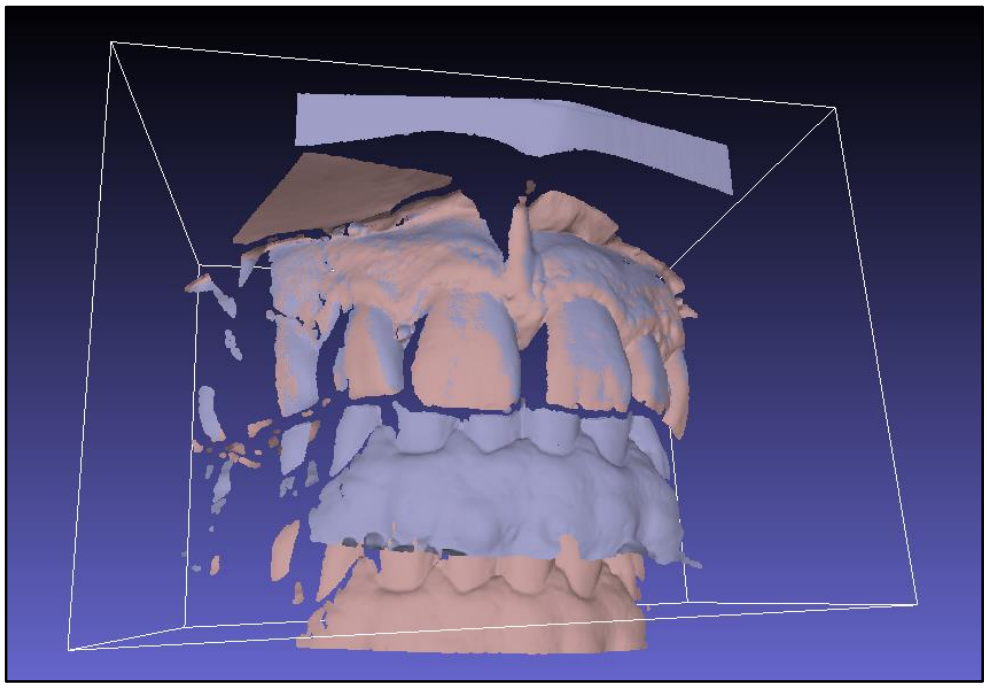

**Figure 13 Stage 2 of the Proposed Workflow.**
Creating the common coordinate frame with respect to the upper model. The two bite scans (and their associated full arch alignments) are positioned such that the upper model does not move between the two scans.

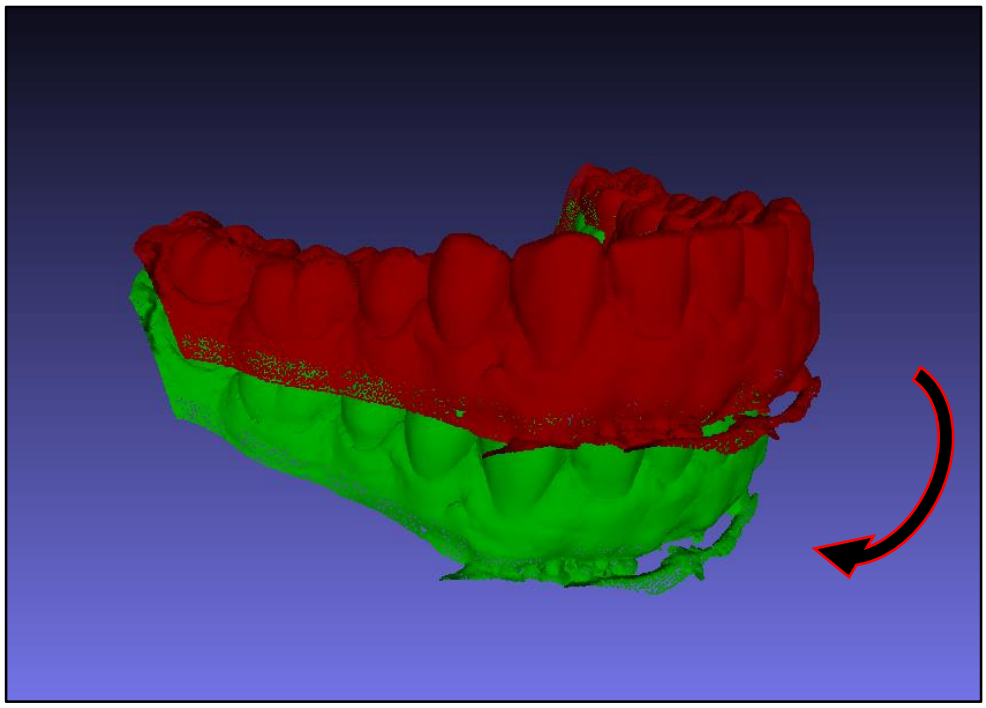

**Figure 14 Stage 3 of the Proposed Workflow.** The transformation (movement) that the mandibular dentition has undergone can now be recovered. This forms the basis for calculating the instantaneous axis of rotation.

## 3.2 The Instantaneous Axis of Rotation

The mathematical modelling of the movement of a rigid object from a start position to a finish position will now be explored. It will be illustrated that, regardless of whether the mandible is performing a pure rotation or a rotation-plus-translation, it is *always* possible to model this movement with a rotation around an axis, and a translation along that axis. This is known as *Chasles' fixed point theorem for Euclidean motions* (Chasles 1830). In modern times, this is generally referred to as the instantaneous axis of rotation (IAR)[2]. Further mathematical details of the calculation of IARs can be found in many modern texts, and the following summary details are adapted from the textbook, Kinematics of Human Motion (Zatsiorsky 1998).

## 3.3

To fully understand the premise of this thesis it is essential to have a working knowledge of IAR theory. This theory generalises the movement of a rigid body in 2D or 3D space. According to the theory, it is always possible to find an axis of rotation (and a translation along that axis), which will correctly position the object in the start and finish positions. For simplicity we will start by considering the 2D case.

### 3.3.1 The Instantaneous Axis of Rotation in Two Dimensions

Let us assume for a moment, that a mandible makes a pure rotation about an axis which passes through the condyles. This movement can be precisely modelled, by defining a rotation of a certain degree about this axis. In this simple case, *all* intermediate positions of the mandible, between the start and finish positions, will also happen to be perfectly modelled (Figure 15).

---

[2] This theory (also called 'screw-axis theory') is a proof that the displacement of any rigid body from a start point to an end point can be modelled by a rotation around an axis coupled with a translation along that axis. Although not well known in dental circles, the theory was used by Bennett in as early as 1908 (Bennett 1908), to describe mandibular motions. Various dental groups have since used this method to describe mandibular motions but the mathematical complexity has, perhaps, limited its widespread clinical adoption.

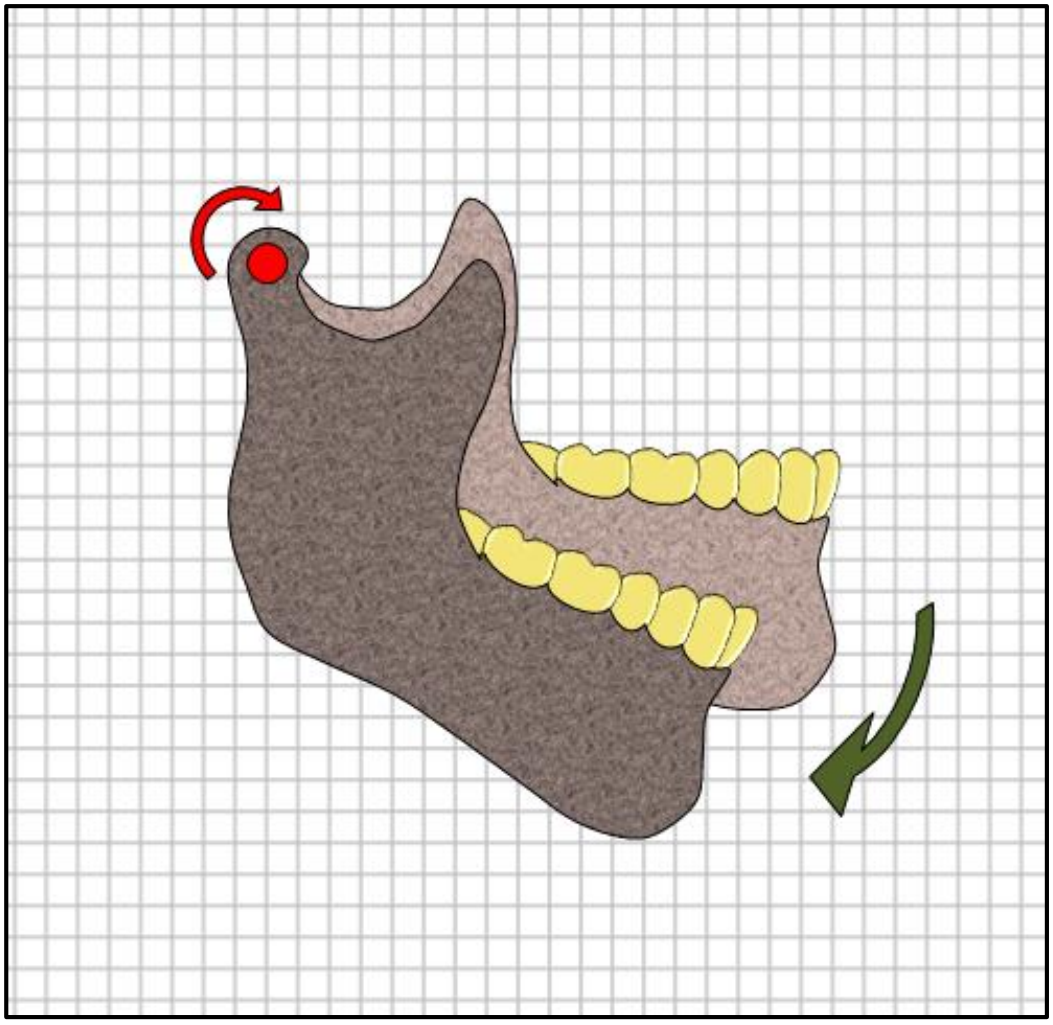

**Figure 15 Modelling a Pure Rotation of the Mandible.** It is assumed that the mandible actually physically rotates about the condylar axis. The observed movement (green arrow) can be precisely modelled by a rotation around an axis located in the condyle (red circle). The start and finish positions, and all intermediate positions, will be correctly modelled by this axis.

Now suppose that the mandible performed a pure translation instead of a rotation. It is still possible to model this movement using a rotation. The axis of rotation will be located at a distance of infinity rather than in the condyle (Figure 16). Again, all intermediate positions will happen to be correctly modelled, in addition to the start and finish positions.

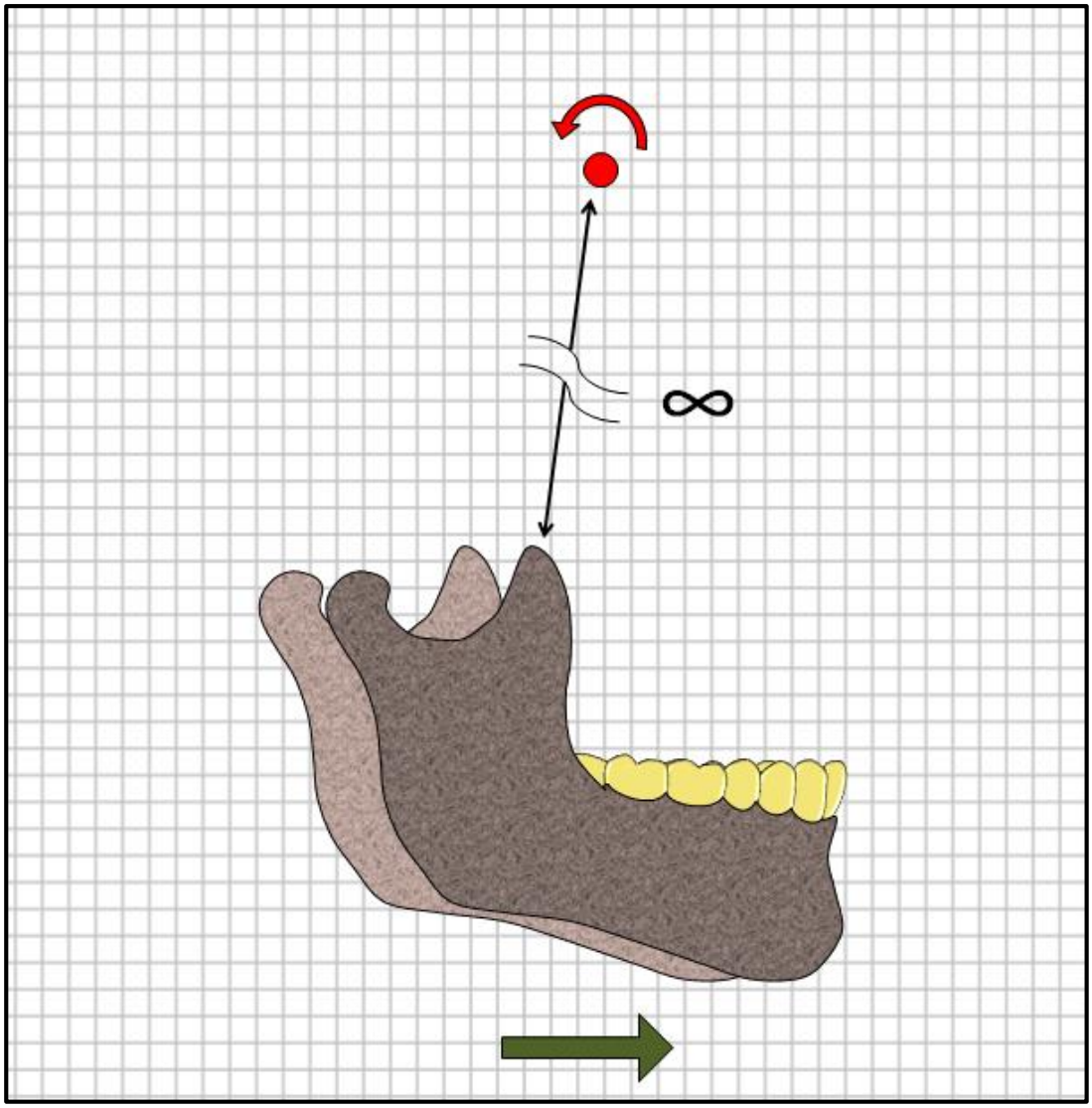


**Figure 16 Modelling a Pure Translation of the Mandible.** The translation (green arrow) is modelled using an axis of rotation (red circle). Despite the fact that no rotation actually takes place, the movement can be precisely modelled mathematically as a rotation about this axis (located at infinity). The start and finish positions, and all intermediate positions, will be correctly modelled by this axis.

In a third case, a combined rotation and translation is modelled using only a simple rotation about an axis. A non-physiological movement is used to emphasise the point that *any* motion of the rigid body (the mandible) can, in fact, be modelled by a simple rotation about an axis (Figure 17). An important difference is that, with a complex motion, *only* the start and finish positions of the movement will be accurately modelled. All intermediate positions (the path taken by the mandible) will be incorrectly modelled by the axis.

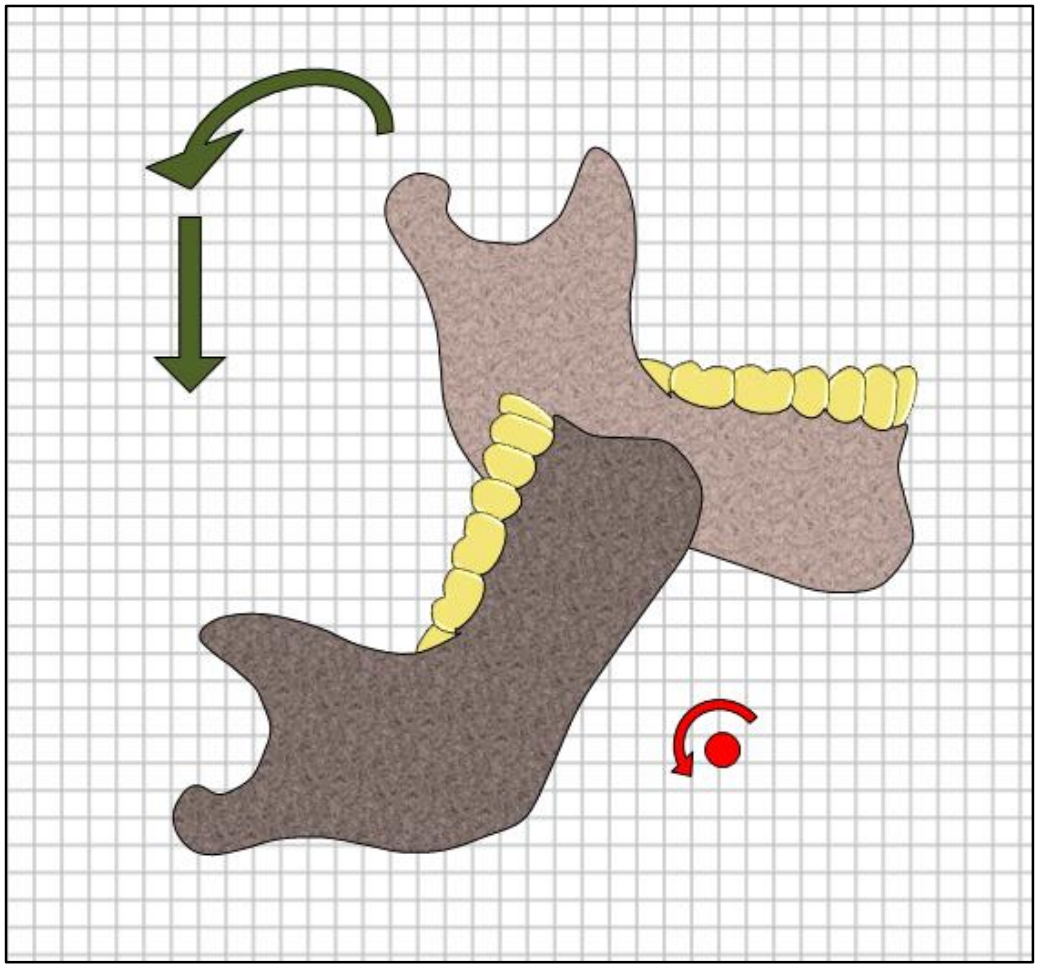

**Figure 17 Combined Rotation and Translation.** Any combined rotation and translation (green arrows) can be modelled as a simple rotation about an axis (red circle). The start and finish positions will be precisely modelled by this axis. However, all intermediate positions - the path taken by the mandible - will be incorrectly modelled.

From a clinical perspective it can be seen that, in the 2D case, *if* the mandible is performing a pure rotation, all mandibular positions within that movement will be correctly modelled. Furthermore this is a kinematic, rather than anatomic, model. As such, the axis of rotation can be located anywhere, be it within the condylar head, at the neck, or at some other location.

However, if the mandibular movement is not a pure rotation, only an approximation of the motion will be modelled by the axis. Only the start and finish positions will be completely accurate.

In order to accurately model a complex movement, the motion can be subdivided, noting checkpoints along the way. Each fraction of the motion can then be represented by its own axis. For example, the compound motion previously

illustrated in Figure 17 could be subdivided into two parts, modelled by two distinct axes (Figure 18).

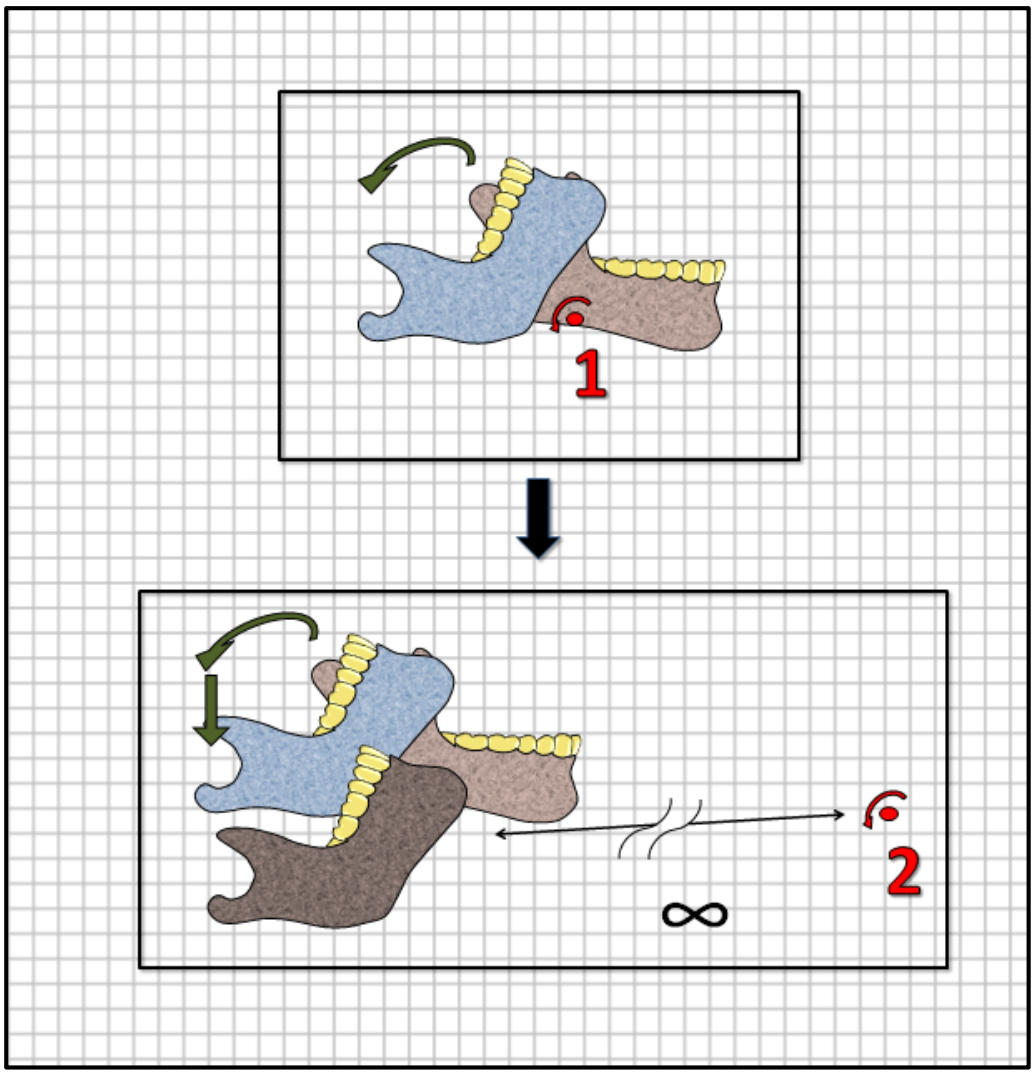


**Figure 18 A Complex Motion Subdivided to 'Capture' a Waypoint.** Here, two axes each model half of the movement (blue mandible represents the waypoint). The first half of the motion is modelled by a rotation about axis 1, whilst the second half of the motion is performed by rotation about axis 2. The start, finish and mid positions of the mandible are accurately described using the two axes. The remaining intermediate positions, whilst not accurately described, are closer to the real motion.

With one subdivision, the model now guarantees accurate positioning of the mandible in three stages of the complete movement (start, mid-point and finish). The remaining parts of the motion still have no guarantee of accuracy, though they are likely to be better approximations of the actual motion.

If a better modelling of the complete motion was required, a further subdivision could be employed, using discrete axes for ever-smaller sections of the complete movement. An example of a physiological jaw-opening movement, comprising

simultaneous translation and rotation from the outset, is shown in (Figure 19) along with multiple discrete axes that would sequentially model the movement.

If these subdivisions are constructed to be infinitely small, we arrive at the ‘instantaneous axis of rotation’. This axis perfectly describes, using only a simple rotation, an infinitesimally small part of a rigid body motion. Each successive step in the complete motion is modelled by another axis. Since the distance between each step of the motion is infinitesimally small, the distance between each discrete axis also tends towards zero. Ultimately, the axis can be envisaged as a single axis, travelling along a continuous path, rather than a series of discrete axes, dotted along that path.

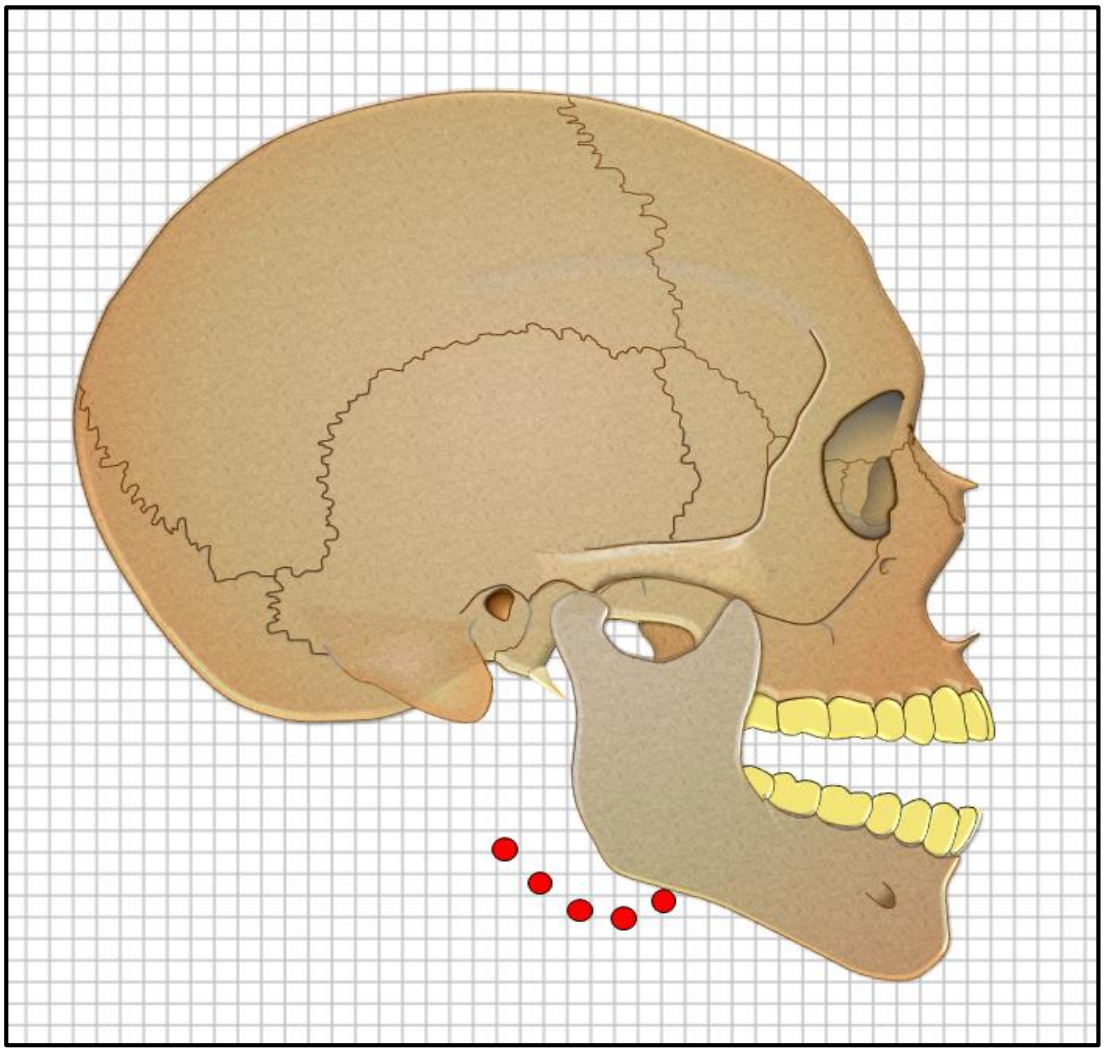

**Figure 19 A Typical Sequence of Discrete Axes of Rotation Modelling a Physiological Jaw-Closing.** This jaw motion comprises simultaneous rotation and translation of the condyle. From the closed position, the leftmost axis provides the initial model of motion. The axis to the right of this can be envisaged as ‘picking up’ the next part of the motion, and so on sequentially from left to right (axes shown as red circles).

### 3.3.2 The Instantaneous Axis of Rotation in Three Dimensions

Section 3.3.1 showed how to model the motion of a rigid body in 2-dimensional space, using the instantaneous axis of rotation. It is clear that the mandible is a 3-dimensional object and that the model must be extended appropriately.

Adding a third dimension poses a problem. It is no longer possible to model *any* rigid body motion by a simple rotation about an axis.

Consider a child's swing. If the swing starts at the neutral position, and moves to a 'forward swing' position, there is no trouble identifying a suitable axis from which to model the movement (the cross-bar of the swing frame). Now imagine the attachment of the swing to the cross-bar can slide along the bar. From a neutral position, the swing slides along the bar to come to rest in another neutral position. An axis can be created perpendicular to the cross-bar and infinitely far away, from which this sliding movement can be generated. Now suppose the two movements are combined – a 'swing forward' and a slide along the bar. Any single axis which models this complete motion must lie parallel to the cross-bar. This is the only way the relative orientation of the start and finish positions of the swing seat can be preserved. However, this being the case, there is nowhere in 3-dimensional space to place this axis to reproduce the sliding motion.

The only solution to this degenerate situation is to allow for movement *along* the axis, in addition to rotation *about* the axis. This is often referred to as a screw axis.

Any motion of a rigid body in 3-dimensions can be modelled using a discrete rotation about an axis, and a discrete translation along that axis. This is known as Chasle's Theorem.

This is much like the action of a screw, with the pitch of the thread determining the size of the translation along the axis for a given rotation. By varying the (mathematical) pitch, one can define and orientate a screw axis in 3D space, such that any movement can be modelled.

As with the 2-dimensional situation, only the start and finish positions will be guaranteed to be correct. The path the object takes may not be accurately modelled by the arc traversed by motion around (and along) the screw axis.

As before, the motion can be subdivided infinitely, to produce a single instantaneous screw axis (sometimes called a helical axis), which will travel through 3D space as the motion takes place. This axis will completely define any rigid body motion. If discrete intervals are used, rather than infinitely small intervals, a series of axes which will closely model a rigid body movement (finite helical axes) will be produced.

### 3.3.3 The Rotation Matrix

Having seen that any rigid body motion can be modelled by using a rotation about an axis and a translation along it, it follows that a convenient way of modelling this rotation is required.

First, consider the 2-dimensional case of a point, **P**, that is rotated around the origin by degree, θ, to **P'** (Figure 20).

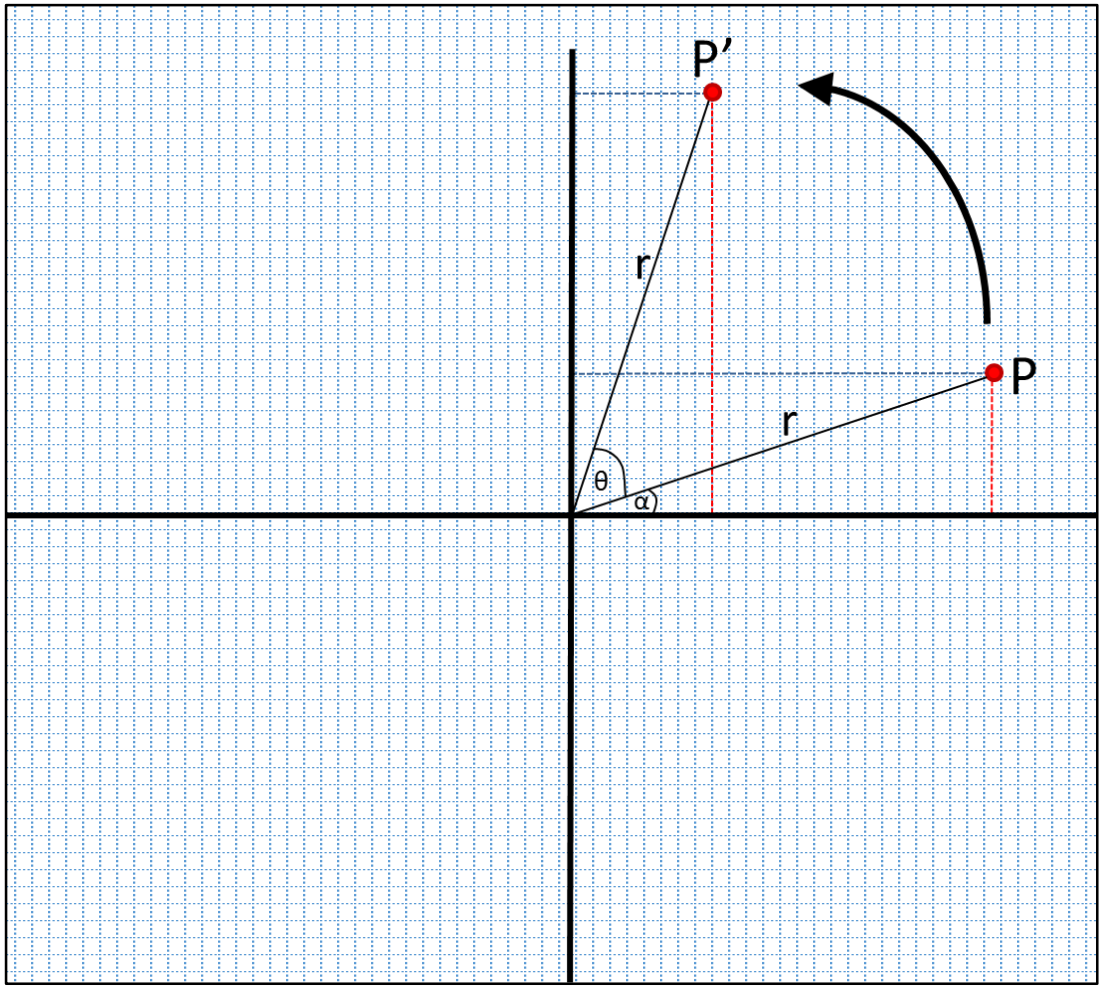


**Figure 20 The 2D Rotation of an Arbitrary Point (P), About the Origin by Degree θ, to P'.**

The aim is to map the coordinates **P**(x,y) to **P'**(x',y'). Starting with **P**(x,y) :

$$x = r\ \cos(\alpha)$$

$$y = r\ \sin(\alpha)$$

and for x' :

$$x' = r\cos(\alpha + \theta)$$

$$\rightarrow \; x' = r(\cos(\alpha)\cos(\theta) - \sin(\alpha)\sin(\theta))$$

$$\rightarrow \; x' = r\cos(\alpha)\cos(\theta) - \mathrm{r}\sin(\alpha)\sin(\theta)$$

$$\rightarrow \; x' = x\cos(\theta) - y\sin(\theta)$$

Similarly :

$$y' = x\sin(\theta) + y\cos(\theta)$$

Matrices can be used to simplify the transformation:

$$\boldsymbol{P'} = \boldsymbol{RP}$$

where ***P*** and ***P'*** are column vectors, and ***R*** is the 2x2 rotation matrix. This can be written as:

$$\begin{bmatrix} x' \\ y' \end{bmatrix} = \begin{bmatrix} \cos(\theta) & -\sin(\theta) \\ \sin(\theta) & \cos(\theta) \end{bmatrix} \begin{bmatrix} x \\ y \end{bmatrix}$$

Hence, for all points, *P*, *P'* can be calculated using simple matrix multiplication. The rotation matrix remains 'fixed', and defines a rotation of θ degrees around the origin.

This protocol can be extended to three dimensions. The 2-dimensional rotation *centre* will become a 3-dimensional rotation *axis*. The rotation matrix, ***R***, is expanded from a 2x2, to a 3x3 matrix. This matrix contains all the information required to rotate any 3D point $\mathbf{P}_{(x,y,z)}$ around a specific axis (which passes through the origin, but may point in any direction), by a fixed degree, θ, to $\mathbf{P'}_{(x',y',z')}$.

Conceptually, this expansion to 3 dimensions can be shown if one considers that any 3D rotation can be accomplished by combining rotations around the x-axis, the y-axis and the z-axis sequentially. A rotation around, for example, the z-axis, will never change $\mathbf{P}_z$, so we are, in effect, performing a 2-dimensional rotation in the x-y plane. The rotation matrix for a 3-dimensional rotation of degree, α, about the z-axis is therefore given by:

$$\begin{bmatrix} x' \\ y' \\ z' \end{bmatrix} = \begin{bmatrix} \cos(\alpha) & -\sin(\alpha) & 0 \\ \sin(\alpha) & \cos(\alpha) & 0 \\ 0 & 0 & 1 \end{bmatrix} \begin{bmatrix} x \\ y \\ z \end{bmatrix}$$

Similarly, a rotation, γ, about the x-axis, will leave $\mathbf{P_x}$ unaltered, and is given by :

$$\begin{bmatrix} x' \\ y' \\ z' \end{bmatrix} = \begin{bmatrix} 1 & 0 & 0 \\ 0 & \cos(\gamma) & -\sin(\gamma) \\ 0 & \sin(\gamma) & \cos(\gamma) \end{bmatrix} \begin{bmatrix} x \\ y \\ z \end{bmatrix}$$

and finally, a y-axis rotation of degree, β, will leave $\mathbf{P_y}$ unaltered :

$$\begin{bmatrix} x' \\ y' \\ z' \end{bmatrix} = \begin{bmatrix} \cos(\beta) & 0 & -\sin(\beta) \\ 0 & 1 & 0 \\ \sin(\beta) & 0 & \cos(\beta) \end{bmatrix} \begin{bmatrix} x \\ y \\ z \end{bmatrix}$$

A single rotation matrix can now be derived, which can be thought of as a rotation, γ, about the x-axis, followed by a rotation, β, about the y-axis, and finally a rotation, α, about the z-axis.

$$\boldsymbol{R}(\theta) = \boldsymbol{R_z}(\alpha)\boldsymbol{R_y}(\beta)\boldsymbol{R_x}(\gamma)$$

Note that the order of matrix multiplication is important.

The resulting matrix, **R**(θ), is a single 3x3 matrix which merges the individual rotations into one combined movement.

The key point is to realise that such a 3x3 matrix can exist for *any* rotation, about *any* arbitrary axis. This axis will always pass through the origin (0,0,0).

This presents a crucial problem. Whilst the orientation and degree of rotation of the axis is correct, the spatial location is not correct (since it would be highly unlikely that the true screw axis passed through the origin). Therefore the result of rotating a rigid body using a rotation matrix will be a correctly orientated object, but in the wrong place in 3D space. A *translation* must subsequently be applied to every point on the rigid body. A 2D version of this process is shown in Figure 21 and Figure 22. This translation will NOT be equivalent to the location of the screw axis.

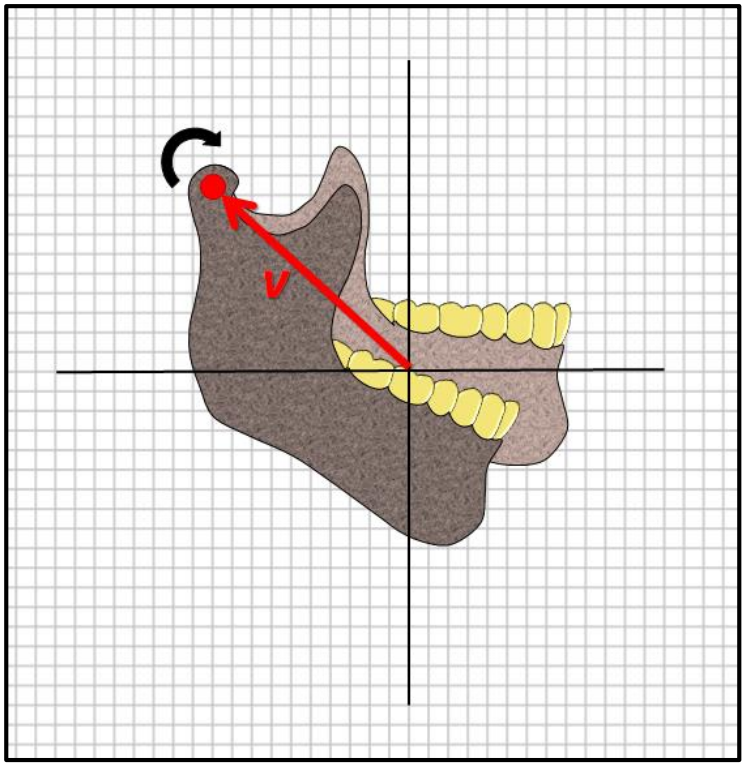


**Figure 21 A Rotation Occurring Around a Point that is not Located at the Origin.** This point is unknown, and defined by the vector, *v*.

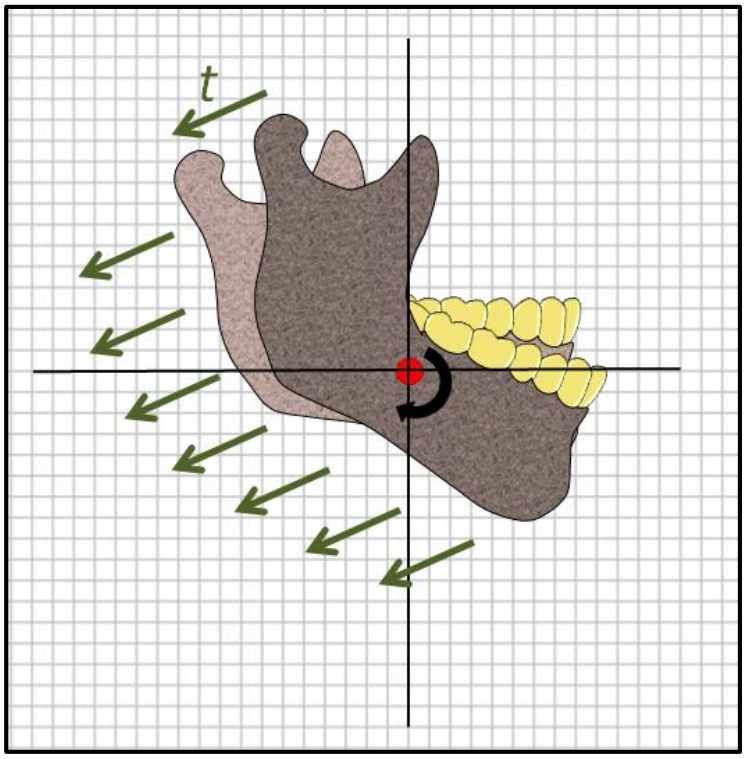


**Figure 22 Modelling the Rotation Shown in Figure 21 Using a Rotation Matrix.** The rotation will occur around the origin. A translation, *t*, (green arrows) is subsequently required in order to correctly position the mandible. The location of the centre of rotation (vector *v* in Figure 21) is not recovered.

The 3-dimensional equivalent situation implies a translation is required (a bodily shift without change in orientation) of the object, after the rotation has been applied:

$$P' = RP + T$$

where P' is the transformed coordinate, R is the 3x3 rotation matrix, P is the pre-transformed coordinate and T is a 3x1 column vector (the 3D equivalent of t in Figure 22), performing the translation. As before, this translation will not indicate where the screw axis is. It is entirely dependent on where the origin of the global coordinate system happens to be.

It is common practice to combine R and T into one matrix, the 'transformation matrix'. This is done by adding another column to the rotation matrix, to hold the elements of T. It is often numerically simpler to maintain square matrices (the same number of columns and rows), so an additional row is inserted which will have no effect on calculations. In order to balance this, the coordinates of all 3D points, P, are homogenised. This simply means an additional row is inserted, usually with the value 1, to enable matrix multiplication. Thus:

$$\begin{bmatrix} P'_x \\ P'_y \\ P'_z \\ 1 \end{bmatrix} = \begin{bmatrix} r_{11} & r_{12} & r_{13} & t_{14} \\ r_{21} & r_{22} & r_{23} & t_{24} \\ r_{31} & r_{32} & r_{33} & t_{34} \\ 0 & 0 & 0 & 1 \end{bmatrix} \begin{bmatrix} P_x \\ P_y \\ P_z \\ 1 \end{bmatrix}$$

### 3.3.4 Recovering the Location of the Screw Axis

Let us assume for a moment that the rotation matrix for a given mandibular opening movement is known. The direction of the axis of rotation and the degree of rotation can be derived from the rotation matrix (as will be shown later). The task is to find the actual location of this axis in 3-dimensional space. In dental terms, this will be the position of the (virtual) articulator hinge, relative to the dentition.

Consider a point, P, undergoing a displacement (d) to P' in 3-dimensional space (Figure 23).

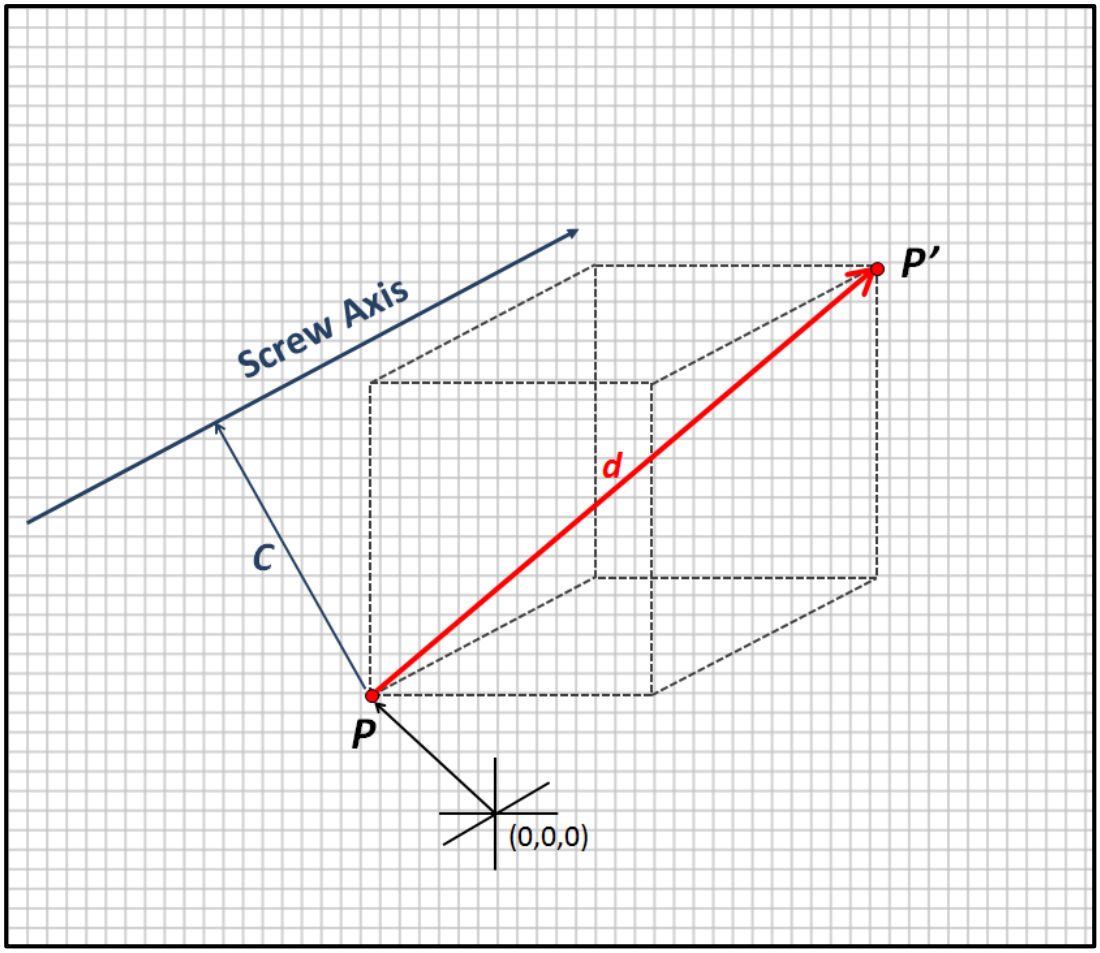


**Figure 23 A Point, P, Undergoes a Displacement, d, to P' in 3D Space.** The transformation is shown with the red line. Vector C (blue line) is a point on the screw axis (relative to P, and constructed perpendicular to the screw axis). The constructed dotted lines are formed in the direction of the screw axis, and orthogonal to the screw axis. In the global coordinate system, the vector P+C will define a point on the screw axis.

The vector P+C must be found, since this will identify a point on the screw axis, in the global coordinate system.

The displacement, d, can be decomposed into two vectors. The first, $d_r$, represents the rotation around the screw axis. The second, $d_t$, represents the translation along the screw axis (Figure 24). The displacement, d, is given by:

$$d = d_r + d_t$$

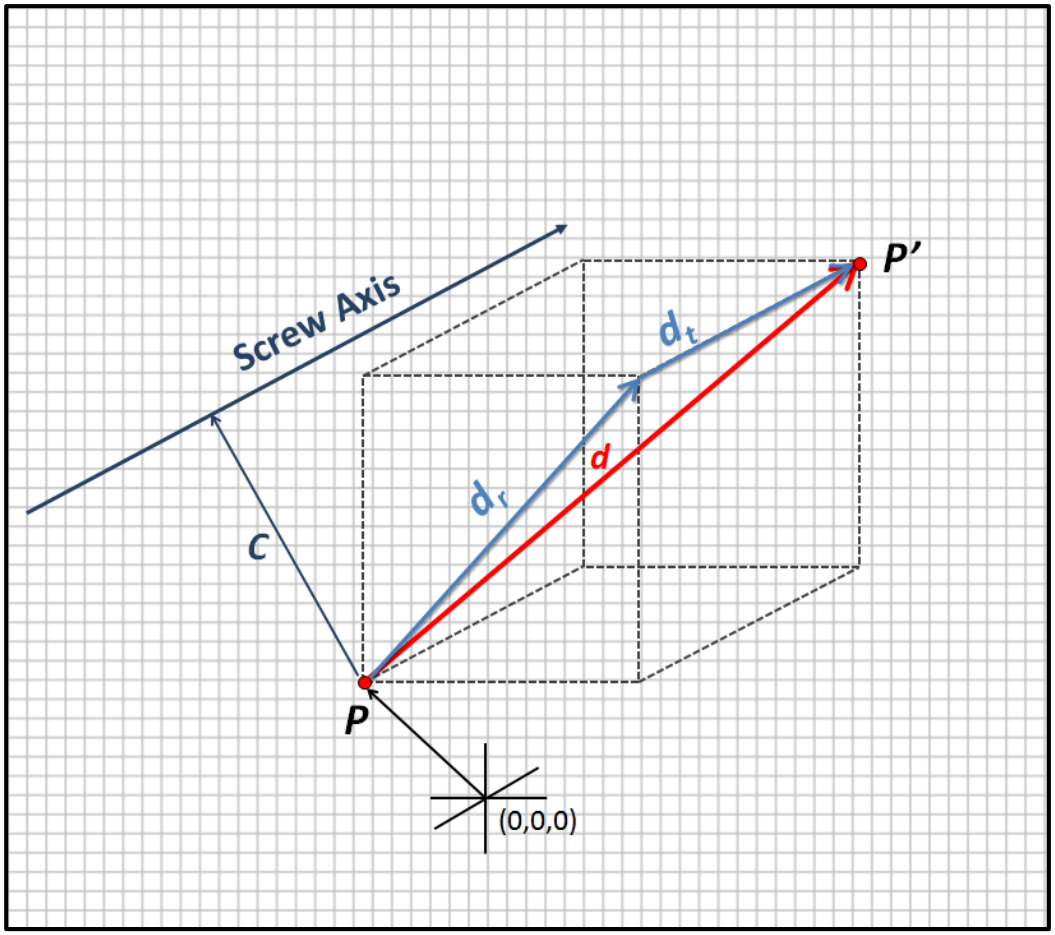


**Figure 24 Decomposing the Motion.** The displacement, d, can be decomposed into a vector, $d_r$, which is confined to a plane perpendicular to the screw axis (representing the pure rotation component), and a vector, $d_t$, representing the pure translation along the screw axis.

Vector $d_t$ can be replaced with the vector, b, given as :

$$b = kS$$

where b is the Rodrigues vector, S is the unit vector of the screw axis, and k is the magnitude of the vector, given by :

$$k = \tan\left(\frac{\theta}{2}\right)$$

where θ is the degree of rotation about the screw axis. This allows vector $d_r$ to be found :

$$d_r = d - b$$

Next, vector C is found, using :

$$C = \frac{b \times (d_r - b \times d_r)}{2b \cdot b}$$

The coordinate of a point, Q, on the screw axis in the global co-ordinate frame is then given by:

$$Q = P + C$$

There is now a direction for the screw axis, and a point on that axis. Dentally speaking, the axis is fully defined in 3-dimensional space, and can be plotted relative to the dentition.

### 3.3.5 Calculating the Rotation Matrix

So far, it has been assumed that the rotation matrix is known. It has been shown that, given this information, the screw axis can be derived. Thus, the problem of locating the axis of opening of the mandible can be solved. However, this relies on being able to calculate the rotation matrix, which will now be considered.

Assume that there is a 3D scanned model (for example the mandibular dentition), and that this model is displaced from a start position, by some unknown transformation, to an end position. These two positions will be clinically determined using the digital (optical) ‘bite registrations’.

Since the same model is used, and simply transformed, all the data points within the model will remain well defined and identifiable. For example, the model may contain 500,000 vertices (3D points). Internally, the order in which these points are stored will remain unchanged. Therefore, it can be said that the first vertex listed in the transformed model, will be the corresponding point to that of the first vertex listed in the original model. The corresponding positions of all 500,000 vertices can be tracked, as they move from the start position to the end position.

The task is to solve:

$$P' = [R|T]P$$

using all 500,000 corresponding values of P and P’, such that the elements of the transformation matrix [R|T] can be determined. This matrix was previously shown to contain 12 variable elements - the last row being fixed at [0 0 0 1]. A system of up to 500,000 linear equations can be set up to solve for these 12 variables. This is called an overdetermined system, because there are far more examples of

individual solutions (P → P') than there are unknowns. In this example, there should be no noise in the data, so the solution will be exact. Theoretically, one could just choose the first 12 points and create enough linear equations to solve the matrix [R|T]. However, computers cannot represent all fractional numbers accurately, so there is a possibility that the transformed coordinates, P', have accumulated minor errors in their locations. This would affect the solution to the system of equations, particularly if only 12 known co-ordinates are used to solve it. The reliability of the result can be improved by using all 500,000 vertices to calculate the solution.

There is a problem with this approach. Once more linear equations are used, than there are variables, the likelihood of there not being a numerically exact solution increases. The answer is to use a numerical technique which minimises the error. A common closed-form method (meaning a repeatable, absolute solution will be found), is singular value decomposition (SVD)[3]. This method is employed to find the elements of the transformation matrix using all the vertices available from the model.

### 3.3.6 Recovering the Axis of Rotation, and Degree of Rotation, From the Rotation Matrix

From the exploration of the nature of the 4x4 transformation matrix, it is known that the rotation matrix is embedded in it, in the top left corner, as a 3x3 matrix. Having determined the elements of the rotation matrix in the previous section, the axis of rotation and degree of rotation about that axis must now be identified.

Given the 3x3 rotation matrix, R, a vector, v, is sought such that:

$$Rv = v$$

In conceptual terms this is a (non-zero) vector which, when undergoing the rotation defined by matrix R, results in the same vector – ie the vector does not move. This means it must be in line with the axis of rotation.

Eigenvectors(s) of a square matrix, A, are defined as vectors which satisfy:

---

[3] Singular Value Decomposition is a linear algebraic technique by which a matrix is decomposed (factorised) into 3 matrices which can be multiplied together to reproduce the original. The elements of the decomposed matrices provide useful information for solving least squares minimisation problems.

$$Ax = \lambda x$$

where x is a non-zero vector, and λ is called the eigenvalue of x, and is simply a scaling factor. In the case of the rotation matrix, λ=1 (since the object, and axis, are not stretched or skewed by the rotation). We must therefore find the eigenvector of R, whose eigenvalue is 1. The original equation can be rearranged, with λ=1, to:

$$(R - I)v = 0$$

where I is the identity matrix. This yields a series of three linear equations which can be used to solve for v.

The degree of rotation about the axis, for a rotation matrix, R, is derived by using the trace of the matrix (the sum of its diagonal elements):

$$Tr(R) = 1 + 2\cos\theta$$

So:

$$\theta = \cos^{-1}\left(\frac{Tr(R) - 1}{2}\right)$$

Now all the necessary information exists, on axis orientation and degree of rotation, to calculate the screw axis.

The entire process for finding the screw axis from a pair of identical 3D models which have undergone some unknown 3-dimensional transformation is summarised in Figure 25.

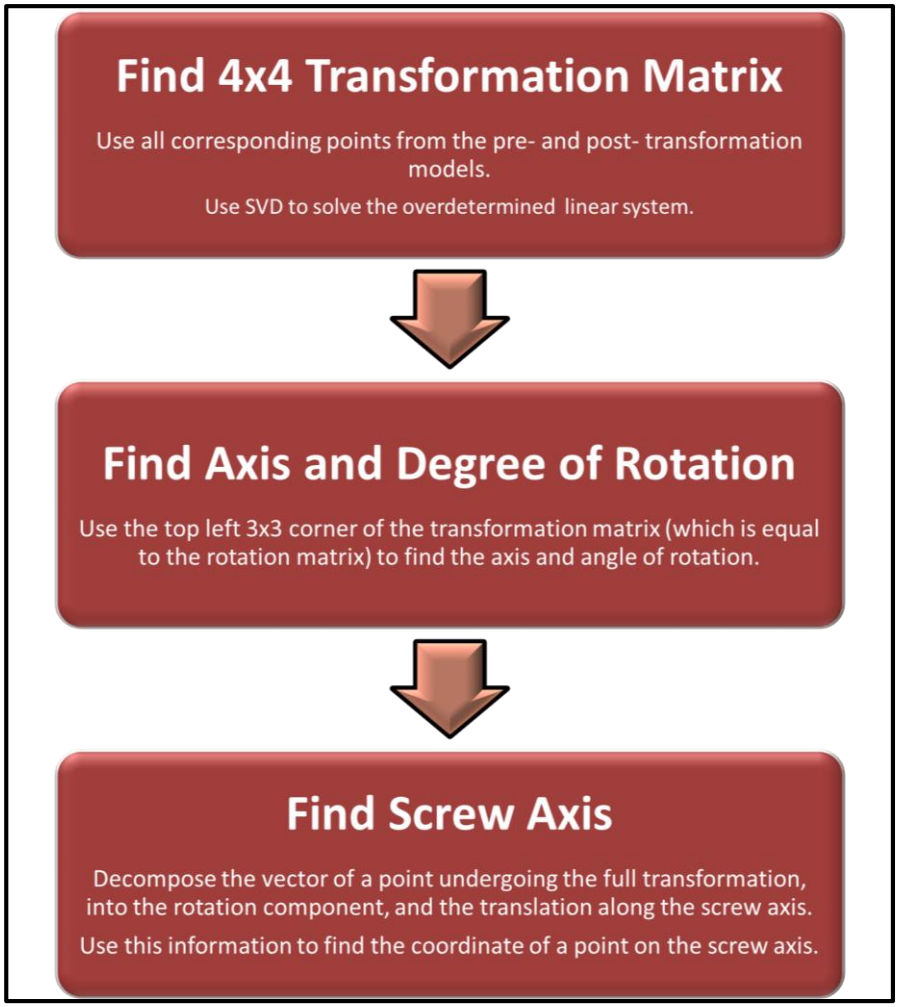


**Figure 25 Summary of the Digital Workflow Needed to Calculate the Screw Axis.** This calculation assumes we have a set of 3D points which have undergone some unknown transformation in 3-dimensional space.

## 3.4 Defining the Required Accuracy of Axis Location in Terms of Clinical Parameters

### 3.4.1 Introduction

Since this is a novel method it is prudent to perform a hypothetical analysis of the likely accuracy of the system. Whilst not fully robust, this will give clues as to which variables need tight control and which may be less critical. It will also prevent time-wasting on a method which is destined to fail.

The proposal has several advantages over the intra-oral method previously attempted (Long 1970) (see Section 1.1.3.4). Firstly, there are no interocclusal recording materials, so no further errors are introduced at this stage. Secondly, with optical scanning, the precision and accuracy should be improved compared to using pencil and paper. Thirdly, the system can consider thousands (or even hundreds of thousands) of sample points (rather than just two) in its derivation of the THA and can therefore arrive at a better consensus.

### 3.4.2 The Simulation Model

A summary of the simulation model used throughout this analysis is given in Figure 10 of Section 3.1). In this case just two points are considered, analysing their movement from jaw-nearly-closed to jaw-open (both in CR). The THA is calculated based on this movement, and only in two dimensions. By using a computer and applying numerical analysis, specific parameters can be varied to introduce measurement errors. In this way, an investigation into the predicted accuracy of the system, and the sensitivity of the system to different parameters, can be made.

A simulation package was written in MS Excel to implement the model. The simulation enabled different parameters to be altered.

### 3.4.3 Analysis of the Variables

The problem can be reduced to that of calculating the orientation of the THA and the spatial location of a point on this axis.

#### 3.4.3.1 Predicted Errors in Deriving the Orientation of the Axis

Since it is envisaged that the scanner will record the labial segment, the model assumes a scanning width of 30mm, which would typically capture almost all four upper incisors and both upper canines. This value is based on the typical 9+7+8mm incisor and canine width (Magne et al. 2016), but assumes the teeth are wrapped around an arch (not completely flat) causing some overlap of their widths. Furthermore, this width is deliberately left small to account for the potential lack of visibility of the canines in both stereo cameras, if they are curving out of sight around the arch. The scanner might actually need a width of view of 40mm, but only collect 3D data in a smaller area.

From this anterior view, the THA will be almost parallel to the labial segment, and errors in its orientation will be determined by the errors in scanning resolution at the extremes of the image. Assuming a scanning accuracy of 0.1mm, the worst case scenario would occur when there are antagonistic errors of this amount at both sides of the scan. So over a 30mm width, the angular error, $\varepsilon$, is given by:

$$\varepsilon = \tan\left(\frac{0.1}{15}\right) = 0.38°$$

where 15=30÷2, the centre point of the THA within the scanners field of view. If the width of scan is reduced by 50% to 15mm (equivalent to fitting less than both central incisors into the width of the scan) the orientation error rises to 0.76º, which is still minimal. Of course the actual width between TMJs is typically closer to 115mm (Mandilaris et al. 1992), or even wider in some populations (Lazic et al. 2006) so the *effect* of orientation errors will be magnified. Even so, the spatial error in location equates to only:

$$57.5 * \tan(0.38) = 0.38\text{mm}$$

at each TMJ. It is therefore concluded that the error in orientation is likely to be acceptable.

### 3.4.3.2 Predicted Errors in Deriving the Spatial Location of the Axis

Given the negligible error in orientation, the problem can be reduced to 2D analysis in X (antero-posterior) and Z (caudo-cranial) as follows. For now, assume only two key points are scanned – the incisal edge and a point 10mm cervical to that edge. By tracing these points over the two scans, one can bisect and construct perpendiculars for each point pair (refer to Figure 10).

The intersection of these perpendiculars will be the THA. Now introducing an error to one of the measurements, one can observe the effect each variable has. First, a measurement error of 0.1mm is applied in 40 positions, in a circle, around the true point. The incisal point is at X=77.2mm and Z=-48.6mm with respect to the THA (which is at 0,0). These figures are taken from a study of 57 dentate individuals (Morneburg & Pröschel 2002). It is assumed that there is an opening of 10º between the two scans. The result is shown in Figure 26.

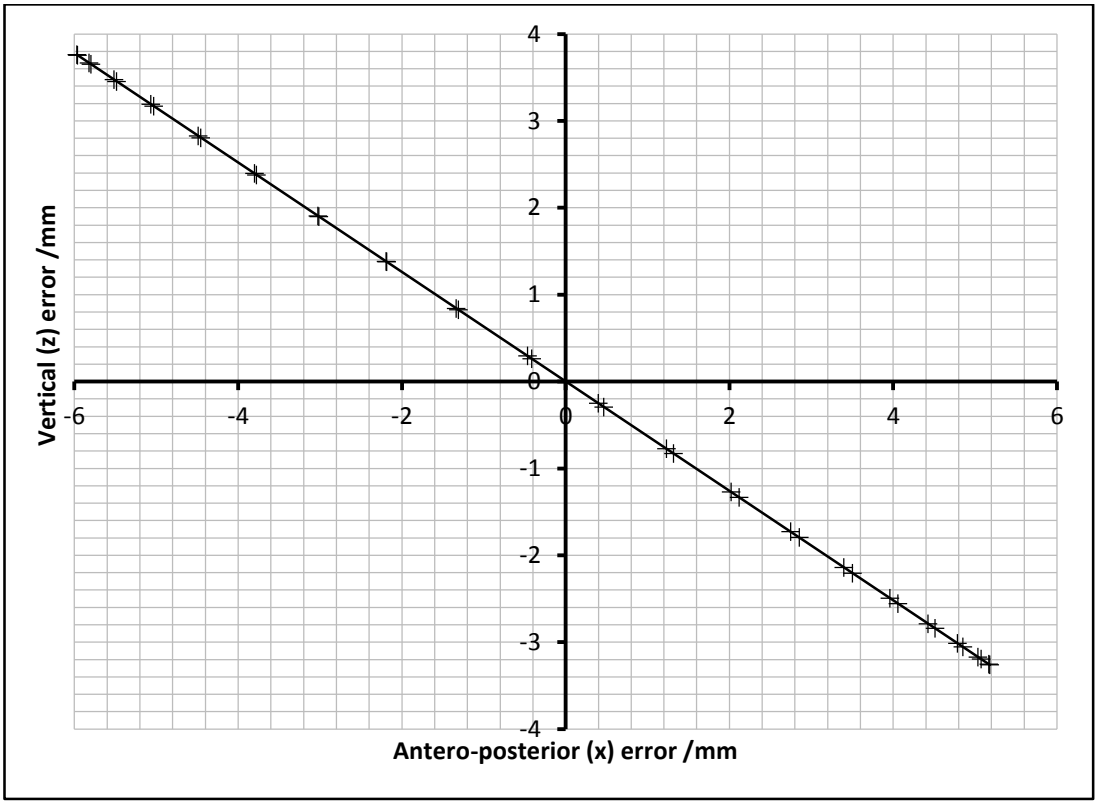


**Figure 26 Effect of a Sample of Measurement Errors of Radius 0.1mm on the Calculated Location of the THA.** 40 samples were taken in a circle around the true value. (True THA is at 0,0).

It is seen that the radial position of the 0.1mm error has a large effect on the location of the calculated THA, and that all errors follow a straight line which connects the midpoint of the measured opening to the hinge axis.

The magnitude of the error in THA location varies depending on the radial position of the measurement error. A polar plot (Figure 27) shows the distribution of these errors over 360º.

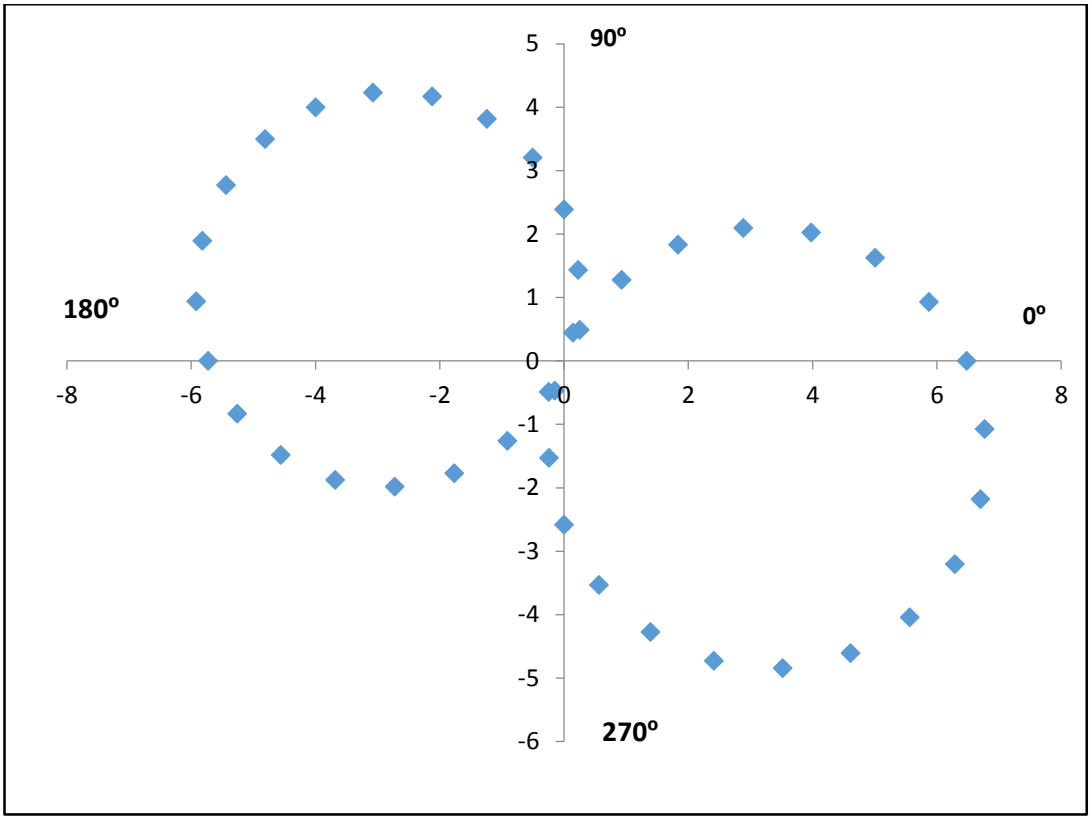


**Figure 27 Polar Chart Showing Magnitude of Error in THA Location with Varying Position of a 0.1mm Measurement Error at the Labial Surface.** For example, if the measurement error of 0.1mm is located at 0º (exactly along the positive X-axis), then the error in calculating the THA location will be 6.5mm. The *direction* of this error at the THA will be along the line shown in Figure 26.

Other workers have looked at this problem in reverse by looking at errors in earbow location of the THA, and their effect on occlusal accuracy (Adrien & Schouver 1997; Morneburg & Pröschel 2002). Their results suggest that the polar direction of some hinge axis location errors will have a much larger effect on occlusal errors than others (Figure 28).

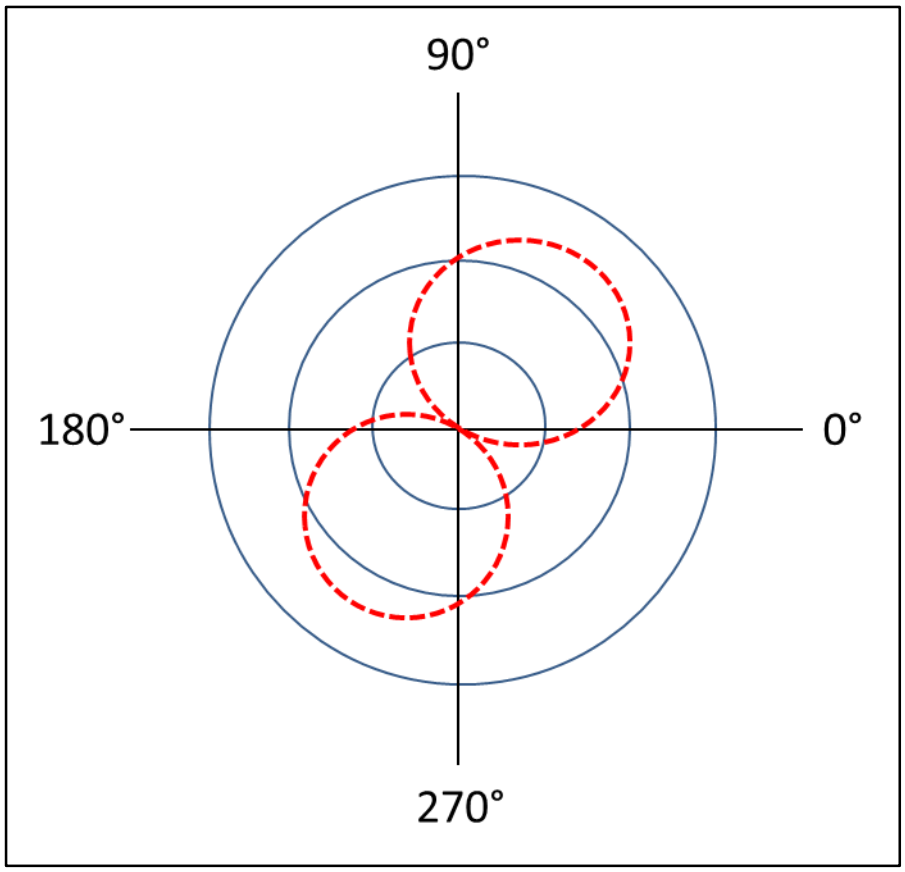


**Figure 28 The Direction of an Error in Hinge Location has a Profound Effect on the Magnitude of Occlusal Errors.** A polar plot is shown, with each blue circle representing an additional 100µm incisal error. The dotted red line shows the data for the predicted magnitude of incisal error, given a particular radial error in THA location. For example, if the THA is incorrectly located in the anterior-superior quadrant, at an angle of 45 degrees, the expected incisal error after 2mm of rotation around this incorrect axis will be 250µm. Here all THA errors are assumed to be 10mm in magnitude. Adapted from (Morneburg & Pröschel 2002) p.361

Unfortunately, the direction of this error is entirely random because earbow errors are scattered around the true THA (Walker 1980; Morneburg & Pröschel 2002). This means resorting to statistical analysis and providing the clinician with a probability of inducing an occlusal error (Morneburg & Pröschel 2011). Whilst this is a commendable analysis it doesn't help the unlucky percentage of patients whose axis location error happens to fall in just the wrong place, and it seems unsatisfactory that these errors can't be predicted on a case by case basis in advance.

Conversely, it can be seen by superimposing Figure 26 on Figure 28, that the proposed method, whilst potentially failing to locate the exact THA, will always locate it somewhere along a *favourable* direction vector (here calculated to be 328º) meaning clinically, the error will have very little effect at the level of the dentition. If it is also possible to keep the majority of errors to within a 5mm radius, comparable to

an arbitrary axis earbow, then a notable improvement in clinical precision might be observed.

Minimising the magnitude of this error radius will now be considered.

Firstly, a simulation was run, varying the vertical height of the labial scan volume from 1mm to 15mm. The degree of opening at the incisors is fixed at 15.9mm (10º) and the scanner resolution is fixed at 0.1mm. The results are shown in Figure 29. It can be seen that the maximum error in radius of hinge axis location increases significantly at low sample heights. At a sample height of 10mm the maximum error is 7.06mm (mean 4.20mm, standard deviation 2.05mm).

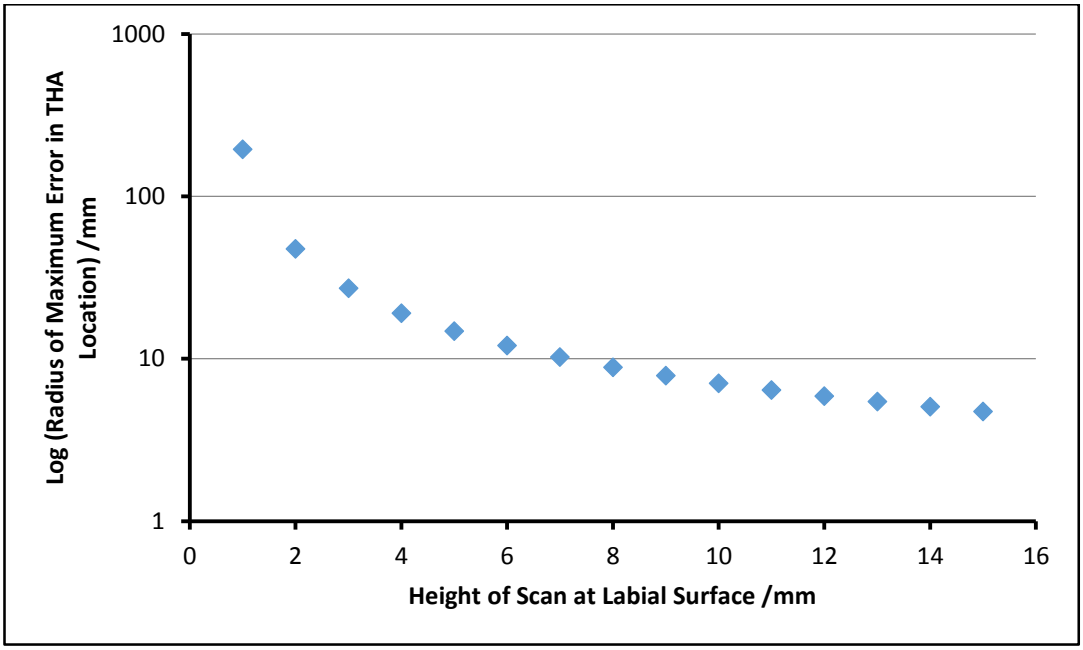


**Figure 29 Predicted Absolute Error in THA Location with Varying Height of Labial Scan.**

It is concluded that if only a small height is captured (for example half the height of a typical, unworn incisor), the error will be large. By advising users to ensure the scan covers at least 10mm in vertical height in each arch, a sufficient amount of information will always be captured. This finding is in agreement with a protocol suggested for digitising study models in maximum inter-cuspation (Solaberrieta et al. 2016), where bilateral molar bite scans were advised to be 15mm in height, to cover the full height of the upper and lower teeth.

Secondly, variations in the trueness of the scanner are investigated, whilst keeping the height of the labial sample fixed at 10mm, and the incisal degree of opening fixed at 15.9mm (Figure 30).

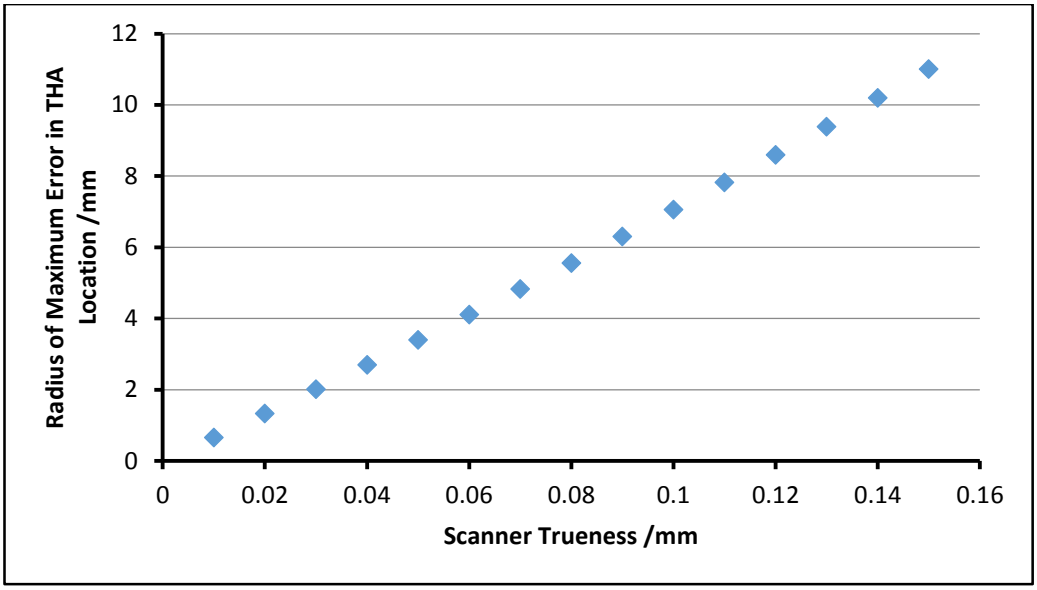


**Figure 30 Effect of Varying Scanner Trueness on Predicted THA Location Error.**

There is a linear relationship between scanner resolution and THA location error and at a resolution of 70µm, all points fall within an error radius of 5mm.

Thirdly, the effect of the degree of opening between the two scans is explored. The scan height is fixed at 10mm and the trueness at 0.1mm (Figure 31).

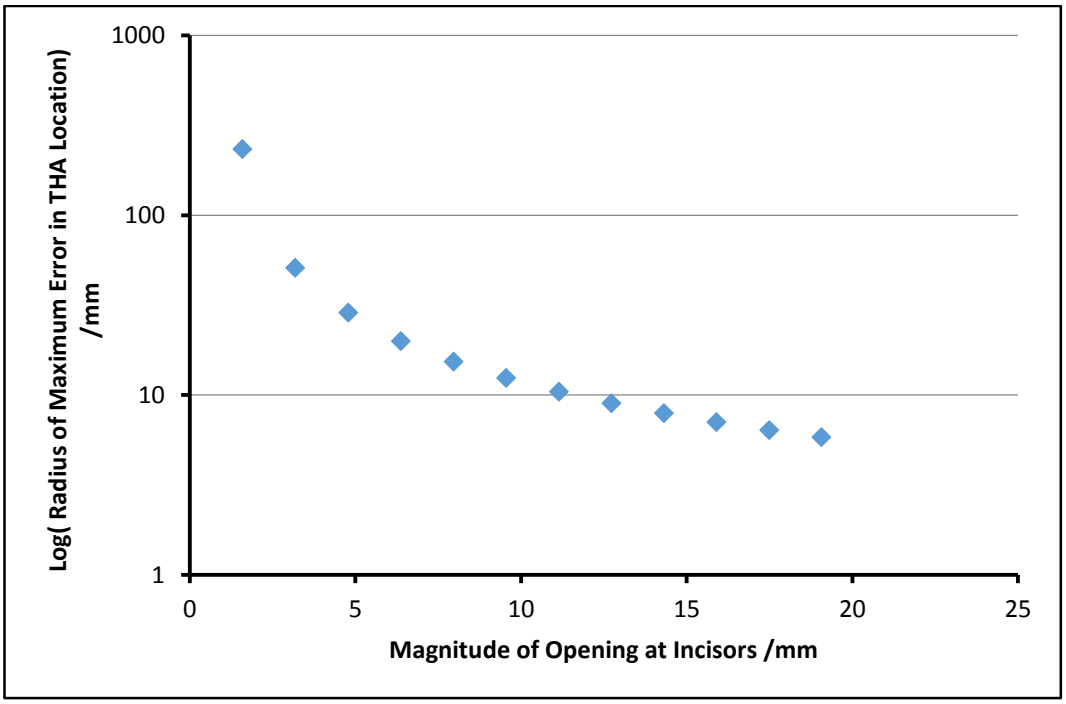


**Figure 31 Effect of Different Degrees of Opening on Predicted THA Location Error.**

It appears to be important to ensure a large degree of opening (>10mm) to improve results. Traditionally, interocclusal records are advised to be recorded at or near the desired OVD to minimise errors. It may therefore seem counterintuitive to advise that one of the scans be obtained with the patient opened by more than 10mm. However, since the other scan will be recorded with the patient almost closed (in CR with the posterior teeth *just* out of contact), and the method dictates that *both* jaw positions will be reproduced with the axis model, the correct occlusion at the patients OVD will be reproduced. The opening must be kept to below the level where translation, as well as rotation, may occur in the TMJ. This is commonly held to be about 20mm (Posselt 1956).

#### 3.4.3.3 Summary of Simulation Findings

This is not an exhaustive study and is only meant to provide an idea of the accuracies that can be expected, and which variables have the largest influence on errors. It should be noted that the worst case scenarios illustrated above would probably not generally occur. For example, the scans will gather hundreds of thousands of points of data (not just two) and provide an average orientation based on these.

The issue of aligning the bite registration scans to the models has been ignored. There will be an error incurred in this process, since there is no definitive mathematical solution to the alignment problem (Besl & McKay 1992). Strictly speaking, it is the accuracy of the *system*, and not the accuracy of the *scanner* which is under investigation. The total error incurred in scanning and aligning data is effectively what is implied by the term ‘scanner resolution’.

Finally the model only simulated an error in one of the two scans. If scanning and alignment errors for both scans are assumed to be similar, one might wish to halve the 0.1mm value used for scanner resolution.

The following conclusions can be drawn:

- The method seems theoretically viable and is worth pursuing
- The scanner resolution should be below 0.1mm, ideally nearer 0.05mm
- The scanner should capture a height of 35mm (equal to 10mm for upper and lower incisors + 15mm opening)
- The two scans should be taken with a difference of at least 10mm of opening at the incisors

# 4 Development of the Scanner

A method is sought, by which the 3-dimensional surface topology of the upper and lower labial segments can be optically recorded. From Section 3.4.3.3, this method must collect data in approximately a 40x40mm area, to capture a sufficiently large region. This is based on the mean widths of upper central incisors (~9mm) upper lateral incisors (~7mm) and upper canines (~8mm), bearing in mind there will be some overlap because the labial segment is not flat (Magne et al. 2016). It should demonstrate a trueness to 50µm (or better), if the THA is to be located with a clinical accuracy comparable to axiographic methods.

## 4.1 Overview of Optical 3D Methods

### 4.1.1 Passive Stereo

Passive stereo is probably the simplest technology and mimics the way humans observe the 3-dimensional world. Two cameras are separated by a known baseline distance and at known angulation to each other. A scene is observed and common points viewed in both cameras are identified and used to triangulate the data, thereby determining the 3D location of that point (Figure 32).

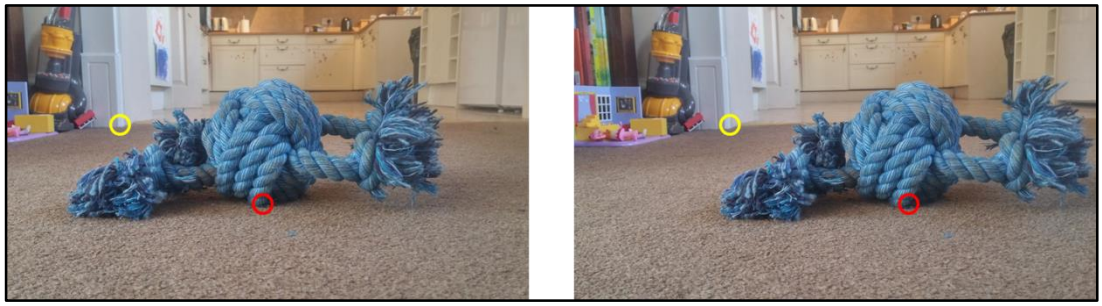

**Figure 32 Stereo Matching.** Given a stereo-pair of images, a search algorithm looks for matching pixels in both images. Here two such matches are shown (red and yellow). The 3D location of these points can easily be calculated from triangulation if the stereo cameras are ‘calibrated’. Areas in the scene containing less ‘interesting’ textures (such as the white cupboards) are difficult to match.

The apparatus can be simplified even further, to a single camera, which moves around in 3D space. Different consecutive images form stereo pairs due to the camera movement between frames. Hobbyist ‘structure from motion’ has become extremely popular in recent years, with mobile phone apps, such as 123D Catch (Autodesk Inc, San Rafael, USA) fuelling the appeal.

The simplicity of the hardware is attractive, but masks a more complex software problem – identifying stereo correspondences in the left and right images. This is the subject of much research (Mohan & Ram 2015; Lohot & Sonawane 2015), and the algorithms require ‘tuning’ to the particular task at hand. They perform better in the presence of rich features in the scene, such as patterns or texture. Generally the output is a sparse or moderately dense cloud of 3D data points, which can look good upon visual inspection, but which provides neither dense data, nor high accuracy.

### 4.1.2 Active Stereo

In an effort to improve the accuracy of the 3D data and the density of correspondences, a pattern (or patterns) can be projected onto the scene. These illuminate the scene in specific ways, helping to solve the correspondence problem, particularly if there are few features in the scene. Broadly, these illuminated patterns can be static (one-shot) or sequential (multi-frame).

#### 4.1.2.1 Multi-Shot

The highest accuracy can be achieved by projecting a sequence of patterns onto a static scene and matching corresponding pixels in the stereo images. In fact, sub-pixel accuracy is achievable, with reports of precisions of $1/5^{th}$ of a pixel (Scharstein et al. 2014). The generally accepted standard is sinusoidal phase shifting (Geng 2011; Lau et al. 2010; Liu et al. 2010a; Wang et al. 2010). Here, a sine wave pattern is projected onto the scene, and progressively marched (or shifted) across the image. Each pixel is illuminated by a varying amount over the sequence of images, a little like watching a lighthouse. The temporally varying illumination can be fitted to a sine wave to determine the phase of that particular pixel, in a process termed phase unwrapping. An example of a 3-step phase shifting pattern is shown in Figure 33. Corresponding pixels in the stereo-pair of images can be found by matching the phase of each observed pixel. In some systems, the projector actually

replaces the second camera, and triangulation occurs between the single viewed image and the projected image.

For higher accuracy, a larger number of phase shifts are used to compensate for any non-linear illumination effects (the 'gamma' in the display) (Hoang et al. 2010; Liu et al. 2010b; Li & Li 2011). In addition, a higher frequency may be used. For example, a wavelength of 16 pixels projected from an 800 pixel wide display, will produce 50 repeating phase patterns across the scene. It is this high frequency that enables such accurate sub-pixel matching, but this comes at a cost. There will now be up to 50 potential matching candidates in the stereo-pair of images. In order to choose the correct match, an additional set of low frequency sine waves can be marched across the scene (here, the wavelength would be 800 pixels, meaning each pixel is unambiguously identified). The lower frequency pattern is less accurate, but sufficient to allow absolute identification of the high frequency correspondences.

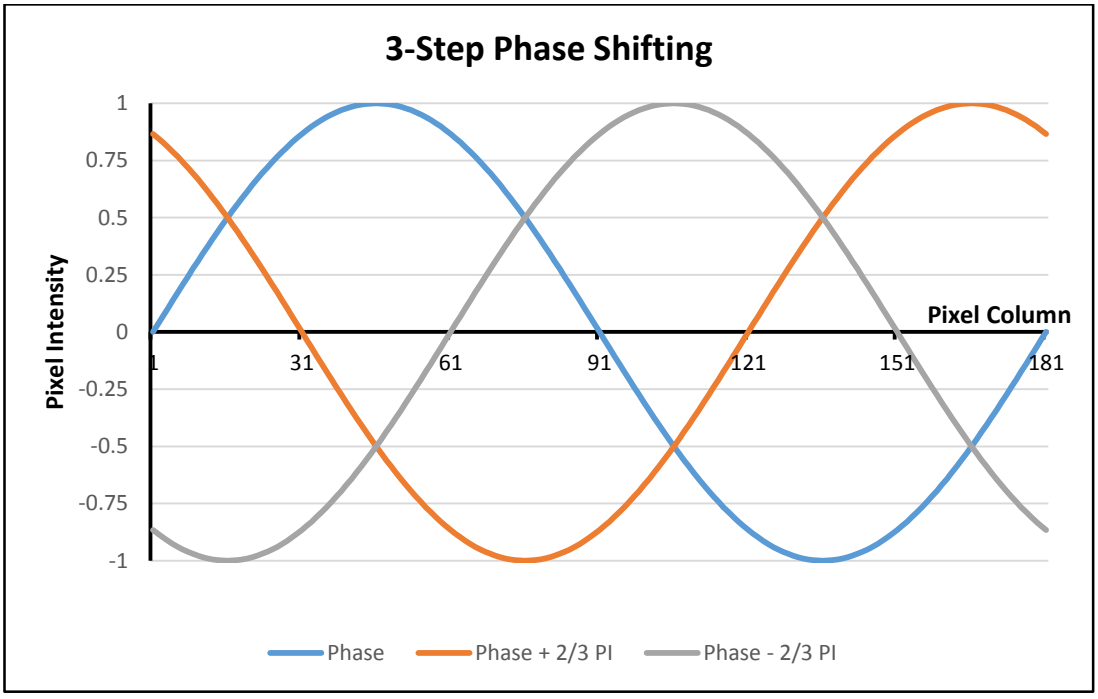


**Figure 33 3-Step Phase Shifting.** An image is projected, whose intensity varies in a sinusoidal manner with pixel column (blue line). Subsequent images are projected which are identical except for a uniform phase offset (orange and grey lines). When the camera views these patterns, the change in illumination of any pixel over the sequence can be used to determine which projected pixel column is being viewed.

#### 4.1.2.2 One-Shot

The main disadvantage of the multi-shot technique is the fact that the object being scanned must remain stationary during the scanning process. When scanning a moving target, a single static image can be projected onto the scene to provide texture to help the standard passive stereo matching algorithms (Konolige 2010). In general the cost of this rapid data capture is either in accuracy, data density, or both.

An alternative technique is to use multiple colours in the one-shot pattern, so that more information can be encoded in the scene. However, the drawback of this technique is that colours within the scene itself may preclude accurate measurement. For example, a red object will only reflect the red component of a projected pattern, leading to measurement errors.

Other techniques make use of stripe boundaries (Hall-Holt & Rusinkiewicz 2001). The sharp edges of the projected stripe patterns can be very accurately identified (with sub-pixel precision). However, the measured 3D data is generally less dense because of the need for dark spaces between each stripe. A further problem is identifying precisely which is the corresponding stripe in the second image.

### 4.1.3 Time of Flight

These sensors emit a pulsed light signal of very short duration (a few nano-seconds), and have specialised CMOS receptor arrays to receive the reflected light. The time delay between sending and receiving the packet of light can be used to calculate the distance that each ray of light has travelled. This technique is fast but the accuracy is poor for two reasons. Firstly, the receptor arrays tend to be available with only a small number of pixels (typically 320 x 240). Secondly, the depth resolution is generally limited to approximately 10mm because the speed of light (299,792,458ms$^{-1}$) is so fast that an interval of only ~1x10$^{e-10}$ seconds will elapse over a distance of nearly 30mm. In order to approach resolutions in the micrometre range, intervals of a few picoseconds (1x10$^{e-12}$) would need to be accurately measured. This is currently beyond all but the most expensive electronics.

### 4.1.4 Confocal Methods

A tightly focussed scanning laser, or a laser grid, is projected onto the target. The depth of focus is altered rapidly over a range, and multiple images are collected for the scene. For each pixel, the most sharply defined image *for that pixel* is noted, and the corresponding focal plane is retrieved to give the depth. The software for this technique is relatively simple, but the hardware is specialised to provide the high frame rate, laser projection and moveable focussing lens.

## 4.2 Choice of Method

The goal is to provide an affordable and accurate solution for recording the transverse horizontal axis. Standard digital camera technology continues to improve, whilst prices remain artificially low. For this reason, if the system is constructed using such cameras it will be easily upgradeable as the technology improves (for example better pixel resolution), and will potentially remain affordable. This eliminates time of flight and confocal methods, leaving the stereo method as the preferred technique.

Given that the novel method for finding the THA is entirely untested, it should primarily be ascertained whether, given sufficiently accurate and dense stereo correspondences, the hinge axis can be found using 3D labial scans. To this end, it is prudent to start with the most accurate available correspondence method – phase shifting. The explosion in availability of Digital Light Projectors can be harnessed to provide an inexpensive, flexible and accurate method for generating the projected patterns.

The disadvantage is that the multiple projected images will not allow for clinical testing, since the patient might move slightly during the exposure time. However, the principle can be tested *in vitro*, to confirm whether the active stereo apparatus has the potential to work clinically. The implementation of the phase shift scanning method in this thesis takes 0.5 seconds per scan.

As the machine vision field continues to develop, one might expect higher resolution cameras, better one-shot imaging strategies and faster multi-shot imaging techniques to be developed. Using these innovations, one could move the solution to a clinical setting, pending encouraging laboratory results.

## 4.3 Scanner Design

### 4.3.1 Hardware

Having decided upon an active stereo 3D system, the cameras (to collect the images) and the projection method (to display the sinusoidal patterns) must be specified.

High fidelity is required from the cameras in order to take accurate measurements. To this end, monochrome cameras offer an immediate advantage. Each pixel on the receptor grid has a direct one-to-one mapping with the eventual image. By contrast, colour cameras have receptor grids with an alternating pattern of red-green-blue-green pixels. They create the eventual image by interpolating the colour over a 4x4 pixel grid, and so they suffer some loss of accuracy. To combat this, 3CCD cameras are available that have individual red, green and blue receptor grids, and split the incoming light onto each. This maintains the one-to-one pixel mapping but they suffer the drawbacks of very high cost, and reduced light intensity on any one receptor (leading to a potential decrease in the signal-to-noise ratio).

For these reasons the use of monochrome cameras is indicated, which are both inexpensive and accurate, but this does limit the potential projection pattern to monochrome. This is a disadvantage when considering one-shot patterns, since by projecting colour it is possible to encode three separate images in the red, green and blue channels simultaneously. However, it has already been stated that the goal is to ascertain whether the proposed method is viable under optimal conditions, prior to attempting optimisations for clinical use. As such, a multi-shot monochrome phase shift pattern offers the best resolution.

Webcams generally have poor lens quality. This is important because it is not only the number of pixels in the camera, but the quality of the lens, that ultimately determine how accurate the system will be. By using industrial machine vision cameras, the option of using good quality lenses becomes available. There is also the ability to choose the focal distance.

Two IDS uEye LE monochrome cameras (IDS, Obersulm, Germany) were chosen, which offer USB 2.0 connectivity (making them as easy to use as a webcam) and 1280x1024 pixel resolution. The lenses chosen were Tamron M118FM16 lenses (Tamron, Saitama, Japan) which offer a low level of lens distortion (-0.7%).

For flexibility of projection, it is sensible to use a digital light projector. This can be run as a second monitor from any PC or laptop, and the patterns can be readily

altered. In recent years, pico-projectors have become popular, and their diminutive size and short focal distance make them good candidates. The Optoma PK201 (Optoma Europe Ltd, Watford, UK) offers a small in-focus screen, with a diagonal of 12.7cm. In practice the screen can be focused at a slightly shorter distance to make it even smaller. One caveat to all these projectors is that they use the same underlying DLP technology – the DLP2010 microchip (Texas Instruments, Dallas, Texas). This has the projection pixels arranged in a diamond formation, and has an unconventional native resolution of 854x480 pixels. The Optoma electronics up-scales this to 1280x720, but this involves signal processing which will warp the highly specific projection patterns. As such, the projector must be run at a reduced resolution of 640x480, allowing the PC to map pixels in a one-to-one relationship. This reduction crops the sides of the projected screen, meaning it projects onto an area of approximately 60x40mm. This is close to the desired projection area of 40x40mm, and negates the need for custom modifications.

The USB cameras can be controlled simultaneously by using 2 separate processors (available in all modern multicore computers). The projector images can be preloaded onto the graphics card in the computer, and all projection routines can be controlled via the graphics processor unit (GPU). This is an efficient configuration, and obviates the need for any external hardware synchronisation. The hardware design of the system is shown in Figure 34.

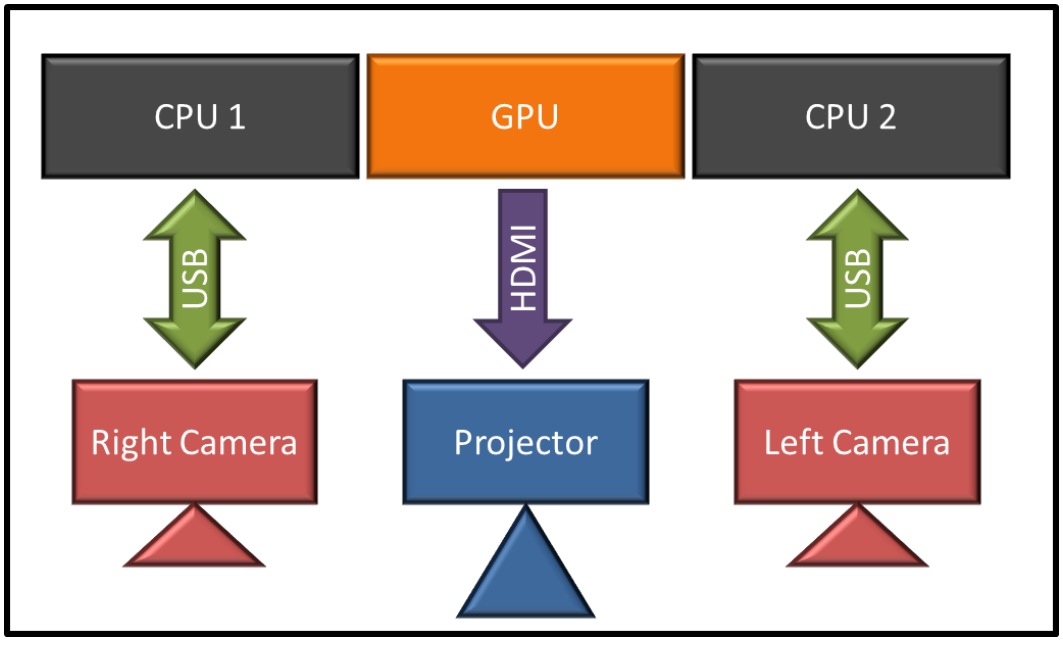


**Figure 34 Outline of the Hardware.** The grey and orange boxes are all components within the controller computer. The cameras are triggered synchronously via parallel processors. The projector frames are displayed via the graphics processor for increased efficiency.

### 4.3.2 Camera and Projector Positioning

In order to create stereo vision, the cameras must be separated, much like human eyes. The projector should ideally be situated exactly between the cameras, to ensure maximum viewing overlap in the scene.

An immediate question arises; ‘how far apart should the cameras be?’, or more formally, ‘what is the ideal angle of intersection of the light rays traveling to the left and right cameras, in order to optimise 3D recovery?’.

The answer will invariably be a compromise. Larger angles offer better depth resolution at the cost of decreased commonality between the left and right images (more areas which will only be viewed by one of the cameras). This has an adverse effect on the ability to find stereo correspondences, and reduces the density and accuracy, of the 3D data. Furthermore, as the angle increases, the ability to discriminate which pixel column in the left image is intersecting with the right image, decreases. Taken to its logical conclusion, if one camera was positioned at 90º to the other (ie looking side on), the depth resolution would be ideal, but there would be little or no information in the x (lateral) direction. This is similar conceptually to imagining looking at a vertically striped piece of card. Viewed from the front, the individual stripes are clear, but as the card is turned closer to side on, the individual stripes will merge, and become harder to discern.

These trade-offs will now be examined in more detail, in order to determine an optimal camera angle for the system.

Let us assume the left camera will form the global co-ordinate system. Straight ahead is the z-axis, whilst the x and y axes map directly to those of the 2D camera image. The right hand camera is now positioned such that its field of view overlaps that of the left camera at some angle, α (Figure 35).

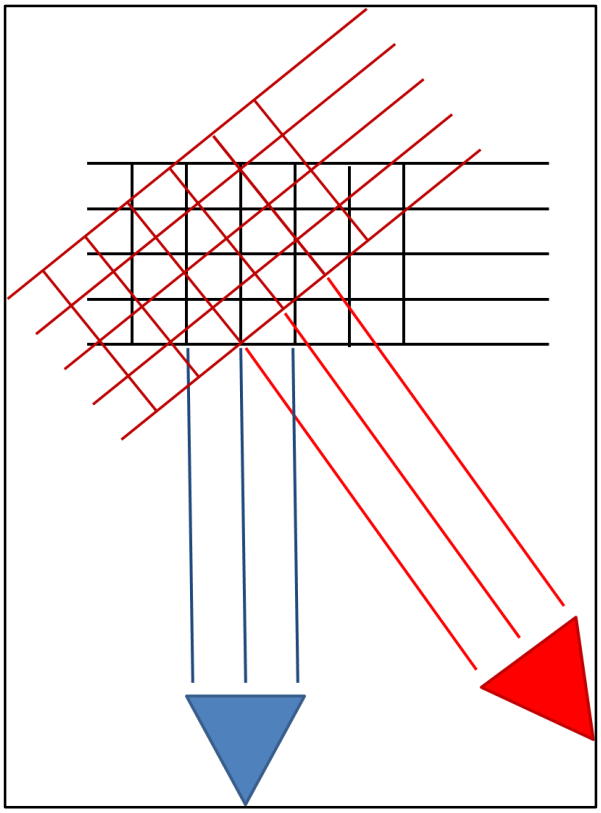

**Figure 35 A Stereo Camera Layout.** The left camera (blue) forms the basis of the global co-ordinate system. The right camera (red) will view the scene from a different perspective. Intersections between the red and black lines show the potential 3D coordinates that the system can 'read' (assuming whole-pixel resolution, rather than sub-pixel).

For simplicity, it is assumed that the system has whole-pixel resolution (ie it is unable to discern fractions of a pixel). It can be seen that the effective depth resolution, z, is inversely related to the sine of the angle between the cameras (Figure 36). This depth resolution is also directly related to the pitch of the camera pixels.

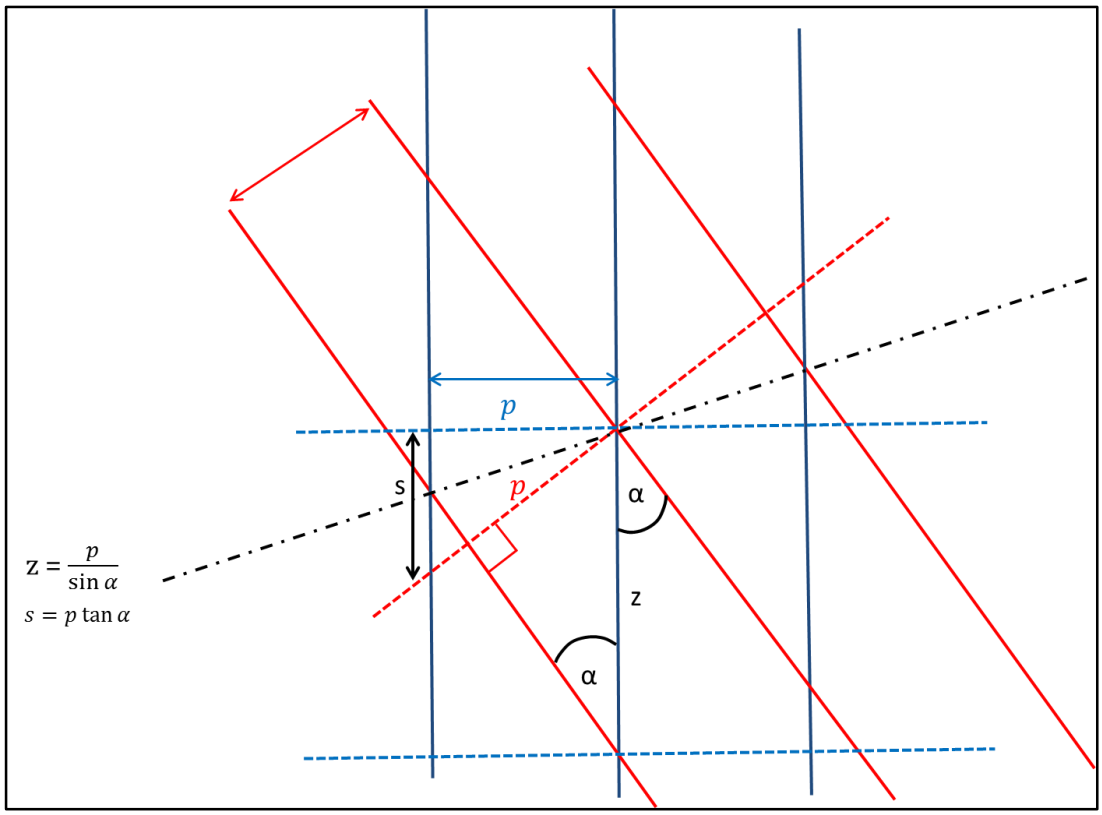


**Figure 36 Close Up View of Two Pixels from Each Camera.** The pitch of the pixels, p, represents the distance (in the scene) between camera pixel units. The depth, z, is the difference between two consecutive pixels in the right camera, intersecting with a single pixel in the left image. If a whole-pixel resolution for the system is assumed, this z value is the depth resolution of the system.

The phrase 'discriminatory ratio' is now proposed, to describe the compromise in stereo acuity[4] that is inherent with an increased camera angle. Using the XY resolution (the pixel pitch, p), the relative discriminatory ratio, $\partial$, is calculated as:

$$\partial = \frac{p}{d}$$

where:

$$d = z \tan \propto$$

[4] Here, the term acuity refers to the sharpness of the image in relation to the angle of view. As the viewing angle becomes more acute, individual features in the scene will become less discernable, and hence the acuity decreases

This ratio gives a value for the expected ability of the system to identify stereo correspondences (with a ratio of one meaning no loss in acuity, and a ratio of zero meaning no ability to discern stereo correspondences). This is illustrated in Figure 37 and Figure 38.

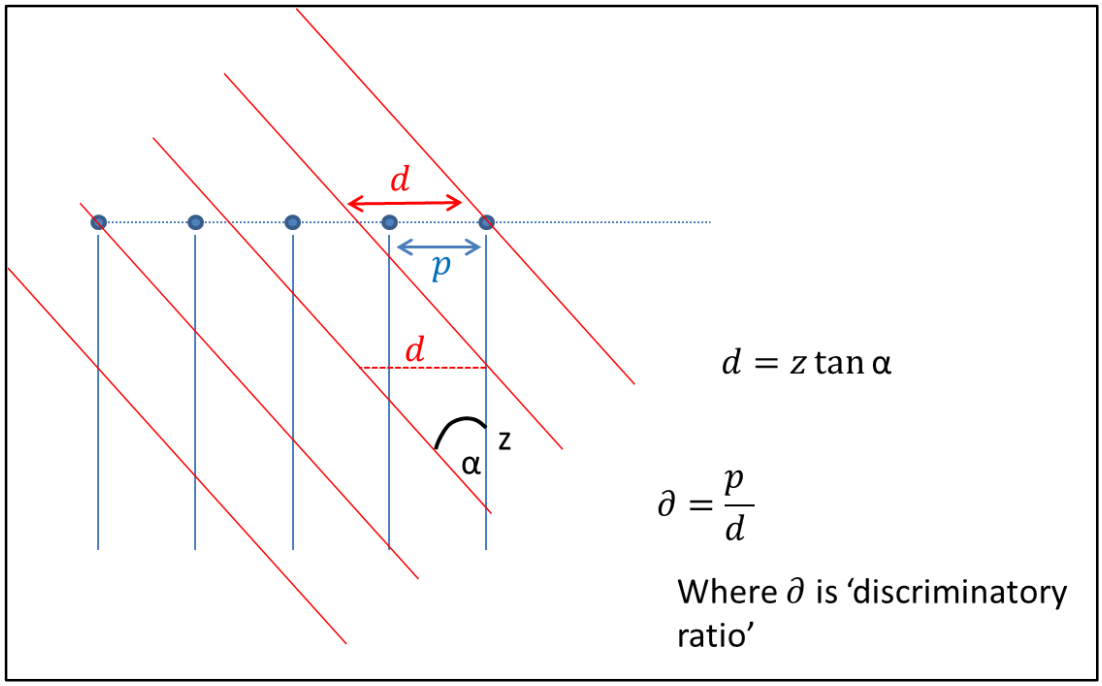


**Figure 37 Calculation of the Discriminatory Ratio.** This ratio is a measure of the likely ability of the system to identify stereo correspondences.

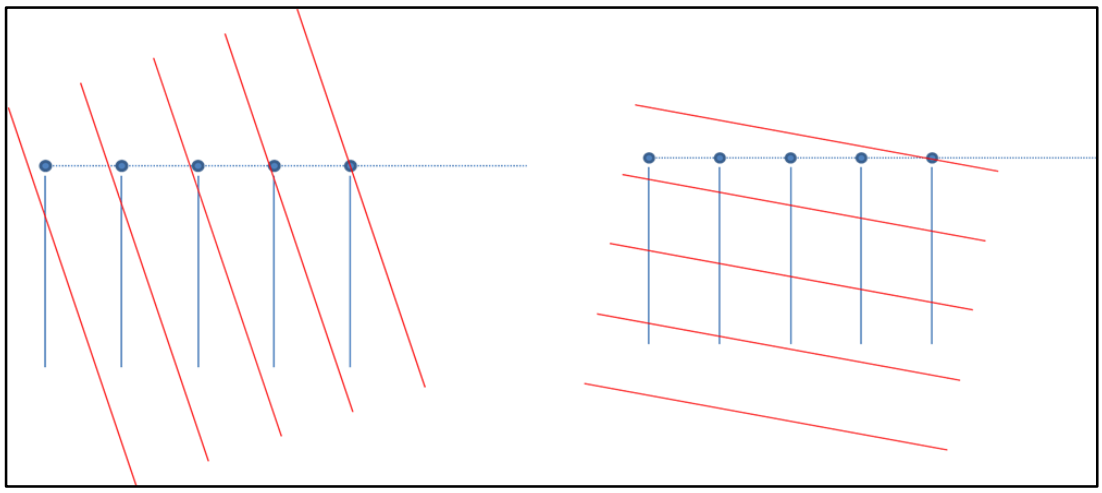

**Figure 38 The Effect of Different Camera Angles on the Fidelity of Stereo Correspondences.** The left image has a low camera angle. Each pixel in the right camera (red lines) maps almost one-to-one with the left camera (blue lines). On the right image, the camera angle is high and a pair of pixels from the right camera will straddle multiple pixels from the left camera. Ultimately, since the co-ordinate frame is equal to the left camera (blue), the stereo acuity of the scanner will be compromised with increasing angle.

A simple model was created in Microsoft Excel to simulate the effect of variation in camera angle on the relative depth resolution (Figure 39), and the discriminatory ratio (Figure 40).

An angle of 30º would seem to be a reasonable compromise.

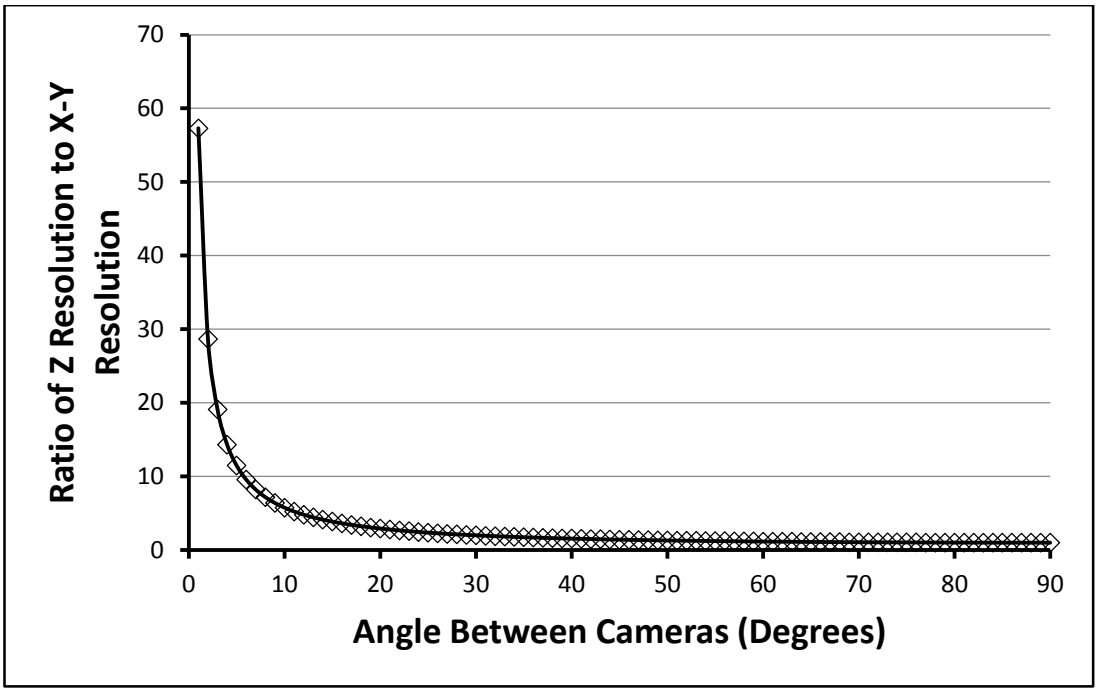


**Figure 39 The Effect of the Angle Between Two Cameras on the Depth (Z) Resolution of the 3D Scanner.** At an angle of 30º, the depth resolution is precisely half of the XY resolution.

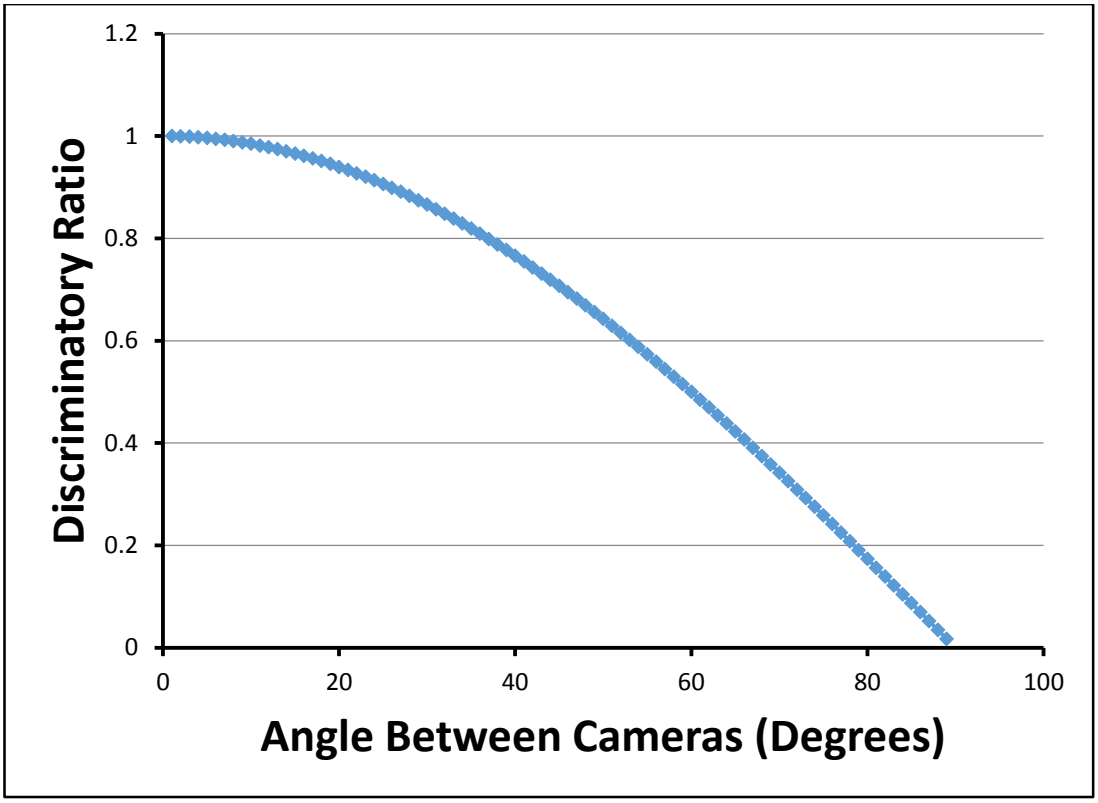


**Figure 40 Discriminatory Ratio vs Camera Angle.** The ability to discern stereo correspondences decreases with increasing angle. At 30º, the ratio is 0.87.

The cameras and projector are shown in Figure 41, mounted on a rigid bar.

**Figure 41 The Cameras and Projector Mounted on a Rigid Brass Bar.**

### 4.3.3 Software

Sourcing the hardware is a relatively simple task. The key hurdle lies in instructing this hardware to perform useful tasks – in this case, ultimately to be able to find the THA in a patient. To do this, software must be written.

The first decision is simply which language should the software be written in. There are many programming languages, all offering different advantages and disadvantages. Some are tailored towards specific problems, and many form layers on top of another language. For example, Python (http://www.python.org/) is a general purpose language, upon which the Theano extension can sit (Bergstra et al. 2010). This addition provides support for use of the multiple graphics processors available in modern computers to speed up Machine Learning and Artificial Intelligence algorithms.

Many higher level languages such as Python and Java are quite simple to learn. Their aim is to allow widespread access to the power to develop simple software, by keeping the instructions quite generic (and human readable). The alternative approach is to use a low level language, which is generally less intuitive to read. For example, suppose one wished to program a car to drive from A to B (as yet, an unsolved problem). Assuming for the moment that such a grand problem had been solved, a high level language might simply have a command 'Drive From A To B', where the programmer merely inserts data for 'A' and 'B'. No information about how fast to drive, which route to take etc will be given. By contrast, a low level language would require a full instruction set to be written (switch engine on, get in gear, depress clutch…etc). It can quickly be seen that the task facing a low level programmer is far more onerous.

For this work, there are some serious flaws with the high level approach. The languages offer less flexibility, which can be problematic when trying to write software to solve novel problems. The code tends to run at a much slower speed, which could be problematic when dealing with millions of 3D data points, alongside employing complex 3D processing algorithms. In fact there is often an exponential growth in the number of discrete calculations required as the number of data points increases, so the calculations could take days to complete if we use high level code.

Finally, much modern software is written using pre-existing helper libraries. For example, OpenCV (http://opencv.org) is an open source (freely available) library for solving common machine vision problems (generally for 2D images), whilst the PointCloudLibrary (http://pointclouds.org), is a similar community effort to develop

3D processing algorithms. Neither are languages *per se*, but both provide support for software written in a low level language.

In fact, almost all modern software libraries, and all modern high performance software, is written in a low level language called C++. This developed from one of the original languages, C, which has been around since the dawn of computing.

C++ offers the coder full control over all aspects of the computer and any associated hardware (such as cameras), full optimisation capabilities (speed) and full access to every additional software library ever written. The trade-off of the additional difficulty, in favour of all the benefits gained, is therefore accepted.

It is worth noting that this decision proved fruitful later on in this thesis. There is a general agreement that if one can program in C++, it is easy to turn ones hand to any other language. In Section 8.2, a mobile application (Android™) is developed to solve a camera calibration issue. Having become experienced with C++, it was relatively simple to apply the skills to Android and write the app.

Throughout the thesis, several major pieces of software were written. These are summarised in Figure 42, Figure 43 and Figure 44, as connected graphs illustrating the various pieces of software written and used. An overview of the functions performed by each software library is given in Table 1.

All source code is available in the CD accompanying this thesis. To give the reader a feel for the process, a screenshot of the development environment is shown in Figure 45. In this particular example (part of the software to perform 3D scanning), multiple helper libraries have been written (visible in the small window pane at the top right), and the main window shows an example of the C++ code.

It is good practice to compartmentalise code into libraries to facilitate reuse. For example, the code to drive the cameras will be the same, regardless of which projection pattern is being used. Different exposure times may be required, but the process of capturing and storing images in synchronisation will be the same. For this reason, a library to perform these functions was written which could accept, as input, some useful specifications such as camera exposure time.

In this way, the hardware and software for the project were developed and refined throughout the period of research. A good understanding was also gained as to what is possible with current technology, and which non-dental research areas to monitor for potential enhancements applicable to dental applications.

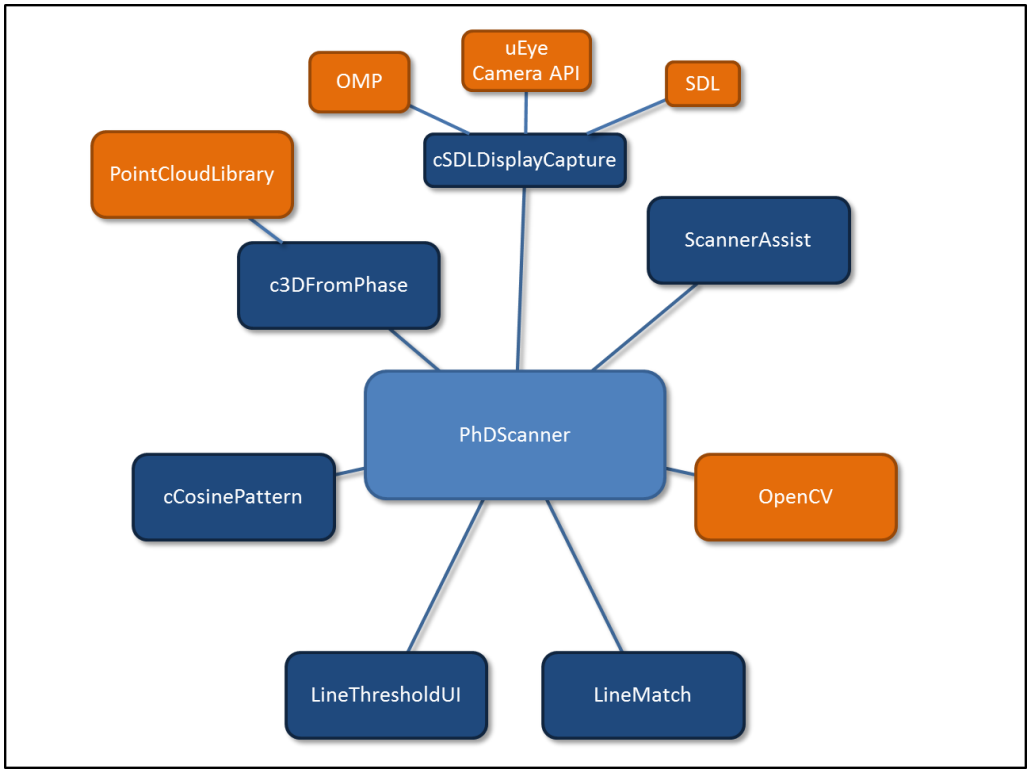


**Figure 42 The Main Scanning Software Architecture for Scanning and Creating 3D Models.** Each box represents a library, or class, of software. Blue boxes are original pieces of software, written for this thesis. Orange boxes are third party pieces of software. The main roles of each library are given in Table 1.

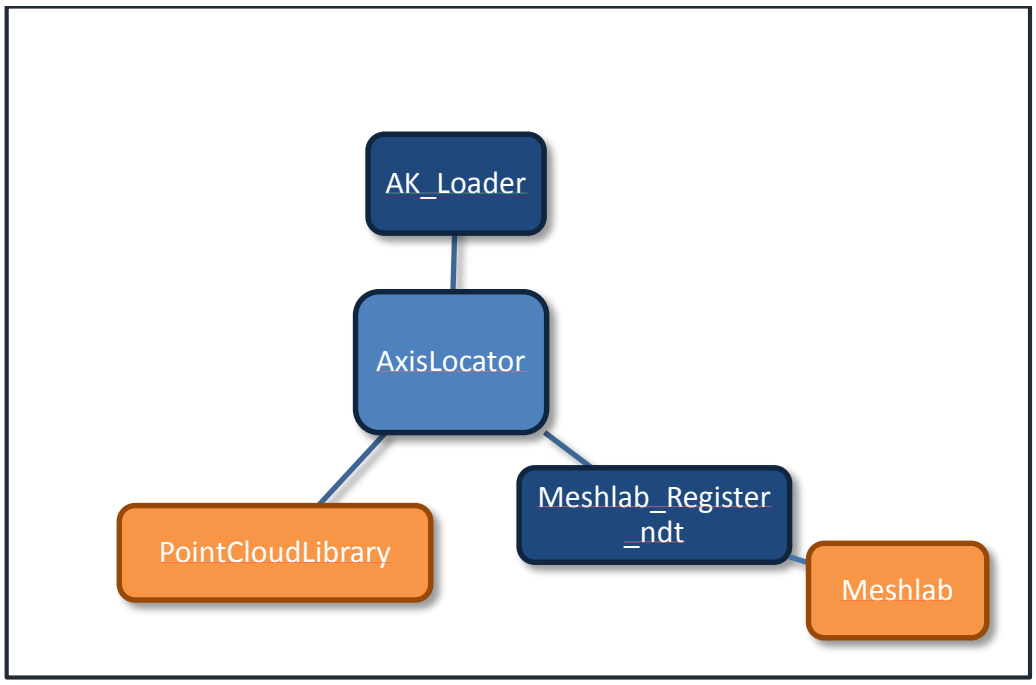


**Figure 43 Axis Calculation Software.** Each box represents a library, or class, of software. Blue boxes are original pieces of software, written for this thesis. Orange boxes are third party pieces of software. The main roles of each library are given in Table 1.

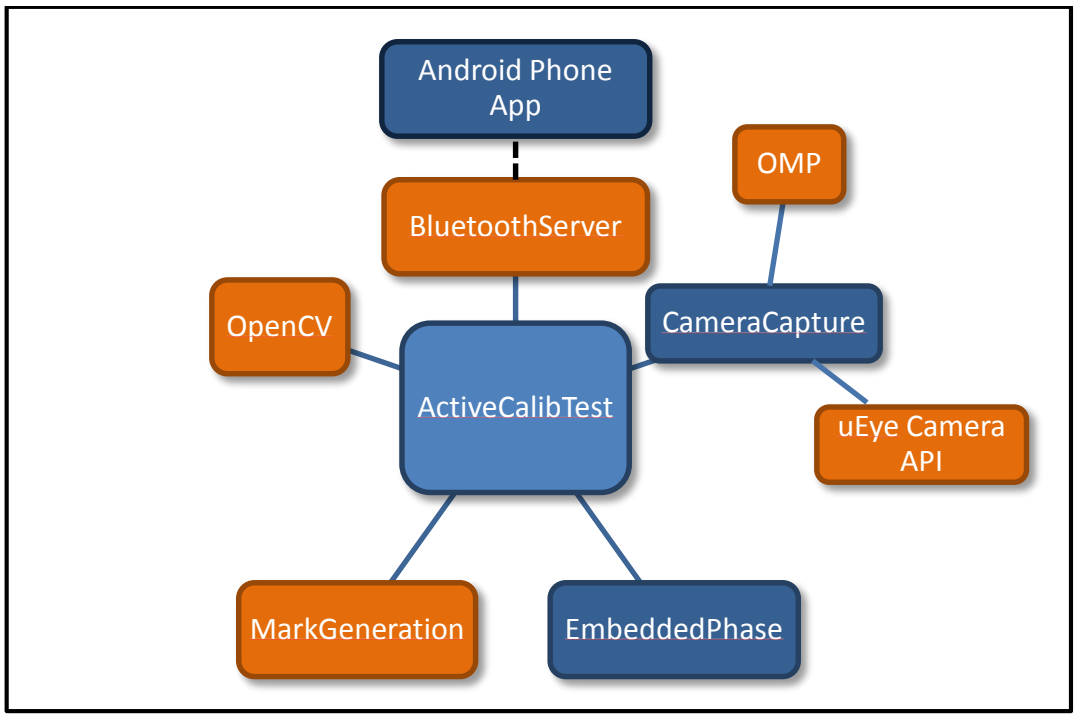


**Figure 44 The Novel Mobile Phone-Based Camera Calibration Software.** Each box represents a library, or class, of software. Blue boxes are original pieces of software, written for this thesis. Orange boxes are third party pieces of software. The main roles of each library are given in Table 1.

| | |
|---|---|
| PhDScanner | Orchestrates the overall scanning |
| c3DFromPhase | Calculates 3D data from phase maps |
| cCosinePattern | Creates the cosine scanning patterns and decodes them |
| LineThresholdUI | A user interface to set the correct threshold for identifying the jailbar line pattern |
| LineMatch | Stereo correspondence calculation for jailbar line pattern |
| ScannerAssist | Sundry routines such as saving/loading files etc |
| cSDLDisplayCapture | Pattern projection and collection of stereo images |
| PointCloudLibrary | 3D data manipulation library |
| OpenCV | 2D data manipulation library |
| SDL | Interface to graphics card for efficient projection of images |
| uEye Camera API | Interface to camera hardware |
| OMP | Allows parallel processing to ensure simultaneous capture of stereo images |
| AxisLocator | Calculates hinge axis from transformation matrix |
| AK_Loader | Helper functions for AxisLocator such as matrix loading |
| Meshlab | Freeware for initial scan alignment |
| Meshlab_Register_ndt | Takes the initial alignment from Meshlab and refines using the normals distribution transform |
| CameraCapture | Synchronised camera capture without projector patterns |
| EmbeddedPhase | Creates embedded phase patterns (Moreno et al. 2015) to display on mobile phone. Decodes the observed patterns. |
| ActiveCalibTest | Orchestrates camera calibration |
| Android Phone App | Displays a sequence of embedded phase shift patterns. Advances each frame via Bluetooth signal from ActiveCalibTest |
| MarkGeneration | Creates calibration marks from the observed, decoded patterns |
| BluetoothServer | Enables Bluetooth connection from PC to Android |

**Table 1 Summary of the main functions performed by each library. Blue boxes denote original software, orange denotes pre-existing software.**

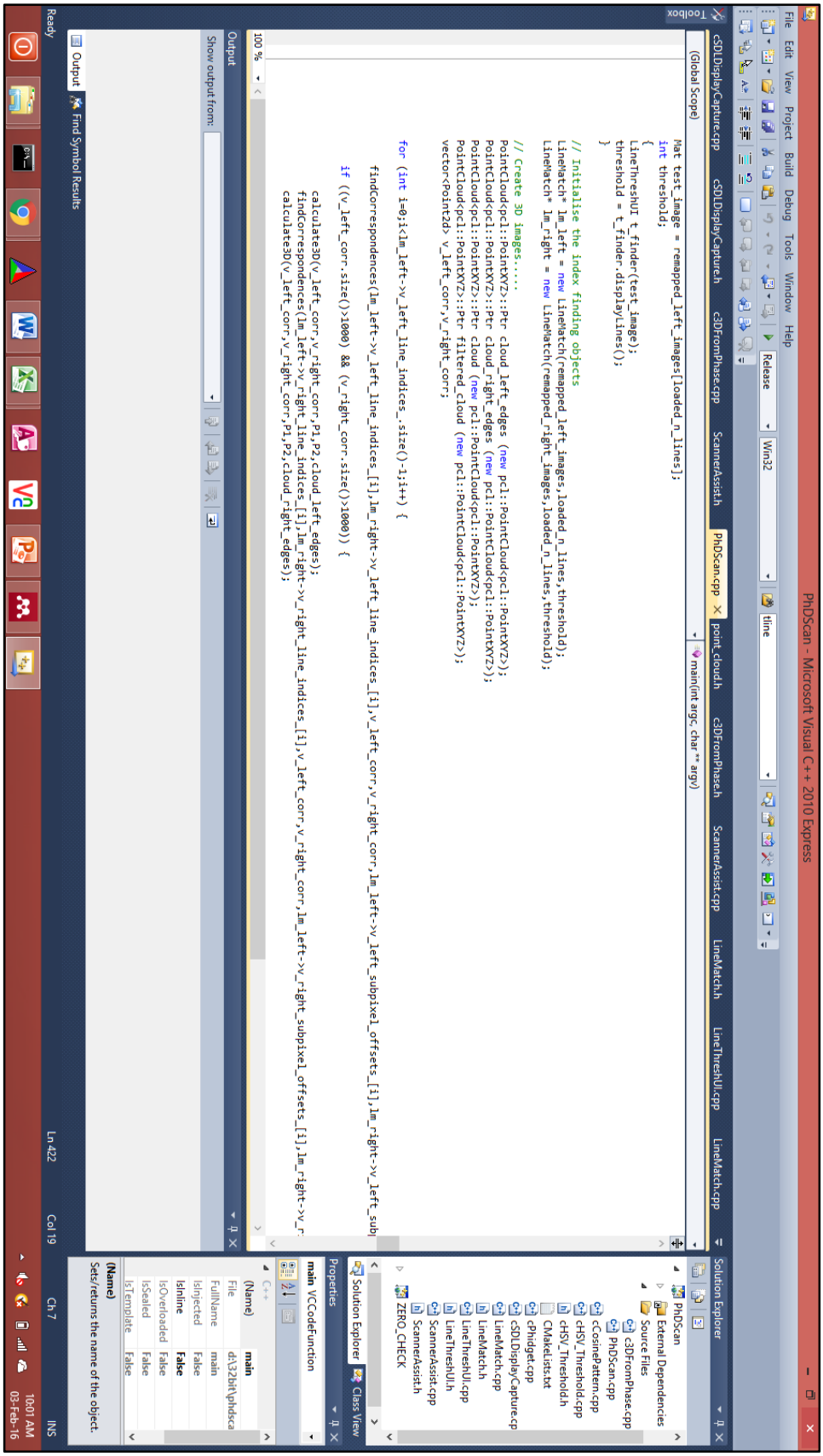


**Figure 45 Example of the Software Development.** The software for scanning in 3D is shown. In the small right hand panel, multiple supporting libraries (all written by the author) are visible. The main window shows an example of some C++ code which orchestrates the stereo correspondence matching.

# 5 An *In Vitro* Study into the Accuracy of a Novel Method for Recording the Mandibular Transverse Horizontal Axis

## 5.1 Introduction

The proposed method is tested for accuracy in locating the hinge axis *in vitro.* Dental study models, mounted on an articulator to simulate the patient, are used.

When assessing positional accuracy, the terms ‘trueness’ and ‘precision’ are common. Trueness quantifies how closely a measure lies to the actual value. Precision describes how closely a series of repeated measures align to each other.

In the following experiment, the precision is given as the standard deviation of multiple repeated measures. A lower value will imply multiple measurements produce similar results. A higher value would imply a larger spread of data from multiple repeat measurements, and thus a poorer precision.

The trueness is given as the distance of the calculated axis, as compared to the true hinge axis location. The results are then considered in the context of existing methods to decide whether there is clinical potential, and if so, what further work is required prior to this.

## 5.2 Aim

- To quantify the trueness and precision of hinge axis location *in vitro* using the novel optical technique.

## 5.3 Objectives

- To quantify the trueness of hinge axis location, measured in the sagittal plane at positions 57.5 mm lateral to the midline.
- To quantify the precision of hinge axis location, measured in the sagittal plane at positions 57.5 mm lateral to the midline. Precision is considered as the standard deviation from the mean of all measurements.
- To quantify the precision in angle between multiple calculated axes.
- To quantify the precision in calculated degree of rotation, about the calculated axes.
- To assess the effect of different viewing angles on axis location.

## 5.4 Method

### 5.4.1 Scanning Equipment

A structured light 3D scanner was constructed using a DLP projector (Optoma PK201, Optoma Europe Ltd, Watford, UK) and two monochrome CMOS cameras (UEye UI-1240LE-M, IDS Imaging, Obersulm). Phase modulation patterns were encoded in the projector and gamma compensation was applied to the projector-camera pairs. The cameras were mounted on a rigid metal bar at an angle of 30º to each other, and a baseline separation of 90mm, such that their principle points were focussed on the same point in space. To calibrate the system, a calibration target of circles was printed using an Epson Stylus Photo 1400 (Epson UK Ltd, Hemel Hemstead), and mounted on an aluminium block which had been machined flat using a toolmakers block and a milling machine (Clarke CL500M, Clarke International, Epping). The relative alignment of the cameras was calculated using this target and bespoke software which utilised the OpenCV library (http://opencv.org). The projector was mounted equidistant between the two cameras. The field of view allowed a scanning area of 60 x 50 mm at a working distance of 150 mm. This meant one scan could typically capture six upper, and six lower teeth of the anterior labial segment. The projector served only to provide 'phase texture' to the scanned object, in order to reliably identify corresponding pixels in both camera images for 3D calculations. Software was developed to record and process 3D data using the PointCloudLibrary (http://pointclouds.org). The scanner was tested by scanning the aluminium calibration block, and measuring the deviation from true of a horizontal cross section.

### 5.4.2 Experimental Protocol

Dental stone casts were arbitrarily mounted on an average value Freeplane articulator (DeTrey Freeplane 75, Dentsply DeTrey, Konstanz, DE). Digital models of the stone casts were created as follows. 14 scans of the arches were captured using the new scanner, starting from the left hinge of the articulator, and working around the model to the right hinge. The stone models were then removed from the articulator and scanned in a dental model scanner (Lava Scan ST Scanner, 3M EPSE, St Paul, MN) which has a trueness of 10µm according to testing standard

VDI 2634/2. The scanned models were exported as STL files into MeshLab software (http://meshlab.sourceforge.net/) along with the 14 scans previously taken of the articulated models. These scans were then aligned by 'digitally veneering' the labial scans on to the models. This produced a dense point cloud, based on the highly true and precise ST scans, but with more points on the buccal and labial surfaces.

Three points on the upper model were noted, upper right second molar palatal cusp tip, upper left second molar palatal cusp tip, and upper right central incisor mesio-incisal corner (Figure 46). Three points were similarly identified in the lower arch. These were the points from which all future measurements were taken. In fact, in the following experiments, the new scans can be thought of as vehicles which are used to align the pre-existing models created in the ST scanner, in much the same way as traditional interocclusal records and stone models.

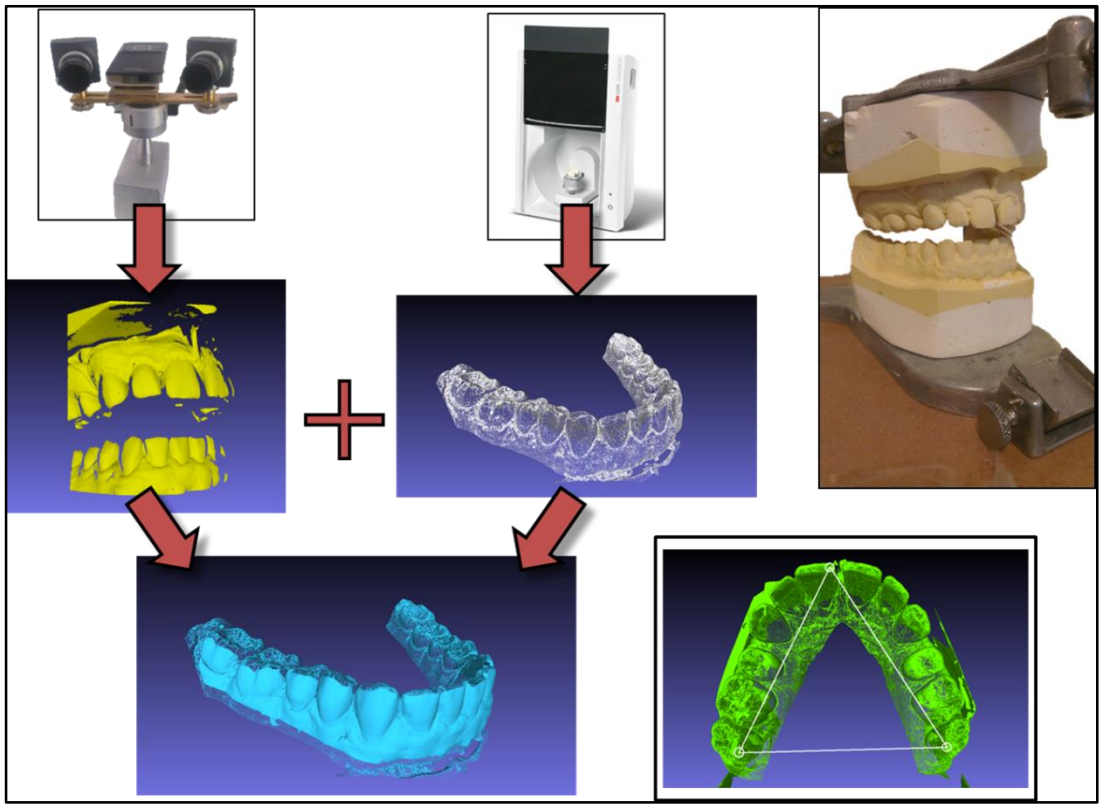

**Figure 46 Building the Models.** 14 buccal & labial scans were taken with the new scanner, starting from one hinge of the articulator and working around to the other (left). The upper and lower models were then scanned using the Lava ST scanner (middle). All scans were merged to produce master models which had been 'digitall veneered' buccally and labially with the dense point cloud scans (lower left). Three points were defined from the ST scan models in a tripod from which to take measurements (lower right).

The 14 buccal scans also captured the hinge of the articulator relative to the upper model, giving an absolute value for the true location of the hinge axis. Any axes calculated using the new method could be compared visually to this axis (Figure 47) and analysed numerically (described later).

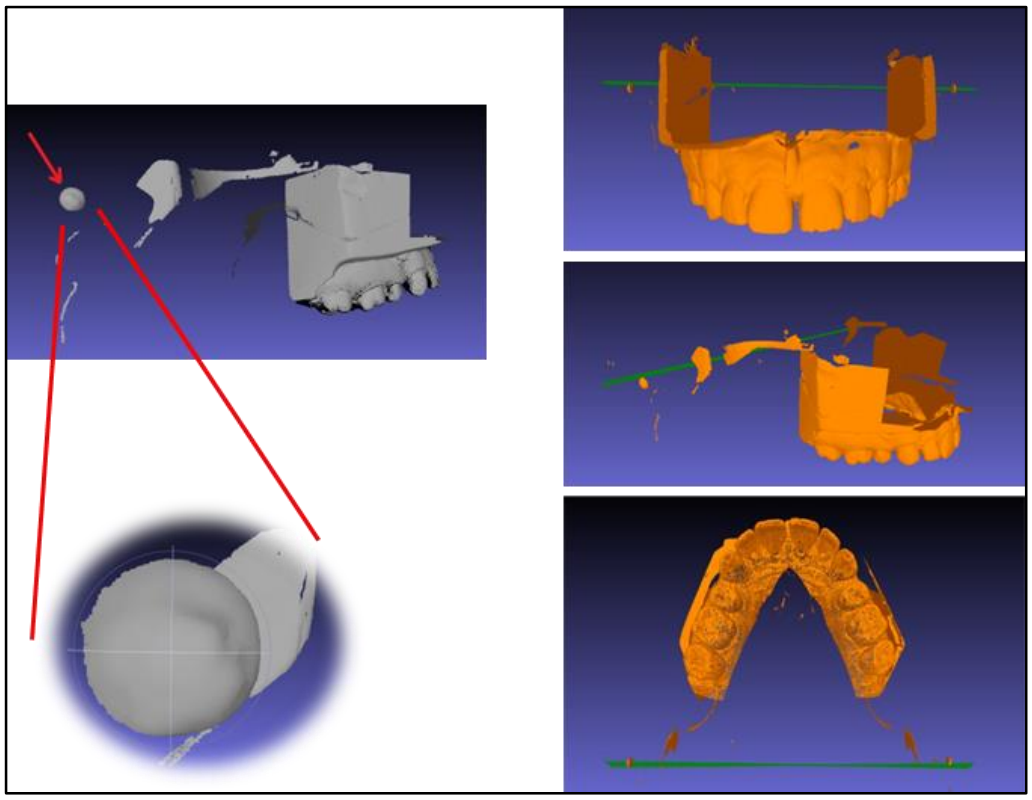

**Figure 47 Identifying the True Hinge Axis.** Shown on the left, the ends of the articulator hinge were identified in the scan and the central axis point was found (right hinge shown in picture). Any axes calculated later on in the experiment could be visually compared to the true axis, and could also be numerically compared (see method for full description). Shown on the right is an example of 100 calculated axes (green) overlaying the true model.

The method for calculating the axis of rotation was tested as follows. With the teeth together in maximum intercuspation, 10 scans were taken with the aim of capturing from the mesial cusps of right first permanent molars, to just beyond the midline anteriorly. Between each scan, the scanner was picked up and replaced to ensure slightly differing viewpoints, simulating the clinical situation. This procedure was repeated with 10 more scans aiming to capture the labial region from right canine to left canine. A final set of 10 scans were taken capturing the mesial cusps of the left first permanent molars, to just beyond the midline anteriorly. The teeth were then separated by inserting a 7mm diameter wooden rod placed between the models posteriorly, behind the last standing molars. This provided approximately 10mm of

vertical separation at the incisors. Without moving the models, the scanning process was repeated as before, to provide 10 more scans of the teeth apart, from each of the three viewing positions. In total, 60 scans were taken, 30 ‘teeth apart’ and 30 ‘teeth together’ (Figure 48).

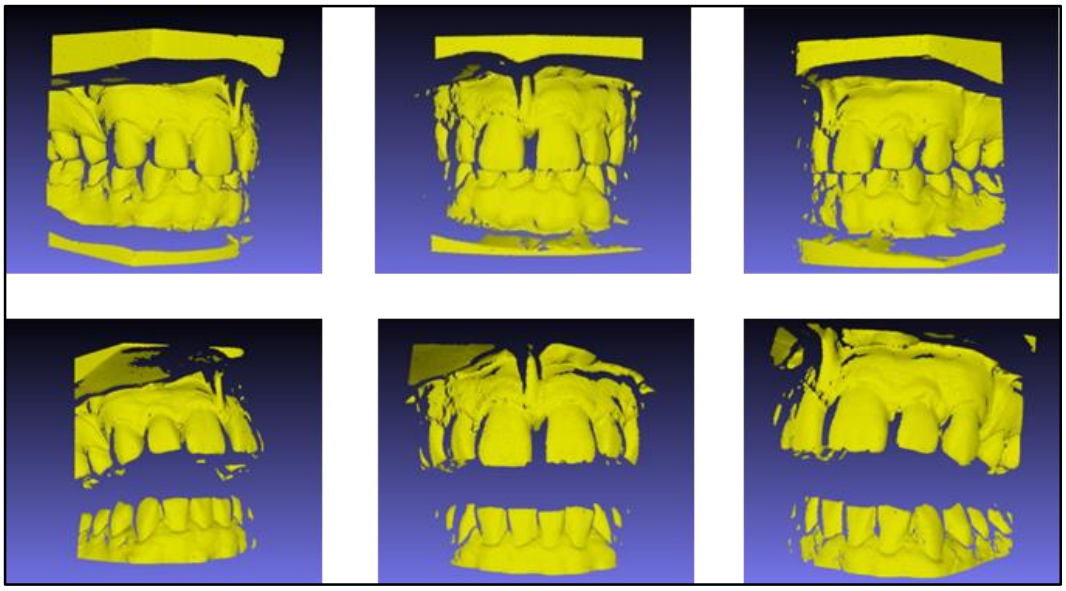

**Figure 48 Examples of the Different Scans.** 10 scans were taken for each viewpoint. In total, 60 scans were performed. Top row : ‘Teeth together’ scans. Bottom row: ‘Teeth apart’ scans. Right-to-left : Right view, Labial view, Left view.

Each of the 60 scans were used as templates to position the ‘digitally veneered’ models relative to each other. The alignment algorithm used was the Normal-Distributions Transform (Magnusson 2009). From each pair of scans (teeth apart and teeth together), an axis of rotation was calculated using a custom software implementation of the method described in Section 3. In total, 900 axes were calculated by using every combination of the ‘teeth together’ and ‘teeth apart’ scans.

Finally, a standard horizontal reference plane was created using three points: the position of the hinge axis at the left and right TMJ (see below) and an arbitrary point located 43mm superior to the upper right incisal edge. The real articulator axis was visible on the scans and the centre point of the 4mm diameter hinge cylinder was selected at the left and right extremes (131mm apart) to define the position of the true hinge (Figure 47).

The locations of these axes were then plotted in sagittal planes located at 57.5mm left and right of the midline to represent the position of the temporo-mandibular

joints (Mandilaris et al. 1992). The trueness and precision of axis location was assessed using the mean and standard deviation. Variation in axis orientation, and variation in degree of rotation about the axis, were similarly assessed.

## 5.5 Results

The scan of the flat board deviated from true with a standard deviation of 14µm. The scanner sampled points every 50µm.

A total of 900 axes were calculated by combining the scans in all possible combinations.

The error radii of axis location for all the pairing combinations are shown in Table 2.

| Group | Left TMJ | | Right TMJ | | Combined | |
|---|---|---|---|---|---|---|
| | Mean | SD | Mean | SD | Mean | SD |
| Labial to Labial | 2.40 | 0.47 | 2.70 | 0.49 | 2.55 | 0.50 |
| Labial to Right | 1.49 | 0.50 | 1.72 | 0.30 | 1.61 | 0.42 |
| Labial to Left | 2.30 | 1.05 | 3.36 | 0.42 | 2.83 | 0.95 |
| Right to Right | 3.12 | 0.33 | 2.40 | 0.93 | 2.76 | 0.79 |
| Right to Labial | 4.00 | 0.28 | 2.58 | 0.65 | 3.29 | 0.87 |
| Right to Left | 3.82 | 1.05 | 2.87 | 0.68 | 3.34 | 1.00 |
| Left to Left | 1.80 | 1.04 | 3.73 | 0.41 | 2.77 | 1.25 |
| Left to Labial | 1.41 | 0.71 | 3.28 | 0.57 | 2.35 | 1.14 |
| Left to Right | 2.22 | 0.83 | 2.46 | 0.47 | 2.34 | 0.68 |
| All Combined | 2.51 | 1.17 | 2.79 | 0.81 | 2.65 | 1.01 |

**Table 2 Mean Error Radius of Axis Location in the Sagittal Plane.** Groups are described in terms of the sets of views used in calculating the axes. For example, ‘Labial to Right’ means that the 10 Labial views of the teeth together, and the 10 Right side views of the teeth apart, were used to calculate 100 axes. (All measurements in mm).

The patterns of axis location error for each combination of views are shown in Figure 49.

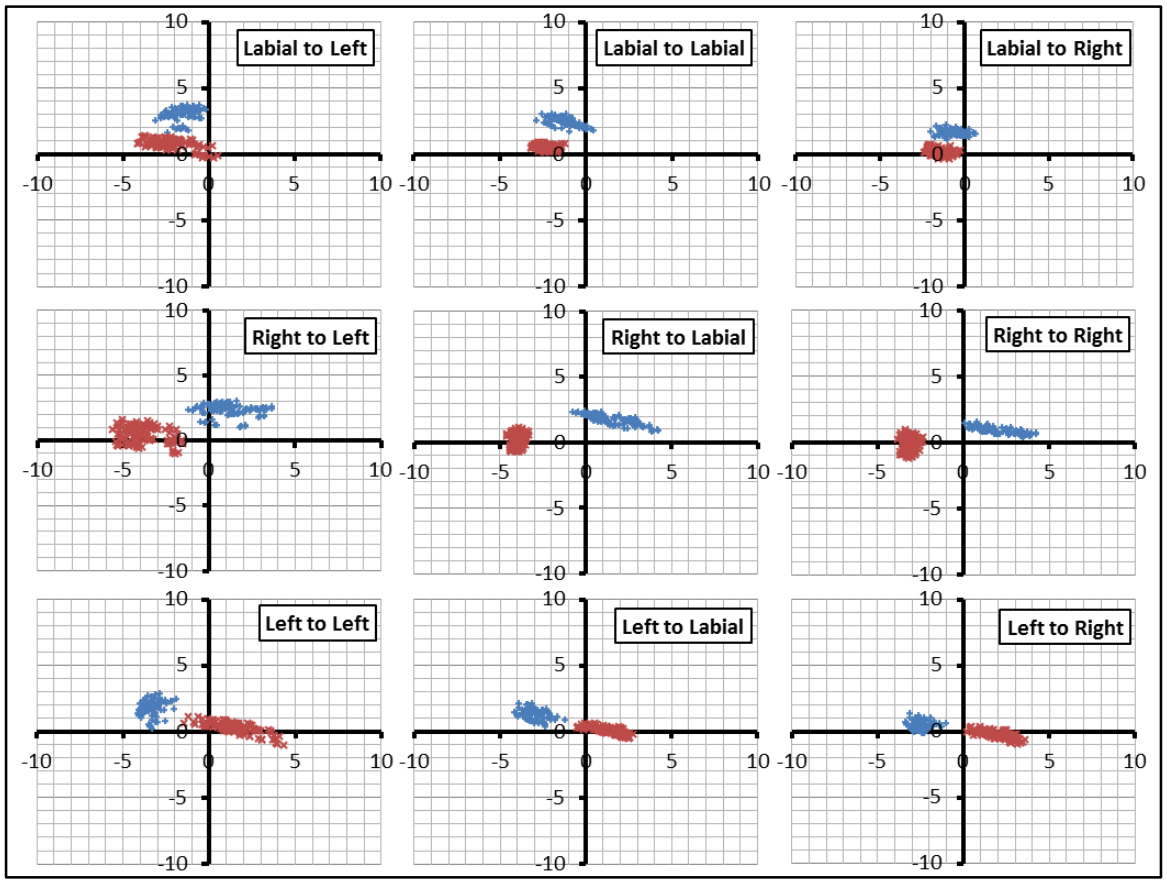


**Figure 49 Distribution and Radius of Axis Location Errors for All Combinations of Scan Sets.** Each chart shows 100 axes, calculated from 10 'Together' views and 10 'Apart' views. The co-ordinates are in mm, with superior-inferior (Y) and anterior-posterior (X), and with positive X pointing anteriorly. (Blue Plus : Left TMJ, Red Cross : Right TMJ).

The mean radius of error for all 900 axes, regardless of viewpoint, and combining the left and right TMJs was 2.65 ± 1.01mm.

61.3% of the axes lay within 3mm of the true axis, and 99.2% of the axes lay within 5mm of the true axis. The maximum error radius was 5.57mm.

The mean calculated degree of rotation around the axis was 7.71 ± 0.09º. The range over the 900 axes was 0.43º (7.51 to 7.94º).

The mean angle between calculated axes and the true axis was 2.11 ± 0.90º. The range over the 900 axes was 4.26º (0.46 to 4.72º).

The mean translation along the axis was 0.24 ± 0.13mm. The range over the 900 axes was 0.62mm (0.00 to 0.62mm).

## 5.6 Discussion

The precision of the calibration target could be questioned as the quality of ink jet printers is probably unreliable below 50µm. This may be the limiting factor in scanning trueness and precision. It would be beneficial to improve the calibration in future experiments.

A 30° angle between cameras was chosen as a mathematically reasonable compromise between depth accuracy and X-Y correspondence accuracy. However, when scanning a more curved labial segment, or when scanning from the left or right views, the commonality between the stereo images may be reduced. If an increase in calibration could be achieved (allowing sub-pixel resolutions), then a decrease in the stereo angle could be considered. This would increase the confidence and number of stereo matches whilst maintaining depth resolution.

The trueness and precision of the new scanner has not been robustly investigated to industry standards. However, all hinge axis calculations, and measurements were performed using points from the models scanned in the Lava ST scanner, which has a trueness of <10µm when tested against testing standard VDI 2634/2. The labial scans are simply a positioning aid for these virtual models. It is cautiously presumed that this positioning is sufficient for clinical use, based on the trueness with which the hinge axis is located, and the fact that the labial scans merged seamlessly with those of the ST scanner. The simple test of deviation from ‘flat’ when scanning a flat target (in this case, a standard deviation of 14µm), is one of the industry standard tests for scanner precision. The new system would therefore seem to be performing with a comparable precision to the Lava ST scanner. However, further verification that the optical interocclusal records are sufficiently true and precise is required,  and this will be the focus of future work.

A problem with the Lava model scanner was the low density of the point cloud of data. It was noted that individual data points were often 100µm apart. Despite the fact that these points might have a trueness of 10µm, the sparse data may lead to poor alignments to the bite scans. For this reason, the ‘digital veneering’ technique was developed to enrich the data in key areas. A cleaner solution would be sourcing a model scanner that produces denser 3D data.

The practical benefit of the novel method is immediately applicable to digital workflows. It may also be possible to articulate conventional stone models using a 3D printed mounting plate and interocclusal record. Current readily available stereolithographic technology will print down to 10µm layers (Digital Wax 020D, DWS Systems, Zane, Italy). The material cost of additive manufacturing is very low,

and would probably be less than the clinical cost of traditional techniques. However, it would seem more sensible to consider CADCAM dental techniques as the first choice in implementing the method, rather than reverse-engineering physical articulated models. In light of the growing number of ‘virtual articulators’, the method could simply be integrated into existing workflows by informing the articulator software on where to position the models, relative to the virtual hinge.

The most commonly used method for locating the THA is to locate an arbitrary point anatomically and record this with an earpiece facebow. This method typically locates the THA with a mean radius of error of 4.7mm and a standard deviation of 2.9mm (see Section 1.1.3.2).

Electronic pantographs are more expensive, take longer to use, and consequently are generally restricted to use in highly specialized practice or as a research tool. Their trueness in locating the THA clinically would seem to be around 2mm (see Section 1.1.3.3).

The proposed method lies somewhere between these two techniques, with a mean radius of error of 2.65 ± 1.01mm. It is interesting to note that this range of error is in good agreement with the predictions made by the mathematical model (Section 3.4.3). The model predicts maximum hinge axis location errors of approximately 5mm, if the scanner trueness is 70µm and sufficient surface area of teeth is captured. There is also the prerequisite that sufficient jaw opening has occurred. The *actual* trueness will be compounded by scanner trueness and precision, scanner noise and alignment algorithm errors. One might surmise that the printed calibration target, coupled with some errors in alignment, combine to form errors in the system of approximately 50 to 70µm. The theoretical model predicts that this might induce maximum hinge axis errors of 5mm, with average errors typically half this value. This fits well with the experimental findings.

It has previously been shown that the *radial* location of this error has a greater effect on introduced occlusal discrepancies than the magnitude of the radius of error (see Section 1.1.4). Broadly speaking, errors in the posterior-superior and anterior-inferior quadrants have less influence on occlusal discrepancies. In this experiment, if the ‘Closed’ scan was taken from the labial view, the calculated axis tended to be located in the favourable posterior-superior quadrant (Figure 49). The viewpoint of the ‘Apart’ view had less influence. One reason for this might be the behaviour of the alignment algorithm. When the teeth are closed, the lower arch is partially obscured by the overbite. Alignment relies on a feature-rich surface and it could be that the narrower lower incisor teeth provide more defined embrasures than the wider posterior teeth so the labial views have more useful points to align. The alignment of the ‘Apart’ views may show less variation because a sufficient

area of the lower arch is always visible, regardless of viewpoint. Furthermore, the relatively flat labial segment may produce more dense scans with many points being visible to both cameras. Conversely, the ‘Right’ and ‘Left’ views may have less mutually visible points due to the curvature of the arch. It could be beneficial to reduce the angle between the cameras (currently 30º), to try and enhance the number of mutually visible points in the left and right images.

The pattern of axis locations when a less favourable viewing angle has been used appears to be broadly linear horizontally, particularly on the side from which the scan took place. This might imply that alignment is successful superior-inferiorly, but that the lower model can ‘slide’ antero-posteriorly when insufficient data are captured. The effect of this linear error on the quality of the interocclusal records needs further investigation. Furthermore, the effect of using different dental models, with different tooth morphologies and arch forms requires investigation.

Visual inspection of the location of all axis errors shows that errors located near the ‘worst’ polar co-ordinates (60º and 240º, according to the simulation in Section 0) never exceeded 3mm. In other words, the larger observed radial errors (>3mm) were always located in a favourable direction and would cause only a small incisal occlusal discrepancy.

The orientation of the calculated axes was always close to that of the real axis (2.11 ± 0.90º). If analysis was restricted to labial ‘Closed’ scan sets (but any ‘Apart’ view) the deviation of the orientation of the axes improved to 1.12 ± 0.33º. Previous analyses of the occlusal effects of axis location errors tend to have simplified the problem to 2D, and considered the left and right TMJs in isolation. However, the real situation is 3D, and each axis is defined by a pair of points (left and right TMJs). Future work could be directed at the effect of the skew in the axes in 3 dimensions.

The calculated degree of rotation about the different axes showed very little deviation (7.71 ± 0.09º), hinting that the method calculates the relative orientations of the occlusal planes with good precision. Small errors in the ‘virtual’ interocclusal records will be a cause of differences in degree of rotation about, and angulation of, the calculated axes. The magnitude and effect of these errors at the occlusal level requires further investigation. The interocclusal records need to be far more true and precise than the hinge axis location.

It is the aim of future work to investigate the trueness and precision of the interocclusal records, but indirect evidence can be gained by looking at the predicted magnitude of occlusal errors for an axis located in the posterior-superior quadrant. Morneburg and Pröschel (Morneburg & Pröschel 2002) showed that, with

a 5mm radius error, and an opening of 2mm, one can expect occlusal errors up to a maximum of 180µm, and generally less than 100µm, at the second molar region, providing the *direction* of the erroneously located axis is favourable. At half this error radius (as the novel method produces) one can predict that the optical interocclusal records may typically show a trueness of below 100µm but further work is needed to verify this.

The magnitude of the translation along the axis should theoretically be zero. However, inaccuracies in scanning and alignment lead to slight inaccuracies in the angulation of the axis, and 'force' the computer to introduce a shift along the axis to compensate. If several scans have been taken, as would seem sensible clinically, the axis with the smallest translation should be the one most closely aligned to the true axis. Of course, this method assumes that there is no actual bodily shift of the mandible and that a pure rotation has taken place.

In the system, the projector is set to a screen resolution of 640x480 (its maximum native resolution) and the cameras are 1.3 Mega pixels (1280x1024). These are low by today's standards, and illustrate how quickly cheap technology becomes available. An upgrade in hardware would only cost a few hundred pounds, and one could expect a 2 to 4 times increase in resolution. This is a key benefit of the use of digital technology in dentistry.

Another benefit is the complete lack of any further distortions or warping of the data – the errors are absolute. In general practice, many unknowns such as storage time and temperature of materials, incorrect handling of materials, loosening of screws on transfer jigs during postage/transportation or human error accumulate during the mounting of study casts and the fabrication of prostheses. It seems reasonable to expect that, with a reduced number of variables in the procedure, a more consistent result will be achieved. A clinical comparison of traditional techniques and the new method is warranted.

The clinical method would require the patient to be positioned in CR. This may decrease the precision of the method, although with minimal training, or using patient-guided techniques, this position is considered reproducible (see Section 1.2.2). The use of a small anterior jig to position the patient in CR seems advisable, followed by the use of a thicker jig to provide the 'Apart' record. The use of a jig will obscure a small part of the two upper central incisors, and so there will be less useful data collected in the labial scan. This might affect the quality of the alignment, although this is doubtful if sufficient tooth structure is visible either side of the jig (for example, all the way around to both canines). Furthermore, the hidden lower incisal edges of the 'Closed' scans may have impacted detrimentally on the trueness. The clinical procedure suggested above may actually improve the

alignments, because the lower incisal edges are more likely to be visible in both scans when an anterior jig is worn.

Finally, it is important to stress that the method simultaneously aligns *both* the upper and lower dentition relative to the THA. Comparisons with earbows are therefore only half of the story. The error induced in the traditional mounting of the lower model on an articulator must also be considered (see Section 1.2.3). With regards to the hinge axis location, the novel method performs a task traditionally performed with an earbow *plus* an interocclusal record. It is conceivable that the method may display clinically noticeable improvements in trueness and precision over the cumulative errors accrued with the traditional workflow.

## 5.7 Conclusion

The proposed method for locating the THA showed good trueness and precision, within clinically acceptable limits, *in vitro*. The mean radial axis error was 2.65 ± 1.01mm, over 900 calculated axes.

The method works best when the first scan of the pair is captured viewing the full anterior labial segment.

The trueness and precision of the interocclusal scans requires further investigation to determine if they are sufficient at the level of the occlusion, and not just the THA, to justify clinical use.

Sources of inaccuracy will come from calibration errors, scanner noise and alignment algorithm errors. These aspects will need addressing if the performance is to be improved.

A faster scanning pattern (ideally a one-shot pattern) will be required for clinical applications.

# 6 An *In Vitro* Study into the Trueness and Precision of the Optical Interocclusal Record

## 6.1 Introduction

The experiment in Section 5 has shown that a novel optical method involving 3D scanning the labial segment can locate the kinematic hinge axis on articulated models with good trueness and precision.

However, before testing this approach clinically, it is important to understand the trueness and precision with which the relationship between the upper and lower dentition is recorded. This is because the optical interocclusal record is central to the novel method for locating the THA.

Furthermore, a true and precise interocclusal record is extremely clinically relevant, since ultimately this determines the relationship between the occlusal planes of the upper and lower dentitions.

## 6.2 Aim

- To assess the trueness and precision of an optical method for recording interocclusal relationships.

## 6.3 Objectives

- To measure the trueness of multiple optical bite registrations by exploiting the precise (known) change in position of the mandibular model, when moved using a linear stage.
- To measure the precision (in terms of standard deviation from the mean) of multiple optical bite registrations, taken with multiple simulated mandibular positions.

## 6.4 Method

A jig was created which held a maxillary dental model rigidly, and allowed precise relative movement of the mandibular model, using an XYZ positioning table (LSSZ1106 Jiangxi Liansheng Technology Co. Ltd., Nanchang, China) (Figure 50).

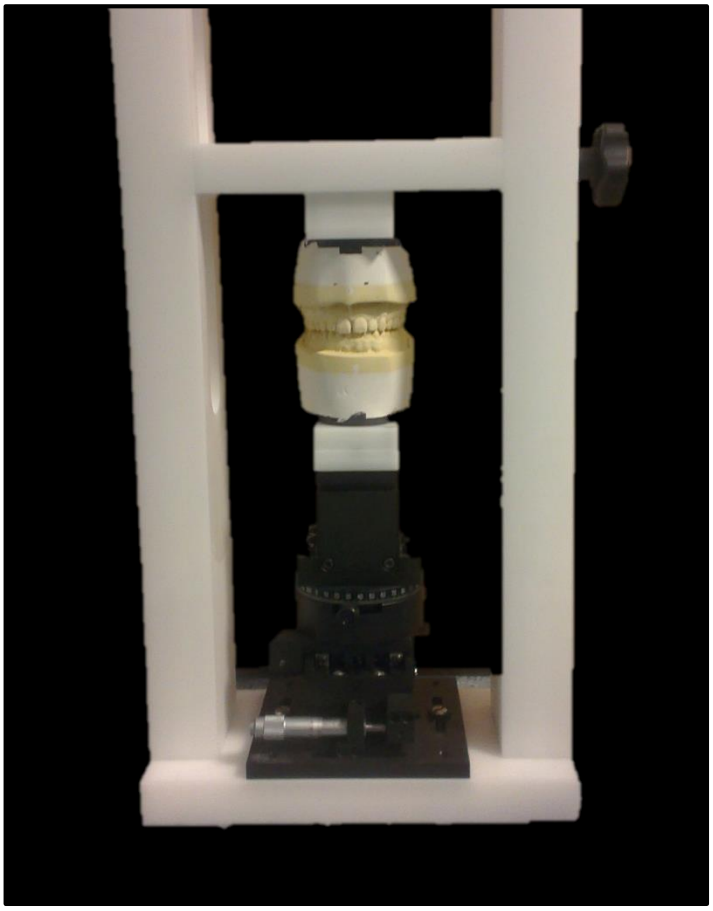

**Figure 50 The Custom Test Rig.** This allowed for precise movements of the lower model (using an xyz linear stage) whilst keeping the maxillary model stationary

A 3D optical scanner was constructed using off-the-shelf components, capable of recording all upper and lower incisors/canines simultaneously (see Section 5.4.1).

### 6.4.1 Precision

The mandibular model was positioned to simulate left lateral excursive position (10mm lateral displacement) and 5 labial interocclusal scans were taken as described in Section 5.4.2. Between each scan, the camera was picked up and

replaced by hand, to simulate the clinical variation in position when taking a 3D photograph. This process was repeated for a right excursive position (10mm lateral displacement), a protrusive position (6mm anterior displacement), a retrusive position (2mm posterior displacement), an open position (5mm vertical displacement from MICP) and a closed position (MICP), giving a total of 30 scans (Figure 51).

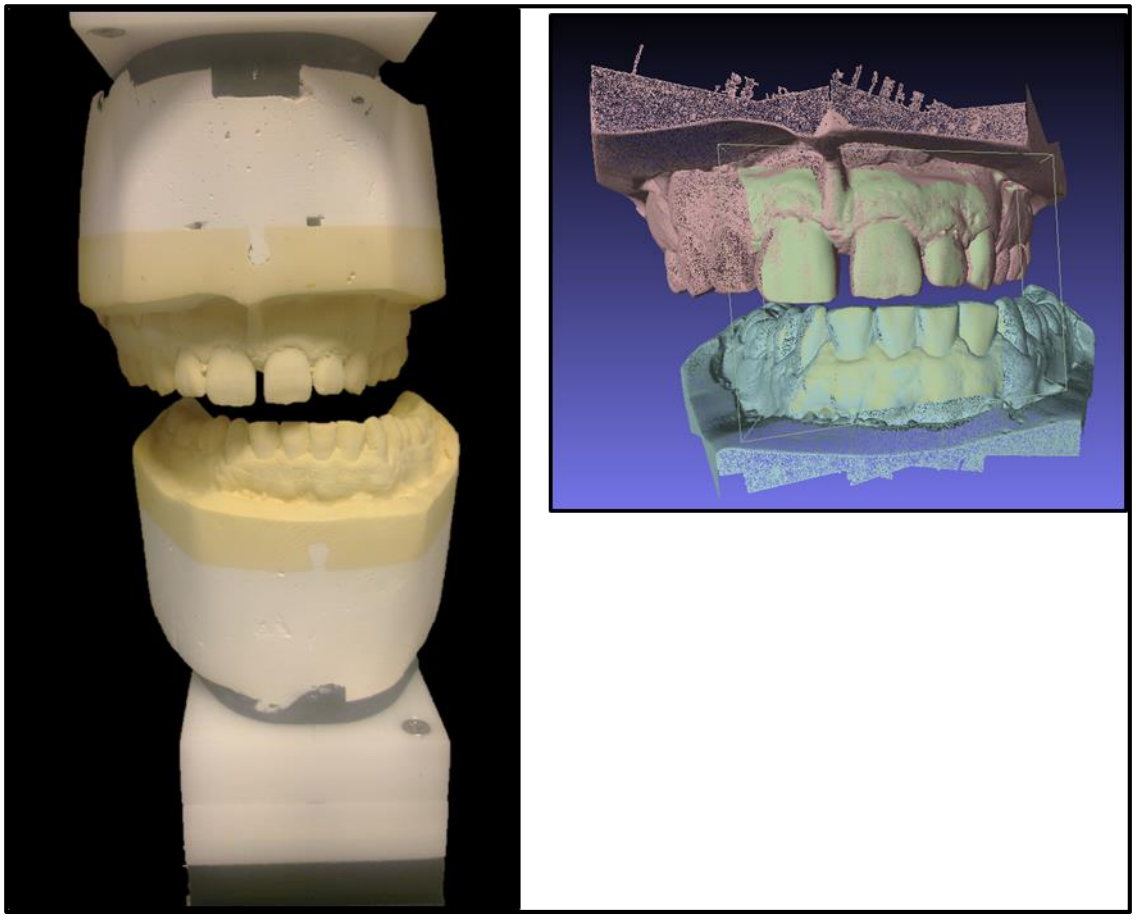

**Figure 51 An Example of a Simulated Left Mandibular Excursion and the Corresponding Optical Scan.** The full arch digital models (orange and blue) superimposed on the bite scan (green). Five such scans were taken for each of six simulated mandibular excursions.

The stone models were then digitized (Rexcan DS2, Europac 3D, Crewe) and 3 reference points were identified on both virtual models. On the upper model, these were the mesio-palatal cusp tips of the upper left and upper right first molars, and the mesio-incisal corner of the upper left central incisor. On the lower model, these were the mesio-buccal cusp tips of the lower left and lower right first molars, and the mesio-incisal corner of the lower left central incisor. In this way, a triangle was created in the upper arch, defining the upper occlusal plane. Similarly, a lower

occlusal plane triangle was created, whose three vertices were well distributed around the arch (Figure 52).

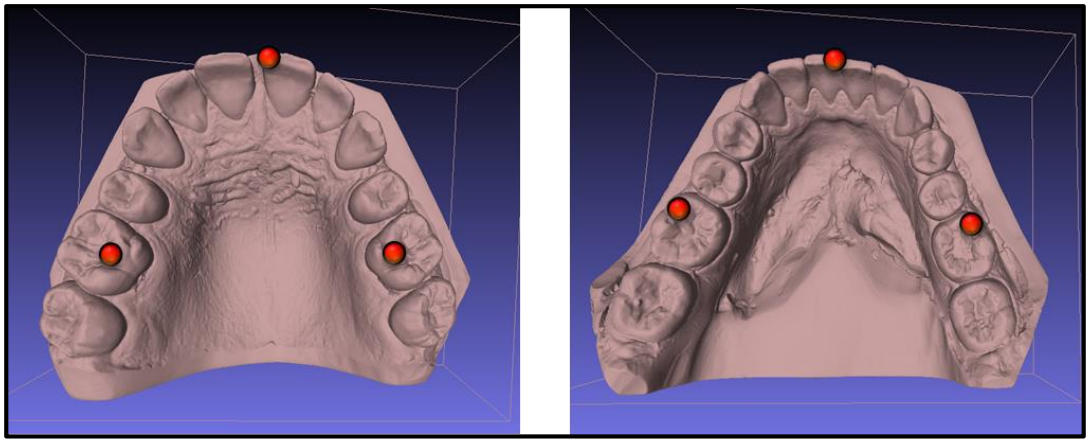

**Figure 52 The Reference Points Selected on Both Full Arch Models.** All measurements were taken from these point, for all experiments.

Custom software was written which performed the following steps. Firstly, the scanned full arch models were aligned with each optical interocclusal scan in turn. Next, these aligned models were both transformed to a common global co-ordinate frame. The three maxillary reference points were used to define this co-ordinate system. Thus, the point on the upper right molar was transformed to (0,0,0) and the point on the upper left molar was located along the positive x-axis. The incisal point was positioned at y=0, effectively making the occlusal plane level with the plane y=0. By standardising the co-ordinates in this way, the absolute positions of the three lower reference points could be compared directly between each of the interocclusal alignments.

The precision of each of the lower reference points was calculated as the standard deviation from the mean position, for each set of 5 scans. Any differences in the precision of the interocclusal records, based on different mandibular positions, were assessed using Levene's Test. The tests were performed using MS Excel (2010), running an implementation of Levene's Test from the Department of Statistics, University of Florida (http://www.stat.ufl.edu/~winner/computing/excel/levene.xls).

### 6.4.2 Trueness

The trueness of the interocclusal records was investigated as follows. Firstly, the mandibular model was positioned in MICP. Five labial scans were taken and

averaged to create a baseline position for the upper and lower digital casts. Next the mandibular model was lowered by 100µm, and a single scan was taken. This process was repeated 10 times until the model had been lowered by 1mm (Figure 53).

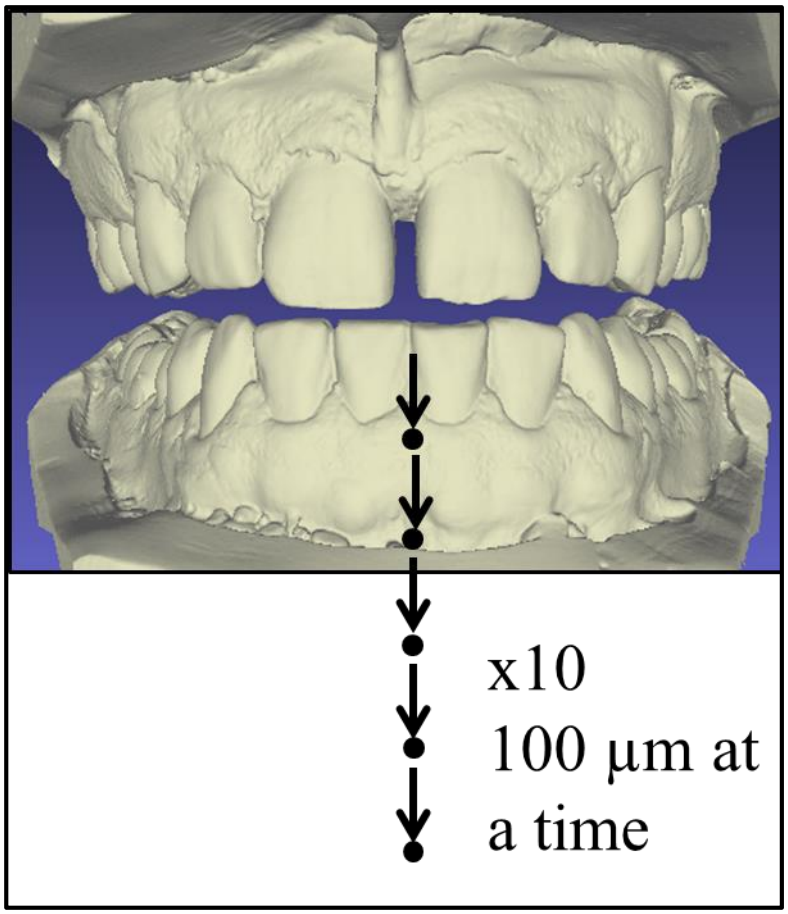


**Figure 53 Assessing the Trueness of Optical Bite Registrations.** The mandibular model was lowered by 100µm, and an optical bite registration taken. This process was repeated 10 times.

The virtual full arch models were registered to each of these scans as described previously, and the calculated distances traversed by the mandibular reference points between each scan were compared to the known distances.

Two methods of analysis were employed. Firstly, the linear distance travelled for each of the single scans was compared to the 'start' position (which was calculated as the mean of the five initial scans). The displacement of each of the three reference points was plotted against the known displacement, and linear regression performed to assess quality of fit.

Secondly, the absolute distances between all possible pairs of scans were used. For example, the distance between reference points in scans 1 and 2 would be expected to be 100µm, whilst the distances between scans 4 and 7 would be

expected to be 300µm. Over the ten 100µm intervals, 45 individual comparisons were possible (from T(10) = 45 where T(x) is the Triangular Operator n + (n-1) + (n-2) + …. + 1).

The distribution of errors in absolute distance was assessed using QQ Plots (Microsoft Excel 2010) to confirm normality, and reported as mean ± standard deviation.

## 6.5 Results

The transformed co-ordinates of the maxillary reference points, used to align all interocclusal registrations to a common co-ordinate system, showed a mean alignment error 0 ± 0µm.

The QQ plots for error distributions of the trueness measurements are shown in Figure 54, Figure 55 and Figure 56. These show the data at all three reference points to be normally distributed.

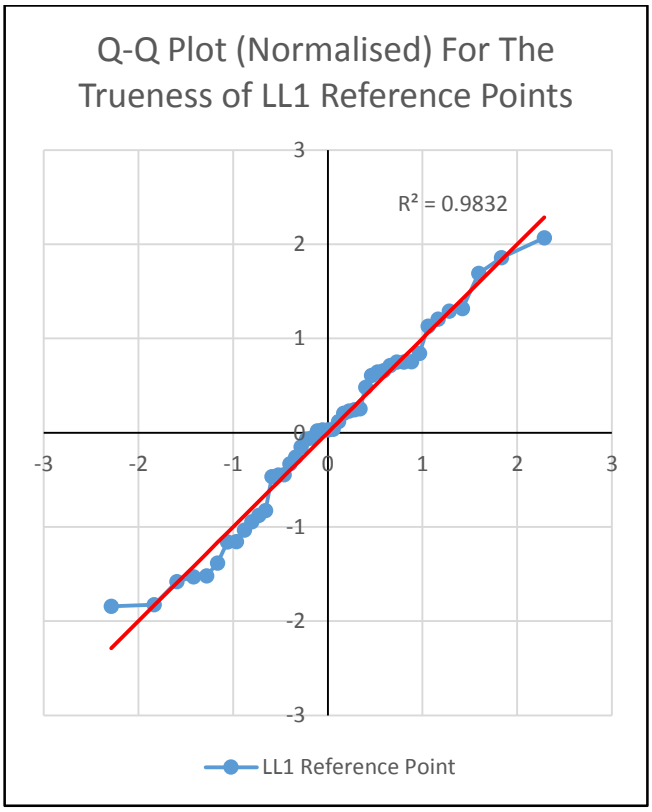


**Figure 54 Q-Q Plot (Normalised) for the Trueness of the LL1 Reference Point**

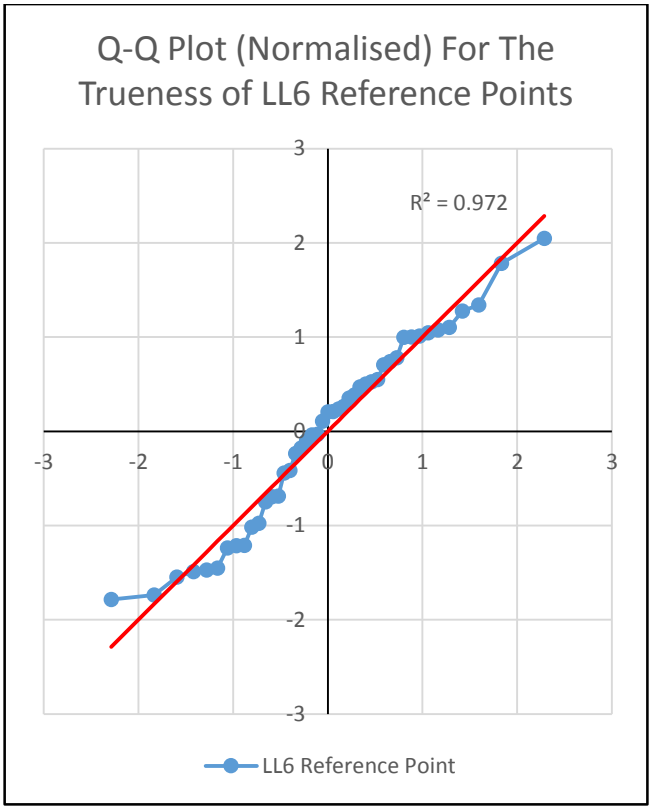


**Figure 55 Q-Q Plot (Normalised) for the Trueness of the LL6 Reference Point**

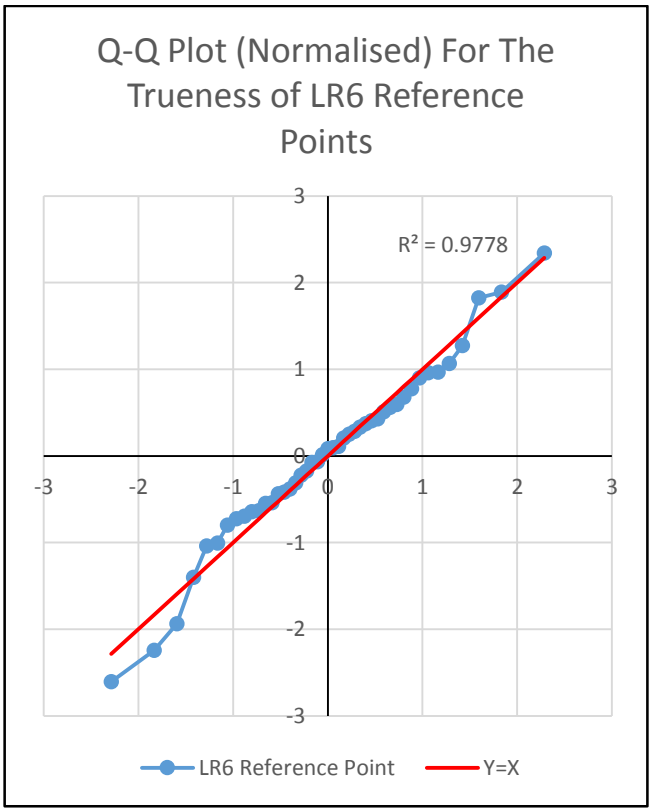


**Figure 56 Q-Q Plot (Normalised) for the Trueness of the LR6 Reference Point**

### 6.5.1 Precision

The precision of reference point location for each set of 5 interocclusal records is shown in Table 3.

Levene's test showed no significant difference in precision between the six groups, and thus a pooled standard deviation was calculated using all 30 scans. The standard deviations of the derived positions of the mandibular reference points were 22µm (LL1), 39µm (LL6) and 46µm (LR6).

The precision was significantly poorer for LL6 and LR6, compared to LL1 using Levene's Test (p=0.003 LL1,LR6 and p=0.007 LL1,LL6).

| Mandibular Position | Standard deviation of distance to mean position (µm) | | |
|---|---|---|---|
| | LR6 | LL1 | LL6 |
| Left lateral | 40 | 24 | 35 |
| Right lateral | 62 | 17 | 32 |
| Retrusive | 49 | 24 | 47 |
| Protrusive | 46 | 20 | 52 |
| Open | 31 | 29 | 39 |
| Closed | 46 | 9 | 13 |
| Pooled Result | 46* | 22 | 39* |

**Table 3 Precision of Each Mandibular Reference Point, for Each Group of 5 Scans and Each Mandibular Posture.** Levene's Test showed no significant difference in precision between the six groups. A pooled standard deviation could therefore be employed. *Denotes significance (p<0.01) (see text).

### 6.5.2 Trueness

Linear plots of the calculated mandibular position for each of the 10 lowering steps are shown in Figure 57, Figure 58 and Figure 59. Step ‘zero’ is extrapolated as the origin, and linear regression best fit lines are plotted to show the correlation with the known distances moved.

The trueness of the calculated distances moved between each combination of steps (45 different distances in total) were -15 ± 22µm (LL1), -93 ± 121µm (LL6) and 4 ± 53µm (LR6).

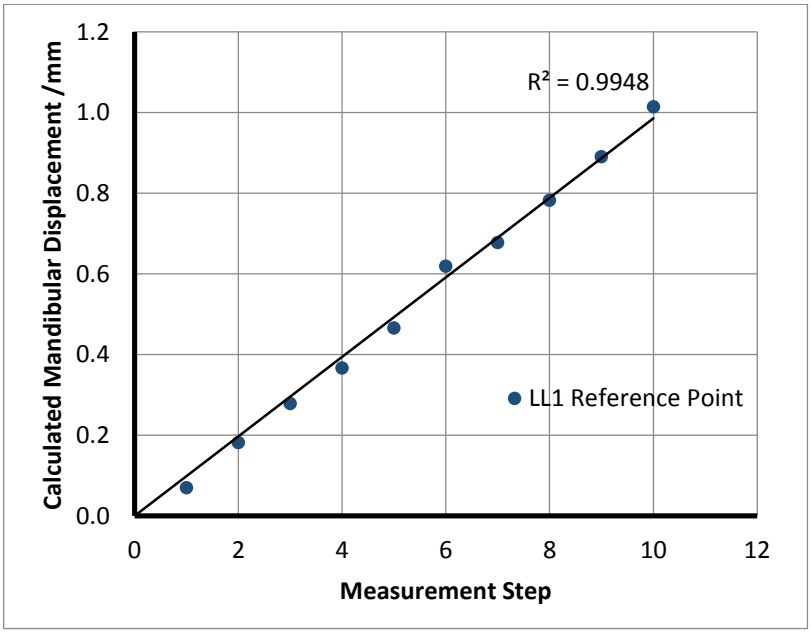


**Figure 57 Graph Showing the Calculated Displacement of LL1 Reference Point, Relative to the Start Position, at Each of the Ten 100µm Incremental Movements.**

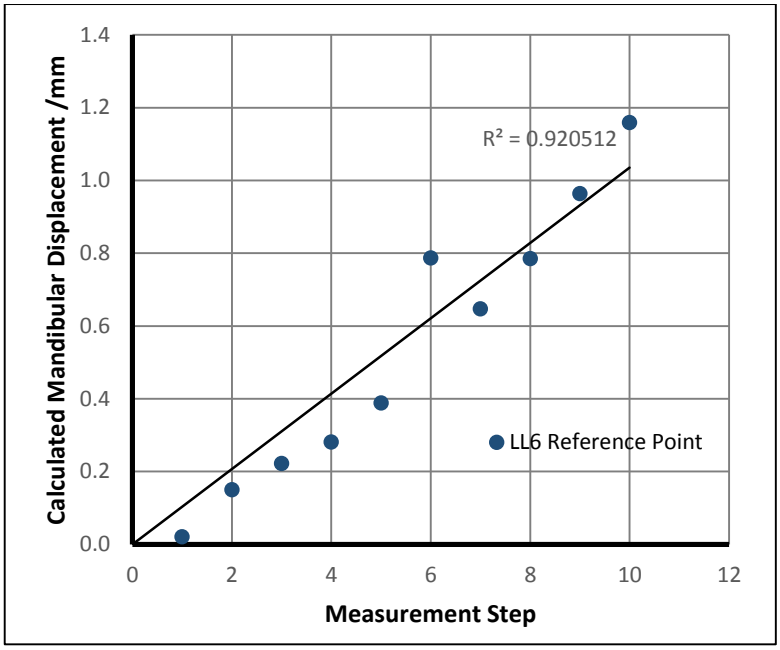


**Figure 58 Graph Showing the Calculated Displacement of LL6 Reference Point, Relative to the Start Position, at Each of the Ten 100µm Incremental Movements.**

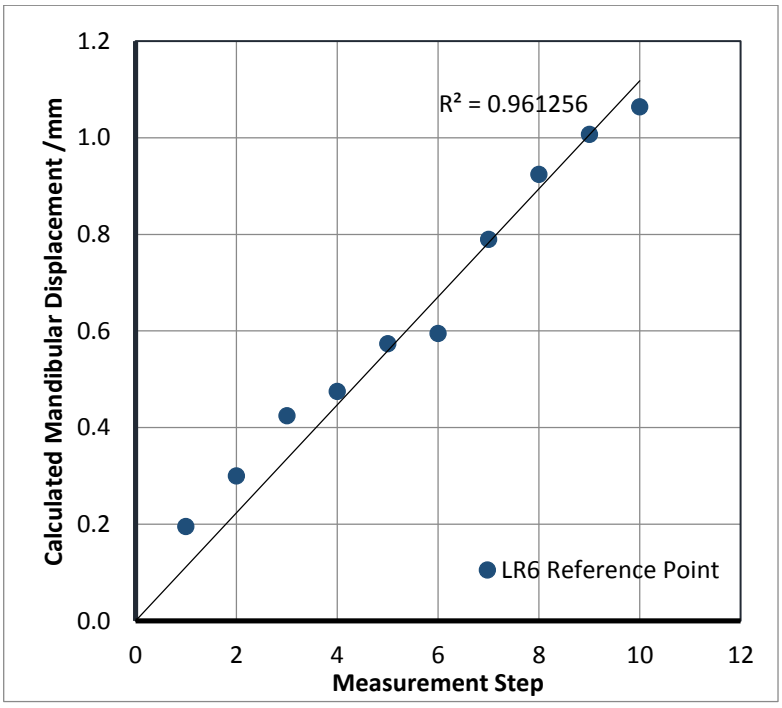


**Figure 59 Graph Showing the Calculated Displacement of LR6 Reference Point, Relative to the Start Position, at Each of the Ten 100µm Incremental Movements.**

## 6.6 Discussion

It is important to note that this methodology captured the entire interocclusal error, in the same manner as keeping a mounted maxillary dental model ‘fixed’, and aligning the mandibular model via a traditional bite registration. The precision with which the digital maxillary model remained fixed during the alignment process required investigation.

This investigation is needed because computers use floating-point representations of fractional numbers, and a limited degree of precision (ie decimal places). If a sequence of complex mathematical operations are being performed (such as a matrix multiplication to transform the co-ordinates of a digital model) it is worth confirming that no loss of numerical precision is encountered. In the method presented, the common co-ordinate frame was produced by aligning the maxillary digital model to a particular reference set of co-ordinates. If floating-point errors accumulated, one would expect that these alignments might have very small errors. This potential numerical error was investigated and all upper digital models were confirmed to be aligned to within 0 ± 0µm of each other. It can be concluded that, at a one micron level of precision, no numerical errors occurred in the transformation calculations.

Section 1.2.3 showed that the weight of evidence for the precision of traditional methods suggests a typical figure in the range of 0.3 to 0.5mm. However, some of this variation is due to clinical differences each time a patient is positioned into centric relation. Even so, the method appears to show a 10-fold improvement in precision. Such a large improvement is unlikely to be entirely due to clinical variation. At the very least, it would seem worth testing the method clinically to compare the precision of traditional wax records against the proposed technique.

As discussed in Section 1.3.2, previous workers using maximum intercuspation intraoral digital bite scans have shown the record to be true and precise near the scan, but cross-arch errors to be large (typically 0.5mm or more). The same effect is found here, where the trueness and precision of the incisal positioning is significantly better than that of the molars, more distant from the scan. However, even at these distant sites, the method shows improvements over intraoral scanner buccal bites, with errors typically below 100µm in the present experiment, compared to reports of >500µm using an intraoral scanner bite registration (Iwaki et al. 2013).

This improvement is probably due to the larger volume of information that is captured when using the proposed labial bite scan. This larger volume yields more

information for the alignment algorithm, constraining the solution to one that is closer to the ‘real’ solution. Furthermore, the bite scan is the product of a single optical scan. Intraoral bite scans are the product of multiple smaller scans, digitally stitched together. This process might produce greater errors in the overall bite registration, and help to explain the observed improvement seen with the novel method.

Further improvements might be gained by aligning the dense point cloud (labial scan) to the meshed version of the 3D models created by the Rexcan DS2 scanner, rather than the point cloud version. The difference is subtle but important. The density of the data points (vertices) from the commercial scanner is typically less than the density with which data is collected from the novel scanner. This mismatch could be partially compensated for by aligning each vertex from the bite scan data, to the closest point on the *mesh*, rather than the closest *vertex*. Effectively, this would align the vertices onto a surface, rather than onto another cloud of vertices, and might produce a small improvement in the result.

In the previous experiment (see Section 5), this mismatch was compensated for by ‘wallpapering’ the dense labial scans over the top of the commercial model. However, this technique may still be prone to alignment errors in the wallpapering. Furthermore, the commercial scanner used in that experiment produced even less dense data than the one used here. The density of the data from the scanner used in the present experiment was considered sufficient to negate this wallpapering stage. However, this data was still less dense than the data produced from the bite scanner. In the future, scanning the dental models using a modified version of the novel scanner, to ensure the data is as dense as deemed necessary, might be indicated.

It is difficult to explain the larger, and more diverse, distribution of errors in LL6 trueness shown in the second experiment. This may be due to differences in morphology between the left and right regions of the scan. The standard deviations for LR6 and LL1 seem to agree with the findings in the first experiment, whilst LL6 seems to be an outlier. Even considering the decreased trueness of LL6, all reference points showed potentially higher positional trueness than existing methods.

## 6.7 Conclusion

The optical 3D labial bite registration technique relates maxillary and mandibular models with good trueness and precision *in vitro*. There is potential to demonstrate similar results *in vivo* and a clinical investigation seems justified. However, the scanning time (approximately 0.5sec) is too long to expect the patient to remain completely still, when considering the sub-100 micron levels of precision required.

# 7 Adapting the Technology Towards a Clinically Viable Solution

## 7.1 Introduction

The previous experiments have confirmed the predictions of the feasibility study (Section 3.4) in terms of the specification of the hardware. So far, the hardware has been operating as optimally as possible by implementing standard phase shifting projection patterns. This produces the most dense, true and precise 3D data (Section 4.1.2.1).

There is, however, a problem. The scanning time is approximately 0.5 seconds, because multiple phase shift patterns must be projected, and the cameras and projector are not synchronised, leading to an artificially long delay between frames to avoid any image tearing. When considering the desired level of trueness and precision, it is almost certain that a handheld scanning device with a 'live' patient, will not remain perfectly still for this length of time, and the images will become noisy. For example, common wisdom amongst photographers suggests a shutter speed no slower than 1/50$^{th}$ second, when hand-holding a camera, in order to preserve visible image sharpness. The proposed method uses the images to take precise measurements and is therefore particularly intolerant to image blur.

There are two solutions to this problem. Firstly, the frame rate of the cameras and projector could be increased. In fact, projectors natively run at faster than 60 frames per second because, in that time window they must project separate red, green and blue images. Typically they run at 240 fps (red, green, blue and white ) and it might be possible to take advantage of this. Unfortunately, to do so would entail replacing the colour LEDs with white ones, which would be a difficult procedure on a sealed unit projector. Furthermore, the cameras would be required to run at a similar frame rate which would add significantly to the cost. Finally, there would have to be perfect synchronisation, and the HDMI signal does not lend itself easily to identifying the vertical synchronisation (V-SYNC) pulse (it is encoded within the signal and requires additional decoding hardware).

The second solution is to move to a one-shot pattern. The hardware can remain unchanged (or even become simplified), keeping the cost down. The problem now is one of generating sufficiently true, precise and dense data from a single projected

image. If a colour pattern is used, pixel resolution will decrease because colour cameras have repeating arrays of red, green and blue pixels, and interpolate the data to produce a full image. This degrades the data, and the only way to avoid this is to use a 3-CCD camera (which has separate, full resolution sensors for red, green and blue). These cameras are around ten times the cost of ‘standard’ colour cameras.

The one-shot technique seems preferable, but in order to maintain a subpixel resolution, monochrome images must be used. A promising option is to employ edge detection techniques to solve the correspondence problem.

## 7.2 Designing the One-Shot Scanning Pattern

The use of a series of vertical lines is proposed (‘jailbar patterns’) from which sub-pixel accuracies can be theoretically obtained (Figure 60).

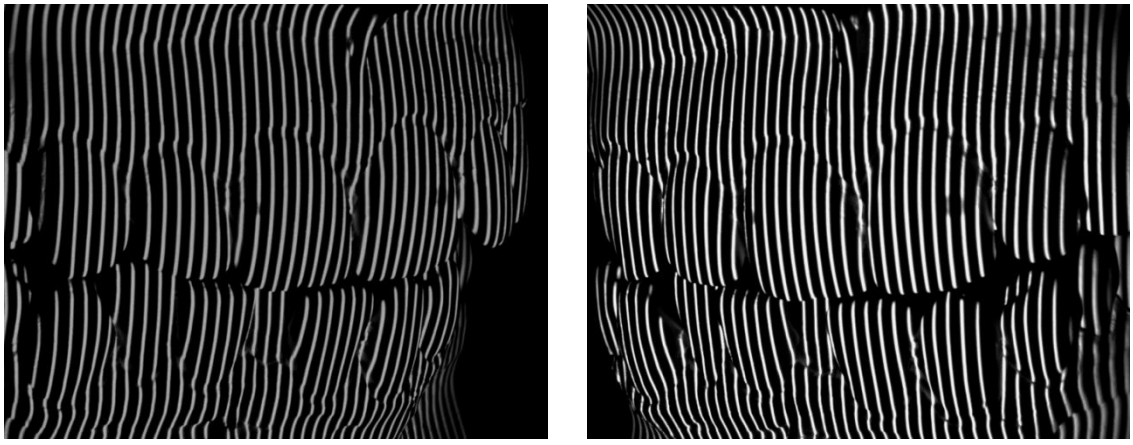

**Figure 60 Left and Right Image Captures of the Proposed ‘Jailbar’ Pattern.**

Each horizontal scan line from an observed image will produce a series of peaks and troughs in pixel intensity (Figure 61).

If the projected lines happened to be *exactly* one camera pixel wide, and in perfect focus, the intensity would vary digitally – going from zero for one camera pixel, straight to ‘full on’ (255 in an 8-bit image) for the next pixel, then back to zero again for the next. Of course, this will never happen. There will always be a mismatch between camera pixels and projector pixels, such that each projected line will straddle several camera pixels. Additionally, small changes in focus will alter the profile of the line such that the edges ‘decay’ in a Gaussian manner, rather than

being a sharp step. The edges will therefore be slightly blurred when viewed close up in the camera image (Figure 62).

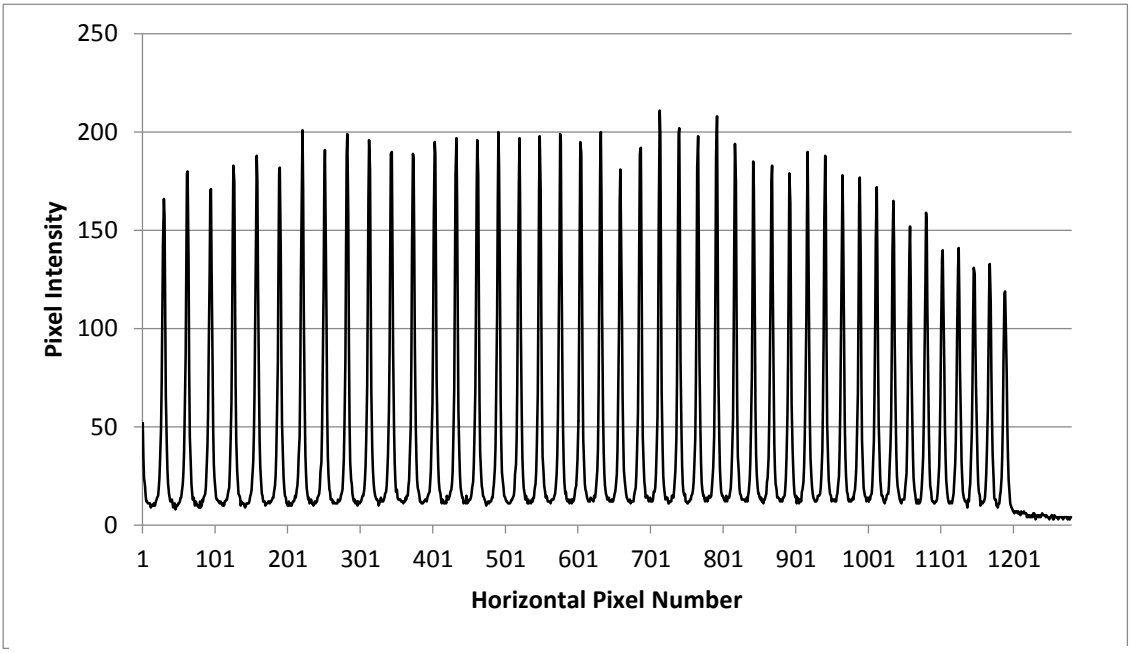


**Figure 61 Camera Pixel Intensities for a Horizontal Sample Line Across One of the Images in Figure 60**

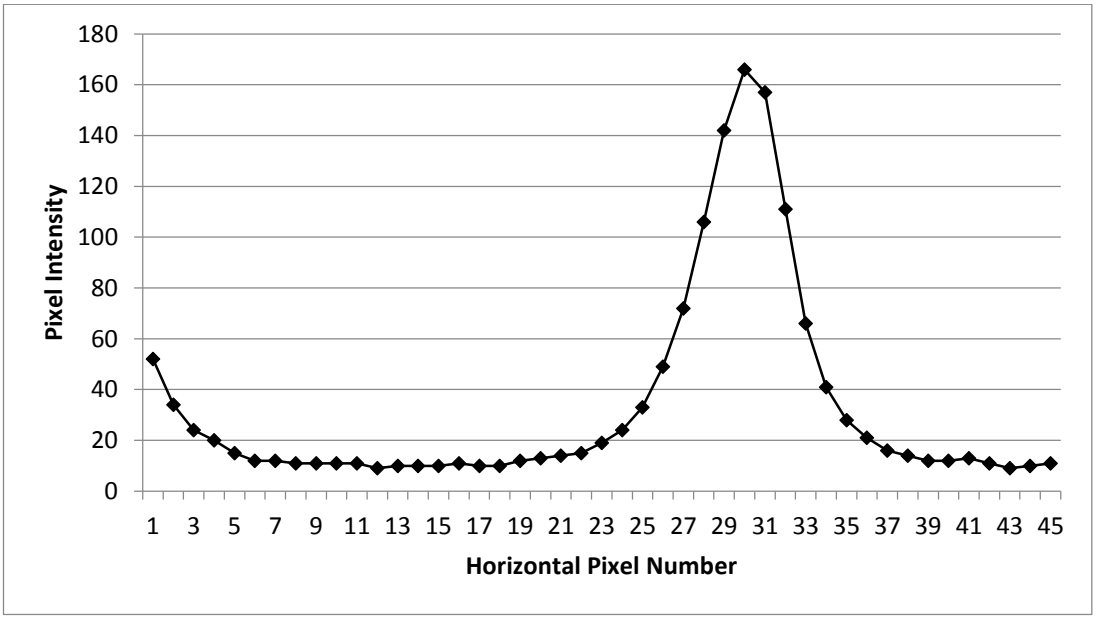


**Figure 62 A Close Up View of a Section of the Sample Line Shown in Figure 61.** The profile of an edge straddles several pixels and is slightly blurred.

The ‘edge’ of each line is defined as the subpixel position of the maximum intensity gradient. This is calculated using the zero-crossing of the second order derivative of the local pixel region (Figure 63).

Each projected line yields a left edge (where the zero-crossing moves from positive to negative) and a right edge (the zero-crossing moves from negative to positive). The number of edges (ie vertical lines) projected in the image should be sufficient to produce reasonably dense data, but not so dense as to contaminate the dark areas in between each line. Such contamination would reduce the contrast of each edge.

In this way, all of the sub-pixel locations of the edges in the left and right camera images can be labelled. However, one problem still remains - identifying corresponding edges in both images, in order to calculate the 3D data. If, for example, 34 vertical stripes are projected, the *index* of each observed stripe is not known. It is merely known that an edge exists at a particular, precise location in the image, but not *which* edge. For this reason, the corresponding edge in the other stereo image cannot be found.

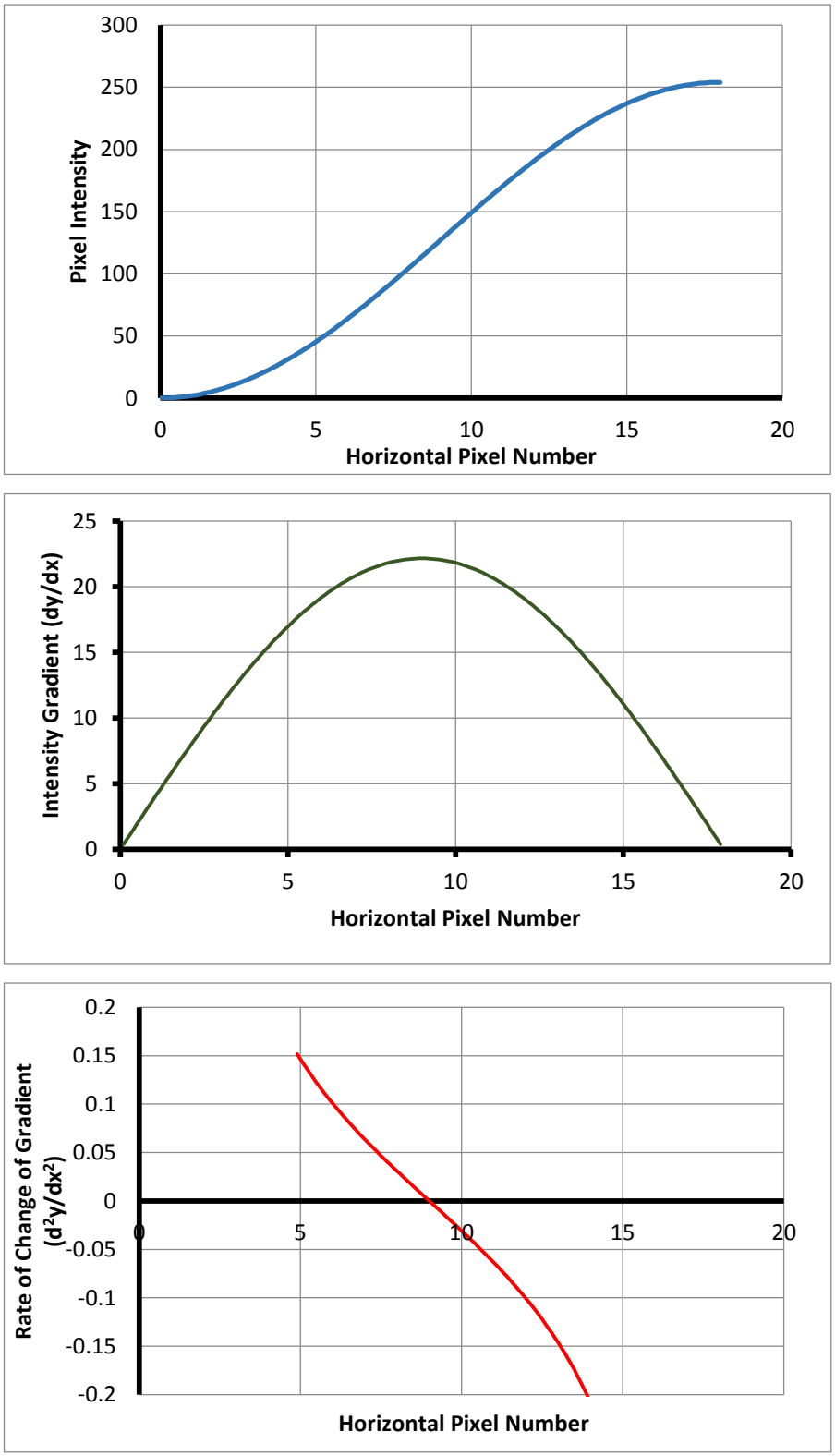


**Figure 63 Edge Detection with Sub-Pixel Resolution.** The edge of a projected line is not sharp in the camera image because of image blur and an imprecise mapping of projector pixels to camera pixels. A rising edge (left edge), similar to that shown in Figure 62, is depicted in the top graph (blue line). The gradient of this edge (first derivative) is shown in the middle graph (green line). The second-order derivative is shown in the bottom graph (red line). The point where this line crosses y=0 (here pixel 9.0) is defined as the edge of the line.

A method is needed for indexing the observed edges. For example, it must be known that a particular edge in the left image is the 21st stripe, and the corresponding stripe in the right image can then be sought. The stripes in an image cannot simply be counted, starting from the leftmost and moving across. There is no guarantee that the leftmost stripe is ‘stripe 1’, since some of the projected stripes may fall outside of the field of view of the camera. In addition, some stripes may be obscured from view (for example, hidden in an interproximal space that is not visible to one or both cameras).

A form of temporal encoding is proposed to solve this indexing problem. The method starts by projecting only ‘stripe 1’ and recording a stereo-pair of images. The edge is found in each horizontal scan line of the left and right images, and these are known to all correspond to ‘stripe 1’.

In the next frame, stripes 1 and 2 are projected, and an image pair recorded. Importantly, this second image is projected only 1/60th or 1/30th of a second after the first, meaning there is little movement between the images (maybe a few pixels). As before, the edges in each image are found, and any edges that are very close to the previously viewed edges (within a few pixels), are labelled as ‘stripe 1’. All new edges are labelled as ‘stripe 2’.

The entire image is built in this way, until all 34 stripes are being projected. This process will take around 1-2 seconds and should be tolerant to object motion, provided the movement between any two consecutive frames does not exceed half of the spacing between stripes. The sole purpose of this pattern building process is to index the stripes - no 3D measurements are taken at this stage (Figure 64 and Figure 65).

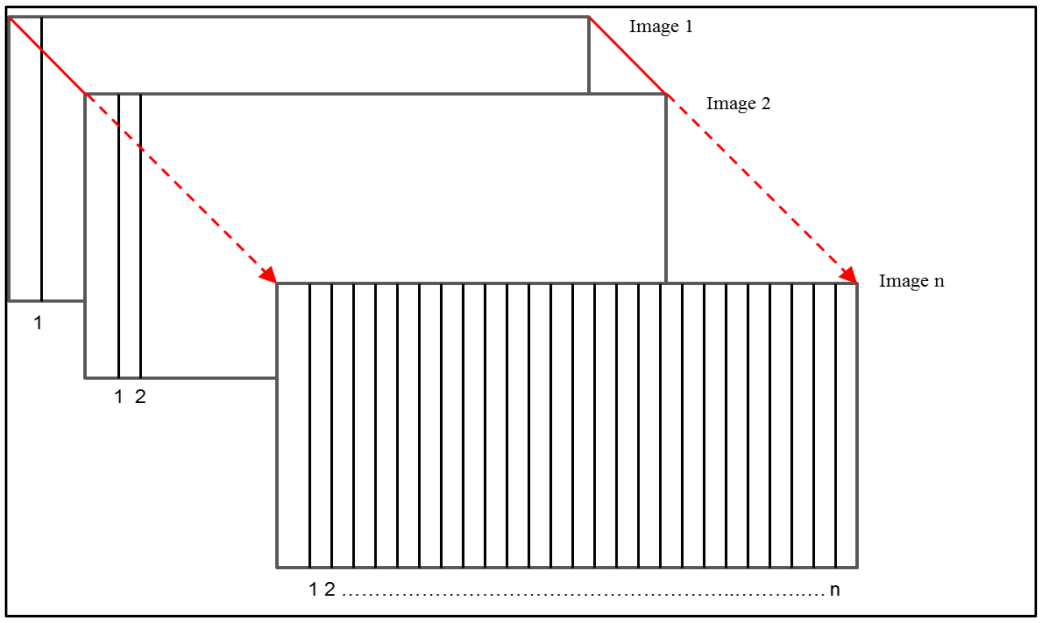


**Figure 64 The Projection Patterns Used to Sequentially Build the Full Jailbar Image.** With each frame, a line is added to the projected pattern, until all lines are being projected. Stripe indices are labelled underneath each image. (For clarity, black lines are shown on a white background, but the true image is a negative of this).

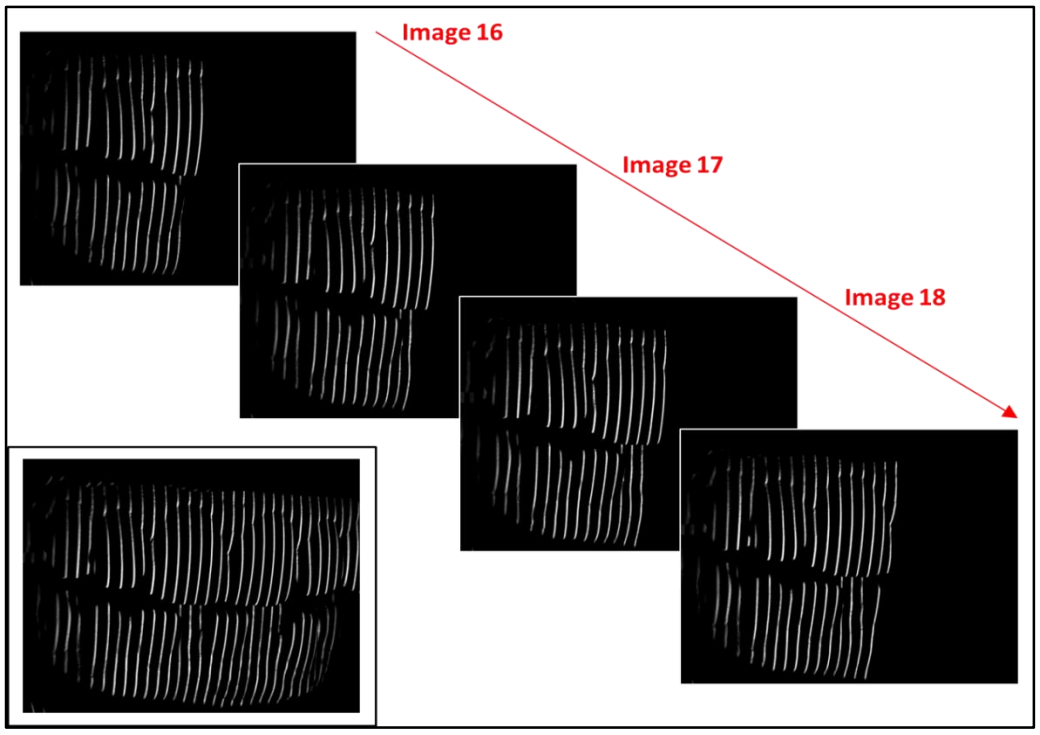


**Figure 65 Example of the Jailbar 'Build' Images, Observed by the Left Stereo Camera.** A sample of 4 sequential images are shown (diagonal), taken from the middle of the build process. The upper right central incisor can be seen increasingly clearly as more stripes are added to the image. The inset (lower left) shows the fully built image, consisting of 34 projected stripes in total. At this point, the image is 'built', with all stripes indexed. 3D data capture can now commence.

Upon completion of the ‘build’, a further sequence of images can be recorded. The projector continues to project the static (full) jailbar pattern, consisting of all 34 stripes, whilst the stereo cameras collect images. Again, the frame rate must be sufficient to the software doesn’t lose track of the stripe indexing between any two frames. These ‘post-build’ images should provide sufficient data for 3D reconstruction.

It should be noted that the method will not produce sufficiently dense data to reconstruct the observed labial segment. Rather, it will be relying on the existence of the previously scanned dentition (via a model scanner or intra-oral camera), upon which to map the sparse, but precise, 3D jailbars.

It is postulated that by sampling from a sufficiently large volume (as before, from approximately left canine to right canine in both arches), the alignment of the two pre-existing dense 3D models of the dentition to the jailbar labial bite scan will be as true and precise as the optimal sine wave scanning patterns.

## 7.3 Experiment : Precision of Optical Interocclusal Records Using a One-Shot Technique

### 7.3.1 Outline of Aims

- To test the proposed one-shot method outlined in Section 7.2 to determine its precision *in vitro,* when recording mandibular excursive positions
- To perform a pilot assessment of the precision of interocclusal records *in vivo*

### 7.3.2 Objectives

- To assess the precision using standard deviation in the location of three reference points as an indicator
- To assess precision of optical interocclusal records using dental study models and using a single live subject

### 7.3.3 Method

A 3D-video recorder was constructed using a DLP projector (Vivitek Qumi Q5, Vivitek Corporation, Hoofddorp, NL) and two CMOS cameras (uEye 1240LE, IDS

imaging, Obersulm, Germany). The projector was fitted with a macro lens, to shorten the focal length, allowing a field of view projection width of 60mm and height 40mm. Due to the size of the projector body, the stereo camera pair were offset slightly, above the projector at an angle of 30 degrees (Figure 66).

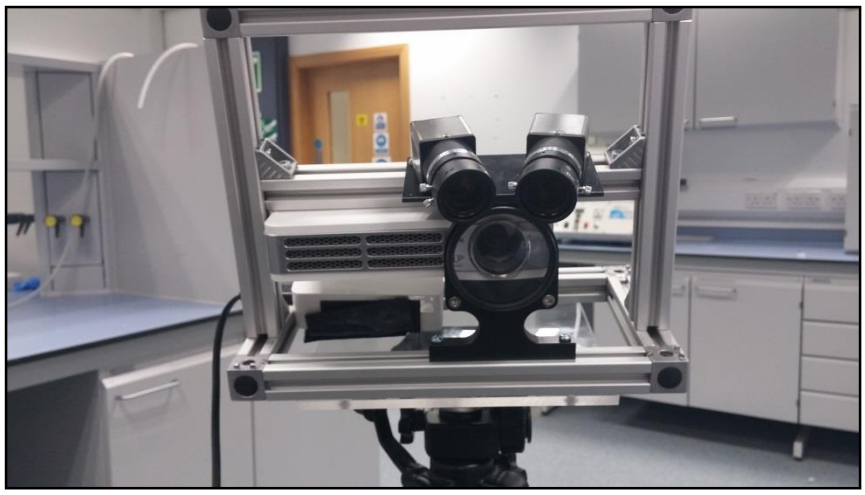

**Figure 66 The 3D Video Scanning Apparatus.**

Calibration was achieved using an asymmetric circles pattern grid, as in previous experiments. However, this grid was chrome etched on a glass slide (rather than printed on paper), using a stereo-lithographic technique (Micro Lithography Services Ltd, Chelmsford, UK). The precision of this process is reported to be 0.8µm.

Software was written to encode, project, capture and process jailbar patterns, as previously described in Section 7.2. This enabled ‘contour lines’ of the scanned object to be recorded in a single exposure (following a ‘build’ period of just over 1 second). In fact, following the build phase, the software allowed for a ‘free running’ 3D video capture mode. This captured individual frames (of exposure 1/60$^{th}$ second) at a frame rate of 15fps.

Each frame captured a field of view covering the upper and lower labial segment (approximately 60mmx40mm, typically covering the upper and lower canines and incisors).

In summary, following the one second pattern build phase (where small movements of the patient were irrelevant), the system captured a full interocclusal record every 1/15$^{th}$ of a second. The equipment cost was less than £1000.

Ethical approval advice was sought from the Leeds School of Dentistry DREC panel. For this pilot study, formal approval was not considered necessary by the panel.

Alginate impressions (Xantalgin, Heraeus Kulzer GmbH, Hanau, Germany) in stock disposable trays (Unodent Disposable Impression Tray, Unodent, Witham, UK) were taken of a 41 year old male subject with intact dental arches, missing only the upper third molars, and no history of TMD. Dental plaster models (Dental Plaster, John Winter, Halifax, UK) were poured within 4 hours of taking the impressions. The models were positioned in an anterior protrusive position, giving a clearly observable set of contacts (two incisors and bilateral molars).

Two seconds of 3D-video was recorded of the labial segment, yielding thirty optical interocclusal protrusive registrations. During the two second scan, the models were carefully moved continuously within a 2mm envelope (whilst maintaining their relative positions) to simulate a patients involuntary head movements. This was achieved by having the models positioned on a flat tray of Perspex which could be hand held and gently swayed, without toppling the models.

The models were then positioned in a left lateral excursive position , again ensuring clearly visible contacts (left canines, second premolar and bilateral molars) and two seconds of 3D-video was used to record thirty lateral registrations.

The ‘live’ subject was also recorded. The subject manually retracted their lips and a coating of intra-oral scanning powder (CEREC Optispray, Sirona Dental Systems, Salzburg) was applied to the labial segments. The subject was positioned into a slight open bite by biting on a small block between their molars. This led to a 4mm incisal separation, and stabilised the upper and lower dentition from moving. Twenty-nine occlusal registrations were obtained using two seconds of 3D-video scanning.

All scans were performed under ambient room lighting. This was possible because the aperture of the cameras was very small, being set to the lowest possible F-stop (16). This meant only the brightly illuminated stripes were visible in the image.

In total, 89 bite registrations were obtained, with 30 representing the protrusive excursive position on the stone models (PM), 30 being the left lateral excursive position on the stone models (LM), and 29 ‘live’ open registrations (OL).

The stone models were digitized (ArKive Dental, Ripon, UK) to create dense ‘point clouds’. These models were aligned to all 89 occlusal registrations as follows.

Firstly, an initial manual guess was supplied for the protrusive models (PM) by aligning the digital models to the first bite scan using Meshlab

(http://meshlab.sourceforge.net/). The transformation matrices required to move the upper and lower models into this rough alignment were saved. This process was repeated for the first scan of the lateral excursive model set (LM), and then for the live subject (OL). In this way, three initial guesses were created (Figure 67).

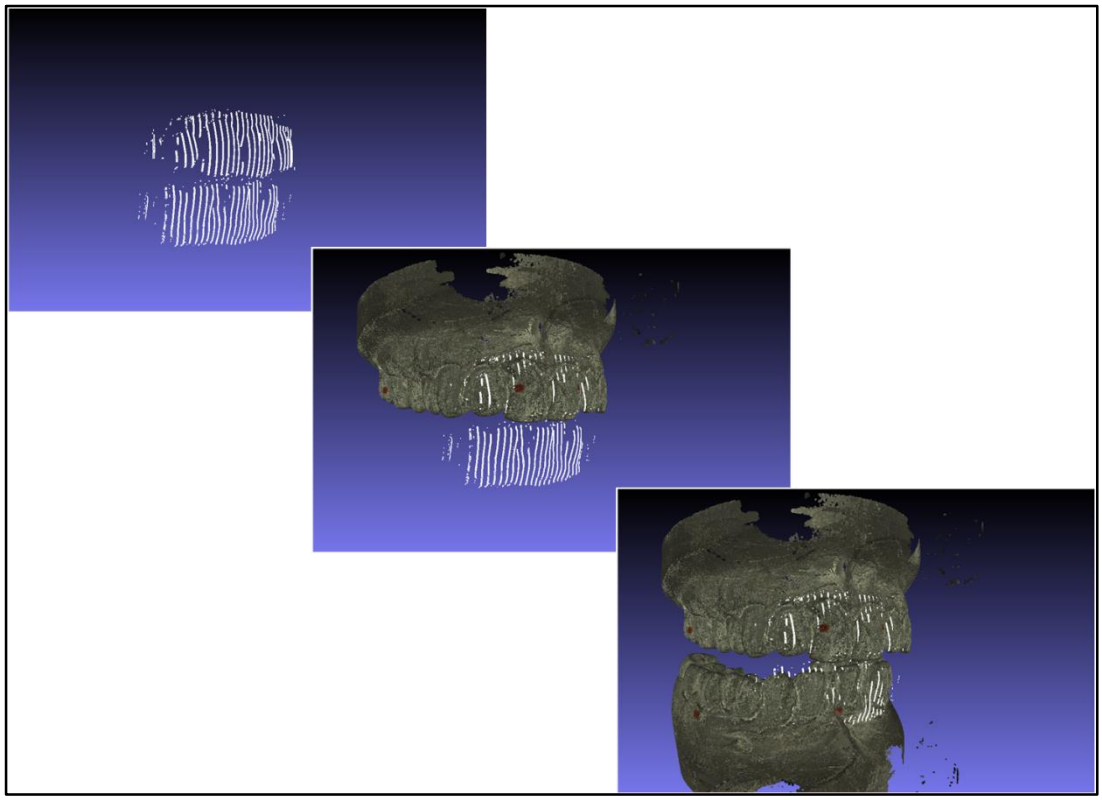

**Figure 67 Initial 'Rough' Alignment of a Jailbar Bite Scan to Dense Point Clouds of the Dental Models.** The upper and lower models are manually aligned in Meshlab, to within a few mm of the correct position. The transformation is saved and provides the initial guess for the custom-written alignment software. A gap between the last standing molars (which are in contact on the stone models) is clearly visible.(Protrusive models shown, PM).

Next, custom software was written using C++ and the PointCloudLibrary (http://pointclouds.org), which iteratively refined the alignment of the digital models, starting from the initial guess to produce a final alignment using the Iterative Closest Point method (Besl & McKay 1992) (Figure 68). The software saved the final transformation matrices, and also passed this alignment on to the next bite scan in the sequence. The models were then aligned to this second scan, using the alignment found in the previous scan as the initial guess. This process was repeated until transformation matrices had been generated for all the bite scans in a particular sequence.

This fine alignment procedure was run three times, once for each of the three sets of scans (PM, LM and OL).

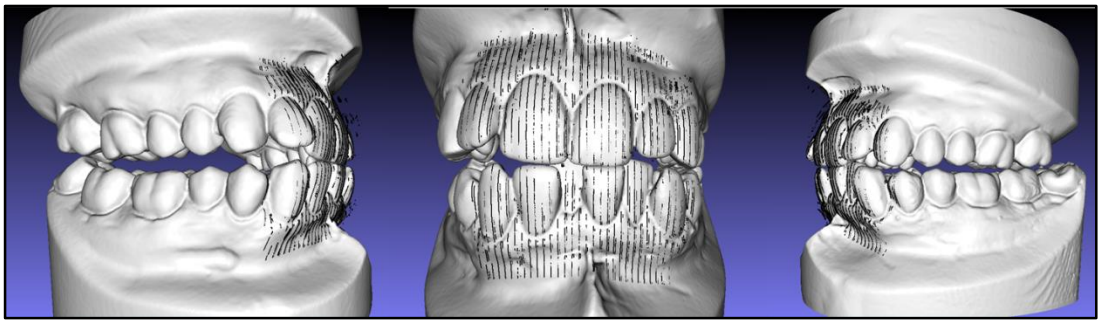

**Figure 68 Fine Alignment of the Models to the Jailbar Bite Scan.** The initial guess (taken from Figure 67) has been processed in the custom software to produce the final protrusive bite registration for one of the 'PM' alignments. For clarity, surfaced models are shown, but in reality the software used dense point clouds (which contain the raw scan data). The gap between the last standing molars has now been corrected.

Finally, custom software was written which loaded these transformation matrices, aligned the upper model to a standard frame of reference (with antero-posterior along the z axis, and the plane y=0 considered horizontal), and then aligned the lower model using the bite registration. In this way, the absolute location of three reference points in the lower model (lower right central incisal tip, LR1, and lower left and right second molar mesio-buccal cusp tips, LL7 and LR7), could be compared directly between bite registrations. Precision was assessed by comparing the variation in distance between these reference points. Differences between the mean variation in reference point location were tested using Friedman's two-way analysis of variance by rank. These were used to test for differences within each group (eg differences between the anterior and the posterior reference point variations) and to test for differences between the groups (eg differences between reference point variation between PM, LM and OL).

The trueness of the 'model' scans was assessed by visually comparing the digital and actual contact points, for the two sets of stone model bite scans (PM and LM). This was readily possible because PM and LM had both been positioned in such a way as to produce easily visible cusp tip contacts around the arch. Each set of aligned surfaced models were loaded into Meshlab and a proximity search performed, considering contacts at two thresholds of separation, 75µm and 150µm. An example of the contact points on a left lateral excursion upper model is shown in Figure 69. The locations of these points was noted for each of the model scans (PM and LM), as either present, or absent, for each tooth.

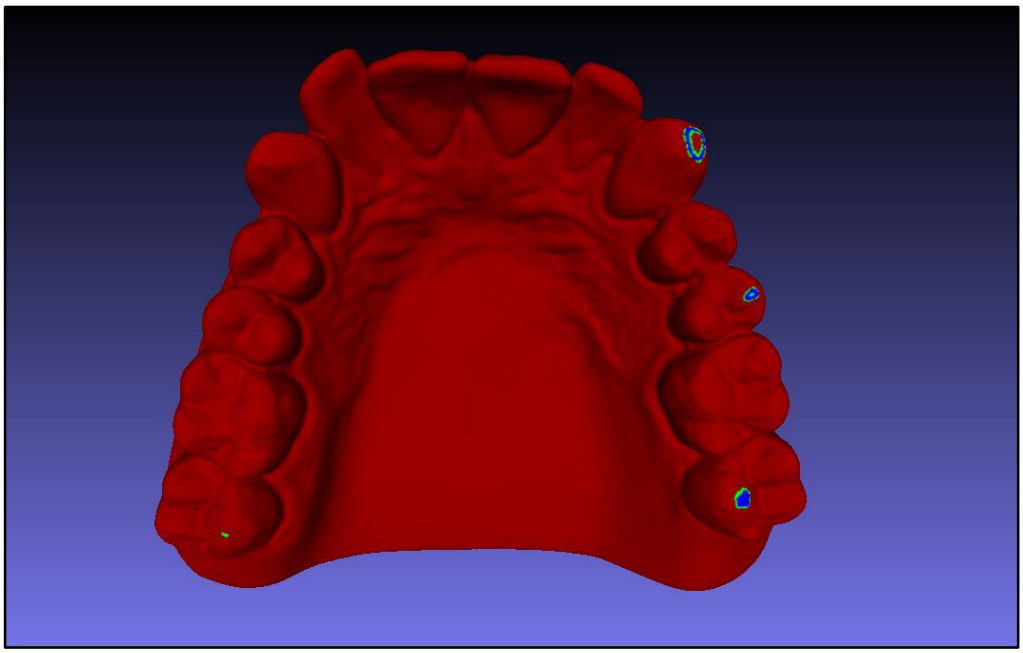

**Figure 69 Visual Assessment of Contact Points.** Contacts within 75µm are labelled in blue, and contacts within 150µm are labelled in green.

### 7.3.4 Results

#### 7.3.4.1 The Data

The scanned models contained between 1.3 and 1.5 million points each.

The bite registration scans of the models typically contained between 50 and 60 thousand 3D points, whilst the scans of the live subject contained 30 thousand 3D points. The number of points in the bite scans decreased as the video frames advanced, with the last frame in a sequence yielding less data than the first (Table 4).

| | Number of 3D Points in First Bite Registration | Number of 3D Points in Last Bite Registration | % Loss of 3D Data of the Capture Sequence |
|---|---|---|---|
| **Protrusive Model, PM (30 frames)** | 56,248 | 51,908 | 7.7 |
| **Lateral Model, LM (30 frames)** | 66,462 | 61,258 | 7.8 |
| **Open Live, OL (29 frames)** | 32,200 | 30,268 | 6.0 |

**Table 4 The Amount of Raw Data Captured With Each 3D Scan.** The number of points captured in each individual scan decreased as the software 'lost track' of some of the edges of the jailbars during the two second video.

Examples of aligned bite registrations for PM, LM and OL are shown in Figure 70 to Figure 74. (See Appendix B for more example scans).

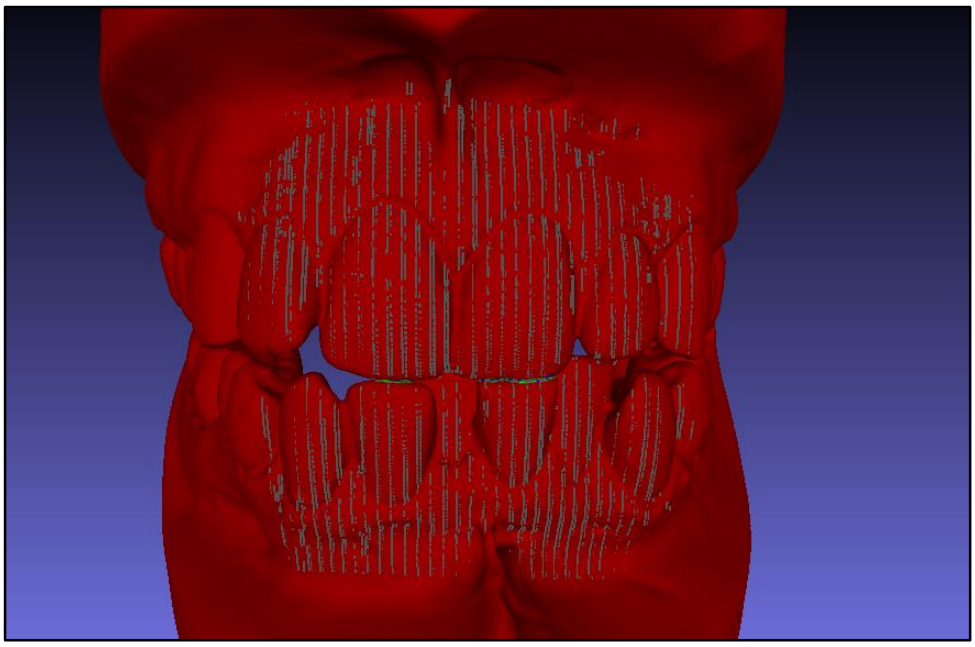

**Figure 70 Example of a Protrusive Model (PM) Bite Registration.** The 20th registration in the sequence of 30 is shown above, along with the fully aligned models. The jailbar pattern extends from the UR2/LR3 region across to the UL3/LL3 region. The gingival margins and beyond are captured in both arches. The bite registration does not extend to the model base.

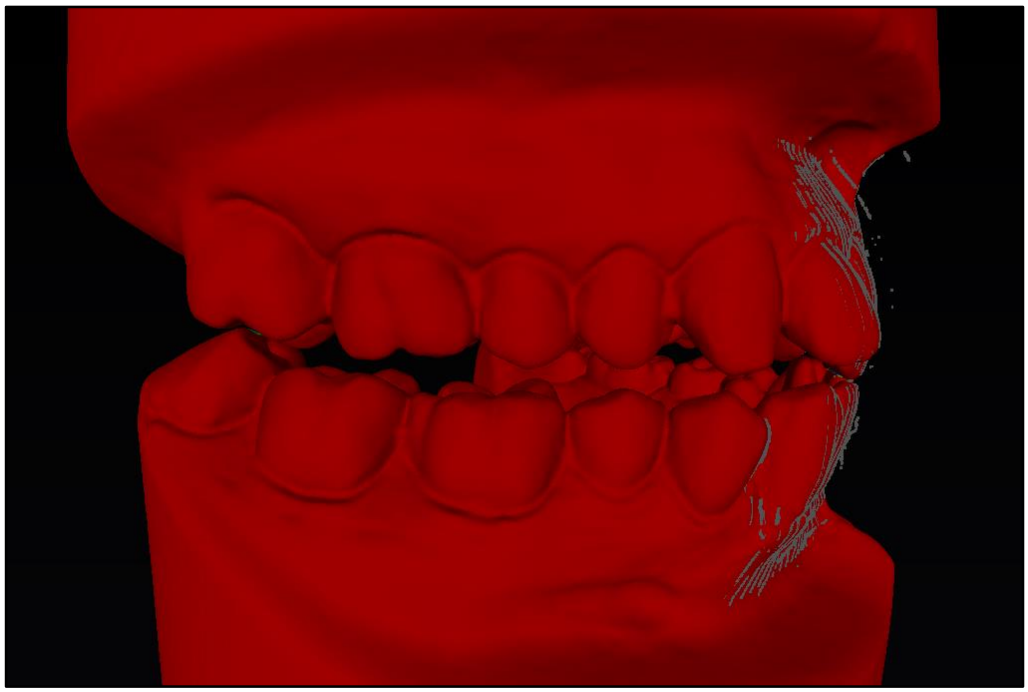

**Figure 71 Protrusive Model (PM) Registration Viewed from the Side.** The same bite registration as Figure 70, viewed from the side. Some noise in the jailbar pattern is visible (background has been blackened to enhance the view). These noisy data represent incorrectly identified stripes, and consequently, 'shifted' 3D locations. Such points do not contribute to the final model alignment.

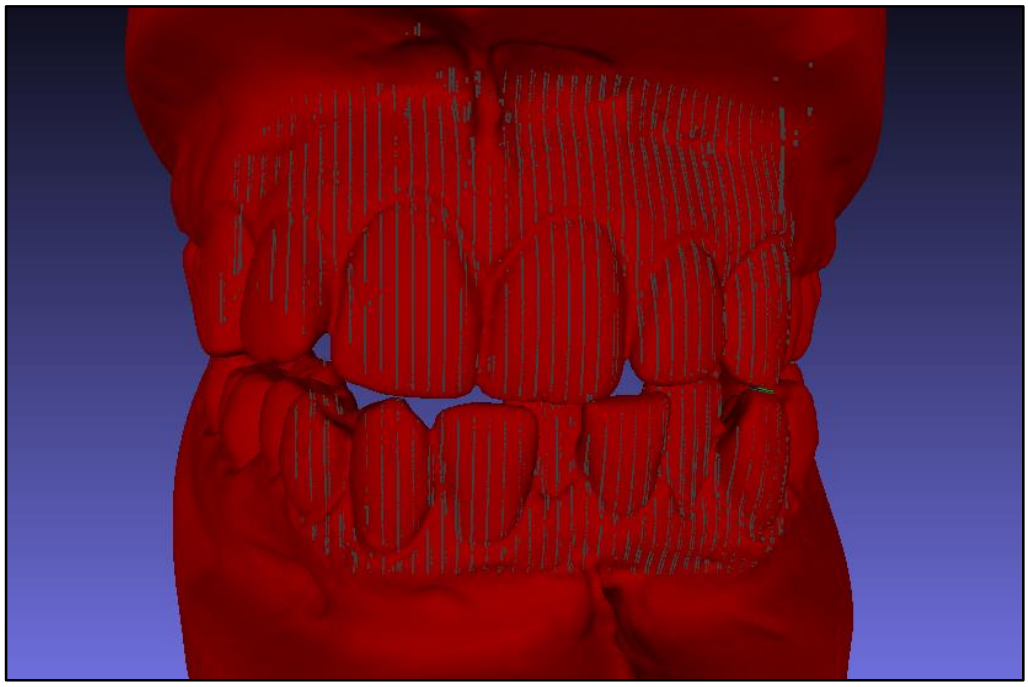

**Figure 72 Example of Lateral Bite Registration on Model (LM).** The 20$^{th}$ bite registration in the sequence of 30 is shown. The jailbar pattern captured the labial region from canine to canine, even capturing a good proportion of LR4.

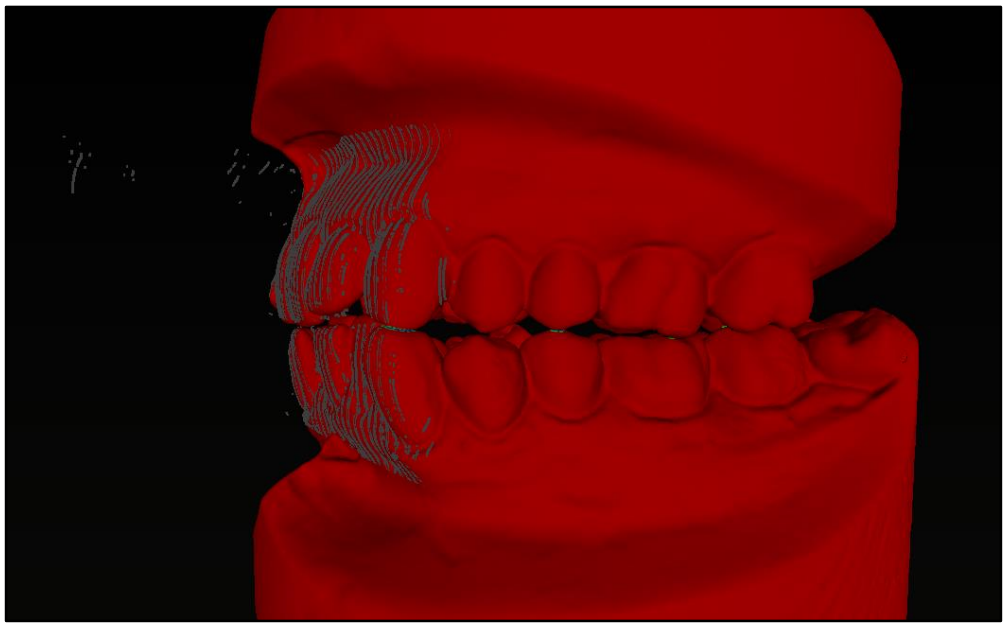

**Figure 73 Lateral Bite Registration Viewed from the Side.** The same registration as shown in Figure 72. Noise is clearly visible in the jailbar scan, but the vast majority align accurately with the model.

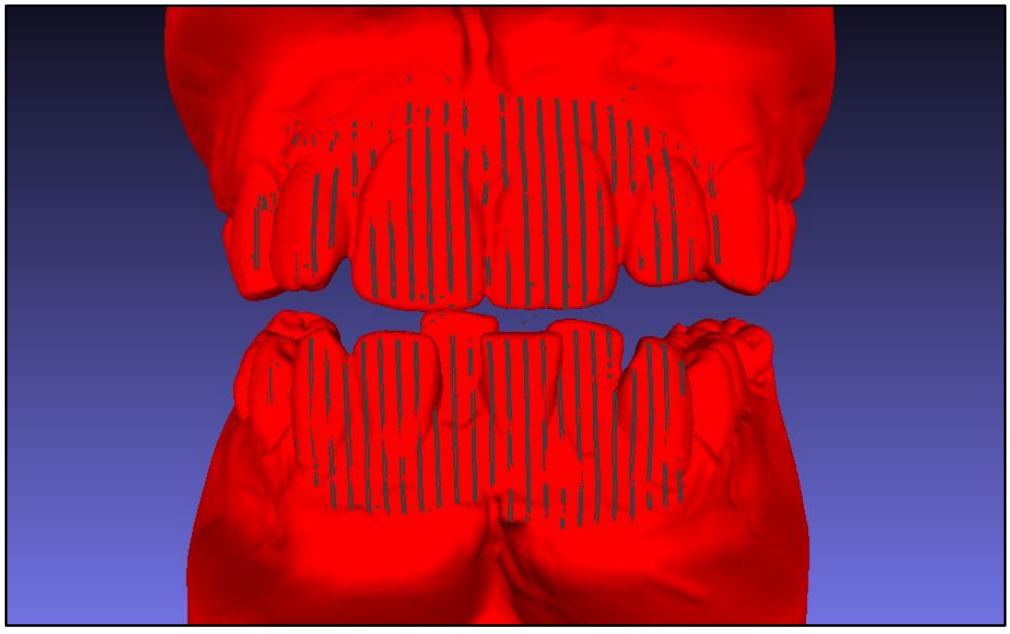

**Figure 74 Example of Live Bite (OL).** The 20$^{th}$ bite registration is shown, viewed from the front. The subject was biting on a small prop posteriorly to ensure the teeth remained stable throughout the 2 seconds of bite registrations. A 3-4mm separation at the incisal level is evident.

### 7.3.4.2 Precision of Reference Point Location

The precision in position of each reference point over each sequence of bite registrations is shown in Table 5. For example, when considering the position of the lower incisor reference point (LR1) for OL, the following can be said; the absolute distance between the position of LR1 taken from any single bite registration and the mean position (taken from all 29 registrations), will average 31 micrometres, with a standard deviation of 10 micrometres.

| | Protrusive Model (PM) | Lateral Model (LM) | Open Live (OL) |
|---|---|---|---|
| LR7 Reference | 79 ± 53 µm | 78 ± 44 µm | 70 ± 36 µm |
| LL7 Reference | 43 ± 20 µm | 123 ± 89 µm | 65 ± 31 µm |
| LR1 Reference | 30 ± 21 µm | 45 ± 24 µm | 31 ± 10 µm |

**Table 5 Variation from the Mean in the Magnitude of Displacement of Each Reference Point.** Each value is expressed as the mean radius of error ± standard deviation.

Distribution of the Data

Q-Q plots, created using SPSS (Armonk NY: IBM Corp) for all the reference point data are shown in Appendix C. With the exception of the LR1 reference point for the OL scans, the data was not normally distributed. Non-parametric statistical tests were indicated.

Comparisons Within Each Group of Bite Registrations

The Wilcoxon Signed Rank Test was used to look for differences within each group.

In OL, the LR1 differed significantly from both LR7 and LL7 ($p<0.01$). There was no significant difference between LR7 and LL7 ($p=0.699$).

In PM and LM, the variation in all three reference points differed significantly ($p<0.01$).

Comparisons Between Each Group of Bite Registrations

The variation in each specific reference point location between sets of scans was compared using Friedman's two-way analysis of variance by rank. The LR1 and LR7 reference points showed no significant variation, regardless of the type of bite registration (PM, LM or OL). However, the LL7 reference point showed significant variation between PM, LM and OL ($p<0.001$).

Scatter plots are shown in Figure 75 to Figure 83, plotting the distribution of the reference points for each sequence. In all cases the distributions have been centred about the origin for ease of comparison.

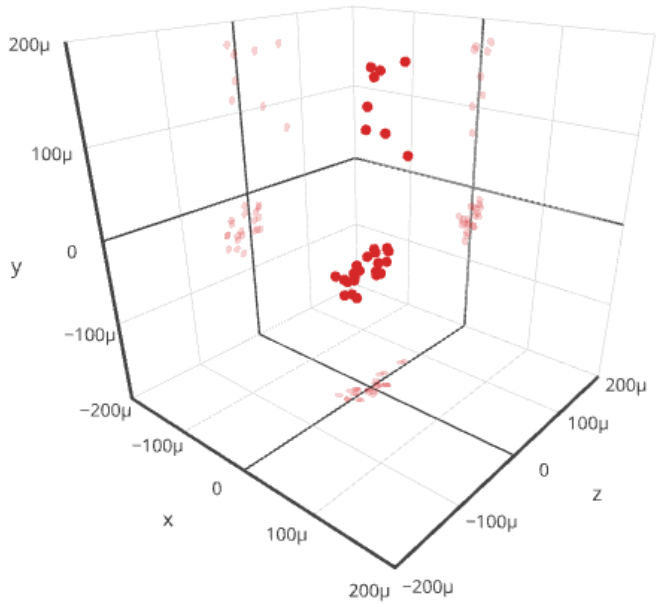


**Figure 75 Variation of LR7 Reference Point Location Over 30 Protrusive Bite Registrations (Sequence PM).** The plane y=0 is horizontal, with the z-axis denoting 'depth' and x-axis left-right.

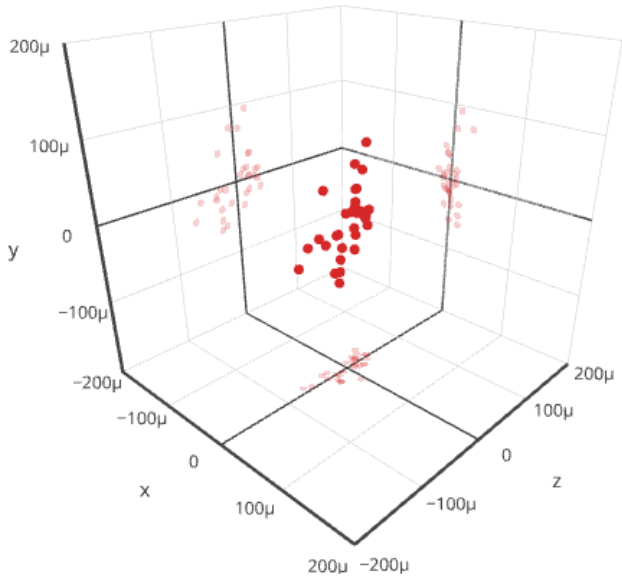


**Figure 76 Variation of LL7 Reference Point Location Over 30 Protrusive Bite Registrations (Sequence PM).** The plane y=0 is horizontal, with the z-axis denoting 'depth' and x-axis left-right.

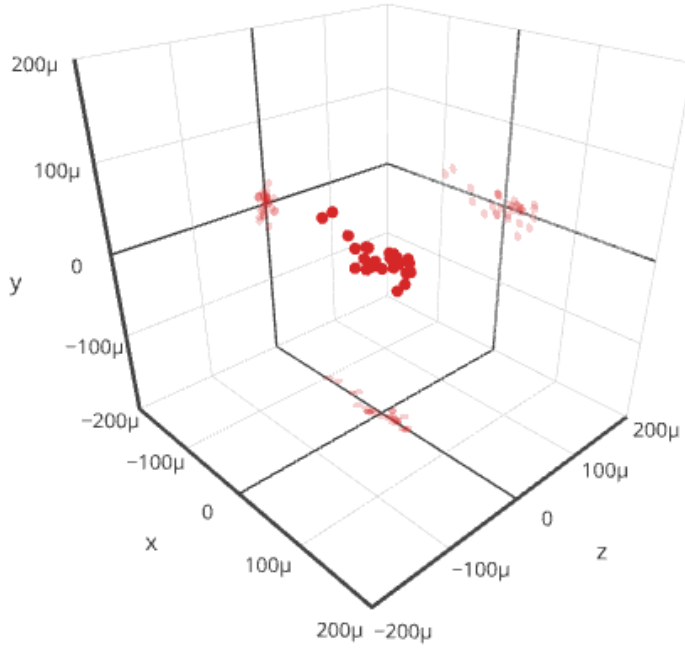


**Figure 77 Variation of LR1 Reference Point Location Over 30 Protrusive Bite Registrations (Sequence PM).** The plane y=0 is horizontal, with the z-axis denoting 'depth' and x-axis left-right.

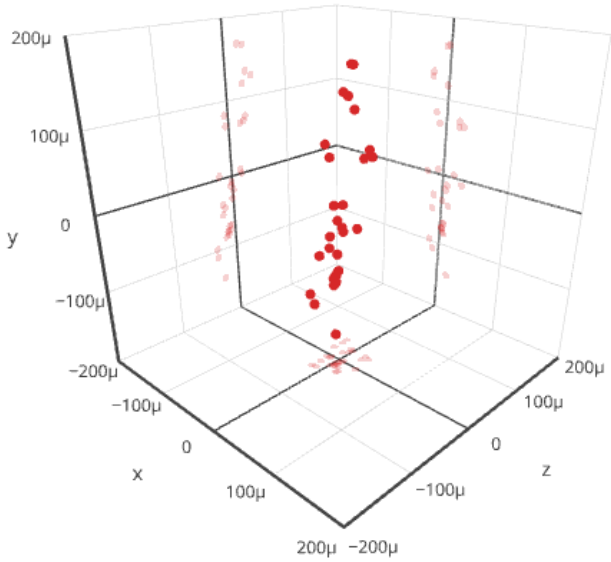


**Figure 78 Variation of LR7 Reference Point Location Over 30 Lateral Bite Registrations (Sequence LM).** The plane y=0 is horizontal, with the z-axis denoting 'depth' and x-axis left-right.

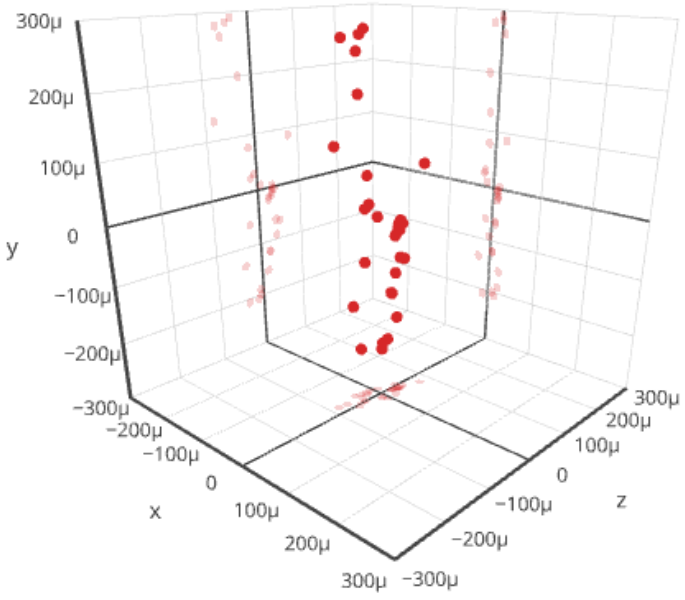


**Figure 79 Variation of LL7 Reference Point Location Over 30 Lateral Bite Registrations (Sequence LM).** The plane y=0 is horizontal, with the z-axis denoting 'depth' and x-axis left-right. (Note the larger scale compared to the other figures).

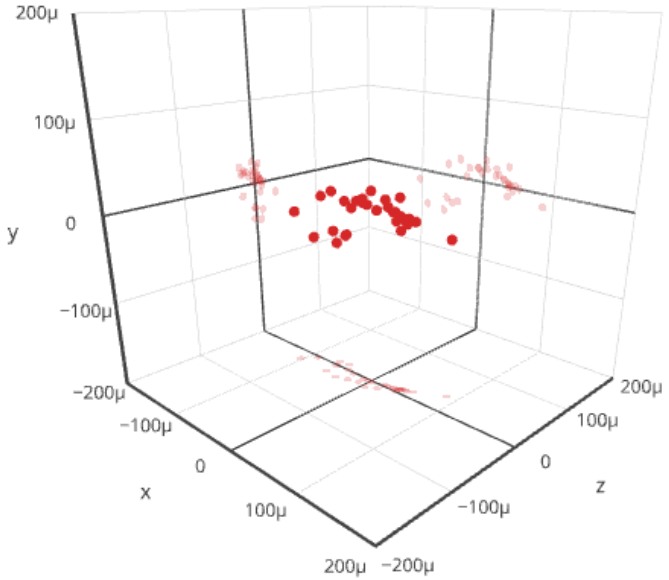


**Figure 80 Variation of LR1 Reference Point Location Over 30 Lateral Bite Registrations (Sequence LM).** The plane y=0 is horizontal, with the z-axis denoting 'depth' and x-axis left-right.

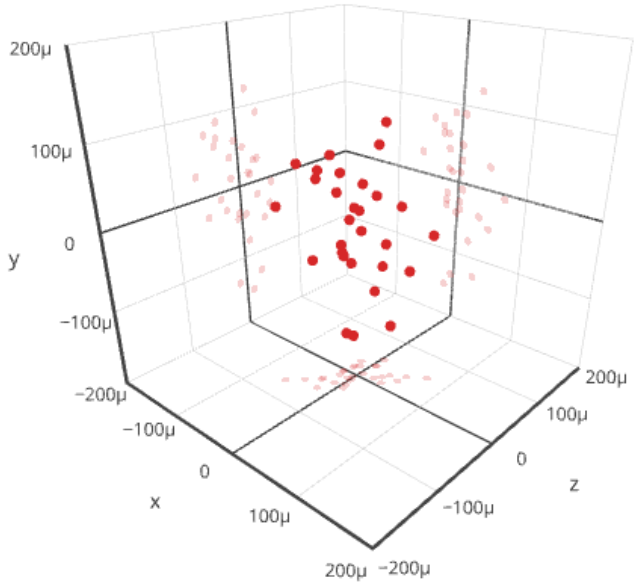


**Figure 81 Variation of LR7 Reference Point Location Over 29 Open Bite Registrations (Sequence OL).** The plane y=0 is horizontal, with the z-axis denoting 'depth' and x-axis left-right.

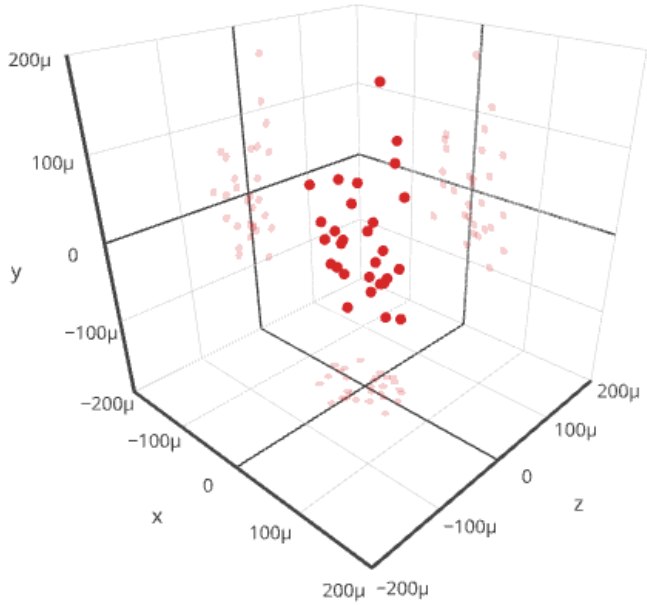


**Figure 82 Variation of LL7 Reference Point Location Over 29 Open Bite Registrations (Sequence OL).** The plane y=0 is horizontal, with the z-axis denoting 'depth' and x-axis left-right.

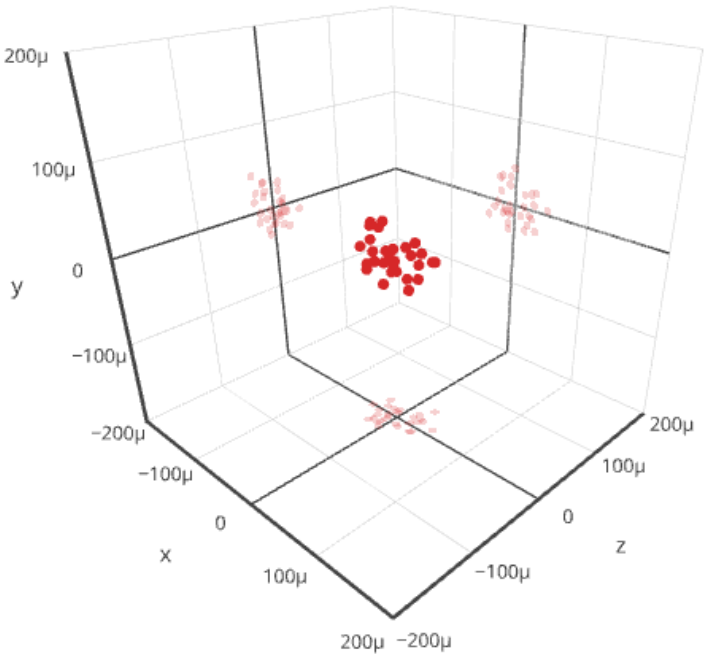


**Figure 83 Variation of LR1 Reference Point Location Over 29 Open Bite Registrations (Sequence OL).** The plane y=0 is horizontal, with the z-axis denoting 'depth' and x-axis left-right.

In all cases the mean variation was lower for the anterior reference point than for the posterior reference points.

### 7.3.4.3 Trueness of Occlusal Contacts

For the two sets of model scans (PM and LM), the models had been positioned such that the contact points were known. Over the 30 bite registrations for each, the percentage success in recording known contacts (sensitivity), and the percentage of occurrences of incorrect contacts (false positives) are shown in Table 6 and Table 7. Examples of the contacts visible on the digital models are show in Figure 84 and Figure 85.

| Contact Distance Threshold | Location of Tooth Contact | | | | |
|---|---|---|---|---|---|
| | UL1/LL1 | UR1/LR2 | UR7/LR8 | UL7/LL7 | UL1/LL2 |
| 75 µm | 100 | 90 | 73 | 13† | 0 |
| 150 µm | 100 | 100 | 73 | 73 | 53 |

**Table 6 Protrusive Model Contact Points.** Over the 30 registrations, the percentage of correct (green cells) and incorrect (red cells) contact points are shown for the two different distance thresholds. †On one occasion, a digital contact was recorded on the lower tooth, but not on the upper tooth.

| Contact Distance Threshold | Location of Tooth Contact | | | | |
|---|---|---|---|---|---|
| | UL3/LL3 | UL5/LL5 | UL7/LL7 | UR7/LR8 | UL6/LL6 |
| 75 µm | 100 | 100 | 80 | 10 | 27 |
| 150 µm | 100 | 100 | 87 | 63† | 50 |

**Table 7 Lateral Excursion Contact Points.** Over the 30 registrations, the percentage of correct (green cells) and incorrect (red cells) contact points are shown for the two different distance thresholds. †On one occasion, a digital contact was recorded on the lower tooth, but not on the upper tooth.

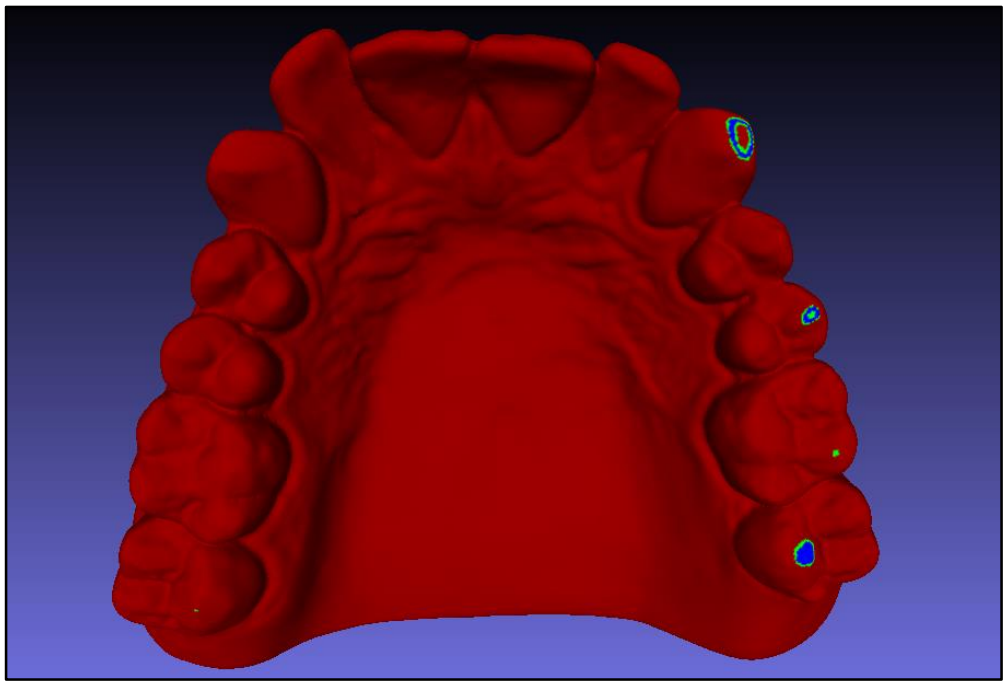

**Figure 84 Example of Upper Model Contact Points for Lateral Bite Registration (LM).** Blue contact points are within 75µm, whilst green contact points are within 150µm. This example shows registration number 20 out of 30. The UR7 contact is only correctly identified at the 150µm threshold, whilst a false positive on UL6 is also present at this threshold.

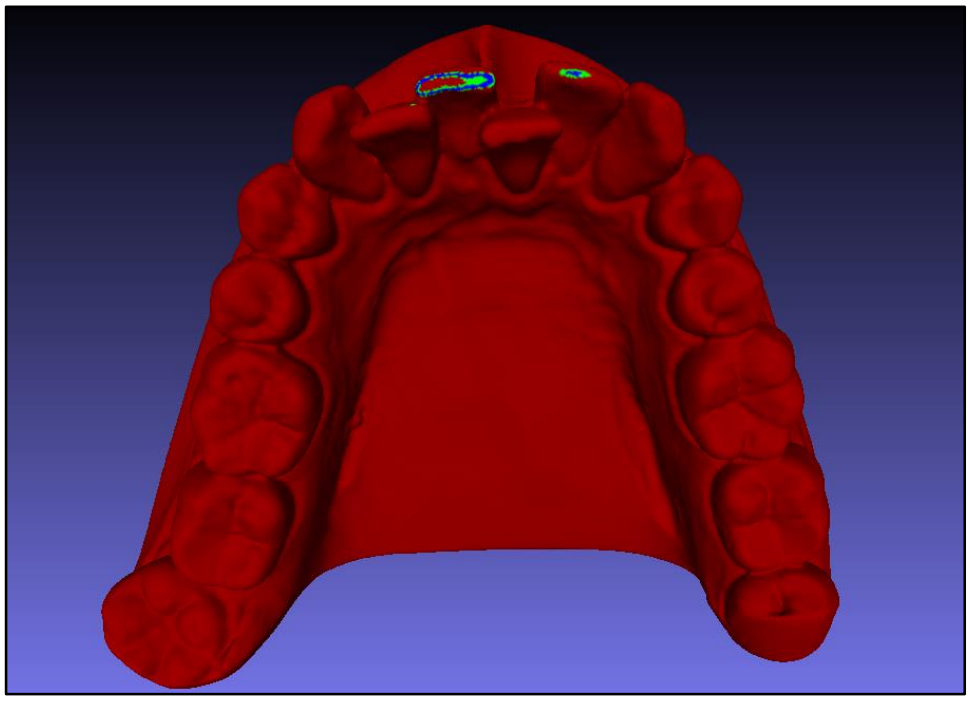

**Figure 85 Example of Contact Points on Lower Model from a Protrusive Registration (PM).** The 10$^{th}$ registration from the sequence of 30 is shown. Neither molar contact is recorded (both contacts were >150 µm apart). A false positive is just visible on the LL2, caused by a 150µm proximity to the palatal surface of UL1.

### 7.3.5 Discussion

#### 7.3.5.1 Hardware Improvements

In comparison to the previous experiments (Section 5 and Section 6), the projector used here had a higher resolution (native 1280x1024 pixels) and a greater light intensity output (500 lumens). These enhancements may help to improve the signal to noise ratio of the scanner. This is important because the static pattern being projected is less robust to noise than the phase shifting pattern. It is hoped that some compensation for this loss of fidelity is provided by the improved hardware. These improvements could be tested robustly against the older system, although logistically this is difficult because the cameras were recycled for use in both systems. For the present, it is considered satisfactory to look at the overall performance of the whole system. Future work may be directed at identifying, and improving, individual technical aspects.

The calibration target was also improved by having a high quality pattern etched on a glass slide. The pattern is the same as has previously been used (meaning no changes were needed to the calibration software), but now the precision of the 'printing' is below 1µm, and the absolute flatness of the target is assured. There is a cost implication though – the target was over £200, compared to effectively zero cost for the printed target. Furthermore, static targets such as the glass slide, with limited calibration features, have been shown to produce inferior results compared to 'active calibration targets' (Schmalz et al. 2011). Future work should therefore be directed at enhancing the calibration method of the system. Ideally, the cost should be decreased too, since glass targets are prohibitively expensive.

It would have been interesting to compare these results with those obtained using this hardware and the sine wave phase shifting scanning patterns. However, given that the current experiment simulated patient movement over the 2 seconds of recording, it would be difficult to do a like for like comparison, since the models would have to remain absolutely still during any phase shift scan. As previously mentioned, scanning a live subject would not be possible as the patient is likely to undergo some movement during the scan.

### 7.3.5.2 Stripe Indexing and Stereo Correspondence

The method by which the index of individual stripes are identified (by comparing to the previous frame and updating a running tally of stripe indices) seems partially effective. A clear pattern emerged in all cases, where less points were correctly identified, as the frame number increased. Factors such as image sensor noise, 'hot pixels' and anomalies such as 'double stripes' (where a single stripe passes through a small crevice and is counted by the software as 2 stripes) will all accumulate to produce lower quality scans as the sequence progresses.

More seriously, as soon as a stripe is incorrectly indexed, this error will propagate down the sequence of later frames.

Incorrectly identified stripes cause a step error in 3D calculation. For example, if stripe 2 in the left image is mistakenly paired with stripe 3 in the right image, the 3D depth location will be incorrect by about 2mm (Figure 86).

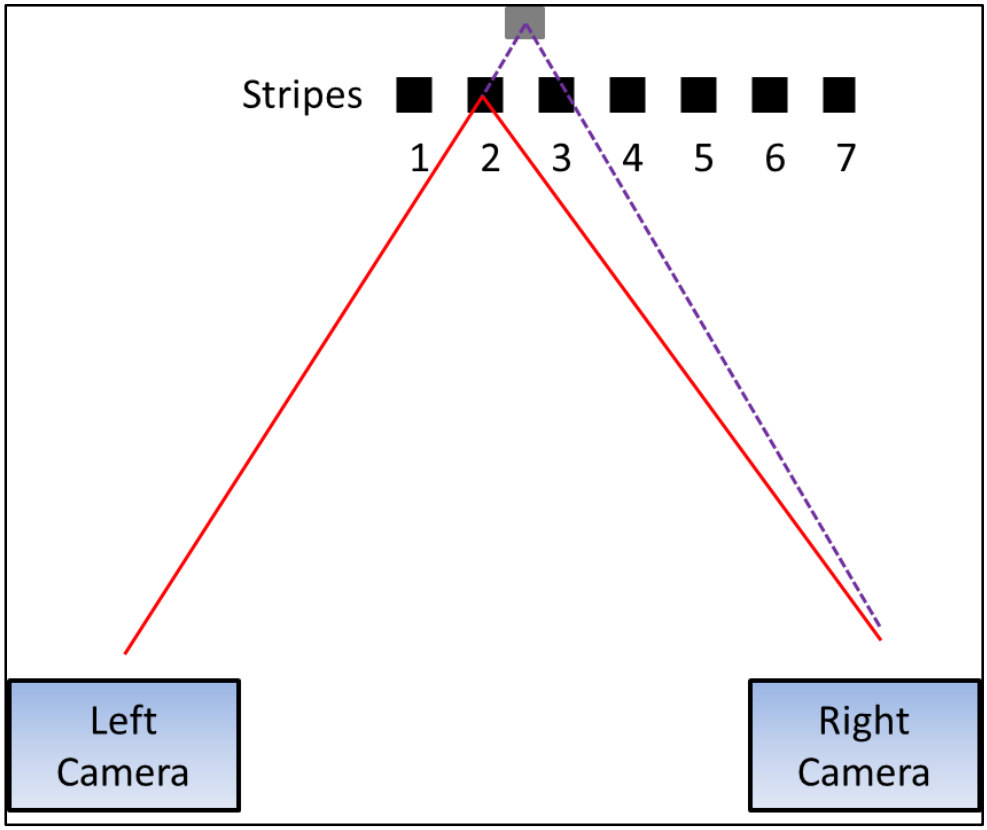


**Figure 86 Step Error in 3D Calculation Caused by Incorrect Stripe Indexing.** Top view of a jailbar pattern. The correct 3D location of stripe 2 is calculated by triangulating the red lines from the stereo cameras. If a stripe index from the left image is paired with the wrong index in the right image, a step error in the calculated 3D position will result (purple dotted lines).

The iterative nature of the alignment algorithm will ensure that these grossly misplaced points will not contribute to the quality of the eventual alignment. They will not 'pull' the alignment in their direction because any grossly distant points are ignored during the latter stages of alignment.

However, they do decrease the quantity of valid 3D measurements, and it is reasonable to assume that with less input data, the output alignment may deteriorate.

Future work should be targeted at improving the robustness of the stereo correspondence algorithm. Given the need to use a one-shot pattern (and the inherent deterioration in stereo matching robustness compared to the standard phase shifting technique), this seems like a sensible avenue for investigation.

It is interesting to note that all digital intra-oral bite registration techniques operate by recording a 3D bite scan (such as employed here). They all create the 3D bite scan with the same level of noise as their dental arch scans, and unlike the proposed method, also often include errors from aligning multiple small scans to create the bite scan. This means they are using a warped and smoothed bite registration to align the digital models.

The quality of the bite registration scan could be improved by taking advantage of the *a priori* knowledge that must exist – namely, the 3D data for the upper and lower dental arches. Any bite registration must be paired to dental models in order to be of any use! Given that these models exist, the stereo matching algorithm could be supplied with information about the shape of the object it is *expecting* to calculate, and the correspondence search could be refined in this way. This approach has been used for 3D facial scans (Aissaoui et al. 2012) and more recently, to solve the difficult problem of 3D mapping for self-driving cars (Güney & Geiger 2015). Here, the authors solve the problem of mapping relatively featureless, flat surfaces (the painted bodywork panels of cars) by providing the stereo matching algorithm with models of what a car might look like. They show that this approach currently ranks top in the KITTI benchmarking system for machine vision stereo correspondence (Geiger et al. 2012). The dental problem is not dissimilar in that it is trying to match the smooth and relatively featureless surfaces of incisors and canines. The stereo algorithm could be supplied with not only a generic model of what a set of teeth might look like, but the *actual* model of that patient's teeth. This would be an improvement on the self-driving car work, akin to knowing exactly which car is on the road in front of you, including any dents and

rust in the bodywork. This is certainly an avenue to explore in future work as, to the authors knowledge, the dental field has not yet adopted this novel approach.

#### 7.3.5.3 The Distribution of the Data

Unlike the experiment in Section 6, the data was generally not normally distributed. There are two stark differences in the methodology. Firstly, the bite scans here consisted of much less data – a series of precise stripes, rather than a full coverage cloud. Secondly, the alignment algorithm used (Iterative Closest Point) differed from the Normals Distribution Transform (NDT) method previously employed. The reason for the difference was technical – the sparse stripes do not provide enough data to create the discrete probability density functions required in NDT. This subtle difference may be the cause of the change in data distribution. Aligning points to points, rather than points to probability functions, discretises the alignments and will cause 'step jump errors' in alignments rather than smooth continuous errors.

A possible solution would be to create denser scans to allow the NDT algorithm to be used. Or the labial scans could be aligned to *surfaced* models, seeking the closest point on the surface of the target model, rather than the closest point in the point cloud. The latter would rely on the creation of extremely true and precise surfaced models, which in itself is difficult because surfacing involves an averaging (or smoothing) process.

#### 7.3.5.4 Live Scan Data vs Model Scan Data

The OL scans only captured around half the number of data points, compared to PM and LM. When viewing the data this can be explained by the tendency for the live scans to capture less of the vertical height of the gingivae – generally around 2mm of gingival extension compared to 5 or 6mm for the model scans. This may be due to the lack of sufficient lip retraction (the subject simply parted their lips), and shadowing from the lips obscuring the cameras view of the gingivae. This could be improved with the use of cheek retractors.

However, the theoretical simulations (Section 3.4.3) suggested that capturing a vertical area such that 1 or 2mm of gingivae were scanned in both arches, would give sufficient trueness. The results of the variability study showed no significant difference between OL and PM or LM when considering two of the three reference points (LR1 and LR7). This is in agreement with the simulation model, which

predicts limited benefit when extending the scan area vertically, so long as about 10mm of height in each arch has been captured.

In addition, the powdering may have improved the contrast and definition in the intraoral scan, compared to less well defined morphology on the un-powdered stone models.

This explains the counterintuitive result that, despite only capturing about half the amount of data, the live scans (without lip retraction) show no significant deterioration in their ability to align the dental arches.

Of note, the third reference point (LL7) showed significant variation amongst the different scans, but the OL scan significantly outperformed LM. This is a further indication that the lower yield in data points for OL did not impair the quality of the bite registration alignments.

#### 7.3.5.5 Precision of Reference Point Location

The results indicate that the anterior reference point showed significantly less variation than either posterior reference point in all cases. In addition, for OL, there was no significant difference between the LL7 and LR7 variation. For PM and LM, the posterior reference points differed significantly in their degree variation.

Of note was the unusually high precision of the LL7 reference point on the protrusive models (PM). Slightly more of the upper left canine tended to be captured in the PM scans, whilst the rotated upper right lateral incisor seemed to obscure the view of the upper right canine (see Figure 70 and Appendix B for typical examples). Perhaps there was an inadvertent operator bias – for example, positioning the left camera to look straight at the models, meaning the stereo field of view would be biased to the left. A decrease in the stereo angle of the cameras may help to alleviate this bias, along with improving the efficiency of the correspondence search. However, a reduction in stereo angle would require an improvement in camera calibration to enhance the subpixel detection and compensate for the reduced whole-pixel depth resolution.

By contrast, the highest variability was also seen in LL7, in the LM scans. The area captured appears to be comparable on the left (Figure 72), although slightly more of the upper dentition was typically captured on the right. This might imply an issue with the alignment algorithm ‘pulling’ the model towards the data. This would explain findings in previous work (Section 5), where the best results were obtained when the scan was taken from straight in front of the subject. As newer, and more

robust, methods of aligning 3D scans are developed, the technology can be adopted. For now, perhaps this finding serves as a reminder of the ill-posed mathematical problem of aligning scans. Users of dental CAD software may be naïve to this fact, and assume that the alignments that seem to be produced by the computer are ‘perfect’. Unfortunately, they are just ‘best guesses’ under varying assumptions (see Section 0).

Generally, the type of bite registration (protrusive, lateral etc) did not affect the trueness and precision of the registration. The only exception was again, the comparison of LL7, where the contrast between the sets of scans was significant, as previously discussed.

Similar levels of trueness and precision were found with all of the occlusal positions tested including open and closed positions. This is in agreement with findings in Section 6, and is of clinical significance.

The method for finding the THA relies on two true and precise interocclusal centric bite registrations, at different degrees of opening. Section 1.2.3 showed that recording this position is fraught with variability when using traditional physical techniques. Some of this will be related to actual clinical variability. However, factors such as inducing jaw deflections as the patient closes into a setting material, and the simple inaccuracies inherent in aligning stone dental models using physical bite registrations, will contribute to the well reported variability of up to 0.5mm. The method proposed in this thesis does not suffer the latter drawbacks, and also enjoys the benefit that multiple ‘check bites’ can easily be obtained.

The pattern of variation may be clinically significant. The scatter plots show a trend for the molar errors to be larger in the vertical direction. This will lead to posterior open bites or anterior open bites, depending on the signed direction of the error. This would seem to be related to small angular errors in the alignment of the labial scans leading to magnified errors at more distant sites. The quality of, and parameters used in, the alignment algorithm is likely to be a weak link in the chain.

#### 7.3.5.6 Trueness of Contact Points on the Models

The assessment of contact points is crude, and serves mainly to show whether or not the mean alignment of the models was representative of the actual alignment.

Contact points within or near the bite scan (LR2 and LL1 for the PM, LL3 and LL5 for the LM) were reliably identified in almost all cases, showing a high sensitivity at both distance thresholds (75µm and 150µm). A false positive result occurred about

half the time on LL2 PM, at the larger threshold of 150µm. This was caused by the proximity of the palatal aspect of UL1, and it is conceivable that this tooth lay somewhere between 150µm and 200µm from the LL2 on the real model. As such, when considering the trueness in alignment of the arches near the bite scan, the specificity becomes poorer when a larger threshold is used to define occlusal contacts.

Contact points situated distant to the bite scan (LR8 and LL7 for both PM and LM) were identified with more sensitivity when the threshold was larger (150µm). However, a tooth that was close, but not in contact (LL6 LM) was wrongly identified as a contact in 50% of cases. This again, implies a trade-off between sensitivity and specificity as the contact point threshold distance is increased.

Ultimately, whilst contact point analysis is clinically intuitive, it may not be that helpful. It is more useful to understand how spatially true the lower arch position is. For example, a model with multiple contacts around the arch might be slightly misaligned, such that only one contact point is actually present. An analysis of contact points would show this to be a clinically disastrous result, and yet a minor ease of the offending contact may instantly bring all others into line. The trueness of the method has been previously assessed (albeit using a different scanning pattern) in Section 6.5.2. The contact point analysis here broadly agrees with what might be expected from the previous work. The pattern of greater trueness in the anterior region persists, and the typical distance for which a contact point might be defined seems in agreement with the precision that has been reported in the preceding chapters. The values in the present experiment are slightly poorer than the previous work, and this is likely a reflection of the change in scanning pattern.

It was not possible to measure the trueness of contact points in the live case (OL) because the subject was biting on a block posteriorly, meaning no contacts were present. It is only possible to infer that the aligned scans were as true as PM and LM, based on the similarity between the variations discussed in the previous section. This inference is not entirely satisfactory, but does provide a strong rationale for continuing this work, since to date, none of the data collected contradicts the theory that *in vivo* scans are of a similar quality to *in vitro* scans, using the proposed method.

A caveat relevant to this, and other published work concerning measuring 3D surfaces should be raised. Comparison software generally works by sampling every vertex (3D point) on one model, and finding the closest point on the *surface* of the other. In the present case, the models are the upper and lower dental arches. This method generally works well, but is prone to errors if the vertex density or distribution are unfavourable. For example, in Figure 87 the contact point will only

be labelled on the upper model, and not on the lower. This is impossible, since by definition a contact point should be present on both models. In the current experiment, this anomaly occurred on one contact point over the 60 models analysed. This is favourable and illustrates the benefit of using dense point data. It is very common for commercial 3D dental data to be down sampled. Furthermore, most down sampling preserves high point densities in areas of high curvature, at the expense of sparse point densities in relatively flat areas. Researchers should be cautious using such data, and ensure that the points are evenly distributed, and sufficiently dense, before drawing conclusions using commercial comparison software.

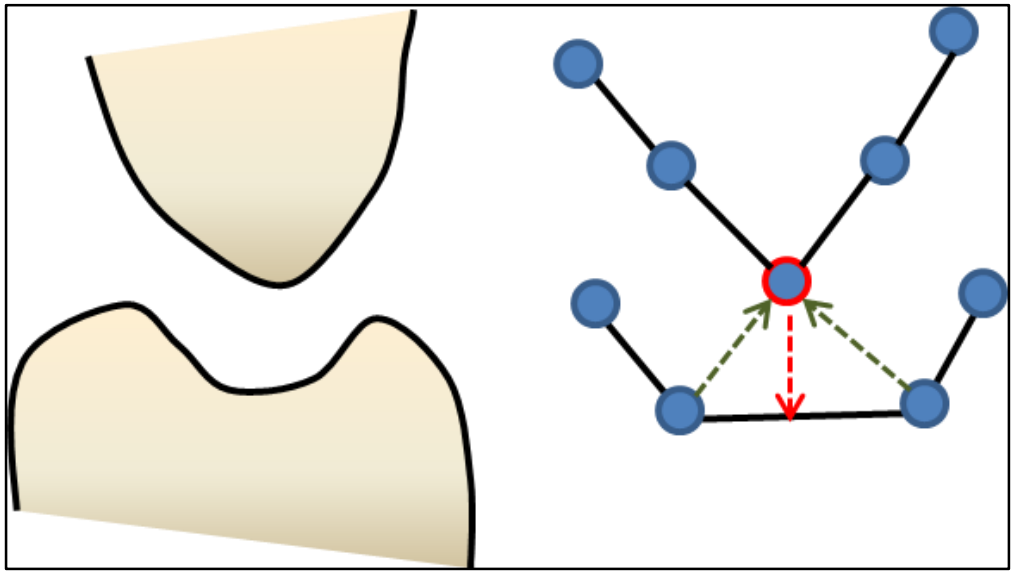

**Figure 87 Measurement Errors When Comparing 3D Meshes.** An upper cusp and lower fossa are shown on the left, and their digital scan simulated on the right. Each vertex (blue dot) is joined by a straight line (in 3D these are triangles). The distance of the upper cusp tip to the lower tooth falls within the contact point threshold, and is marked as a contact on the upper tooth (red arrow). Conversely, the distance from the lower tooth to the upper tooth is greater than the distance threshold. No contact point will be marked on the lower model (green arrows).

### 7.3.6 Conclusion

Within the limitations of the study, the following can be concluded :

A single shot ‘jailbar’ pattern can be used in an inexpensive 3D camera rig to provide digital bite registrations of dental models and live subjects.

The variability (precision) in alignment of dental models, over multiple bite registrations, is typically below 150µm, and is even more precise anteriorly, near the region covered by the actual digital bite scan. This variability is lower than that reported in the literature for traditional techniques.

No significant differences exist between the variability of *in vitro* and *in vivo* alignments.

The trueness of the *in vitro* alignments appears to fall in a similar range to the precision, although more rigorous investigation is required.

# 8 Camera Calibration

To date the experiments have identified potential areas for improvement. One such area is the method by which the stereo cameras are calibrated. This section will explore the theory behind camera calibration, and propose a novel method for calibration, accessible to almost all dental practitioners at no cost. The camera and calibration theory presented in section 8.1 can be found in more detail in the textbook, Multiple View Geometry for Computer Vision (Hartley & Zisserman 2004).

## 8.1 Camera Basics

Cameras are familiar devices, used for recording images of the world around us. They collect light from a scene, and focus it onto an image receptor. In recent years, the term *camera* has become synonymous with *digital camera*[5]*.* This refers to the method of image data collection. Traditional light-sensitive film has been largely superseded by digital sensors. These consist of a digital grid of receptors (pixels), which change their 'state' according to the amount of light falling upon them. Following this exposure, the state of each pixel is stored as an image file.

A pinhole camera is the simplest design. This device has no lens, merely a very small hole in an otherwise light-proof box. The small diameter of the hole limits the divergent rays of light, which originate from a single scene point. Only a particular ray will pass through the hole, and thus a focussed image is formed on the camera receptor (Figure 88).

[5] Even so, some enthusiasts still maintain the use of traditional film is of artistic benefit in certain situations.

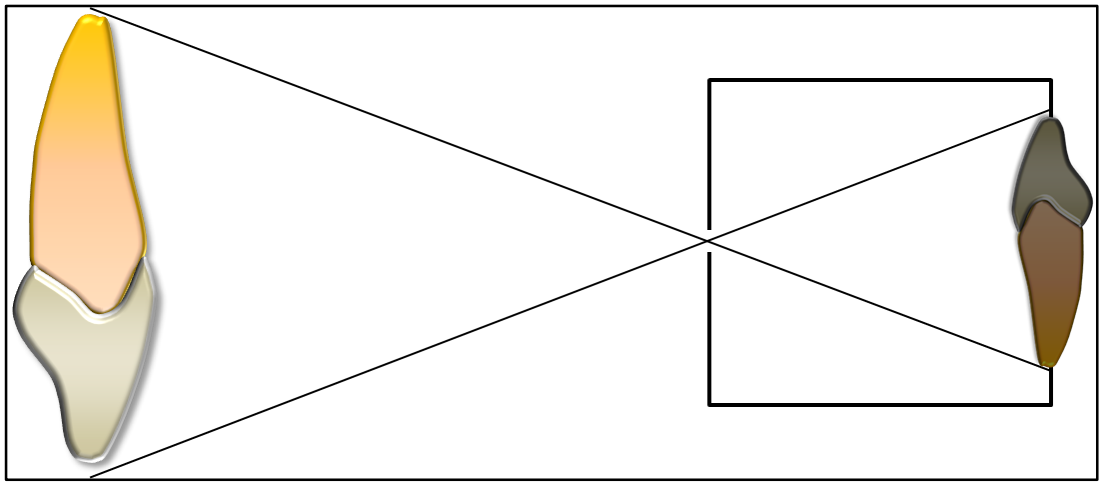

**Figure 88 A Pinhole Camera.** A very small hole is present on the front face of a light-proof box. This limits the direction from which light rays entering the box may travel, casting an inverted and (theoretically) fully focussed image on the back wall of the box. Only a single light ray from each point on the object contributes to the image. This means the image is very dark.

These cameras have an almost infinite depth of focus, and are easy to model mathematically. This is because, in theory, each point in a scene is uniquely recorded by a single, straight ray of light.

Unfortunately, pinholes suffer from two significant disadvantages. Firstly, the amount of light, and therefore information, received is very small. This results in extremely dim images. Secondly, the images are slightly blurred. This is a result of the pinhole diameter. Too large, and several diverging rays of light from a single scene point will enter the camera and hit slightly different points on the receptor. Too small, and diffraction will occur, causing bending of the light rays onto the receptor.

To overcome the shortcomings of pinhole cameras, most ‘real’ cameras incorporate a lens. This refracts light, in accordance with Snell’s Law. The thickness of the lens varies across its surface. In this way, the amount of ‘bending’ of any particular ray of light can be controlled. The result is that multiple diverging rays of light, originating from a single scene point, can be collected across the surface of the lens, and focussed to converge at a single point on the receptor. The distance at which the receptor must be positioned is called the ‘focal distance’ of the lens (Figure 89).

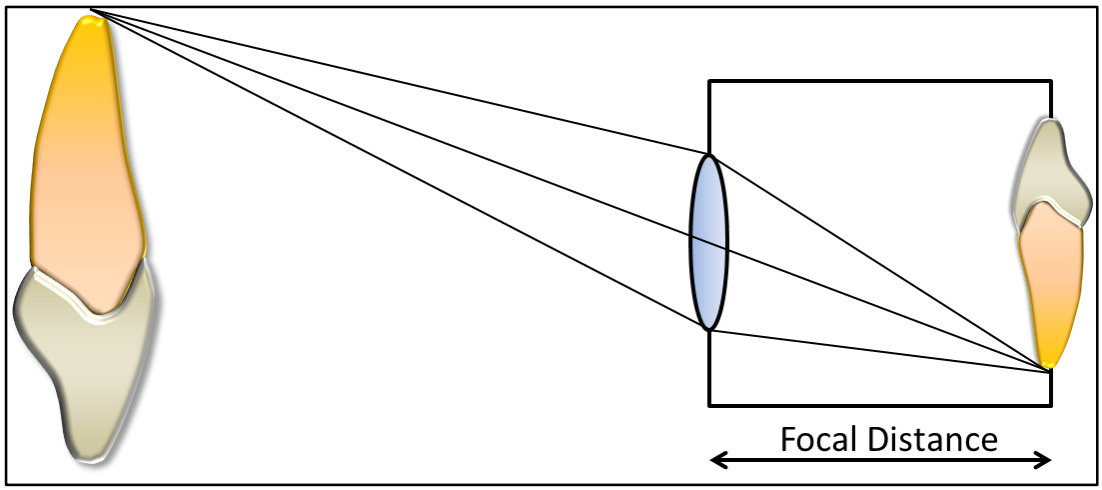


**Figure 89 Using a Lens to Focus an Image.** Unlike the pinhole model, multiple rays of light emanating from a single scene point are now focussed on the image plane. This leads to a brighter image and a better signal-to-noise ratio. The distance from the lens to the focussed image is called the focal distance.

The focal distance will change in proportion to the distance to the real-world object. Camera lenses can be moved forwards and backwards to accommodate for this change and 'focus' on near, or far, objects respectively.

A significant advantage of a lens over a pinhole is the increase in the amount of light entering the camera. In data terms, a larger amount of information is collected.

There are several disadvantages incurred by using a lens. Firstly, the quality of the lens is important. Minor imperfections on the surface of the lens, or in its curvature, will lead to inaccuracies in the image. In particular, distortions known as 'barrelling' and 'pin-cushioning' occur (Figure 90). Secondly, the depth of field (the range of viewing distances in which an object will appear in focus) is reduced, in proportion to the size, or aperture, of the lens.

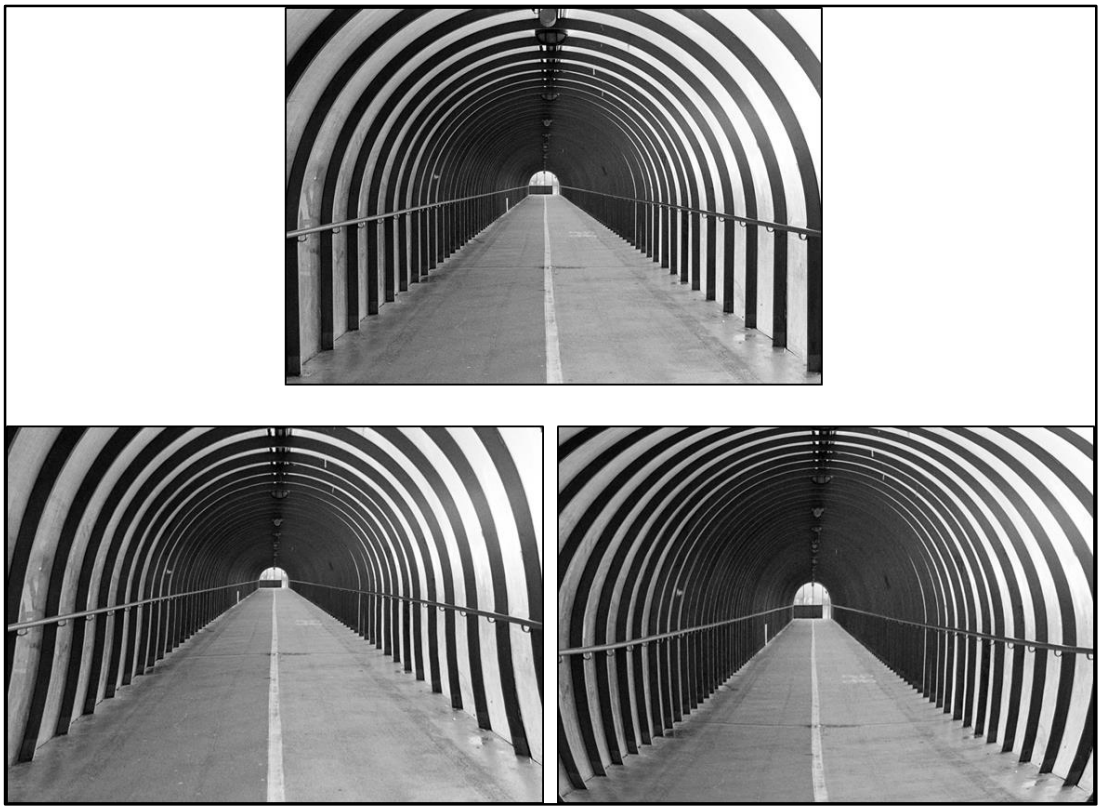

**Figure 90 Lens Distortions.** The original image is shown on top. Underneath are examples of pincushion (left) and barrel (right) distortions. All lenses create such distortions to a varying degree. Whilst generally imperceptible, these must be corrected for, if scientific measurements are to be taken from a photograph. (With thanks to Cecilie Osnes for images).

Other disadvantages include the fact that different wavelengths (colours) of light are diffracted by different amounts, as they pass through the lens. This results in chromatic aberration - a ‘splitting’ of white light into its constituent wavelengths.

A high quality lens will reduce many of these artefacts, and transmit light onto the receptor with greater efficiency. However, some residual image distortion will remain, which will require mathematical correction.

These factors result in the need to calibrate a camera before it can be used as an accurate measuring tool (Tsai 1987). This calibration serves two purposes. Firstly, it determines the *intrinsic* parameters of the camera. These relate to the physical characteristics within the camera, such as focal distance. Secondly, the *external* parameters must be calibrated. These relate the spatial position and orientation of the camera relative to the world co-ordinate system.

The aim of camera calibration is to accurately map observed 3-dimensional ‘world’ points onto the recorded 2-dimensional ‘image’ grid. Initially, a simple pinhole camera model is used (lens distortions will be modelled later). More formally :

$$s\tilde{p} = A[R\ t]\tilde{P} \quad (1)$$

where $s$ is a scale factor (usually 1), $\tilde{p}$ is the homogeneous 2-dimensional image co-ordinate $[u, v, 1]^T$, $\tilde{P}$ is the homogeneous 3-dimensional world co-ordinate [X, Y, Z, 1]$^T$, $A$ is the intrinsic camera matrix and $[R\ t]$ are the extrinsic camera matrices, describing its rotation, $R$, and translation, $t$, in the world co-ordinate system.

### 8.1.1 Intrinsic Camera Parameters

The intrinsic camera parameters are represented by the 3x3 matrix, :

$$A = \begin{bmatrix} f_u & \gamma & c_u \\ 0 & f_v & c_v \\ 0 & 0 & 1 \end{bmatrix} \quad (2)$$

where $f_u$ and $f_v$ are the focal distances (in pixel units) in the horizontal, and vertical, axes respectively. The optical centre, (the 'principal point') is located at the pixel co-ordinate ($c_u$, $c_v$), and $\gamma$ represents the skew of the image axes.

If the image pixels are square (which is common for digital imaging grids), the focal distances, $f_u$ and $f_v$, can be considered to be equal. This implies an aspect ratio ($f_u / f_v$) equal to 1. The skew, $\gamma$, can similarly be considered to be zero, since the angle between the image grid axes, U and V, is generally 90˚.

Typical physical sizes for the image pixels range from 2 to 5μm, and the manufacturing tolerances to produce these pixel grids will be significantly better (<1μm). It is these incredibly fine tolerances, readily available at low cost, that allow the assumptions of zero skew, and square aspect ratio to be made. Even a few years ago, this technology would have only been available at prohibitive cost (or for military use). A recurrent theme throughout this thesis is that of harnessing the 'artificially' low-cost technology now available, and employing it to the benefit of dentistry.

### 8.1.2 External Camera Parameters

In 3-dimensional space, any arbitrary rotation can be represented by a 3x3 rotation matrix :

$$R = \begin{bmatrix} r_{11} & r_{12} & r_{13} \\ r_{21} & r_{22} & r_{23} \\ r_{31} & r_{32} & r_{33} \end{bmatrix} \tag{3}$$

This matrix is therefore capable of representing the orientation of the camera in the world co-ordinate system. The rotation is applied by simple multiplication :

$$\begin{bmatrix} x_r \\ y_r \\ z_r \end{bmatrix} = \begin{bmatrix} r_{11} & r_{12} & r_{13} \\ r_{21} & r_{22} & r_{23} \\ r_{31} & r_{32} & r_{33} \end{bmatrix} \begin{bmatrix} X \\ Y \\ Z \end{bmatrix} \tag{4}$$

Having *rotated* the camera to the correct orientation, it must also be *translated* (moved) to the correct location. This can be achieved by addition, using a simple translation vector, $t$ :

$$t = \begin{bmatrix} t_1 \\ t_2 \\ t_3 \end{bmatrix} \tag{5}$$

and :

$$\begin{bmatrix} x_{rt} \\ y_{rt} \\ z_{rt} \end{bmatrix} = \begin{bmatrix} x_r \\ y_r \\ z_r \end{bmatrix} + \begin{bmatrix} t_1 \\ t_2 \\ t_3 \end{bmatrix} \tag{6}$$

One reason for the use of homogenous co-ordinates in Equation 1 (appending a fourth row of unit value to the matrix [X, Y, Z]$^T$ to create the homogenised form [X, Y, Z, 1]$^T$) is that the rotation and translation can now be concatenated, thus :

$$\begin{bmatrix} x_{rt} \\ y_{rt} \\ z_{rt} \end{bmatrix} = \begin{bmatrix} r_{11} & r_{12} & r_{13} & t_1 \\ r_{21} & r_{22} & r_{23} & t_2 \\ r_{31} & r_{32} & r_{33} & t_3 \end{bmatrix} \begin{bmatrix} X \\ Y \\ Z \\ 1 \end{bmatrix} \tag{7}$$

Finally, from Equation 1, a 2-dimensional image co-ordinate can be mapped to the 3-dimensional world co-ordinate :

$$s \begin{bmatrix} u \\ v \\ 1 \end{bmatrix} = \begin{bmatrix} f_u & \gamma & c_u \\ 0 & f_v & c_v \\ 0 & 0 & 1 \end{bmatrix} \begin{bmatrix} r_{11} & r_{12} & r_{13} & t_1 \\ r_{21} & r_{22} & r_{23} & t_2 \\ r_{31} & r_{32} & r_{33} & t_3 \end{bmatrix} \begin{bmatrix} X \\ Y \\ Z \\ 1 \end{bmatrix} \tag{8}$$

### 8.1.3 Modelling Lens Distortion

The calibration discussed in the previous sections only considers the pinhole camera model. However, real cameras also exhibit some degree of lens distortion. This distortion means the theoretical pixel co-ordinate [*u, v*] will not be the same as the recorded pixel co-ordinate owing to barrelling, or pincushion distortion. This radial distortion can be modelled using a polynomial function. This distorts the ideal image co-ordinate symmetrically about the (previously determined) central pixel, as a function of the radius. The exact degree of the polynomial varies amongst algorithms, although most workers agree that, with high quality lenses, there is little benefit in modelling beyond an order of four (Scharstein et al. 2014). It is also possible to account for tangential distortion (where the planes of the lens and the image grid are not perfectly aligned). Again, with high quality lenses, this is rarely necessary.

An example of a lens distortion polynomial comes from the commonly employed, and openly available, OpenCV (http://opencv.org) implementation :

$$u_{\text{corrected}} = u(1 + k_1 r^2 + k_2 r^4 + k_3 r^6) \quad (9)$$

$$v_{\text{corrected}} = v(1 + k_1 r^2 + k_2 r^4 + k_3 r^6) \quad (10)$$

where u and v are the observed 2-dimensional co-ordinates on the image receptor, and $k_1$ to $k_3$ are the distortion coefficients. The result is a 'corrected' co-ordinate, as would have been seen, if the lens exhibited zero distortion.

Tangential distortion can also be modelled using OpenCV, but is of limited practical benefit when using good quality cameras. In fact, it is generally better to restrict the number of variables, to prevent the minimisation algorithm from converging on an incorrect solution (see next section).

### 8.1.4 Determining the Calibration Parameters

Having formulated a mathematical model for the camera, it is now necessary to find values for the elements of the intrinsic, extrinsic and lens distortion matrices. This is generally achieved by photographing one or more calibration targets. These targets are physical objects, with known dimensions. They must be at least as precise as the expected camera resolution, and ideally more so.

Three dimensional objects, such as cubes with perfectly right angled sides, were traditionally used. However, these targets are expensive and can become damaged. With the explosion in machine vision over recent years, cost-effective targets were needed to accommodate the needs of University researchers, and home enthusiasts. The modern standard calibration target is generally planar, since it is easy to fabricate ‘flat’ targets. The calibration procedure requires that multiple photographs are taken (from different viewpoints, but without adjusting the camera focus).

The targets are decorated in a precise way, using features that can be recognised with machine vision. Examples of these features include chessboards (corner detection), circles (centre detection) and, more recently, QR codes (as QR detection algorithms are becoming increasingly commonplace).

Once these targets have been photographed and detected, the known 3-dimensional world co-ordinates, and corresponding 2-dimensional image co-ordinates, can be used to assemble a system of equations. This system can then be solved to provide the elements for the intrinsic, extrinsic and lens distortion matrices. It should be noted that, due to observational noise and non-perfect lens models, there will not be an exact mathematical solution. Therefore, a minimisation technique is employed, typically Levenberg-Marquart, to solve the non-linear least squares problem.

The planar target calibration technique is surprisingly robust. In particular, the number of different angled views of the target required is small (about five), and the variation in viewing angle can also be small.

### 8.1.5 Problems with Current Calibration Methods

Most applications for inexpensive machine vision seem to operate on large scale data (human, or room sized), and these targets can be easily printed with sufficient trueness and precision.

However, as the desired scanning volume decreases, and the precision and trueness demands increase, even flat targets become more costly. Standard printed targets become inaccurate. Small bleeds in the printer ink will distort the circular targets. Errors in the aspect ratio of the printer will lead to distortion of the calibration circles, making them slightly oval shaped. Specialist printing techniques are required, such as lithography, if the quality of the calibration target is to be sufficient. Furthermore, the target must be perfectly flat, and is usually etched on glass for this reason. These targets are fragile and costly (several hundred pounds each). This limits their mass appeal, and increases the cost of scanning, within the volume needed for this project, and with the required quality.

There are other potential drawbacks to target-based calibrations. Each feature must be in perfect focus, but the targets must also be viewed at an angle to the camera imaging plane. Therefore it is easy for some features to become blurred, reducing the quality of the detected ‘ground truth’ points.

Also, when viewed at an angle, feature detection becomes less reliable. For example, when viewing a circle obliquely, it becomes distorted. In fact, due to the effects of perspective, it will be subtly egg-shaped. The observed ‘centre’ of this feature will not coincide with the real centre of the circle.

These shortcomings have recently been addressed (Schmalz et al. 2011). The group presented a calibration method which combines sinusoidal phase shifting techniques, common in structured light scanning, with the use of a flat-panel computer monitor. They reported a five-fold improvement in the calibration when compared to traditional ‘passive’ targets. Their method exploits the precision with which computer displays are manufactured. The use of phase-shifting patterns negates errors caused from out-of-focus images (since phase shifting is enhanced with slightly defocussed images). Furthermore, calibration points are reliably identified from a variety of viewing angles.

This technique is useful when the anticipated scanning volume is about the size of the monitor. However, the pixel size of a monitor (0.272mm in the case of Schmalz et al) is large when considering dental scanning applications. In the following experiment, a novel, inexpensive, active calibration technique is investigated. It is suitable for accurately calibrating cameras to scan small scale objects, such as the

labial view of a dentition. No specialist calibration equipment is required, instead making use of an everyday object – the mobile phone.

## 8.2 Implementing a Novel Camera Calibration Procedure

### 8.2.1 Introduction

Given the previously mentioned shortcomings of current calibration targets, there is a need to develop a more suitable calibration technique. For the optical bite scanner proposed in this thesis, a calibration system for scanning a volume of space equivalent to the labial segment (~40x40x20 mm) is required. The procedure should be highly true and precise, but should not require costly additional equipment.

### 8.2.2 Outline of Aim

- To implement a true, precise and cost-effective camera calibration procedure, suitable for the optical bite scanner developed in this thesis.

### 8.2.3 Objectives

- To use a mobile phone as an precise and true planar calibration target.
- To implement optimal calibration patterns to be displayed on the phone.

### 8.2.4 Null Hypotheses

1. There is no difference in the quality of camera calibration using the new technique, and the same camera calibrated using a custom-made, lithographic glass plate target. Quality will be assessed by variability of the principal point, and by mean reprojection error.
2. There is no difference in the average stereo reprojection error of a stereo-pair of cameras calibrated with the new technique, and the same pair calibrated using a custom-made, lithographic glass plate target.

## 8.2.5 Method

### 8.2.5.1 Hardware and Software

Two complementary metal-oxide-semiconductor (CMOS) cameras (uEye 1240LE, IDS Imaging, Obersulm, Germany) were mounted on a rigid brass bar, with a horizontal baseline separation of approximately 40mm, and at an angle of approximately 20 degrees[6]. The cameras had a resolution of 1.3 mega-pixels (1280 x 1024).

An Android™ application was written to display a sequence of horizontal and vertical phase shift patterns on a smartphone (LG G3, LG Electronics, Yeouido-dong, Seoul). This phone has a screen resolution of 1440 x 2560 pixels, and a pixel size of 47.2 µm.

The patterns consisted of three sets of frequencies, with wavelengths of 24, 21.33 and 23.63 pixels respectively. Each frequency set was shifted exactly 6 times, in intervals of 60 degrees. A total of 18 horizontal, and 18 vertical patterns were thus created.

The phone application was controlled via Bluetooth® from additional custom C++ software using a laptop PC. This software synchronised the displaying of all 36 patterns on the phone, with image capture by the two cameras (Figure 91). The vertical and horizontal image sequences were then decoded, using the embedded phase shift technique (Moreno et al. 2015). This yielded a single ‘horizontal phase’ image, and a single ‘vertical phase’ image, for each camera. The exact co-ordinate of each display pixel on the mobile phone screen was encoded in these two images.

---

[6] This 20 degree angle represents a reduction when compared to the previous experiments (which used 30 degrees). The reason for this reduction is the suggestion that the curved labial segment reduces the commonality between the stereo views when the cameras are angled at 30 degrees. A 20 degree viewing angle should increase the number of common points viewed in the scene allowing a more dense and precise 3D reconstruction. This will be the case if the calibration method enables good subpixel precision, which in turn will compensate for any theoretical loss in depth resolution when considering whole-pixels. Furthermore, for the calibration experiment described here, the angle is unimportant.

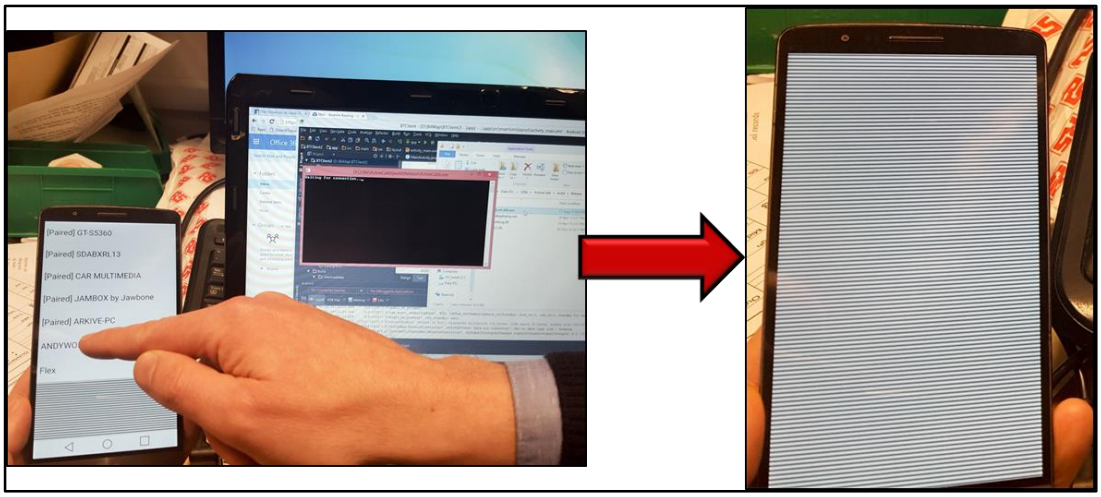


**Figure 91 The Mobile Phone Calibration App.** On the left, the author's phone and laptop are shown. When the app is run, a Bluetooth connection is established by selecting the appropriate 'link' from the list of available connections. On the right, an example of a calibration pattern. Each pattern is a sinusoidal image. There are 36 images in total, and the phone display is controlled by the laptop, which synchronises display and camera-capture. A precise mapping of camera image pixels to phone screen pixels is created, enabling camera calibration.

Additionally, to compensate for differential illumination when viewed obliquely, a second sequence was captured with the camera exposure time doubled. These were decoded to give a second 'High Dynamic Range (HDR) vertical phase' image, and a second 'HDR horizontal phase' image. Finally, a 'master phase' image was created by merging the two pairs of images, choosing the highest quality pixel at each location.

In this way, a precise mapping of each pixel in the camera image to a pixel on the mobile phone screen was created.

#### 8.2.5.2 Experimental Design

Twelve complete image sequences were captured, with the phone screen being repositioned after each sequence by approximately ten degrees, around one or more axes.

Five decoded images were selected, and both cameras were calibrated using this data. In a first stage, the cameras were individually calibrated using the OpenCV calibration library. The aspect ratio was fixed at 1:1, and no tangential distortion parameters were used. Thus, the simplified calibration model entailed a freely moveable principal point, and second, fourth and sixth order radial distortion coefficients.

In a second stage, a stereo calibration was performed, feeding the algorithm the intrinsic parameters derived in the first stage.

The two-stage calibration was repeated for every combination of five images from the twelve. A total of 792 calibrations were performed.

For comparison with a traditional target, an asymmetric circles grid was fabricated on a chrome glass mask, with a tolerance of 0.8µm (Micro Lithography Services Ltd, Chelmsford, UK). The target consisted of 44 circles, 5mm in diameter. To protect the glass, the target was mounted in a 3D printed box (Figure 92).

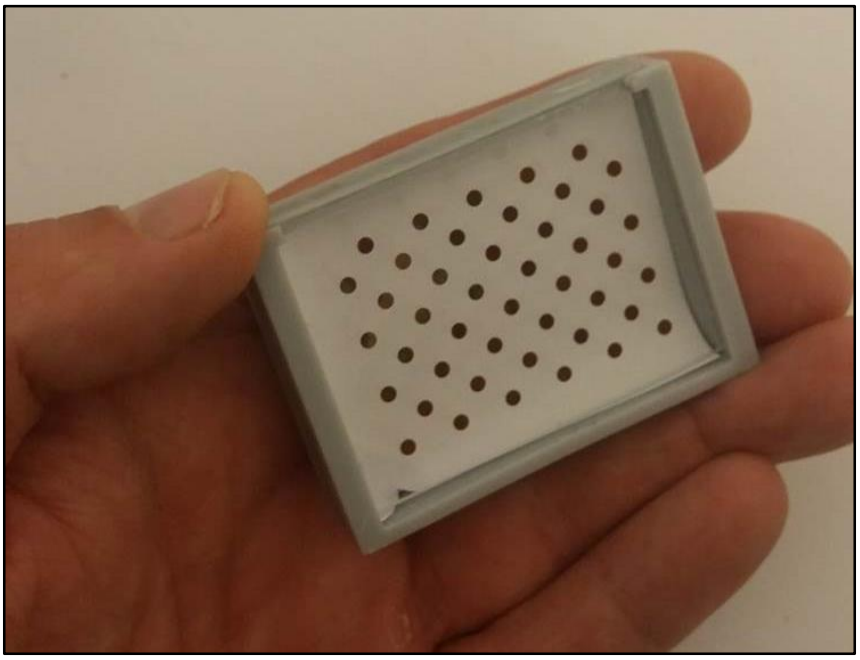

**Figure 92 The Chrome-Etched Glass Calibration Target.** A grid of asymmetric circles, each 5mm in diameter and reproduced with a tolerance of 0.8µm. The glass slide was mounted in a custom-made 3D printed housing. White paper was placed inside this housing to afford good contrast with the black circles.

Twelve images of this grid were captured by the pair of cameras, with small (approximately ten degree), movements around one or more axes between each image.

Both cameras were calibrated individually, then as a stereo pair, using the same software settings as previously described. Five images were used for each calibration. A total of 792 calibrations were performed.

The mean reprojection error was compared between the new, and traditional techniques. This was performed for both cameras. Significance was investigated using an unpaired t-test.

The variation in the position of the principal point was compared. This parameter is difficult to estimate because many reasonable calibration solutions can be found with a broad variation in principal point co-ordinate. It can therefore be considered a highly sensitive measure of the calibration quality. An unpaired Students t-test was used to test for significance.

The mean stereo reprojection error was also assessed, along with the variation in the calculated angle between the two cameras. An unpaired Students t-test was used to test for significance.

Finally, the correlation of the calculated angle between the cameras, and the baseline separation, was investigated using Pearson's *r*.

All statistical data was created using Microsoft Excel, with the Analysis ToolPak add-in.

### 8.2.6 Results

The distribution of all data was tested using Q-Q Plots created in SPSS (Armonk NY: IBM Corp) (see Appendix A). It can be seen that some of the reprojection error data, and some of the error radius data, showed deviations from the normal distribution, particularly in the tails. However, in view of the large datasets (792 values), Students t-test was deemed suitable despite these moderate deviations (Lumley et al. 2002).

The locations of the principal point and mean reprojection errors for the camera calibrations are compared in Table 8 and Table 9. The variation in principle point location was lower using the mobile phone method. Students unpaired t-test showed this to be highly significant ($p<0.001$). The individual, and stereo, reprojection errors were also significantly lower in the mobile phone group ($p<0.001$).

| | Mobile Phone Method | | | Traditional Glass Target | | |
|---|---|---|---|---|---|---|
| | $C_u$ | $C_v$ | Mean Error Radius | $C_u$ | $C_v$ | Mean Error Radius |
| Left Camera | 642.92 (0.50) | 497.35 (1.91) | 1.70* (1.01) | 628.78 (4.63) | 491.99 (4.20) | 5.50 (2.97) |
| Right Camera | 644.84 (1.67) | 512.21 (1.23) | 1.82* (1.00) | 638.59 (2.18) | 507.42 (2.91) | 3.28 (1.58) |

**Table 8 Mean Location of Calibrated Principal Point ($Cu$, $C_v$), and Mean Variation in Radius of Principal Point (Compared to the Mean).** All values in pixels (standard deviation). Number of calibrations = 792. * denotes $p<0.001$.

| | Mobile Phone Method | | | Traditional Glass Target | | |
|---|---|---|---|---|---|---|
| | Left | Right | Stereo | Left | Right | Stereo |
| Reprojection Error | 0.13* (0.01) | 0.10* (0.01) | 0.22* (0.06) | 0.18 (0.02) | 0.20 (0.03) | 0.27 (0.04) |

**Table 9 Mean Reprojection Error in Pixels (Standard Deviation) for the Individual Calibrations of the Left and Right Cameras, and Stereo Reprojection Error for the Pair.** Number of calibrations = 792.*denotes p<0.001.

The distribution of the calculated principal points are shown in Figure 93 and Figure 94.

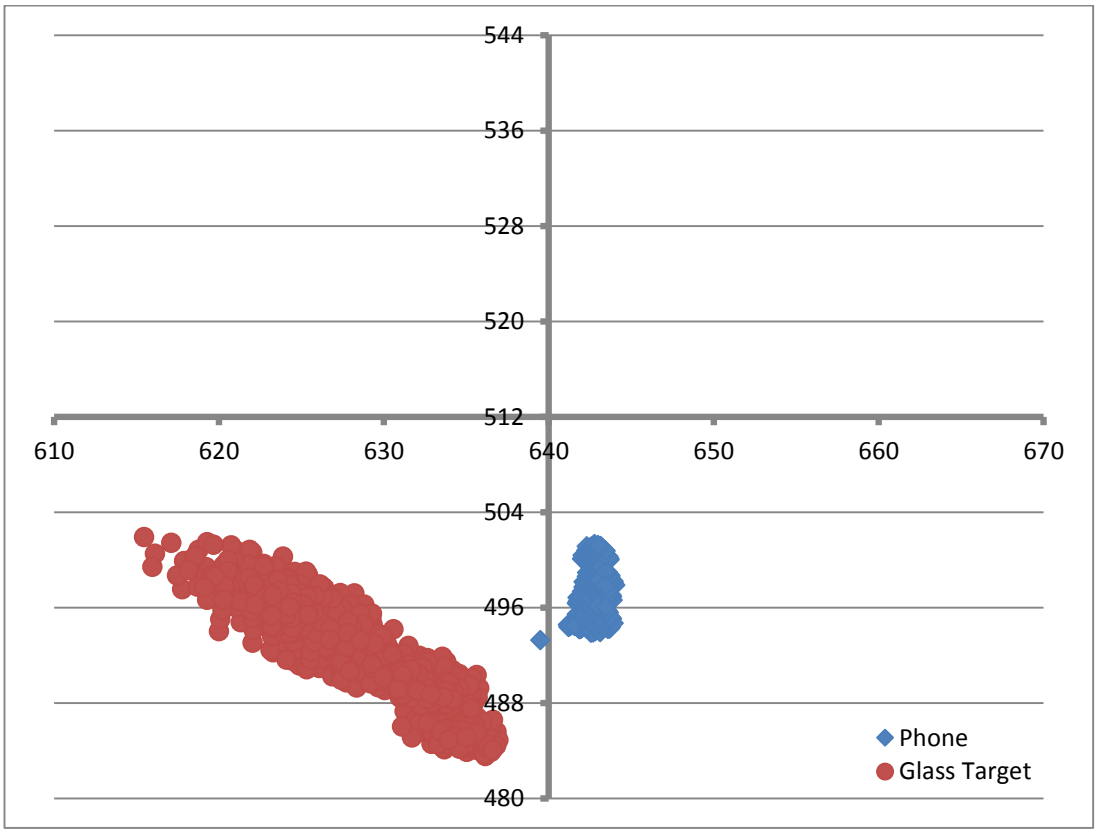


**Figure 93 Variation in the Location of the Principal Point (Over 792 Calibrations) Using the Traditional (Glass) Technique, and the Proposed (Phone) Technique.** Left camera, units in pixels.

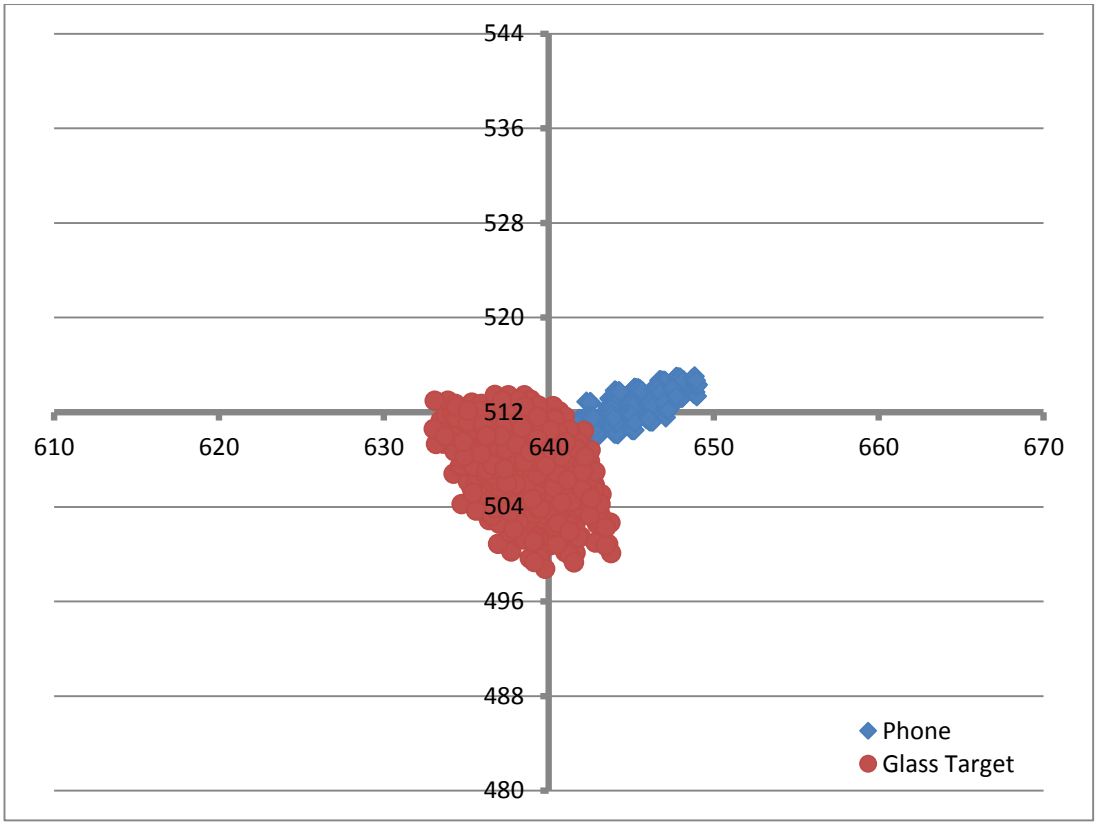


**Figure 94 Variation in the Location of the Principal Point (Over 792 Calibrations) Using the Traditional (Glass) Technique, and the Proposed (Phone) Technique.** Right camera, units in pixels.

The radius of principal point displacement, compared to the mean value, is shown in Figure 95 and Figure 96.

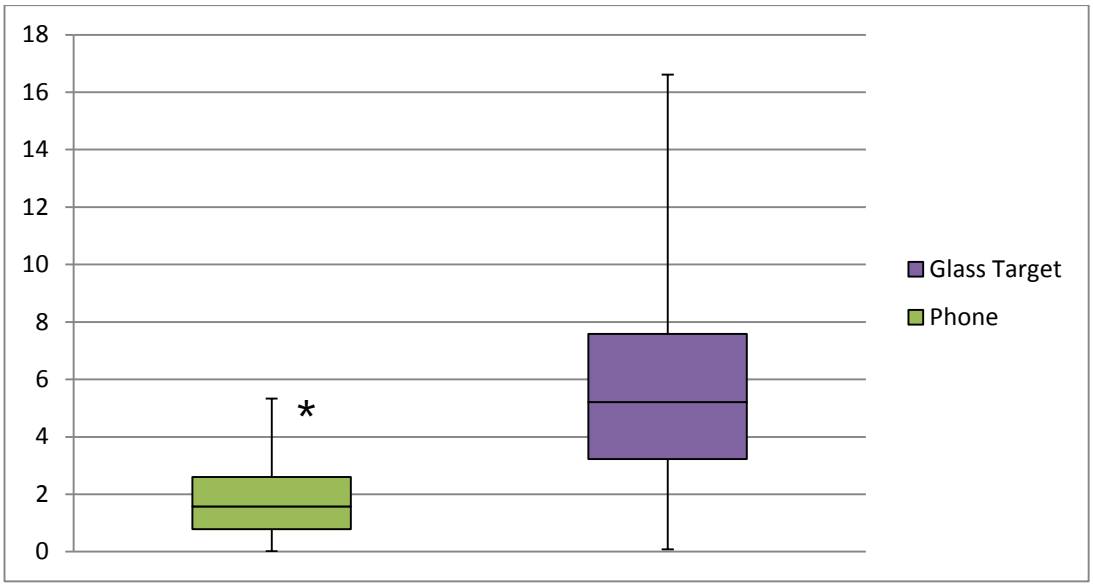


**Figure 95 Radius Error (in Pixels), Compared to the Mean, for the Principal Point.** (Left camera). Box plots show mean and interquartile range. Error bars describe the maximum and minimum observed errors. *denotes significance ($p<0.001$).

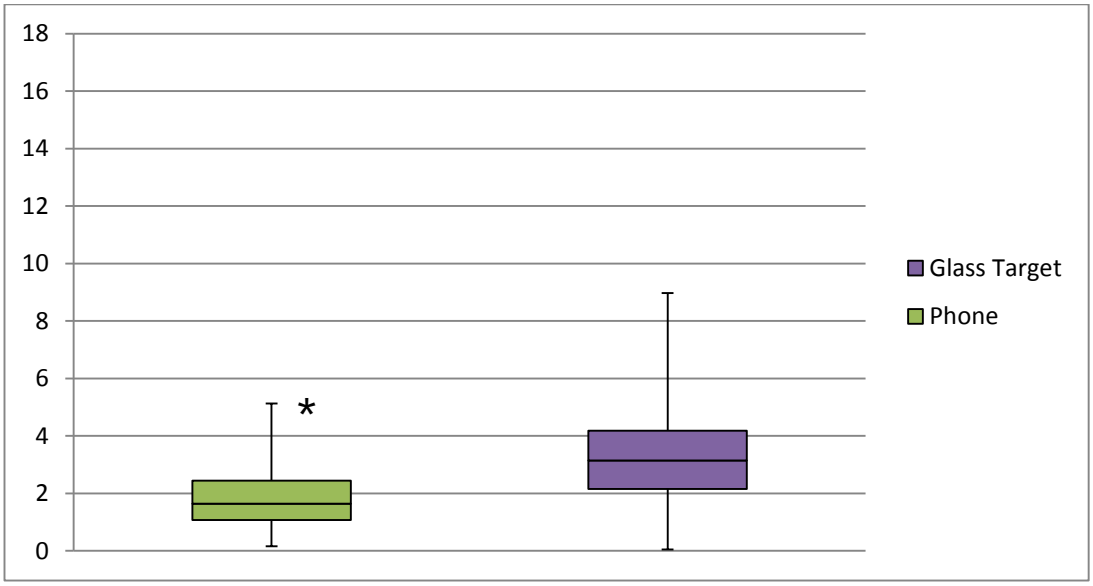


**Figure 96 Radius Error (in Pixels), Compared to the Mean, for the Principal Point.** (Right camera). Box plots show mean and interquartile range. Error bars describe the maximum and minimum observed errors. *denotes significance ($p<0.001$).

The mean stereo reprojection error (in pixels) was 0.22 ± 0.06 for the phone calibration method, and 0.27 ± 0.04 for the glass target. The distribution of errors is shown in Figure 97. An unpaired two-tailed t-test showed the difference between methods to be significant ($p<0.001$).


**Figure 97 Box Plot Comparing Stereo Reprojection Errors (in Pixels) for the Two Calibration Methods**. Box plots show mean and interquartile range. Error bars describe the maximum and minimum observed errors. *denotes significance ($p<0.001$).

There was no significant difference in the calculated angle between the cameras ($p>0.05$). The angles were 20.74° ± 0.06 for the phone calibration method, and 20.74° ± 0.08 for the glass target (Figure 98).

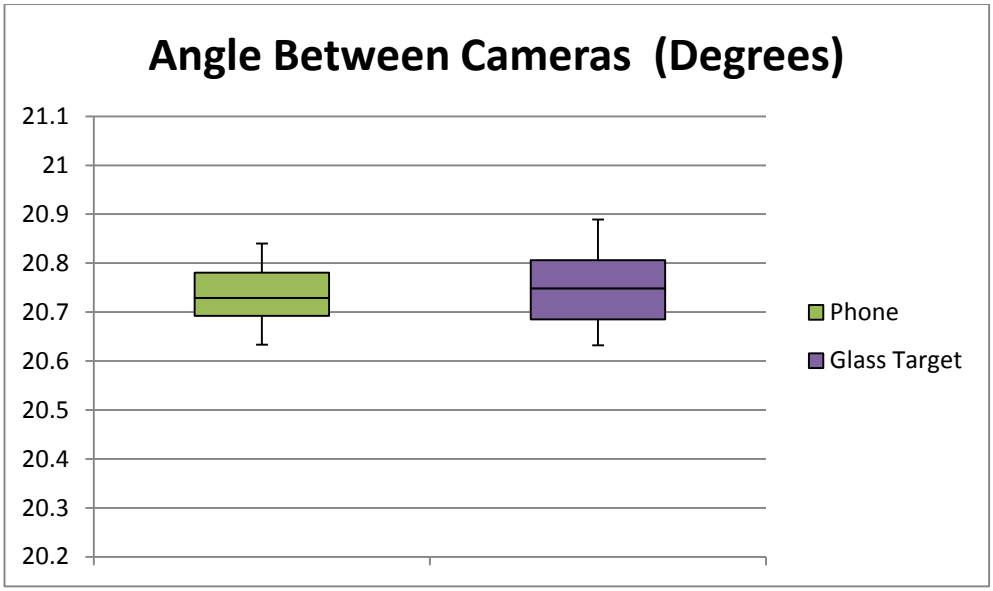


**Figure 98 Box Plot Showing the Calculated Angle Between the Two Cameras for Both Calibration Methods.** Box plots show mean and interquartile range. Error bars describe the maximum and minimum observed errors.

The calculated baseline separation is plotted against the angle between the cameras in Figure 99 and Figure 100.

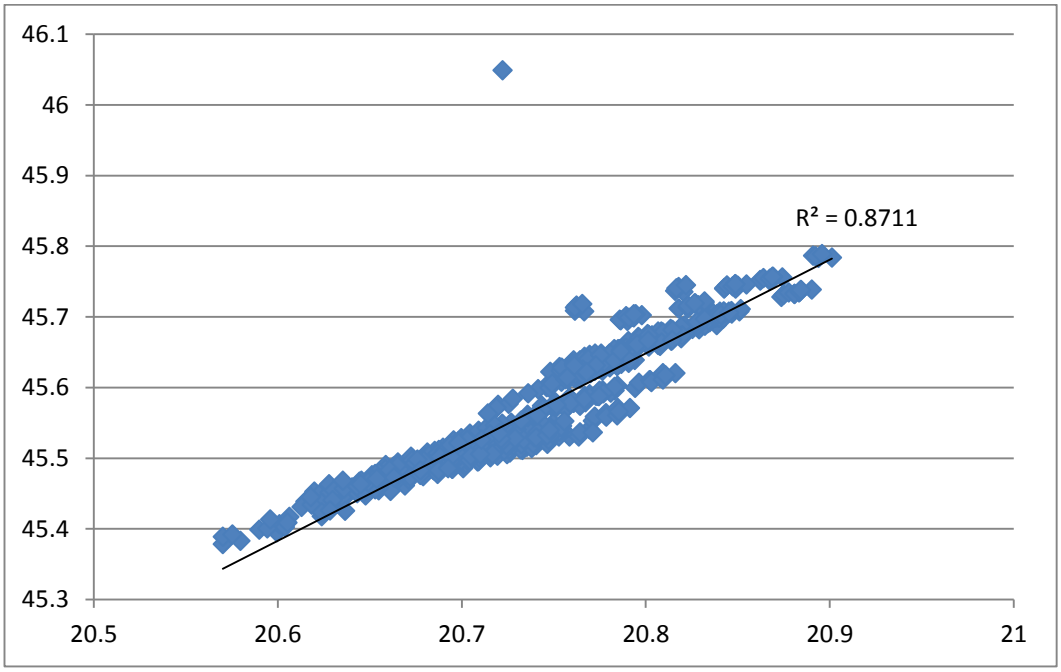


**Figure 99 Calculated Baseline Separation (mm) vs Angle (Degrees), Between Both Cameras (Phone Calibration).**

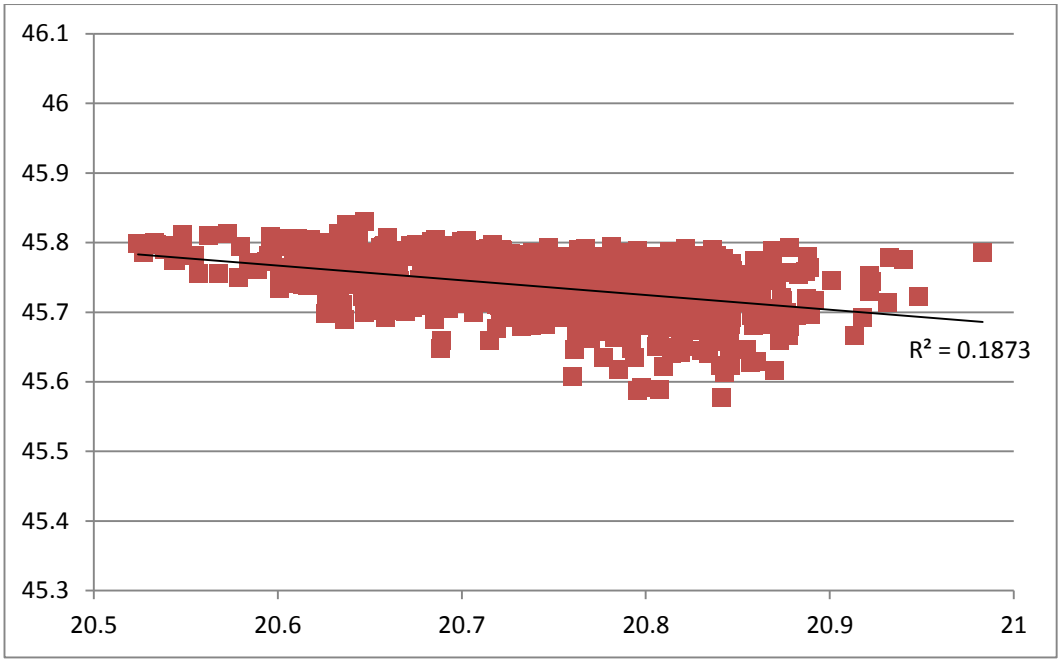


**Figure 100 Calculated Baseline Separation (mm) vs Angle (Degrees), Between Both Cameras (Glass Target Calibration).**

### 8.2.7 Discussion

The precise quality of a camera calibration is difficult to quantify. The mean reprojection error is not a definitive measure of quality, since a low error could be due to an excellent fit of the calibration model, to poorly identified targets. However, it is considered a useful measure in the field. Using the new calibration technique, the reprojection error was significantly smaller for both cameras ($p<0.001$), when compared to the traditional technique.

The principal point is not expected to be perfectly coincident with the centre of the CMOS sensor (640, 512), because of manufacturing tolerances. However, it would be expected to lie close to this. Furthermore, reliable calibration should produce the same principal point, regardless of which calibration images are used.

Additionally, since the camera model compensates radial distortions uniformly in both axis directions, the *u* and *v* values are dependent variables. It is therefore useful to analyse the radial displacement of the principal point, compared to the mean calculated principal point. This error radius was significantly smaller ($p<0.001$) using the new technique (1.70 vs 5.50 pixels for the left camera, 1.82 vs 3.28 pixels for the right camera).

The stereo reprojection error could be considered a better measure of the quality of the calibrated system, since this combines any errors in the individual camera

models. The new method significantly outperformed the traditional method ($p<0.001$) with mean reprojection errors of 0.22 ± 0.06 pixels for the phone calibration method, and 0.27 ± 0.04 pixels for the glass target method. This equates to a 19% improvement in performance.

There was no difference in the calculated angle between the cameras using either method ($p>0.05$). However, the relationship between angle, and baseline separation, was well correlated using the new method ($r =0.87$), but poorly correlated with the traditional method ($r=0.19$). It would be expected that, for a given set of calibration points, if the calibration algorithm 'settled' on a slightly larger angle, the baseline separation would necessarily increase to compensate. This would only be the case if all calibration points had been precisely identified. A larger stochastic error in identifying these points might blur this baseline-angle relationship. It seems plausible that the difference in correlation observed between the two methods offers a further indication that the calibration points are identified with greater trueness and precision, using the new method.

Further refinement may be possible using bundle adjustment, although the added benefit would need to be investigated.

### 8.2.8 Conclusion

Camera calibration using a mobile phone shows significantly lower reprojection errors than the traditional glass target calibration method. The method is effectively 'free of charge', given the ubiquitous ownership of smartphones.

# 9 Summary and Future Work

## 9.1 Summary of Thesis

This thesis was borne from the clinical observation that that the tools available to the general dentist to record a patient's functional articulation are lacking in trueness, precision, affordability and practicality.

A literature review confirmed uptake of current clinical techniques was poor, and the trueness and precision (and clinical benefit unless expertly used) of such techniques seems questionable. What is certain is that no technique is perfect, and there is some way to go as a profession in developing new methods before we can make such claims.

The transverse horizontal axis (THA) was highlighted as one traditional aspect of the patient's functional anatomy that clinicians would like to be able to record and reproduce correctly, and simply.

A simple clinical method was proposed, involving recording centric relation (CR) in two positions of opening, in order to rapidly determine the location of the THA, with good trueness and precision. A review of the literature showed this was not a new idea, and a similar method had been attempted in the 1970's, using the medium of wax to record the two centric bites (Long 1970). However, the author found the inaccuracies of these centric records to be too great for the method to have any clinical use.

It was hypothesised that it would be possible, and cost effective, to build a 3D scanner capable of recording interocclusal records with sufficient trueness and precision to enable this technique for calculating the THA to be viable.

A computer simulation was created to explore the likely trueness that such a scanner might need, the volume of the dentition that should be scanned, and the jaw positions the patient might need to posture into.

Designing and building the hardware and software was then undertaken. The hardware was relatively simple, using readily available cameras and projectors. Writing the software required to turn this equipment into a 3D scanner was complex. Further software to enable digital jaw registration and THA calculation was also written.

Initial experiments were aimed at implementing this system *in vitro* (Section *5*). The experimental results agreed well with the simulation model, enhancing the confidence in the model. The THA was located with a mean error of 2.65 ± 1.01mm.

The need for further specific investigations into the trueness and precision of the interocclusal registrations (upon which find the THA relies) were highlighted. These CR registrations were considered to be the key to the success of the project, and became the focus of the remainder of the work.

In the next experiment (Section 6), the equipment remained unchanged and the trueness of the interocclusal registrations was investigated. When using standard scanning patterns, the hardware was capable of good trueness and precision. Typical positioning errors were below 100µm, while trueness and precision both became poorer, at sites distant from the region of the bite scan. The scanning pattern was too slow to implement clinically.

Section 7 worked on adapting the scanning pattern to a clinical solution. The loss in data density (caused by the faster scanning pattern) was partially offset by the use of a more precise and true calibration target, and higher power projector. However, the calibration target was expensive and the method was identified as an area for further enhancement. The results of *in vitro* and *in vivo* scans showed no statistical difference in precision. The variation was again, greater at sites distant from the area of the scan. The precision was slightly poorer than that previously measured (Section 6), but was still typically less than 150µm posteriorly, and better anteriorly.

Improvements in the measured 3D data will lead to improvements in the jaw registrations. Enhancements will come from better calibration, and better stereo correspondence accuracy.

A novel method to improve the system calibration was implemented, harnessing newly reported scanning patterns (Moreno et al. 2015) coupled with a previously reported enhanced active calibration technique (Schmalz et al. 2011). Experimental results on the quality of calibration showed a significant improvement over previous techniques. The effective cost was reduced to zero by using mobile phone technology.

The second aspect of improving the 3D data (the stereo correspondence problem) will be the subject of future work. As with the calibration work, the aim is to harness techniques being developed from other areas of machine vision. Self-driving car research, an area with significant resource and investment in the current climate, offers a potential solution to the correspondence problem because car panels, and the labial surfaces of teeth, are not dissimilar in terms of texture and morphology (from a machine vision perspective). The *a priori* knowledge methods being developed in this field could be adopted to enhance the trueness and precision of the bite registration scans.

With these two enhancements in place, it is hoped to run full clinical trials assessing the technique. The equipment cost remains in the ‘hundreds of pounds’ and the time taken to collect 29 live bite registrations will continue to be 2 seconds or less. The system is entirely non-contact, requiring no more disinfection than a normal camera used for taking dental photographs. These aspects are viewed as favourable in the general dental setting.

## 9.2 Contributions

**Proposal of a novel method to kinematically locate the THA**

A method has been presented by which, using modern technology, a simple non-contact clinical technique could be used to rapidly record the kinematic THA in a patient.

**Technical specification based on computer simulations**

It has been shown that, if a scanning system could be built whose *overall* error (including any post-processing errors) is 50µm, then the proposed method could be feasible if the entire labial segment is scanned (in a single shot) including an area of 1-2mm of gingivae in both arches. The difference in jaw opening between the two required scans should be 10mm and it follows that a scanning field of view height of 40mm is required to capture this.

**The method can be implemented at minimal cost *in vitro* to give results as predicted by the simulation model**

Using less than one thousand pounds worth of equipment, axis location on an articulator can be found with an error radius of 2.65±1.01mm. The simulation model predicts that the implemented workflow has an overall error of 50 to 70µm. This seems reasonable.

**Cross-arch optical interocclusal registrations lose trueness and precision at sites distant from the registration scan but the deterioration can be minimised**

It has repeatedly been shown that the bite registration is more precise and true where the teeth are scanned, and less so at more distant sites. A contribution in this respect is acknowledging the importance of covering as much surface area as possible with a *single* optical bite scan. The scan should not be composed of multiple smaller scans, since alignment issues may ensue.

Using these guidelines, errors at distant sites can be minimised and are typically below 150µm.

**It is possible to adopt the technology to *in vivo* use**

Using a carefully designed one-shot scanning pattern, this inexpensive apparatus can perform scans on live subjects with a similar degree of precision as *in vitro*.

**A novel camera calibration technique is inexpensive and more accurate**

Using a mobile phone app, stereo cameras can be calibrated with an improvement over traditional methods. The stereo reprojection error decreases to 0.22 pixels using this app compared to 0.27 pixels with a standard technique (19% improvement). This method would be suitable for general dentists, as no expensive calibration equipment is required.

## 9.3 Future Work

### 9.3.1 Skeletal Relationships

There are some stark differences between the functions performed by a facebow and interocclusal record, compared with the proposed optical method. The method only considers the relative position of the dentition to the THA. A facebow attempts to record other skeletal relationships such as the position of the occlusal plane relative to the horizontal and sagittal planes. These relationships have been reported to affect the perceived aesthetics (Kattadiyil et al. 2012) and are an important part of holistic treatment planning. A recent comparison of the ability of the five main facebow systems to reliably reproduce these planar references showed that none of them reproduced these positions precisely (Maveli et al. 2015). The workers concluded that functional and aesthetic repercussions could ensue.

It would appear that a completely reproducible method for relating the occlusal plane to the skeletal base is still lacking. A full solution to the articulation problem would doubtless require this. The proposed method has not addressed this directly, but several modifications could be suggested. Firstly, if one assumes no obvious TMJ asymmetry (as is broadly the case with any earbow), then 'horizontal' could be taken to be equal to this axis. Furthermore, the Denar system used at Leeds University recommends an anterior reference point located 43mm superior to the central or lateral incisal edge. Given the margin of error that this is likely to incur over different sized faces, one could probably produce a similar reference point digitally by plotting a digital point 43mm superior to the incisal edge (as previously reported in Section 5).

A more elegant and robust alternative would be to employ a 3D facial scan. This would enable landmarks such as the inter-pupillary line to be identified. Two obstacles to overcome are the expense of acquisition equipment, and the registration of the dentition relative to the face. Current stereo-matching systems tend not to scan the teeth well (and also produce concave eyes because of stereo-matching problems). The cameras in the system could work at a larger focal distance to capture the face. More simply, the latest generation of mobile phones allows better control of their cameras (fixed focus, F-Stop and exposure). A year or two from now, today's 'latest' phones will be the standard phone in many people's pockets. With the Android programming skills learnt during this thesis, it would be possible to scan a face by taking two or three images using a calibrated phone camera. Starting with the assumption of a conformed generic facial mesh (Aissaoui et al. 2012), the 3D reconstruction could be enhanced, but crucially the a priori knowledge of the dentition (see Section 7.3.4.2) could be included to produce an

acceptable scan and alignment of the teeth relative to the soft tissues. The resolution of such a method would likely be poorer than the sub-100 micrometres work presented in this thesis, but sufficient for aligning the larger anatomy.

### 9.3.2 The Anterior Deprogrammer

The literature review (Section 1.2.2) suggested that a patient-led method for positioning into CR might be sufficiently precise, physiological, and acceptable for most general dentists. This method relies on the ability to 'deprogram' the patient, which requires an anterior deprogramming jig. These can be pre-fabricated (and relined at chairside), or can be constructed chairside with greenstick, acrylic or similar ().

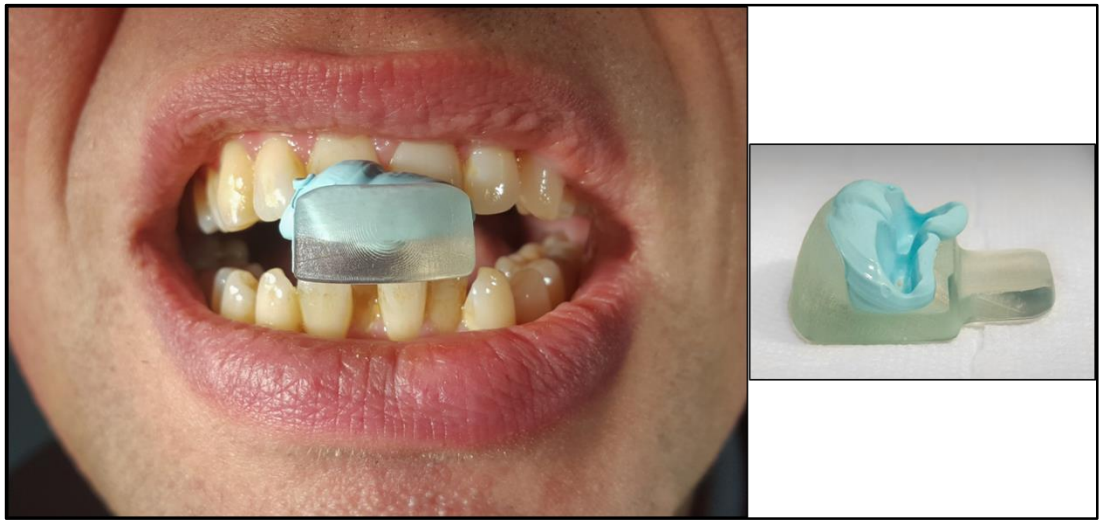

**Figure 101 Example of an Anterior Deprogrammer.** The subject can 'slide' their lower teeth backwards using the underside of the deprogrammer as a guide. Their upper and lower teeth cannot contact, causing them to 'forget' how they bite. The jaw position achieved is therefore entirely derived from muscular and skeletal factors, and not the teeth. For the 3D bite scans, a portion of the central and lateral incisors will be obscured. (The plastic jig has been relined with a silicone material to provide stability).

In any event, a region of the upper incisors will be obscured to the 3D camera, along with some possible shadowing of the lower incisors. It is not known how this reduction in the amount of data collected might affect the quality of the bite registration. It seems likely that, at the very least, this central region of the scan is the most 'favourable' place to be missing data. Using the *a priori* knowledge of the dentition, one might expect almost no detriment to the registration, because all points on the deprogrammer will be ignored during alignment, and a precise alignment in all regions surrounding the deprogrammer should be achieved.

This is another factor that will need exploring in order to move nearer to a complete clinical solution. Furthermore, in patients with a reduced number of anterior teeth, or no anterior teeth, the effect on the precision and trueness of the optical interocclusal record needs investigation.

However, throughout this thesis, the approach has been to test the new methods under ideal conditions first (to see whether the required trueness and precision can ever be achieved), then to address the compromises needed clinically to determine whether the method is still valid. If problems are encountered under non-ideal conditions, issues (such as the calibration) can be addressed to try to compensate.

This agile approach could be considered less scientifically rigorous, but the rationale is based on the need to keep pace with rapid changes in technology. For example, in 2011 (when starting this thesis), it was sensible to use the best affordable equipment and techniques, to assess whether the THA could be found with a reasonable degree of certainty on articulated models. This being the case, as the years have progressed, the projector has improved (at no additional cost), the standard scanning patterns have improved (again implemented at no cost), and the calibration method has improved (by enhancing methods that did not exist until 2015). These improvements have enabled a move closer to a clinically applicable solution, and the recent work in other machine vision fields has provided avenues to explore as a continuation of this work. It is likely that, if the one-shot 'jailbar' system had been implemented from the outset (using paper target calibration and a low contrast, low resolution projector), the error may have been sufficiently large as to reject the optical technique (as Long did with wax in 1970). This would have been a mistake, since the working assumption has thus far proved correct. Namely that as technology advances, any developments that happen to suit dental needs can be rapidly adopted.

To this end, it seems safe to assume that improvements in alignment algorithms will likely compensate for the hole in the scan data that will be caused by the anterior jig, and may also help in the partially dentate and edentulous cases

### 9.3.3 Summary of Future Work

**Improve the creation of the optical bite scan by using *a priori* knowledge of the expected shape**

The trueness, precision and density of the 3D data from the one-shot scanning pattern could be improved by supplying the stereo reconstruction algorithm with data regarding the subject's dentition. 3D facial scanning and integration of the dentition would allow full skeletal relationships to be recorded.

**Retest the trueness and precision of the enhanced system for finding the hinge axis of an articulator *in vitro***

Having created a new one-shot scanner, including the enhanced camera calibration and better 3D reconstruction, repeat the work in Sections 5 and 6. This provides the opportunity to measure the trueness of hinge axis location, and interocclusal recording.

**Development of a scanning technique to record registrations in patients with various occlusal configurations**

An assessment of the effect on bite registration, of an anterior jig, a reduced number of anterior teeth, and no anterior dentition at all, needs to be undertaken. Strategies may need to be developed to overcome such situations – for example by offsetting the scan to one side, where there is more anatomy for the alignment algorithm to use.

**Clinical testing**

With the equipment running smoothly in a 'beta' phase of development, precision of hinge axis location could be tested in a clinical trial. Trueness could also be tested against a clinically accepted pantographic standard.

**Dynamic bite registrations**

The technique could be extended to scanning mandibular positions that are traditionally difficult to record, but would be clinically useful. For example, lateral bite registrations would be of benefit in many dental treatments and should be possible using this technique. The 3D video system would also lend itself to short functional recordings, such as chewing or grinding motions.

# Bibliography


Academy of Denture Prosthetics, 2005. The glossary of prosthodontic terms. *Journal of Prosthetic Dentistry*, 94(1), pp.10–92.

Adrien, P. & Schouver, J., 1997. Methods for minimizing the errors in mandibular model mounting on an articulator. *Journal of Oral Rehabilitation*, 24, pp.929–935.

Aissaoui, A. et al., 2012. Fast stereo matching method based on optimized correlation algorithm for face depth estimation. In *Proceedings of the International Conference on Computer Vision Theory and Applications (VISIGRAPP 2012)*. pp. 377–380.

Bader, J.D., Martin, J.A. & Shugars, D.A., 2001. Incidence rates for complete cusp fracture. *Community Dentistry and Oral Epidemiology*, 29(5), pp.346–53.

Balch, J.H., 2012. *Verification of the accuracy of electronic mandibular movement recording devices: an in vitro investigation*. Masters thesis, The University of Tennessee Health Science Center, USA.

Balkwill, F.H., 1866. On the best form and arrangement of artificial teeth for mastication. *Transactions of Great Britain Odontological Society*, 5, p.133.

Beard, C.C. & Clayton, J.A., 1981. Studies on the validity of the terminal hinge axis. *Journal of Prosthetic Dentistry*, 46(2), pp.185–191.

Bennett, N., 1908. A contribution to the study of the movements of the mandible. *Proceedings of the Royal Society of Medicine, Section of Odontology*, April 27, pp.79–95.

Bergstra, J. et al., 2010. Theano: a CPU and GPU math expression compiler. In *Proceedings of the Python for Scientific Computing Conference (SciPy)*. Austin, TX, pp. 1–7.

Bergstrom, G., 1950. On the reproduction of dental articulation by means of articulators. *Acta Odontologica Scandinavica. Supplementum*, 9(Suppl. 4), pp.3–149.

Besl, P. & McKay, N., 1992. A method for registration of 3-D shapes. *IEEE Transactions on Pattern Analysis and Machine Intelligence*, 14(2), pp.239–256.

De Boever, J.A., Carlsson, G.E. & Klineberg, I.J., 2000. Need for occlusal therapy and prosthodontic treatment in the management of temporomandibular disorders. Part II: tooth loss and prosthodontic treatment. *Journal of Oral Rehabilitation*, 27(8), pp.647–659.

Bonwill, W.G.A., 1864. Articulation and articulators. *Transactions of the American Dental Association*, 26, pp.76–79.

Bonwill, W.G.A., 1885. Geometrical and mechanical laws of articulation. *Transactions of Pennsylvania Odontological Society*, p.119.

Bonwill, W.G.A., 1896. What has dentistry to demonstrate against the hypothesis of organic evolution ? In *Transactions of the Worlds Columbian Dental Congress*. Chicago, pp. 226–240.

Brusco, N. et al., 2007. Metrological validation for 3D modeling of dental plaster casts. *Medical Engineering & Physics*, 29(9), pp.954–66.

Campos, A.A., Nathanson, D. & Rose, L., 1996. Reproducibility and condylar position of a physiologic maxillomandibular centric relation in upright and supine body position. *Journal of Orthodontics*, 76(3), pp.282–287.

Carlsson, G.E., 2010. Some dogmas related to prosthodontics, temporomandibular disorders and occlusion. *Acta Odontologica Scandinavica*, 68(6), pp.313–322.

Celenza, F. V, 1973. The centric position: replacement and character. *Journal of Prosthetic Dentistry*, 30(4), pp.591–598.

Chasles, M., 1830. Note sur les proprietes generales du systeme de deux corps semblables entr'eux. *Bulletin de Sciences Mathematiques, Astronomiques Physiques et Chimiques, Baron de Ferussac, Paris*, pp.321–326.

Chen, D.C. et al., 2000. Contributing factors of mandibular deformation during mouth opening. *Journal of Dentistry*, 28(8), pp.583–588.

Chen, X., 1998. The instantaneous center of rotation during human jaw opening and its significance in interpreting the functional meaning of condylar translation. *American Journal of Physical Anthropology*, 106(1), pp.35–46.

Choi, D.G. et al., 1999. Reliability of an ear-bow arbitrary face-bow transfer instrument. *Journal of Prosthetic Dentistry*, 82(2), pp.150–156.

Cioffi, I. et al., 2015. Short-term sensorimotor effects of experimental occlusal interferences on the wake-time masseter muscle activity of females with masticatory muscle pain. *Journal of Oral & Facial Pain and Headache*, 29(4), pp.331–339.

Clark, D.M., Oyen, O.J. & Feil, P., 2001. The use of specific dental school-taught restorative techniques by practicing clinicians. *Journal of Dental Education*, 65(8), pp.760–5.

Clark, J.R. & Evans, R.D., 2001. Functional occlusion: I. A review. *Journal of Orthodontics*, 28(1), pp.76–81.

Davies, S. & Gray, R.M., 2001. What is occlusion? *British Dental Journal*, 191(5), pp.235–238, 241–245.

Davies, S.J., Gray, R.M. & Smith, P.W., 2001. Good occlusal practice in simple restorative dentistry. *British Dental Journal*, 191(7), pp.365–381.

Dawson, P., 1989. *Evaluation, diagnosis and treatment of occlusal problems.* 2nd ed., St Louis: Elsevier.

DeLong, R. et al., 2007. Accuracy of contacts calculated from 3D images of occlusal surfaces. *Journal of Dentistry*, 35(6), pp.528–534.

Delong, R. et al., 2002. Comparing maximum intercuspal contacts of virtual dental patients and mounted dental casts. *Journal of Prosthetic Dentistry*, 88(6), pp.622–630.

DeLong, R. et al., 2002. Helical axis errors affect computer-generated occlusal contacts. *Journal of Dental Research*, 81(5), pp.338–343.

Donovan, T.E. & Chee, W.W.L., 2004. A review of contemporary impression materials and techniques. *Dental Clinics of North America*, 48, pp.445–70.

Ender, A., Attin, T. & Mehl, A., 2016. In vivo precision of conventional and digital methods of obtaining complete-arch dental impressions. *Journal of Prosthetic Dentistry*, 115(3), pp.313–320.

Ender, A. & Mehl, A., 2013. Accuracy of complete-arch dental impressions: a new method of measuring trueness and precision. *Journal of Prosthetic Dentistry*, 109(2), pp.121–128.

Ender, A. & Mehl, A., 2011. Full arch scans : conventional versus digital

impressions – an in-vitro study. *International Journal of Computerized Dentistry*, 14, pp.11–21.

Eriksson, A. et al., 2002. Clinical factors and clinical variation influencing the reproducibility of interocclusal recording methods. *British Dental Journal*, 192(7), pp.395–400.

Fang, J.-J. & Kuo, T.-H., 2008. Modelling of mandibular movement. *Computers in Biology and Medicine*, 38(11-12), pp.1152–62.

Fenlon, M.R. & Woelfel, J.B., 1993. Condylar position recorded using leaf gauges and specific closure forces. *International Journal of Prosthodontics*, 6(4), pp.402–8.

Fennis, W.M.M. et al., 2002. A survey of cusp fractures in a population of general dental practices. *International Journal of Prosthodontics*, 15(6), pp.559–563.

Ferrario, V.F. et al., 1996. Open-close movements in the human temporomandibular joint: does a pure rotation around the intercondylar hinge axis e? *Journal of Oral Rehabilitation*, 23, pp.401–408.

Ferrario, V.F. et al., 2005. Quantification of translational and gliding components in human temporomandibular joint during mouth opening. *Archives of Oral Biology*, 50(5), pp.507–15.

Fox, S.S., 1967. The significance of errors in hinge axis location. *Journal of the American Dental Association*, 74(6), pp.1268–1272.

Gal, J. a et al., 2004. Analysis of human mandibular mechanics based on screw theory and in vivo data. *Journal of Biomechanics*, 37(9), pp.1405–12.

Gallo, L.M. et al., 1997. Description of mandibular finite helical axis pathways in asymptomatic subjects. *Journal of Dental Research*, 76(2), pp.704–713.

Gallo, L.M. et al., 2006. Relevance of mandibular helical axis analysis in functional and dysfunctional TMJs. *Journal of Biomechanics*, 39(9), pp.1716–25.

Gámez, J.C., Dib, A.K. & Espinosa de S, I.A., 2013. Face bows in the development of michigan occlusal splints. *Revista Facultad de Odontología Universidad de Antioquia*, 25, pp.117–131.

Geiger, A., Lenz, P. & Urtasun, R., 2012. Are we ready for autonomous driving? The KITTI vision benchmark suite. In *IEEE Conference on Computer Vision and Pattern Recognition*. Providence, RI, pp. 3354 – 3361.

Geng, J., 2011. Structured-light 3D surface imaging: a tutorial. *Advances in Optics and Photonics*, 3(2), p.128.

Gordon, S.R., Stoffer, W.M. & Connor, S.A., 1984. Location of the terminal hinge axis and its effect on the second molar cusp position. *Journal of Prosthetic Dentistry*, 52(1), pp.99–105.

Grant, P.G., 1973. Biomechanical significance of the instantaneous center of rotation :tThe human temporomandibular joint. *Journal of Biomechanics*, 6, pp.109–113.

Güney, F. & Geiger, A., 2015. Displets: resolving stereo ambiguities using object knowledge. In *IEEE Conference on Computer Vision and Pattern Recognition*. Boston, MA, pp. 4165 – 4175.

Hall-Holt, O. & Rusinkiewicz, S., 2001. Stripe boundary codes for real-time structured-light range scanning of moving objects. In *Eighth IEEE International Conference on Computer Vision*. Vancouver, BC, pp. 359–366.

Hartley, R.I. & Zisserman, A., 2004. *Multiple View Geometry in Computer Vision* Second., Cambridge, UK: Cambridge University Press.

Hatzi, P., Millstein, P. & Maya, A., 2001. Determining the accuracy of articulator interchangeability and hinge axis reproducibility. *Journal of Prosthetic Dentistry*, 85(3), pp.236–45.

Hellmann, D. et al., 2013. Accuracy of transfer of bite recording to simulated prosthetic reconstructions. *Clinical Oral Investigations*, 17(1), pp.259–267.

Hindle, J.R. & Craddock, H.L., 2006. The use of articulators in UK dental schools. *European Journal of Dental Education*, 10(4), pp.197–203.

Hoang, T. et al., 2010. Generic gamma correction for accuracy enhancement in fringe-projection profilometry. *Optics Letters*, 35(12), pp.1992–1994.

Iwaki, Y., Wakabayashi, N. & Igarashi, Y., 2013. Dimensional accuracy of optical bite registration in single and multiple unit restorations. *Operative Dentistry*, 38(3), pp.309–15.

Jankelson, B., 1969. Electronic control of muscle contraction--a new clinical era in occlusion and prosthodontics. *Scientific and Educational Bulletin*, 2(1), pp.29–31.

Jaschouz, S. & Mehl, A., 2014. Reproducibility of habitual intercuspation in vivo. *Journal of Dentistry*, 42(2), pp.210–218.

Jeon, J.H. et al., 2015. Three-dimensional evaluation of the repeatability of scanned conventional impressions of prepared teeth generated with white- and blue-light scanners. *Journal of Prosthetic Dentistry*, 114(4), pp.549–553.

Jinbao, W., Xiaoming, X. & Jingen, S., 1988. Analysis of the open-closing movement of the human temporomandibular joint. *Acta Anatomica*, 133(3), pp.213–216.

Karl, P.J. & Foley, T.F., 1999. The use of a deprogramming appliance to obtain centric relation records. *Angle Orthodontist*, 69(2), pp.117–125.

Keshvad, A. & Winstanley, R.B., 2001. An appraisal of the literature on centric relation. Part III. *Journal of Oral Rehabilitation*, 28, pp.55–63.

Keshvad, A. & Winstanley, R.B., 2000. Review An appraisal of the literature on centric relation . Part I : Centric relation. *Journal of Oral Rehabilitation*, 27, pp.823–833.

Kois, J.C., Kois, D.E. & Chaiyabutr, Y., 2013. Occlusal errors generated at the maxillary incisal edge position related to discrepancies in the arbitrary horizontal axis location and to the thickness of the interocclusal record. *Journal of Prosthetic Dentistry*, 110(5), pp.414–419.

Konolige, K., 2010. Projected texture stereo. In *IEEE International Conference on Robotics and Automation (ICRA)*. Anchorage, AK, pp. 148–155.

Koralakunte, P.R. & Aljanakh, M., 2014. The role of virtual articulator in prosthetic and restorative dentistry. *Journal of Clinical and Diagnostic Research*, 8(7), pp.ZE25–ZE28.

Lau, D.L., Liu, K. & Hassebrook, L.G., 2010. Real-time three-dimensional shape measurement of moving objects without edge errors by time-synchronized structured illumination. *Optics Letters*, 35(14), pp.2487–2489.

Lauritzen, A.G. & Bodner, G.H., 1961. Variations in location of arbitrary and true hinge axis points. *Journal of Prosthetic Dentistry*, 11, pp.224–229.

Lauritzen, A.G. & Wolford, L., 1961. Hinge axis location on an experimental basis. *Journal of Prosthetic Dentistry*, 11, pp.1059–1067.

Lazic, B. et al., 2006. Intercondylar distances of the human temporomandibular joints. *Collegium Antropologicum*, 30(1), pp.37–41.

Li, Z. & Li, Y., 2011. Gamma-distorted fringe image modeling and accurate gamma correction for fast phase measuring profilometry. *Optics Letters*, 36(2), pp.154–156.

Lindauer, S.J. et al., 1995. Condylar movement and mandibular rotation during jaw opening. *American Journal of Orthodontics and Dentofacial Orthopedics*, 107(6), pp.573–577.

Liu, K. et al., 2010a. Dual-frequency pattern scheme for high-speed 3-D shape measurement. *Optics Express*, 18(5), pp.5229–5244.

Liu, K. et al., 2010b. Gamma model and its analysis for phase measuring profilometry. *Journal of the Optical Society of America.*, 27(3), pp.553–562.

Lohot, P.M. & Sonawane, B.M., 2015. A new approach for stereo matching algorithm with dynamic programming. *International Journal on Recent and Innovation Trends in Computing and Communication*, 3(2), pp.691–696.

Long, J.H., 1973. Locating centric relation with a leaf gauge. *Journal of Prosthetic Dentistry*, 29(6), pp.608–610.

Long, J.H., 1970. Location of the terminal hinge axis by intraoral means. *Journal of Prosthetic Dentistry*, 23(1), pp.11–24.

Lucia, V.O., 1960. Centric relation — theory and practice. *Journal of Prosthetic Dentistry*, 10(5), pp.849–856.

Lucia, V.O., 1964. Technique for recording centric relation. *Journal of Prosthetic Dentistry*, 14, p.492.

Lumley, T. et al., 2002. The importance of the normality assumption in large public health data sets. *Annual Reviews of Public Health*, 23, pp.151–169.

Lux, L.H. et al., 2015. Comparison of the Kois Dento-Facial Analyzer System with an earbow for mounting a maxillary cast. *Journal of Prosthetic Dentistry*, 114(3), pp.432–439.

Maestre-ferrín, L. et al., 2012. Virtual articulator for the analysis of dental occlusion: An update. *Medicina Oral, Patología Oral y Cirugía Bucal*, 17(1), pp.e160–e163.

Magne, P., Gallucci, G.O. & Belser, U.C., 2016. Anatomic crown width/length ratios of unworn and worn maxillary teeth in white subjects. *Journal of Prosthetic Dentistry*, 89(5), pp.453–461.

Magnusson, M., 2009. *The three-dimensional normal-distributions transform — an efficient representation for registration, surface analysis, and loop detection*. PhD thesis, Orebro University, Sweden.

Mandilaris, C.B., Beard, C.C. & Clayton, J.A., 1992. Comparison of the intercondylar distance and the interfacial width as used with the electronic pantograph. *Journal of Prosthetic Dentistry*, 67(3), pp.331–334.

McCollum, B.B. & Stuart, C.E., 1955. *A research report. A basic text for post graduate courses in gnathology*, Ventura, Ca.: Chas. E. Stuart. Available at: http://catalog.hathitrust.org/Record/000300228 [Accessed May 2, 2016].

McKee, J.R., 1997. Comparing condylar position repeatability for standardized versus nonstandardized methods of achieving centric relation. *Journal of Prosthetic Dentistry*, 77(3), pp.280–4.

McKee, J.R., 2005. Comparing condylar positions achieved through bimanual manipulation to condylar positions achieved through masticatory muscle contraction against an anterior deprogrammer: a pilot study. *Journal of Prosthetic Dentistry*, 94(4), pp.389–93.

McMillan, A.S., McMillan, D.R. & Darvell, B.W., 1989. Centers of rotation during jaw

movements. *Acta Odontologica Scandinavica*, 47(5), pp.323–328.

McMillan, D.R. & McMillan, A.S., 1986. A comparison of habitual jaw movements and articulator function. *Acta Odontologica Scandinavica*, 44(5), pp.291–299.

McNamara, J.A., 1973. The independent functions of the two heads of the lateral pterygoid muscle. *American Journal of Anatomy*, 138, pp.197–205.

Millet, C. et al., 2003. Report on the determination of occlusal vertical dimension and centric relation using swallowing in edentulous patients. *Journal of Oral Rehabilitation*, 30(11), pp.1118–1122.

Mohan, D. & Ram, A.R., 2015. A review on depth estimation for computer vision applications. *International Journal on Recent and Innovation Trends in Computing and Communication*, 4(11), pp.235–239.

Moreno, D., Son, K. & Taubin, G., 2015. Embedded phase shifting: robust phase shifting with embedded signals. In *IEEE Conference on Computer Vision and Pattern Recognition (CVPR)*. Boston, MA, pp. 2301–2309.

Morneburg, T.R. & Pröschel, P.A., 2011. Impact of arbitrary and mean transfer of dental casts to the articulator on centric occlusal errors. *Clinical Oral Investigations*, 15(3), pp.427–434.

Morneburg, T.R. & Pröschel, P.A., 2002. Predicted incidence of occlusal errors in centric closing around arbitrary axes. *International Journal of Prosthodontics*, 15(4), pp.358–64.

Müller, H.C., 2010. Registration of occlusion by buccal scan in Cerec software version 3.80. *International Journal of Computerized Dentistry*, 13(3), pp.265–273.

Nagy, W.W., Smithy, T.J. & Wirth, C.G., 2002. Accuracy of a predetermined transverse horizontal mandibular axis point. *Journal of Prosthetic Dentistry*, 87(4), pp.387–394.

Ohm, E. & Silness, J., 1982. The size of the Balkwill angle and the height of the Bonwill triangle. *Journal of Oral Rehabilitation*, 9(4), pp.301–306.

Parfitt, G.J., 1960. Measurement of the physiological mobility of individual teeth in an axial direction. *Journal of Dental Research*, 39, pp.608–618.

Park, N. et al., 1989. Comparison of centric relation recording methods. *Journal of Dental Research*, 68(4), p.693.

Parker, M.H. et al., 1997. Comparison of occlusal contacts in maximum intercuspation for two impression techniques. *Journal of Prosthetic Dentistry*, 78(3), pp.255–259.

Piehslinger, E., Bauer, W. & Schmiedmayer, H.B., 1995. Computer simulation of occlusal discrepancies resulting from different mounting techniques. *Journal of Prosthetic Dentistry*, 74(3), pp.279–283.

Posselt, U., 1956. Hinge opening axis of the mandible. *Acta Odontologica Scandinavica*, 14(1), pp.49–63.

Posselt, U., 1952. Studies in the mobility of the human mandible. *Acta Odontologica Scandinavica*, 10(Suppl 10), pp.19–160.

Pröschel, P.A. et al., 2002. Articulator-related registration--a simple concept for minimizing eccentric occlusal errors in the articulator. *International Journal of Prosthodontics*, 15(3), pp.289–294.

Pröschel, P.A., Maul, T. & Morneburg, T., 2000. Predicted incidence of excursive occlusal errors in common modes of articulator adjustment. *International Journal of Prosthodontics*, 13(4), pp.303–10.

Quoob, A., Ruge, S. & Kordab, B., 2011. GEDAS II – new possibilities in digital contact point analysis. *International Journal of Computerized Dentistry*, 14, pp.105–109.

Ramfjord, S. & Ash, M.M., 1983. *Occlusion* 3rd ed., Philadelphia: WB Saunders.

Razek, M.K.A., 1981. Clinical evaluation of methods used in locating the mandibular hinge axis. *Journal of Prosthetic Dentistry*, 46(4), pp.369–373.

Reeh, E.S., Messer, H.H. & Douglas, W.H., 1989. Reduction in tooth stiffness as a result of endodontic and restorative procedures. *Journal of Endodontics*, 15(11), pp.512–516.

Regli, C.P. & Kelly, E.K., 1967. The phenomenon of decreased mandibular arch width in opening movements. *Journal of Prosthetic Dentistry*, 17(1), pp.49–53.

Reveredo, A.M. et al., 2013. Evaluation of active tactile perception of single tooth implant prosthesis. *International Journal of Oral Implantology and Clinical Research*, 4(1), pp.1–6.

Roth, R. & Rolfs, D., 1981. Functional occlusion for the orthodontist, part 2. *Journal of Clinical Orthodontics*, 15(2), pp.100–123.

Scharstein, D. et al., 2014. High-resolution stereo datasets with subpixel-accurate ground truth. In *German Conference on Pattern Recognition (GCPR)*. Munster, DE, pp. 31–42.

Schmalz, C., Forster, F. & Angelopoulou, E., 2011. Camera calibration: active versus passive targets. *Optical Engineering*, 50(11), p.113601.

Shafagh, I., Yoder, J.L. & Thayer, K.E., 1975. Diurnal variance of centric relation position. *Journal of Prosthetic Dentistry*, 34(5), pp.574–582.

Shodadai, S.P. et al., 2001. Is there a benefit of using an arbitrary facebow for the fabrication of a stabilization appliance? *International Journal of Prosthodontics*, 14(6), pp.517–522.

Solaberrieta, E. et al., 2015. Comparison of a conventional and virtual occlusal record. *Journal of Prosthetic Dentistry*, 114(1), pp.92–97.

Solaberrieta, E. et al., 2016. Determining the requirements , section quantity , and dimension of the virtual occlusal record. *Journal of Prosthetic Dentistry*, 115(1), pp.1–5.

Sprickerhof, J. & Nüchter, A., 2011. A heuristic loop closing technique for large-scale 6d slam. *Automatika*, 52(3), pp.199–222.

Steele, J. & O'Sullivan, I., 2011. *Adult Dental Health Survey 2009*, Available at: http://www.hscic.gov.uk/pubs/dentalsurveyfullreport09 [Accessed May 2, 2016].

Storey, D. & Coward, T.J., 2014. The quality of impressions for crowns and bridges: an assessment of the work received at three commercial dental laboratories. assessing qualities of impressions that may lead to occlusal discrepancies with indirect restorations. *European Journal of Prosthodontics and Restorative Dentistry*, 22(1), pp.11–18.

Storey, D. & Coward, T.J., 2013. The quality of impressions for crowns and bridges: an assessment of the work received at three commercial dental laboratories. assessing the quality of the impressions of prepared teeth. *European Journal of Prosthodontics and Restorative Dentistry*, 21(2), pp.53–57.

Straga, R.W., 2009. *Comparison of occlusal contacts on mounted dental models to contacts identified on digital 3D models using a new virtual alignment method*. MSc thesis, University of British Columbia, Vancouver, CA.

Tanaka, Y. & Hattori, Y., 2012. Dimensional and occlusal accuracy of a novel three-

dimensional digital model of articulated dental arches. *International Journal of Prosthodontics*, 26(3), pp.282–7.

Taylor, M. & Prendergast, P.J., 2015. Four decades of finite element analysis of orthopaedic devices: where are we now and what are the opportunities? *Journal of Biomechanics*, 48(5), pp.767–78.

Tokiwa, H. et al., 2010. Anatomical location of various condylar points for jaw movement analysis in Japanese women. *Journal of Oral Rehabilitation*, 37(4), pp.235–241.

Tsai, R., 1987. A versatile camera calibration technique for high-accuracy 3D machine vision metrology using off-the-shelf TV cameras and lenses. *IEEE Journal on Robotics and Automation*, 3(4), pp.323–344.

Tuppy, F. et al., 1994. The reproducibility of condylar hinge axis positions in patients, by different operators, using the electronic mandibular position indicator. *Journal of Orofacial Pain*, 8(3), pp.315–320.

Türp, J.C., Greene, C.S. & Strub, J.R., 2008. Dental occlusion: a critical reflection on past, present and future concepts. *Journal of Oral Rehabilitation*, 35(6), pp.446–453.

Ueda, Y. et al., 2014. Evaluation of occlusal relationship reproducibility with CAD / CAM techniques. *Asian Pacific Journal of Dentistry*, 14, pp.35–40.

Utz, K.H. et al., 2002. Accuracy of check-bite registration and centric condylar position. *Journal of Oral Rehabilitation*, 29(5), pp.458–466.

Van't Spijker, A. et al., 2009. Prevalence of tooth wear in adults. *International Journal of Prosthodontics*, 22(1), pp.35–42.

Walker, P., 1980. Discrepancies between arbitrary and true hinge axes. *Journal of Prosthetic Dentistry*, 43, pp.279–285.

Walls, A.W., Wassell, R.W. & Steele, J.G., 1991. A comparison of two methods for locating the intercuspal position (ICP) whilst mounting casts on an articulator. *Journal of Oral Rehabilitation*, 18(1), pp.43–48.

Wang, Y. et al., 2010. Maximum SNR pattern strategy for phase shifting methods in structured light illumination. *Journal of the Optical Society of America.*, 27(9), pp.1962–1971.

Weinberg, L.A., 1972. Correlation of temporomandibular dysfunction with radiographic findings. *Journal of Prosthetic Dentistry*, 28(5), pp.519–539.

Weinberg, L.A., 1959. The transverse hinge axis: real or imaginary. *Journal of Prosthetic Dentistry*, 9(5), pp.775–787.

Wilson, P.H.R. & Banerjee, A., 2004. Recording the retruded contact position: a review of clinical techniques. *British Dental Journal*, 196(7), pp.395–402.

Winstanley, R.B., Carrotte, P. V & Johnson, A., 1997. The quality of impressions for crowns and bridges received at commercial dental laboratories. *British Dental Journal*, 183(6), pp.209–213.

Woelfel, J.B., 1986. New device for accurately recording centric relation. *Journal of Prosthetic Dentistry*, 56(6), pp.716–727.

Wood, D.P. & Elliott, R.W., 1994. Reproducibility of the centric relation bite registration technique. *Angle Orthodontist*, 64(3), pp.211–220.

Zatsiorsky, V., 1998. *Kinematics of Human Motion*, Champaign, Illinios: Human Kinetics.

# Glossary of Terms

| | |
|---|---|
| **2-Dimensional (2D)** | Having the dimensions of height and width only. |
| **3-Dimensional (3D)** | Having the dimensions of height, width and depth. |
| **Anterior** | Towards the front of the body. |
| **Articulation** | The static and dynamic contact relationship between the occlusal surfaces of the teeth during function. |
| **Articulator** | A mechanical instrument that represents the temporomandibular joints and jaws, to which maxillary and mandibular casts may be attached to simulate some or all mandibular movements. |
| **Bennett Angle** | The angle formed between the sagittal plane and the average path of the advancing condyle as viewed in the horizontal plane during lateral mandibular movements. |
| **Bridge** | An artificial replacement of one of more missing teeth, being fixed in the mouth to adjacent teeth or implants. |
| **Bruxism** | The parafunctional grinding of the teeth, typically during sleep *or* an oral habit consisting of involuntary rhythmic or spasmodic nonfunctional gnashing, grinding, or clenching of teeth, in other than chewing movements of the mandible, which may lead to occlusal trauma. |
| **Buccal** | Pertaining to or adjacent to the cheek. |
| **CAD/CAM** | Computer Aided Design / Computer Aided Manufacture. Technology allowing the design of an object using a computer, and the fabrication of that object using an automated manufacturing process, typically computer controlled milling. |
| **Canine** | A pointed tooth between the incisors and premolars of a mammal, often greatly enlarged in carnivores. |
| **Caries** | The process of tooth decay. |
| **Cariology** | The study of dental caries (tooth decay) and cariogenesis. |
| **Caudal** | Towards the cauda, or tail, of the body. |

| | |
|---|---|
| **Centric Relation, CR** | The maxillomandibular relationship in which the condyles articulate with the thinnest avascular portion of their respective disks with the complex in the anterior-superior position against the shapes of the articular eminencies. This position is independent of tooth contact. This position is clinically discernible when the mandible is directed superior and anteriorly. It is restricted to a purely rotary movement about the transverse horizontal axis. |
| **Condyle** | Articular prominence of a bone, i.e., in the mandible, an ellipsoidal projection of bone that articulates with the glenoid fossa. |
| **Cranial** | Towards the cranium, or head, of the body. |
| **Crown** | An artificial replacement that restores missing tooth structure by surrounding part or all of the remaining structure with a material such as cast metal, porcelain, or a combination of materials such as metal and porcelain. |
| **Denture** | An artificial substitute for missing natural teeth and adjacent tissues. May be removable or fixed. |
| **Dynamic Occlusion** | The contact relationships of maxillary and mandibular teeth as they move against each other. |
| **Earbow** | An instrument similar to a facebow that indexes to the external auditory meatus and registers the relation of the maxillary dental arch to the external auditory meatus and a horizontal reference plane. This instrument is used to transfer the maxillary cast to the articulator. The earbow provides an average anatomic dimension between the external auditory meatus and the horizontal axis of the mandible. |
| **External Auditory Meatus, EAM** | The passage leading into the ear. |

| | |
|---|---|
| **Facebow** | A caliper-like instrument used to record the spatial relationship of the maxillary arch to some anatomic reference point or points and then transfer this relationship to an articulator; it orients the dental cast in the same relationship to the opening axis of the articulator. Customarily the anatomic references are the mandibular condyles transverse horizontal axis and one other selected anterior point. |
| **Finite Helical Axis, FHA** | A line that is simultaneously the axis of rotation and the line along which translation of a body occurs. The motion is valid for a finite rotation around this line. |
| **Fossa** | An anatomical pit, groove, or depression. |
| **Frankfort Plane** | A plane established by the lowest point on the margin of the right or left bony orbit and the highest point on the margin of the right or left bony auditory meatus. |
| **Glenoid Fossa** | The concavity in the temporal bone by the zygomatic arch that receives the mandibular condyle. |
| **Incisor** | A narrow-edged tooth at the front of the mouth, adapted for cutting. In humans there are four incisors in each jaw. |
| **Infra Orbital Notch** | A groove in the lower orbital rim, palpable clinically. |
| **Instantaneous Axis of Rotation** | In a body which has motions both of translation and rotation, is a line, which is supposed to be rigidly united with the body, and which for the instant is at rest. The motion of the body is for the instant simply that of rotation about the instantaneous axis. (3D) |
| **Instantaneous Centre of Rotation, ICR** | A point on a rigid body whose velocity is zero at a given instant. (2D) |
| **Labial Segment** | The teeth and surrounding structures in close approximation to the lips. |

| | |
|---|---|
| **Lateral Pterygoid Muscle** | A muscle whose inferior head has origin from the pterygoid process, and whose superior head has origin from the sphenoid bone, with insertion into the mandible and the articular disk, with nerve supply from the lateral pterygoid branch of the trigeminal nerve, and whose action brings the jaw forward and opens it. |
| **Mandible** | The lower jaw bone. |
| **Masseter Muscle** | A major jaw closing muscle in the cheek, particularly active during late stage closure, and clenching. |
| **Masticatory System** | The organs and structures primarily functioning in mastication. These include the teeth with their supporting structures, craniomandibular articulations, mandible, positioning and accessory musculature, tongue, lips, cheeks, oral mucosa, and the associated neurologic complex. |
| **Maxilla** | The irregularly shaped bone that, with its contralateral maxilla, forms the upper jaw. It assists in the formation of the orbit, the nasal cavity, and the hard palate; it contains the maxillary teeth. |
| **Maximum Intercuspal Position, MICP** | The complete intercuspation of the opposing teeth independent of condylar position, sometimes referred to as the best fit of the teeth regardless of the condylar position. |
| **Michigan Splint** | A rigid mouth guard designed to fit over all the teeth in the dental arch, allowing the patient an even, prescribed, occlusion and articulation. |
| **Molar** | A grinding tooth at the back of a mammal's mouth. |
| **Non-Working Side** | That side of the mandible that moves toward the median line in a lateral excursion. |
| **Occlusal Vertical Dimension, OVD** | The distance measured between two points when the occluding members are in contact. |
| **Periodontology** | The branch of dentistry concerned with the structures surrounding and supporting the teeth. |
| **Posterior** | Towards the rear of the body. |

| | |
|---|---|
| **Premolar** | A tooth situated between the canine and the molar teeth. An adult human normally has eight, two in each jaw on each side. |
| **Prosthesis** | An artificial replacement of an absent part of the human body. |
| **Static Occlusion** | The contacts relationships of maxillary and mandibular teeth as they bite together but are not moving. |
| **Stomatognathic System** | The combination of structures involved in speech, mastication and deglutition as well as parafunctional actions. |
| **Temporalis Muscle** | A fan shaped muscle on each side of the head, particularly active during jaw closure from a wide gape. |
| **Temporomandibular joint, TMJ** | The articulation between the temporal bone and the mandible. It is a bilateral diarthrodial, bilateral ginglymoid joint. |
| **Transverse Horizontal Axis, THA** | An imaginary line around which the mandible may rotate within the sagittal plane. |
| **Working Side** | The side toward which the mandible moves in a lateral excursion. |

# Appendix A

## Q-Q Plots for Calibration Experiment Data

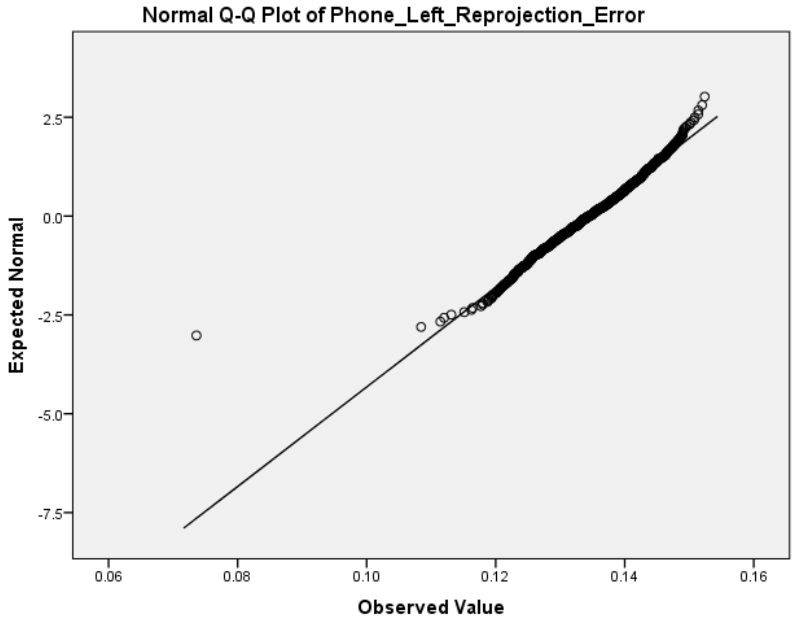


**Figure 102 Q-Q Plot of Left Camera Reprojection Error (Mobile Phone Method)**

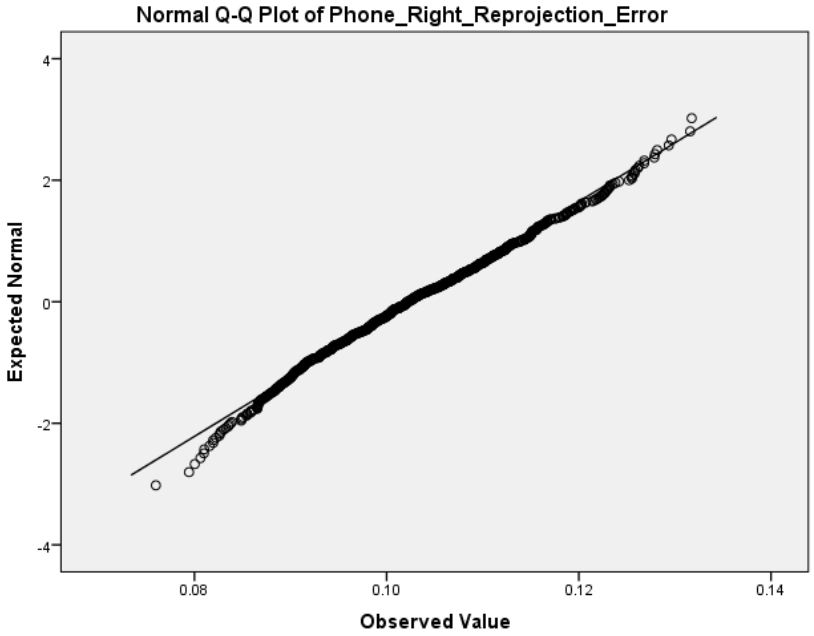


**Figure 103 Q-Q Plot of Right Camera Reprojection Error (Mobile Phone Method)**

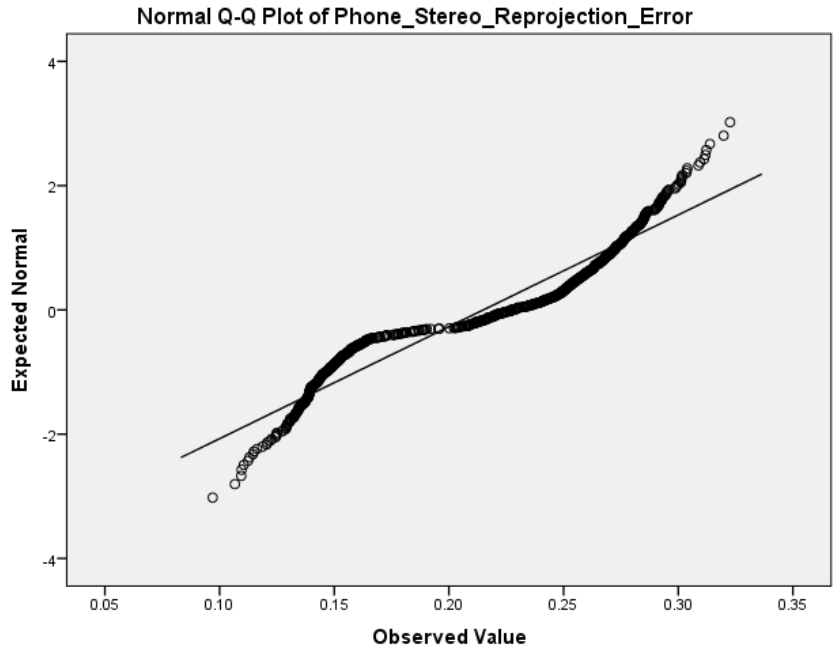


**Figure 104 Q-Q Plot of Stereo Reprojection Error (Mobile Phone Method)**

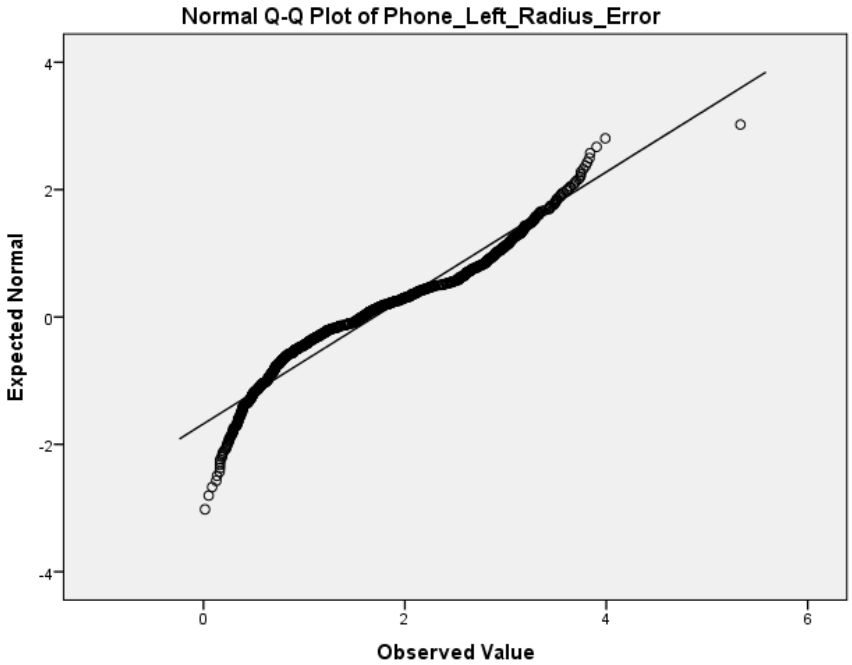


**Figure 105 Q-Q Plot of Principal Point Error Radius for Left Camera (Mobile Phone Method)**

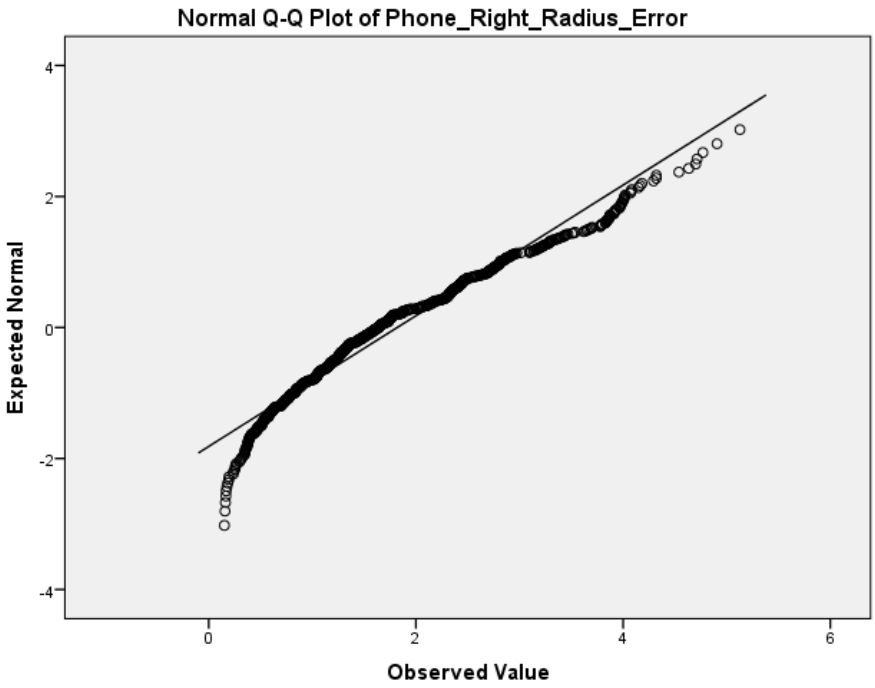


**Figure 106 Q-Q Plot of Principal Point Error Radius for Right Camera (Mobile Phone Method)**

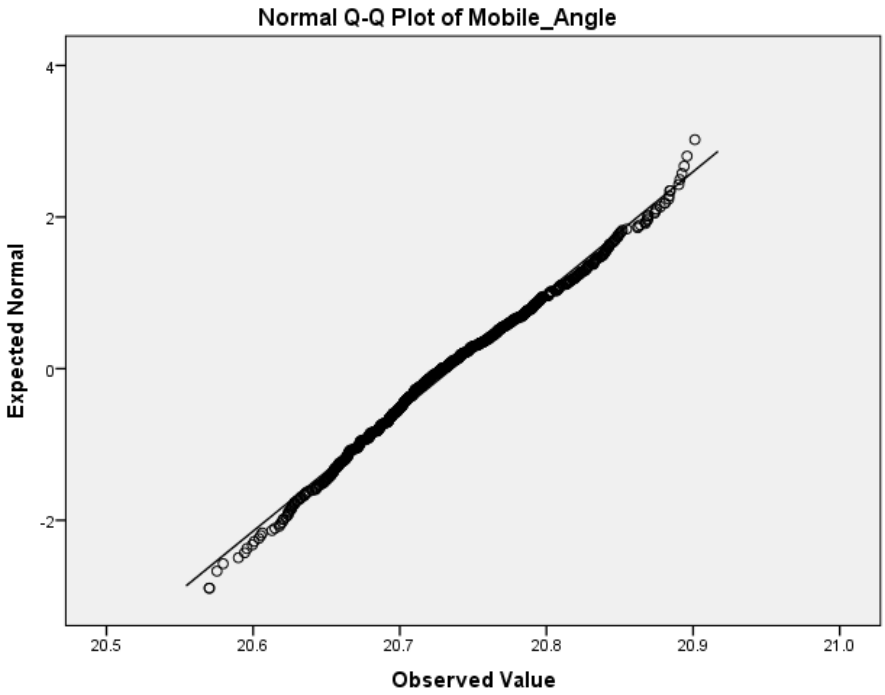


**Figure 107 Q-Q Plot of Estimated Angle Between Stereo Cameras (Mobile Phone Method)**


**Figure 108 Q-Q Plot of Left Camera Reprojection Error (Glass Target Method)**


**Figure 109 Q-Q Plot of Right Camera Reprojection Error (Glass Target Method)**


**Figure 110 Q-Q Plot of Stereo Reprojection Error (Glass Target Method)**

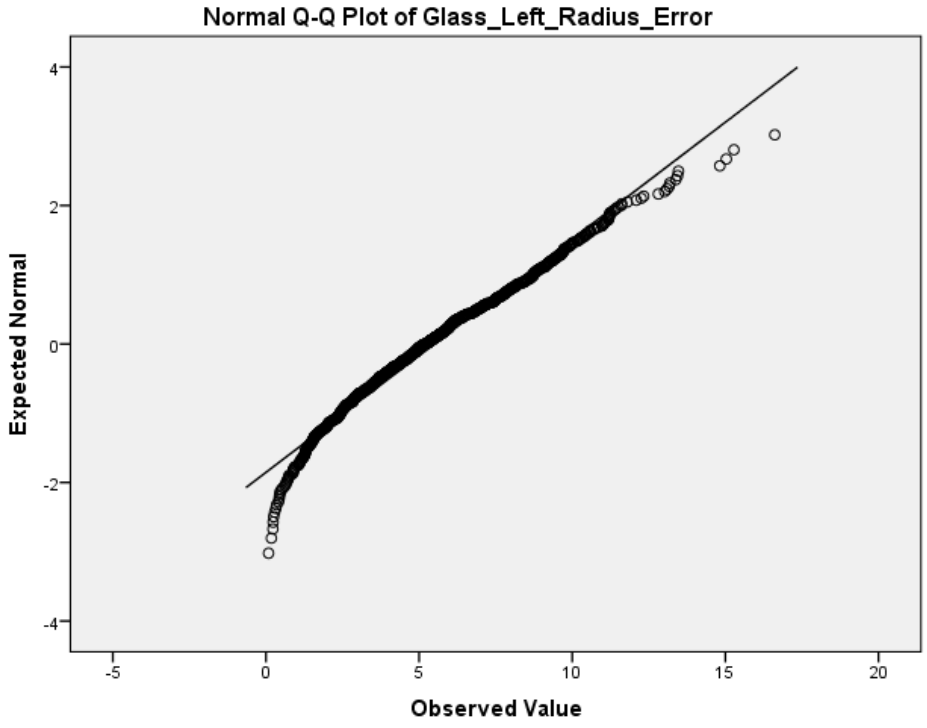


**Figure 111 Q-Q Plot of Principal Point Error Radius for Left Camera (Glass Target Method)**

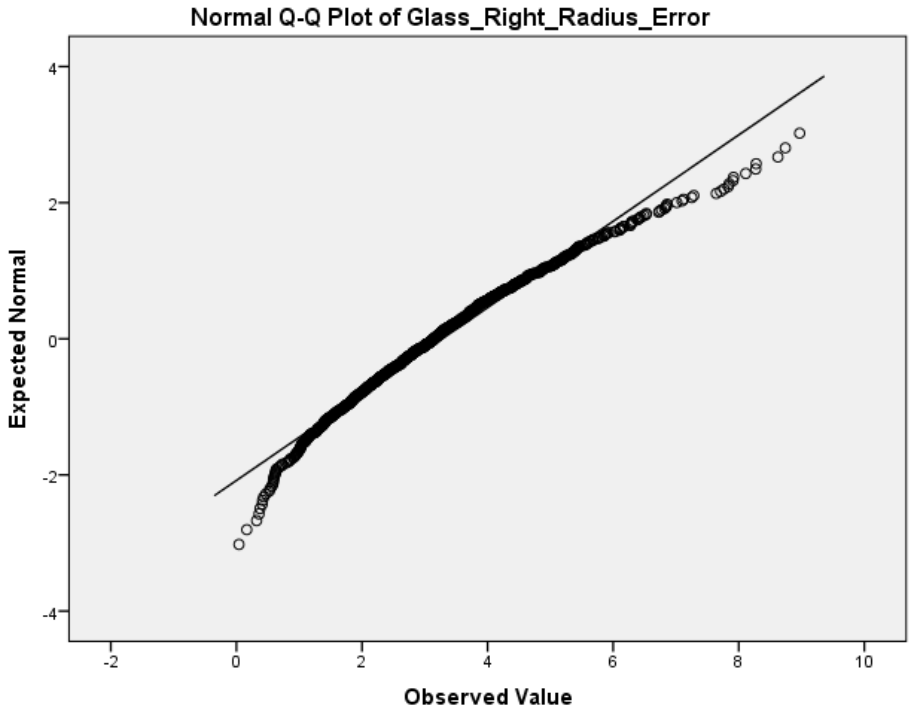


**Figure 112 Q-Q Plot of Principal Point Error Radius for Right Camera (Glass Target Method)**

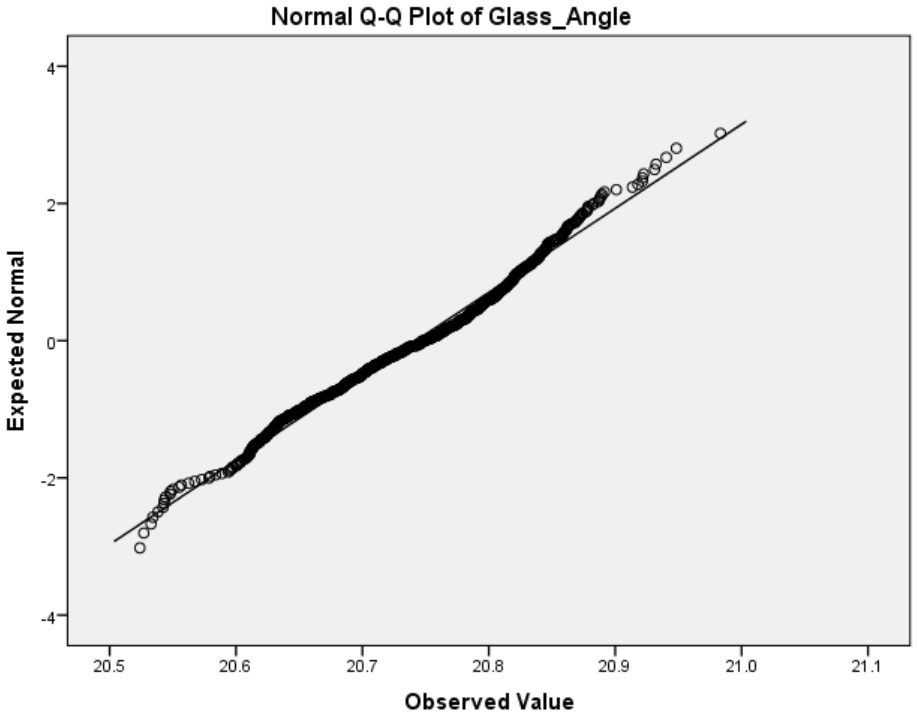


**Figure 113 Q-Q Plot of Estimated Angle Between Stereo Cameras (Glass Target Method)**

# Appendix B

## Examples of Jailbar Scans

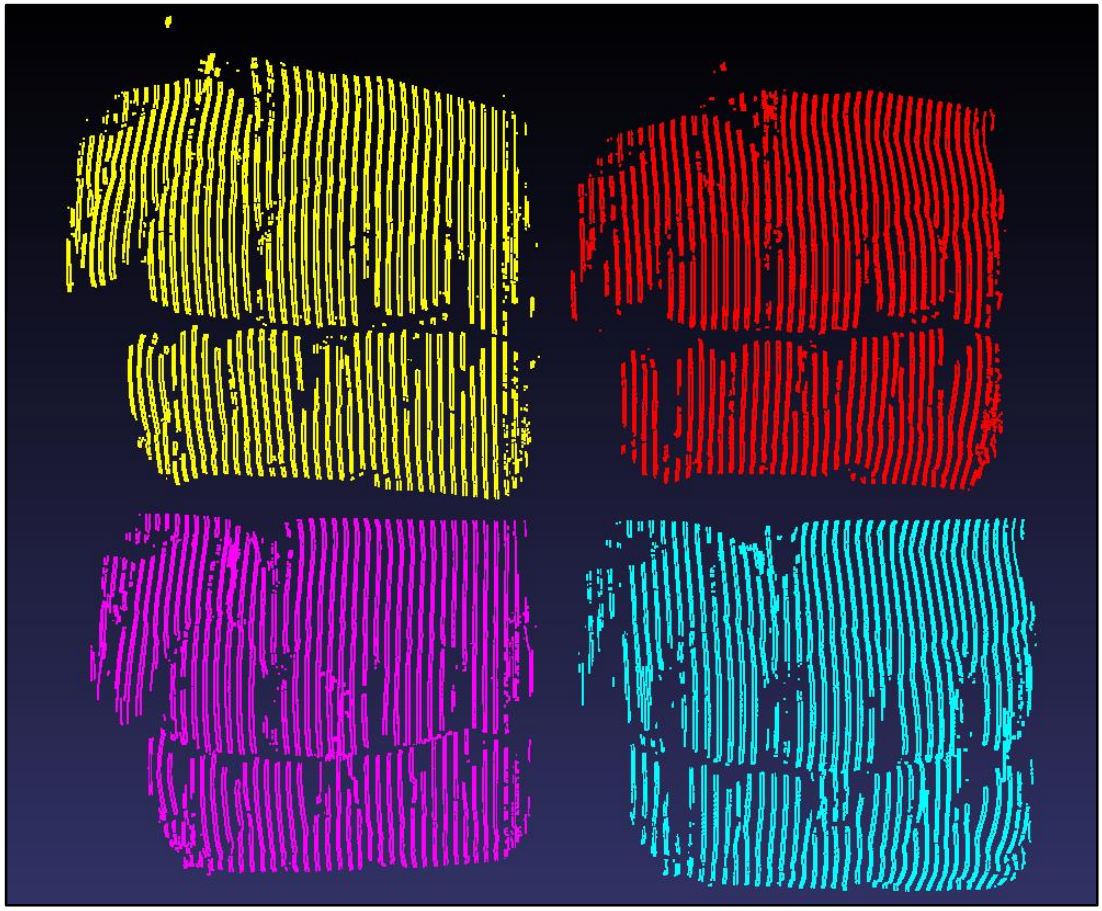

**Figure 114 Four Scans from the LM Set.** The 1st (yellow), 11th (red), 20th (magenta) and 30th (cyan) scans from the lateral excursion model set are shown. The quality of the data decreases over the course of the scan. (First scan : 66462 points, 30th scan : 61258 points).

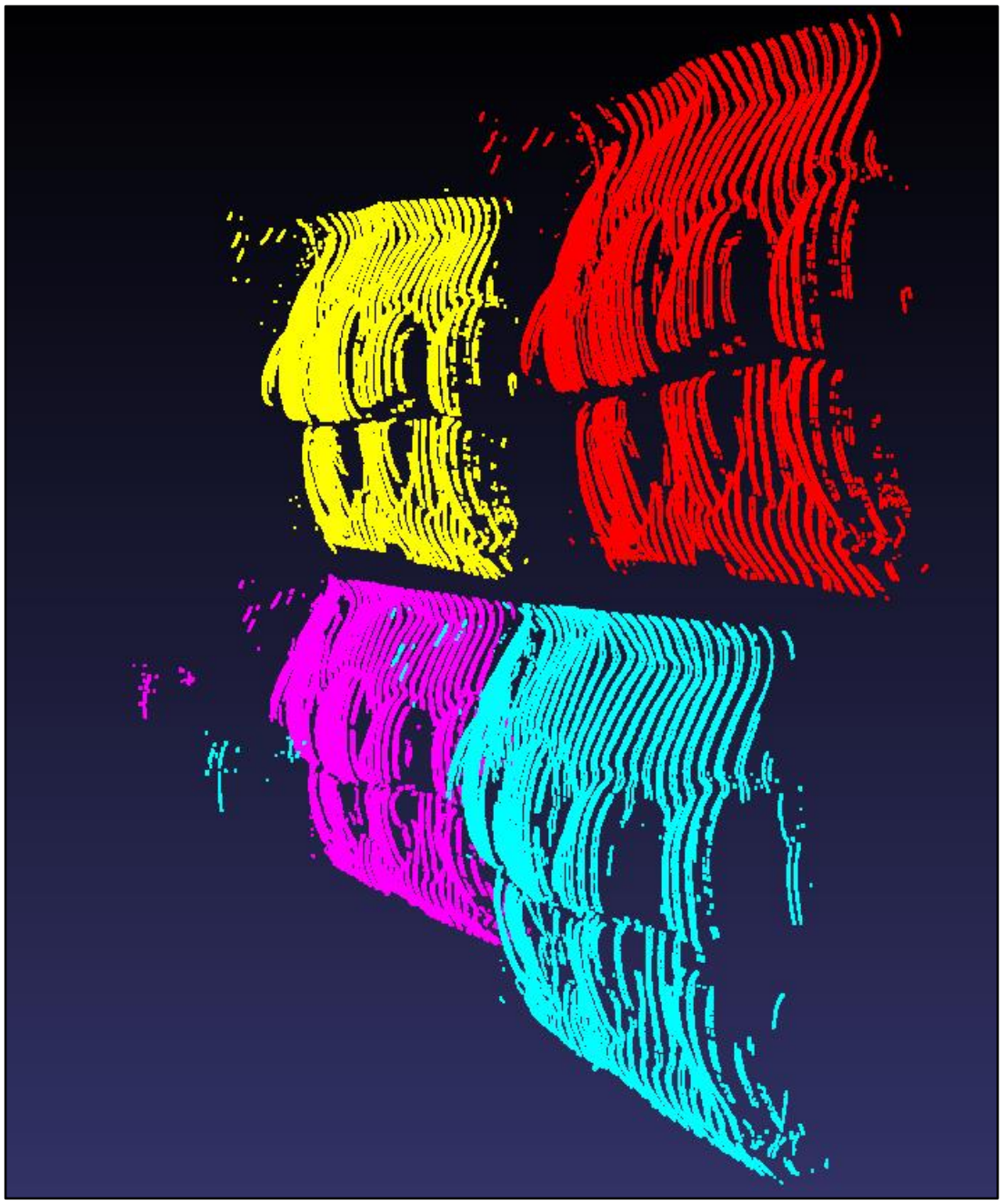

**Figure 115 The Jailbar Scan Data for LM, Viewed from the Side.** The same data as shown in Figure 114. It can be seen that, in addition to losing data over the sequence, the noise in the data increases (particularly visible as noisy points in front of the models). Noise errors are propagated through the remaining scans.

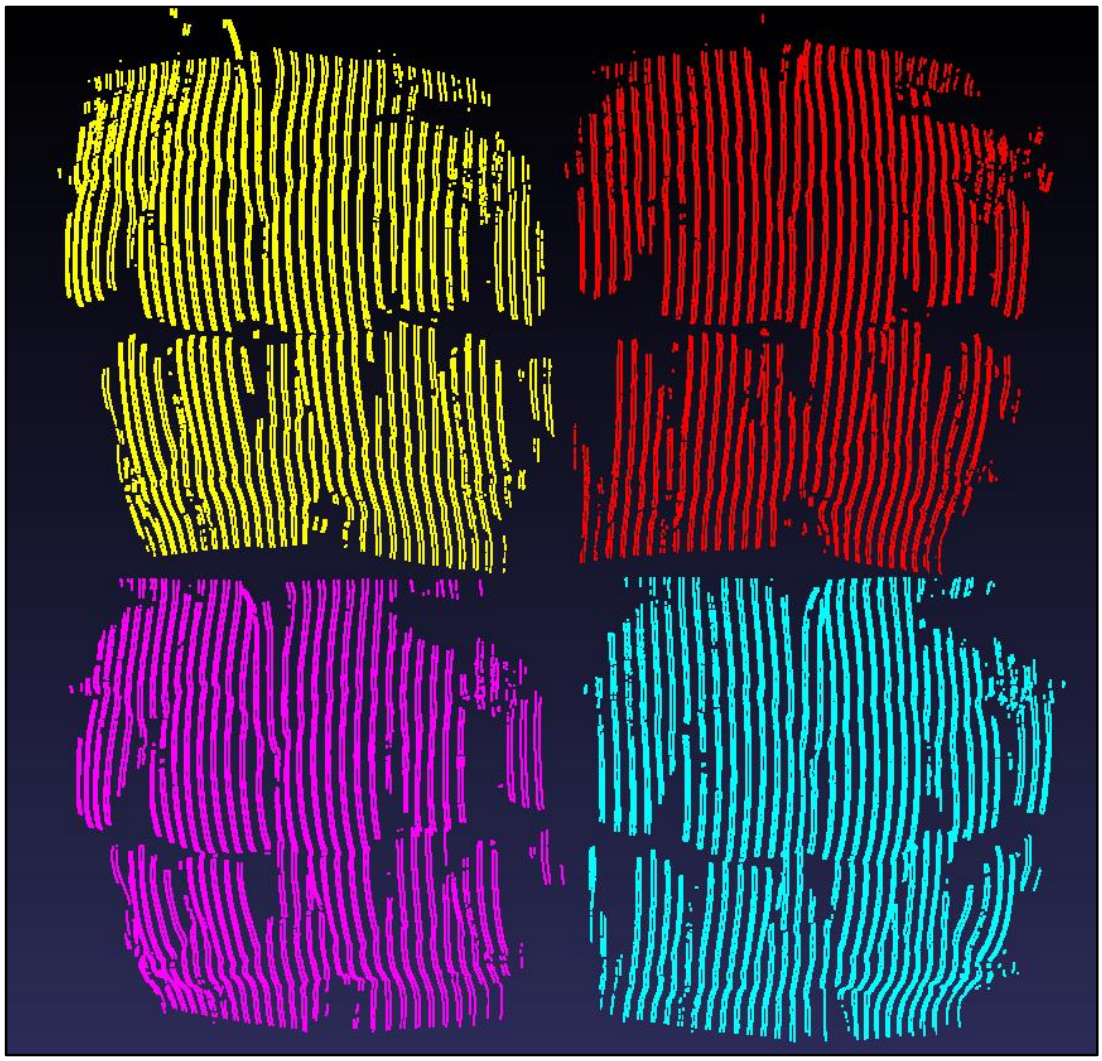

**Figure 116 Four Scans from the PM Set.** The 1st (yellow), 11th (red), 20th (magenta) and 30th (cyan) scans from the protrusive excursion model set are shown. The quality of the data decreases over the course of the scan. (First scan : 56248 points, 30th scan : 51908 points).

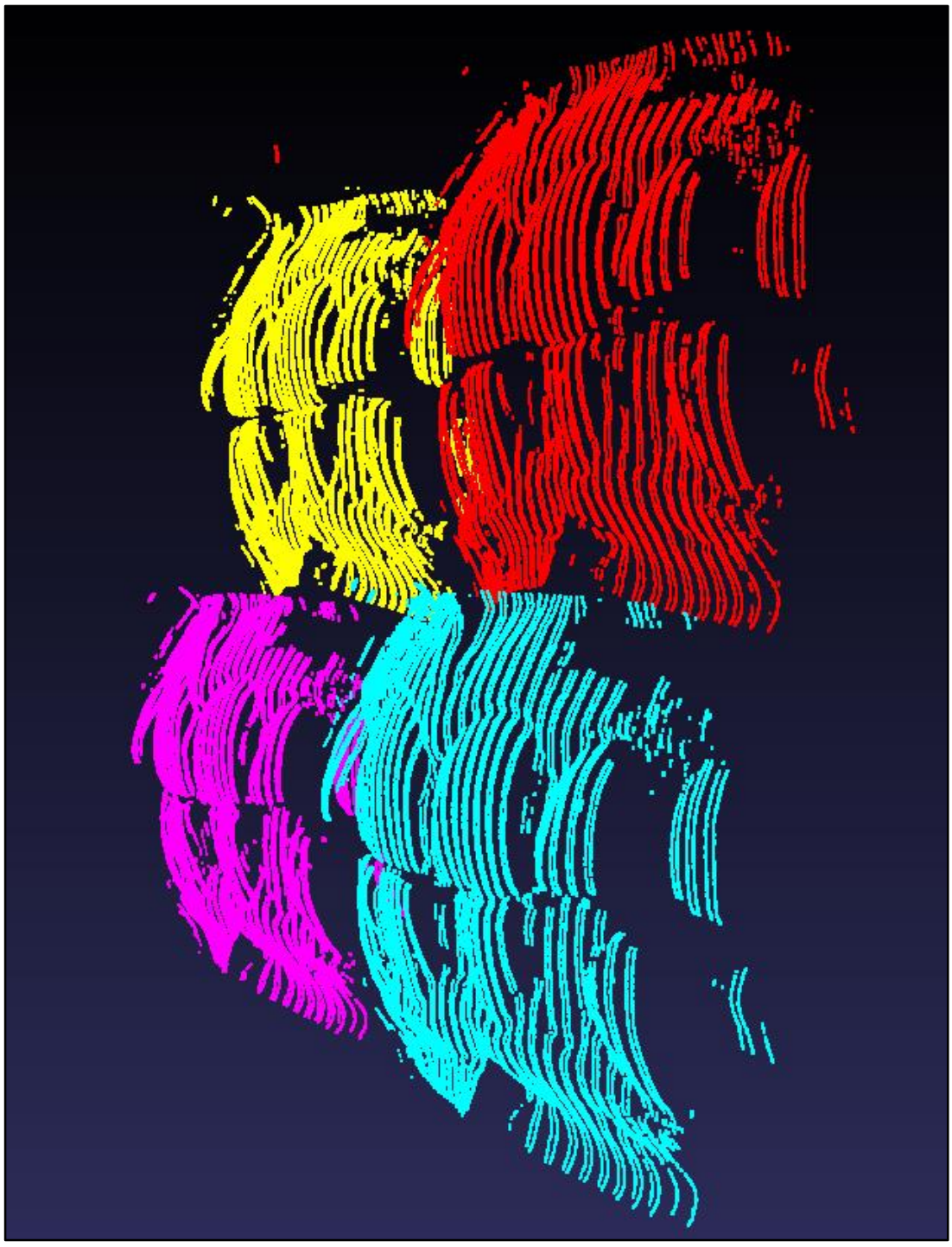

**Figure 117 The Jailbar Scan Data for PM, Viewed from the Side.** The same data as shown in Figure 116.

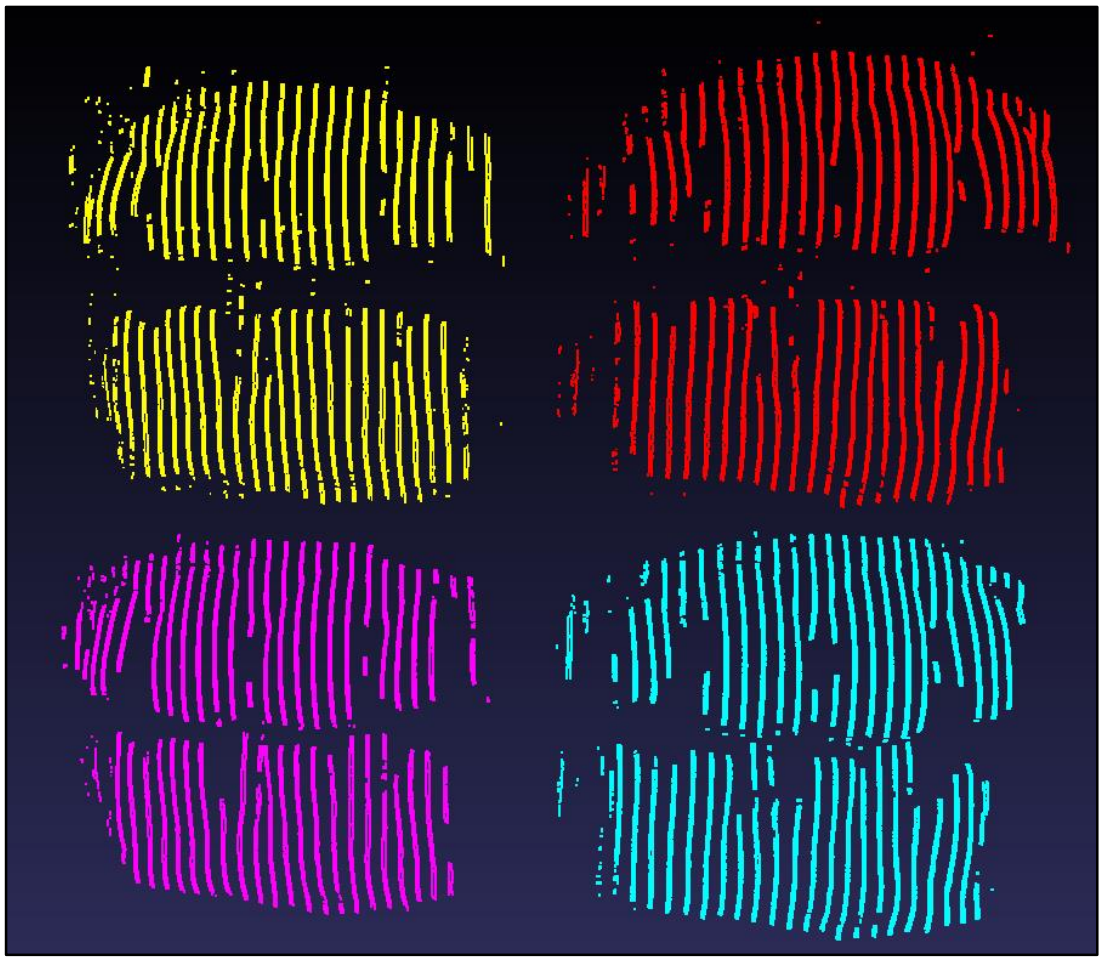

**Figure 118 Four Scans from the OL Set.** The 1st (yellow), 11th (red), 20th (magenta) and 29th (cyan) scans from the live model set are shown. The quality of the data decreases over the course of the scan. (First scan : 32200 points, 30th scan : 30268 points).

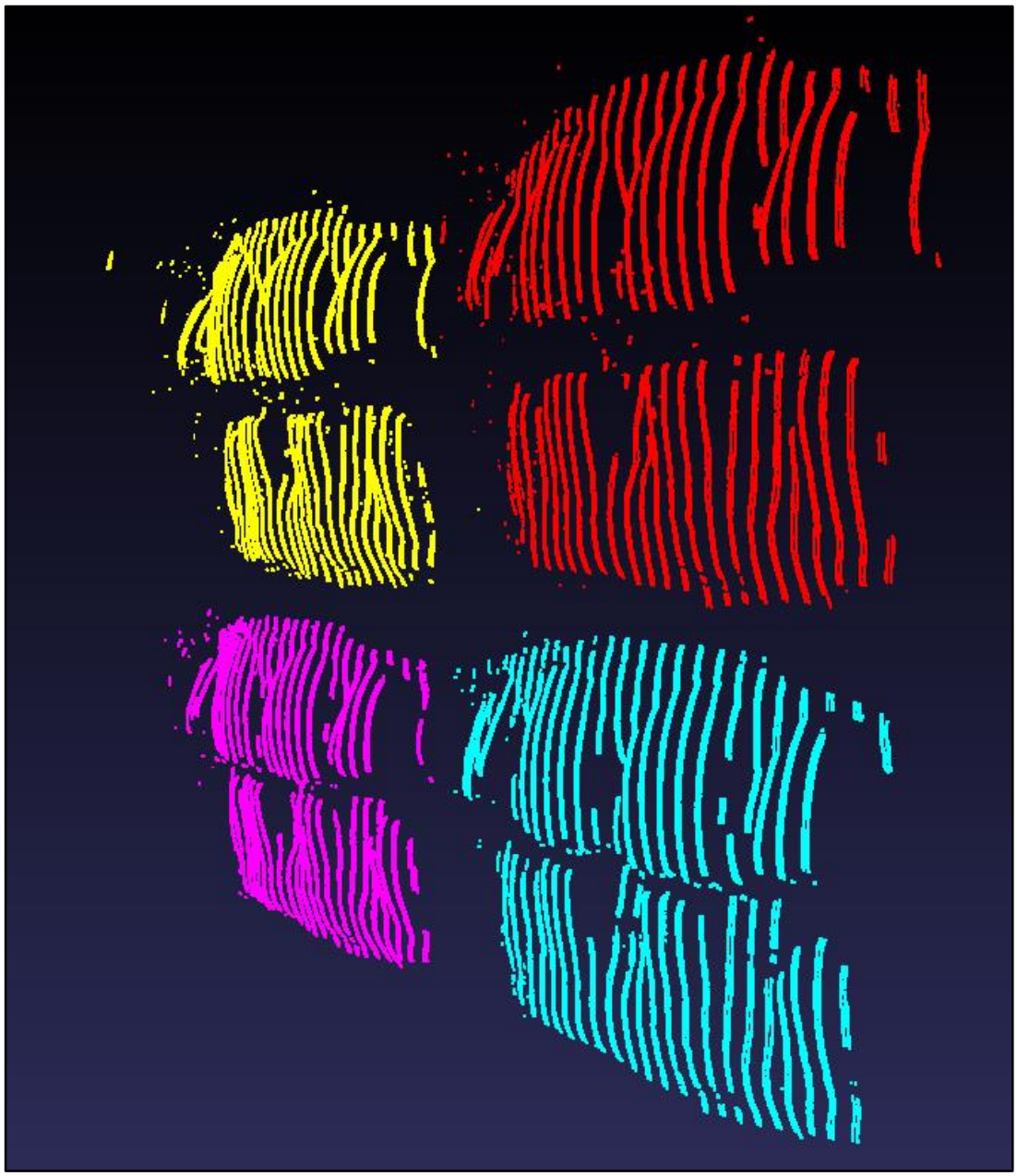

**Figure 119 The Jailbar Scan Data for OL, Viewed from the Side.** The same data as shown in Figure 118.

# Appendix C

## Q-Q Plots for the Jailbar Alignment Variations from the Experiments in Section 7.3

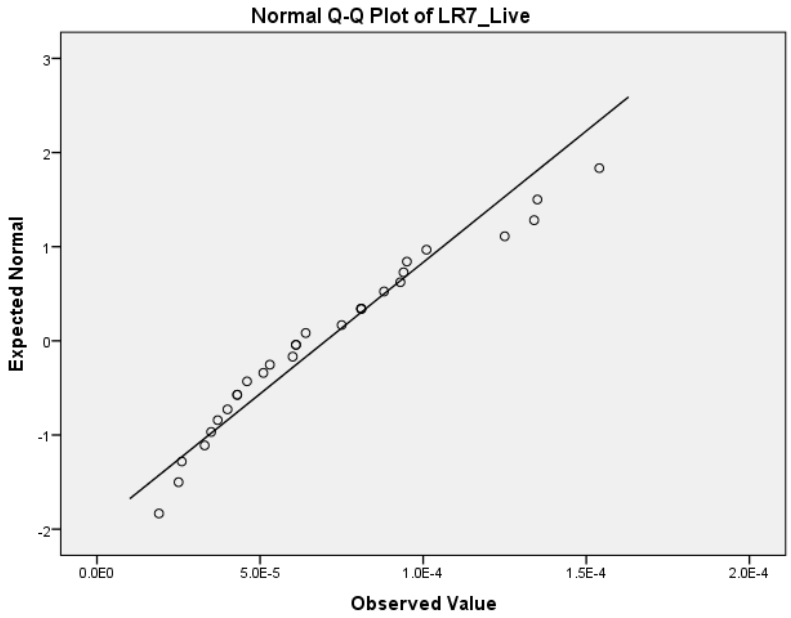


**Figure 120 Q-Q Plot for OL, LR7 Reference Point**

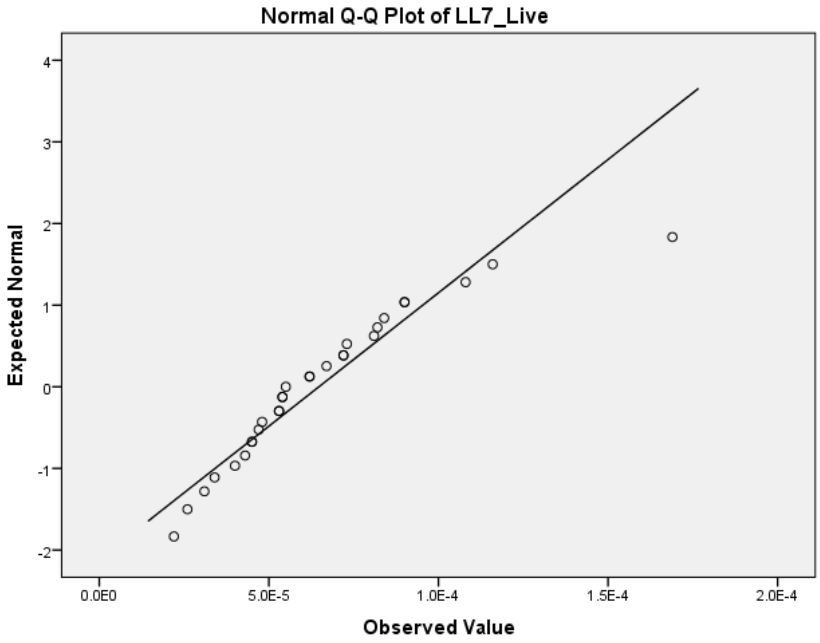


**Figure 121 Q-Q Plot for OL, LL7 Reference Point**

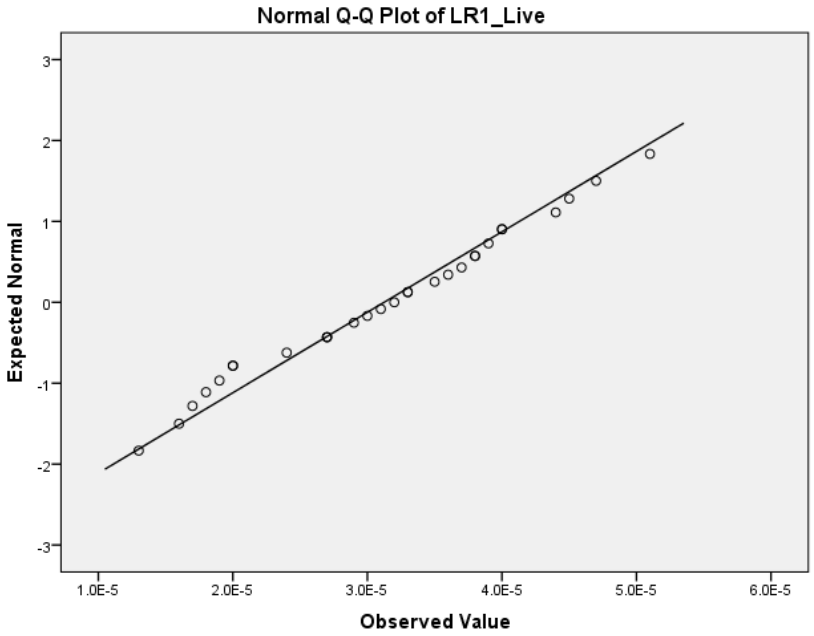


**Figure 122 Q-Q Plot for OL, LR1 Reference Point**

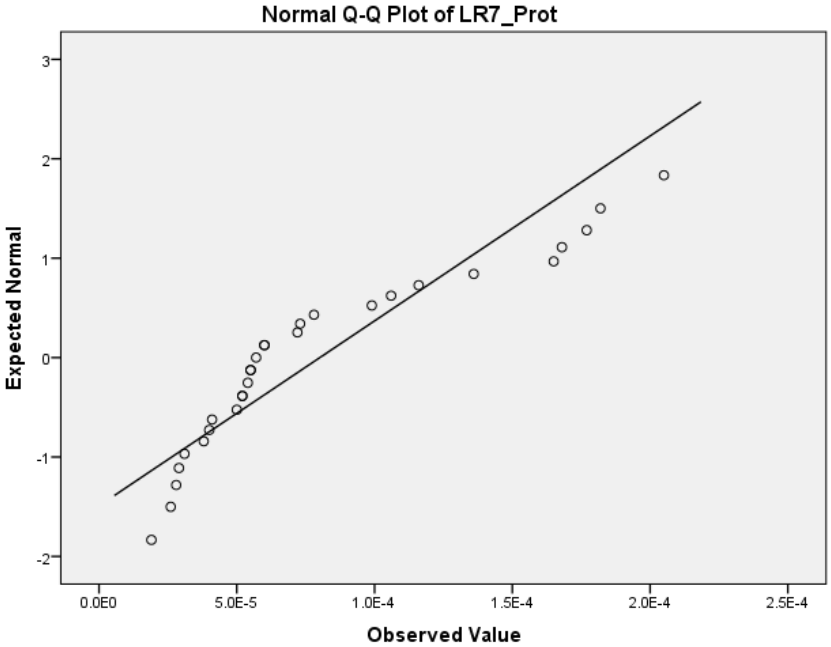


**Figure 123 Q-Q Plot for PM, LR7 Reference Point**

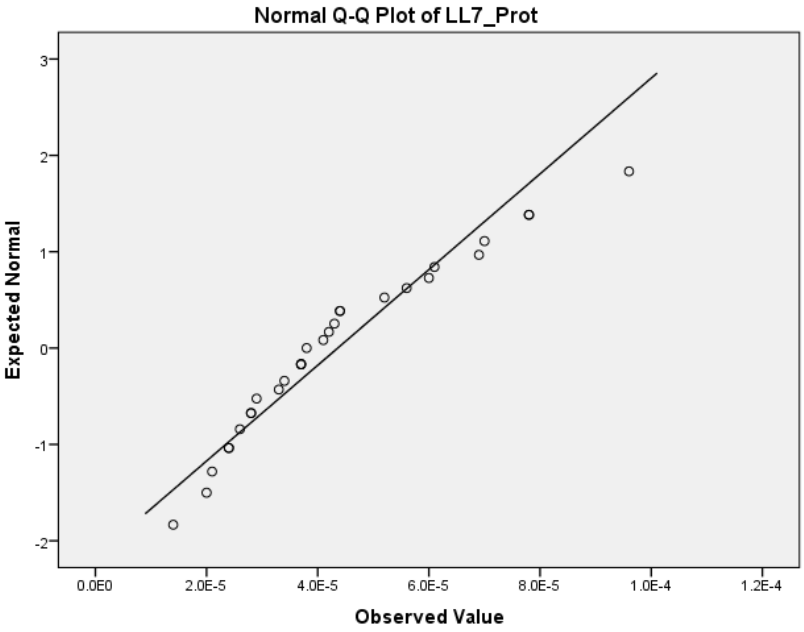


**Figure 124 Q-Q Plot for PM, LL7 Reference Point**

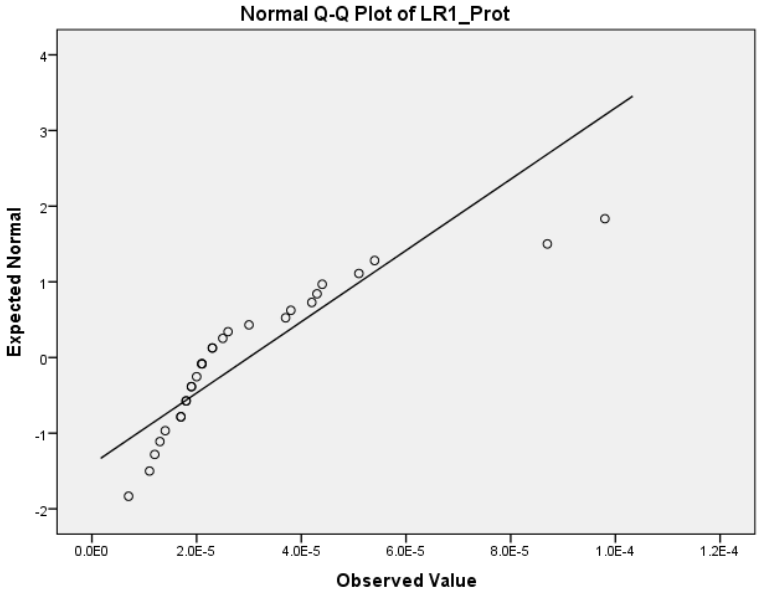


**Figure 125 Q-Q Plot for PM, LR1 Reference Point**

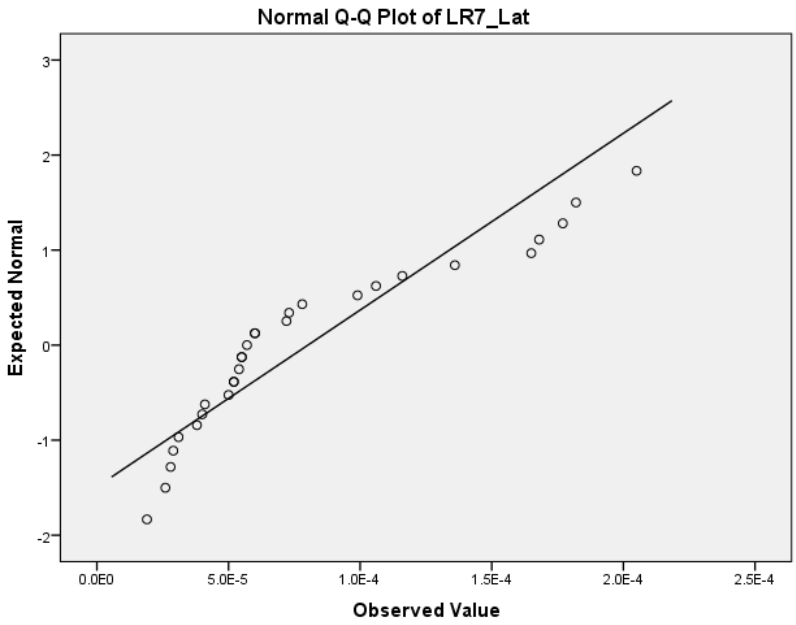


**Figure 126 Q-Q Plot for LM, LR7 Reference Point**

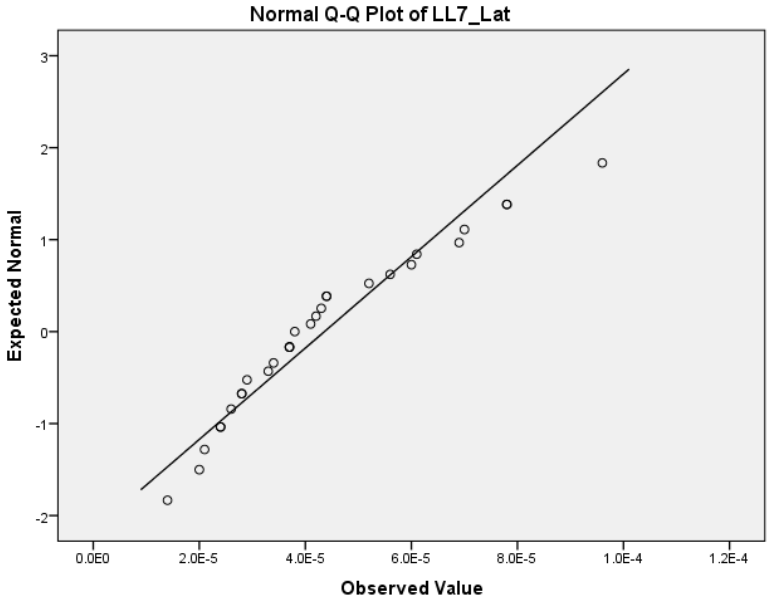


**Figure 127 Q-Q Plot for LM, LL7 Reference Point**

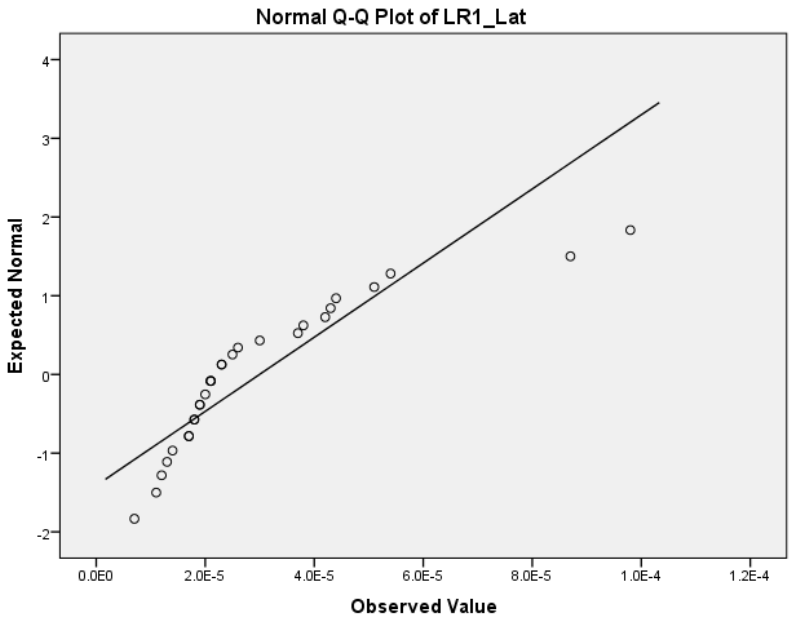


**Figure 128 Q-Q Plot for LM, LR1 Reference Point**

# Appendix D

## The State of the Art (Not a Trivial Problem)

Digital dental technology is developing rapidly. Over the five years since starting this thesis, the marketplace has seen an explosion in model scanners and intra-oral scanners. A move towards ‘powder-free’ scanning, and ‘full arch’ scanning, has also been apparent.

It has been shown that the proposed method relies on the ability to truly and precisely record jaw relationships over the full arch. Whilst intra-oral scanners are still prohibitively expensive for most, it is worth briefly (not rigorously) considering the current state of the art.

One month before submission of this thesis, using the most up to date software on one of the latest intra-oral scanners available, a simple experiment was performed.

In order to assess the trueness of the digital bite, in terms of the full arch occlusion, a set of phantom head teaching models (Frasaco GMBH, Tettnang, Germany) were modified by adding ~3mm of composite to the upper right central incisor, and the palatal cusps of both upper third molars. This ‘tripodised’ the occlusion such that when the upper and lower models were placed together, only these three teeth were in contact (Figure 129 and Figure 130).

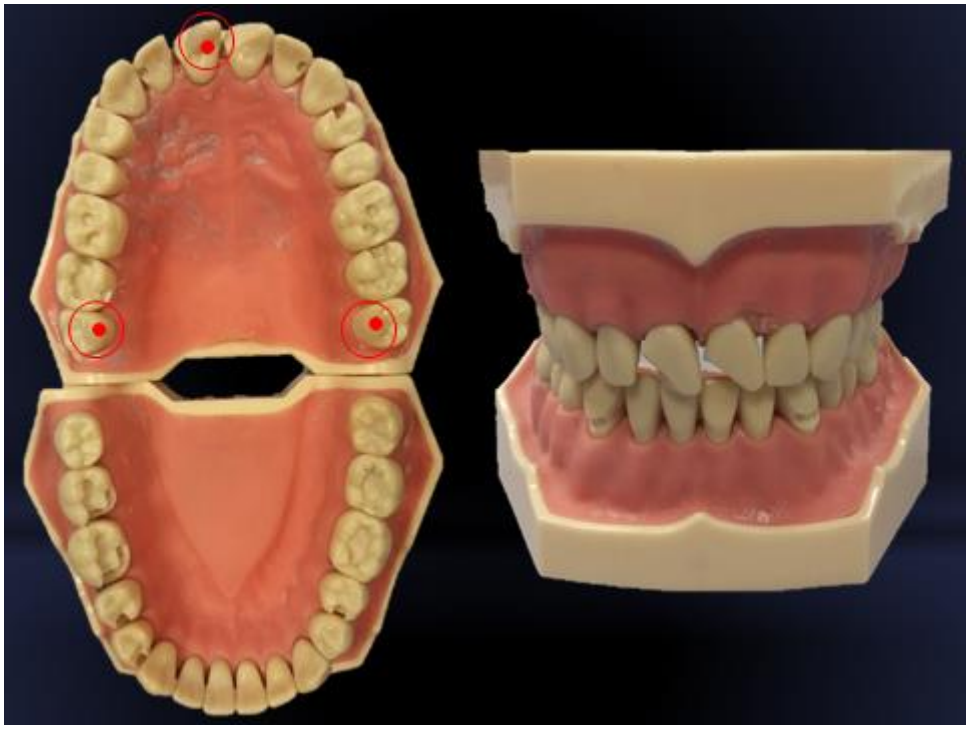

**Figure 129 The Frasaco Models.** 3mm composite stops were added to the upper right first incisor, and the palatal cusps of the upper third molars (circled in red). This 'tripodised' the occlusion causing only 3 points of contact, with all other teeth discluded.

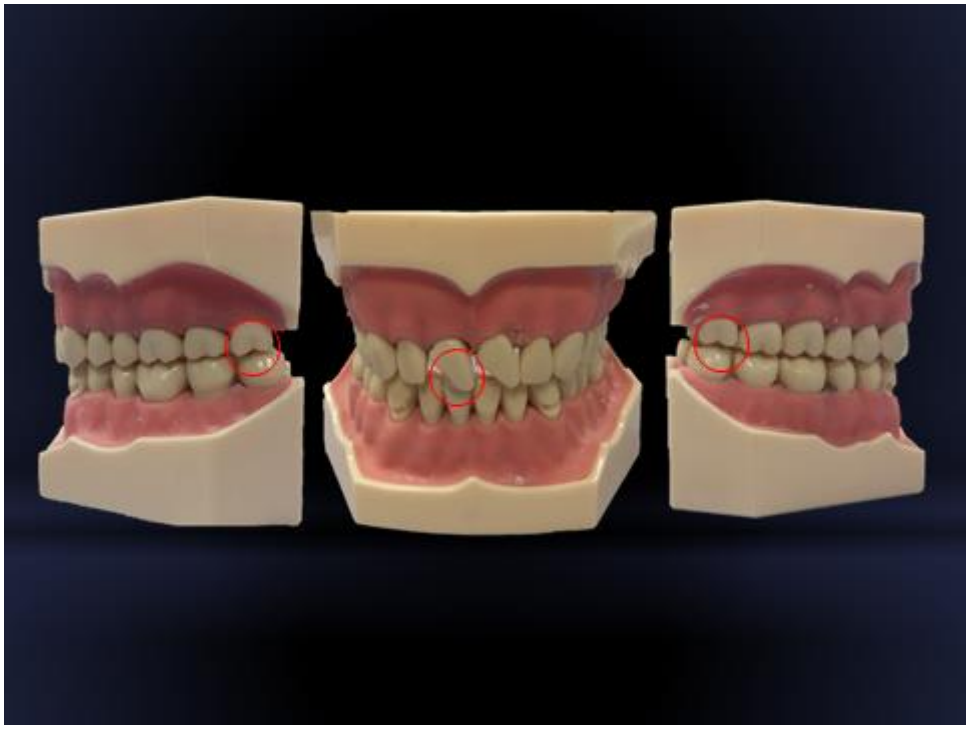

**Figure 130 The 'Tripodised' Occlusion.** Only the third molars and the upper right central incisor occlude. The models are propped open by ~3mm.

The models were scanned using the intra oral scanner to produce full arch scans of the upper and lower dentitions, including the composite stops (Figure 131 and Figure 132).

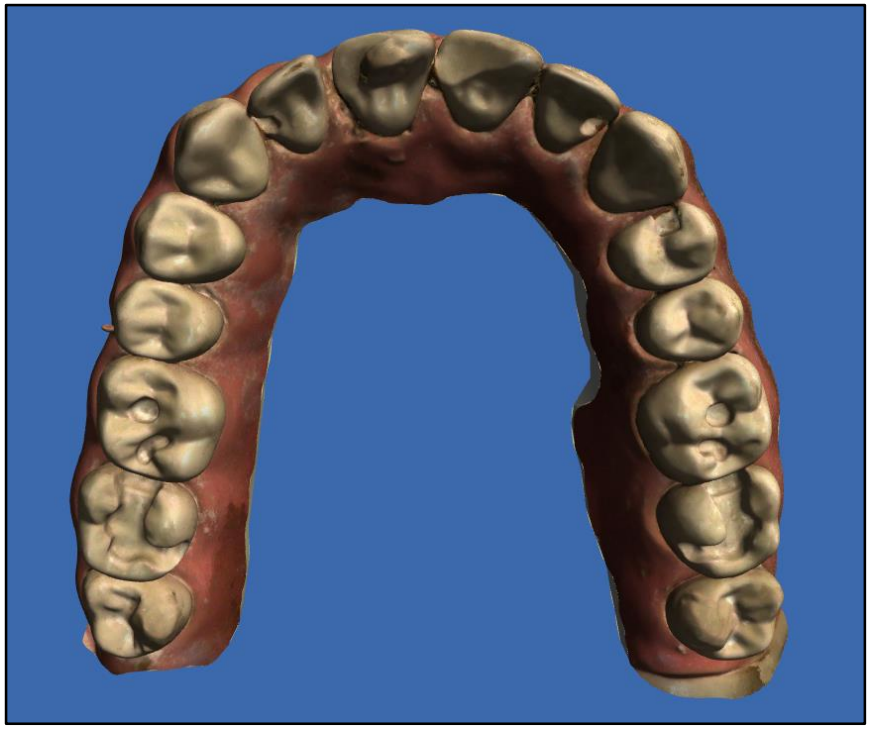

**Figure 131 The Scan of the Upper Arch.**

**Figure 132 The Scan of the Lower Arch.**

Next, two attempts at performing a bite scan were made, trying to capture as much of the labial segment as possible (from first premolar to first premolar). Larger bite registrations failed to align in the software. Both bite scans were used to align the models in the proprietary software, and the best alignment of the two was visually selected (Figure 133 and Figure 134).

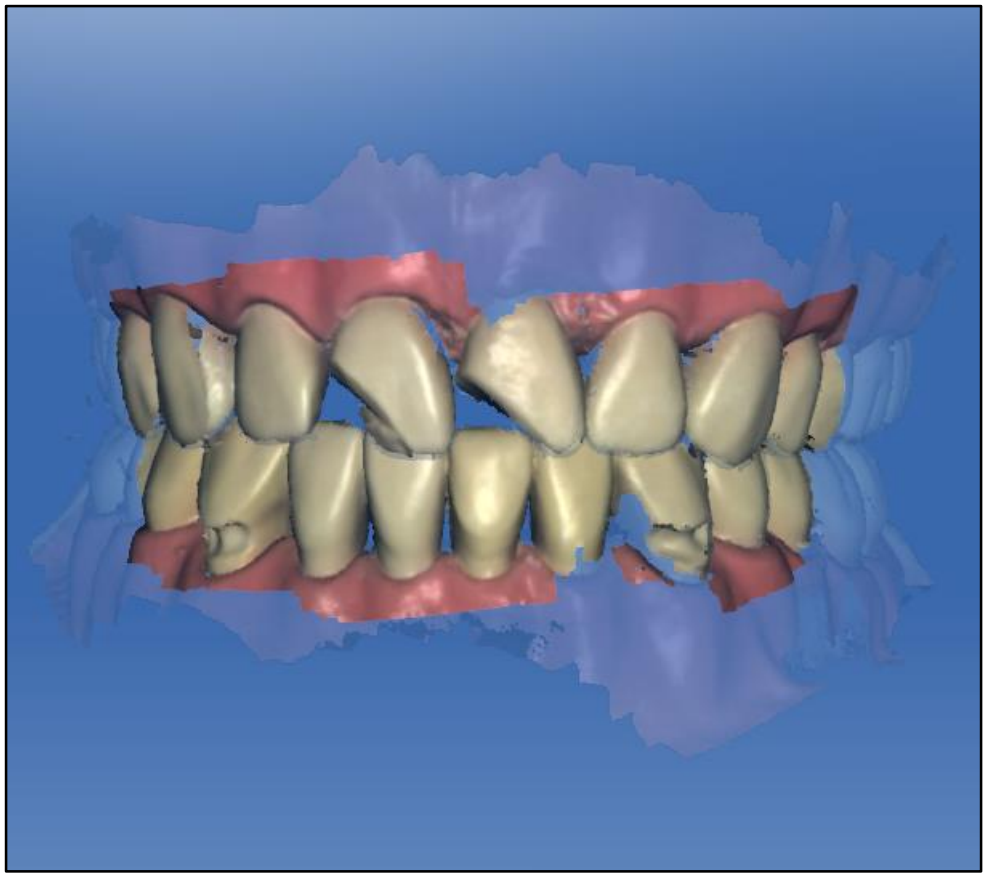

**Figure 133 The Buccal Bite Scan.** The better of 2 scans was selected, based visually on the trueness of the subsequent alignment of the dental arches. The first premolars were captured on both sides.

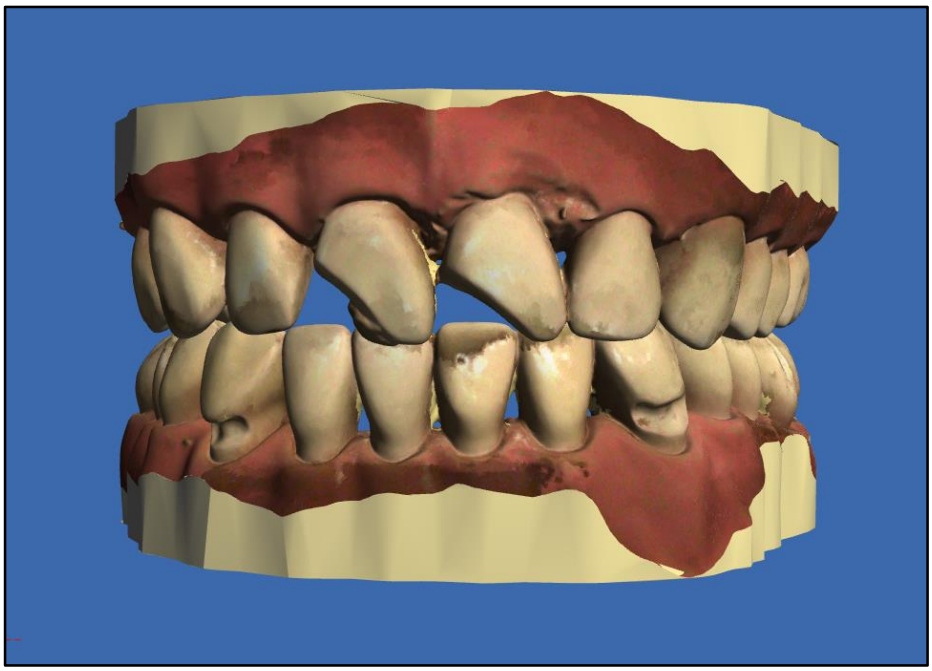

**Figure 134 The Aligned Models**

The software would not allow exporting of the scans for detailed analysis, so within the proprietary crown design software, the occlusal contact points were highlighted on the upper model (Figure 135).

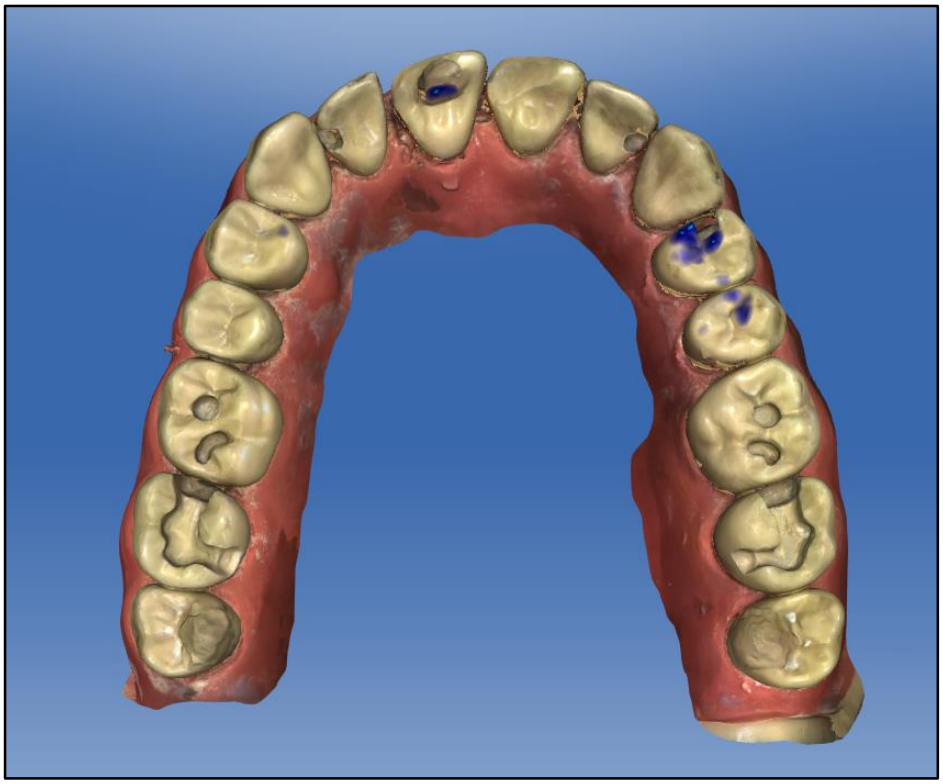

**Figure 135 The Occlusal Contact Points**

The contact point on the incisal composite stop was correctly identified. Incorrect contacts were noted on both upper left premolars, and no contact points were identified on the third molar composite stops.

Visual inspection showed large gaps between the upper and lower third molars (Figure 136 and Figure 137). The measuring tool was used to try and find the shortest distances between the tips of the composite stops on the third molars, and their counterparts in the lower arch. The distance between the right third molars was 2.0mm whilst the distance between the left third molars was 3.4mm. The incisal composite stop was in occlusion.

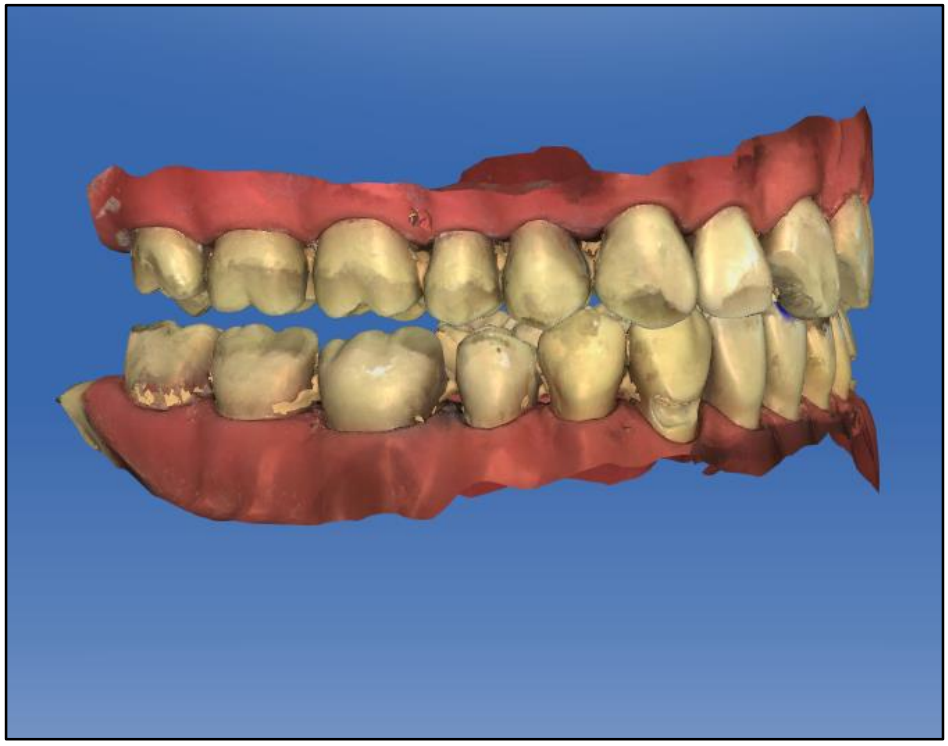

**Figure 136 View of the Right Buccal Segment.** The third molars are not in contact.

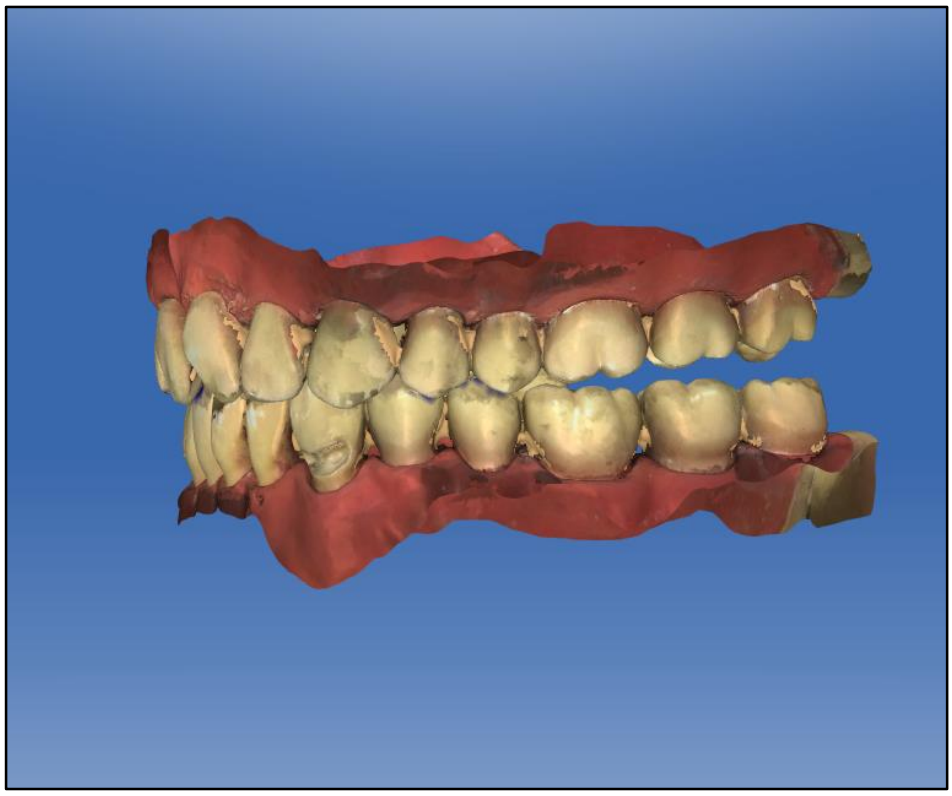

**Figure 137 View of the Left Buccal Segment.** The third molars are not in contact.

These findings are in no way a thorough exploration, given that the number of bite registrations was only two. They merely serve to show the difficulties inherent in the technique, and the errors that are possible. Conversely, it can be stated that, of the 129 bite registrations measured in Sections 6 and 7 of this thesis, not one molar relationship showed a deviation of greater than 300µm. This raises the question; why the difference? Firstly, there are obvious similarities. Both the system developed in this thesis, and the commercial system show greater trueness in the region of the bite scan, and less trueness distal to this. The only difference is the rate of deterioration of the bite registration as one moves posteriorly. This can be explained by the 'weak link' of the scan alignment algorithm. In the case of the novel scanner, the bite scan is a single scan, with no additional errors other than those inherent in the scanning mechanism. Only two alignments are used – the upper arch to the bite scan, and the lower arch to the bite scan – during which some error is expected to creep in. By contrast, the intraoral bite scan is the product of tens, or hundreds, of small field of view video frames. Each frame must be stitched into the 'master' bite scan, and each stitch causes a small error. Perhaps the accumulation of these errors is the reason for the ten-fold increase in the occlusal error at the last standing molars. These stitching errors have only rarely been acknowledged by the profession, with respect to creating full digital dental

models (Brusco et al. 2007), and more recently as a source of error when trying to compare two 3D surfaces, such as crown preparations (Jeon et al. 2015).

This highlights an important area for research. There is an increase in the availability of ‘full arch’ intra-oral dental scanners. Manufacturers tend to quote high trueness values (better than 50µm) which seems correct when one considers the quality of an individual region of the scan. However, this figure would seem to be misleading when considering the quality of the occlusion produced by the system as a whole. Practitioners might presume that if the system scans full arches, and there is a manufacturer protocol for recording the ‘bite scan’, then following the correct procedure will produce a highly true and precise bite registration. This may not be the case, and could lead to undesirable occlusal interferences being created in a prosthesis manufactured from these data. The scientific literature investigating the trueness and precision of full arch digital occlusion is severely lacking.

# Appendix E

# Publication

Keeling, AJ, Brunton, PA and Holt, RJ (2014) An in vitro study into the accuracy of a novel method for recording the mandibular transverse horizontal axis*. Journal of Dentistry*, 42(2). pp. 122-128. ISSN 0300-5712

**TITLE**

**An *In Vitro* Study into the Accuracy of a Novel Method for Recording the Mandibular Transverse Horizontal Axis**

**SUMMARY**

**Objectives** : To assess the accuracy of a novel, non-invasive method for determining the axis of rotation of articulated dental study casts.

**Method**: A 3D structured light scanner was constructed using a projector and two CMOS cameras. Dental stone casts were arbitrarily mounted on an average value articulator. With the teeth together, sets of 10 scans were taken from three different viewpoints. Each scan captured approximately six upper teeth and six lower teeth. The teeth were then propped open, creating 10mm of incisal separation, and the three sets of 10 scans were repeated. From each pair of scans an axis of rotation was calculated using custom software. A total of 900 axes were created this way. The locations of these axes were plotted in sagittal planes located 57.5mm left and right of the midline to represent the position of the temporo-mandibular joints (TMJs). The accuracy of axis location was then assessed.

**Results**: The average radius of error of the individual axes, compared to the real axis, was 2.65 ± 1.01mm. 61.3% of the axes lay within 3mm of the true axis, and 99.2% of the axes lay within 5mm of the true axis.

**Conclusions**: The accuracy of this method is clinically acceptable. Further studies are required to confirm the accuracy of the virtual inter-occlusal records at the level of the dentition. Clinical studies are then indicated to determine whether the transverse horizontal axis on a patient can similarly be determined.

## INTRODUCTION

The transverse horizontal axis (THA) is defined as 'an imaginary line about which the mandible may rotate in the sagittal plane'[1]. In restorative dentistry, recording this axis is important during diagnosis, treatment planning and prosthodontic reconstruction. The method for recording this position has remained largely unchanged for more than a century[2]. Typically, in clinical practice, a facebow is used to determine an arbitrary axis which is assumed to lie close to the true axis. Alternatively, the true axis can be found kinematically, for example, using the Lauritzen Method[3]. Although taught at dental school, most dentists do not continue to use these techniques in general dental practice[4].

The reasons given by general dentists for abandoning the use of these techniques include the clinical time required to perform the recording, the expense of the equipment and the perceived lack of efficacy of these procedures[4]. The findings of recent studies are divided on the latter point. Some workers have found that using a facebow reduces the probability of inducing occlusal errors when compared to mounting dental models using average values[5–7]. Meanwhile, others found no significant improvement in occlusal outcomes[8]. A clear theme is that no method is perfect, and all result in dental prostheses which are likely to need occlusal adjustment in the mouth. However, the amount of adjustment required should be reduced if the models can be mounted in a better approximation to the patient's anatomy.

There is a clinical need to devise a simpler, quicker and more economical method for recording the THA, which will provide a starting point for mounting dental models on an articulator to reproduce the patients jaw movements *in vitro*. This method must be conducive to use in the general practice setting if the majority of patients are to benefit from an improved level of occlusal care.

This paper proposes a novel method for locating the THA, using 3D scans of the labial surfaces of the maxillary and mandibular incisors.

Our new method relies on the mathematical principle of the instantaneous axis of rotation (IAR), initially described by Leonhard Euler, 1775-1776[9], and further refined by Olinde Rodriguez in the 19$^{th}$ century[10]. This states that the movement of a rigid body between two points can be described as a rotation around an axis, and a translation along it. The idea of modelling mandibular movements using IARs is not new[11–14], although this has generally been applied in relation to habitual paths of closure. Our clinical method would require that the recordings be made with the mandible positioned in centric relation (CR), to 'force' the IAR to coincide with the

THA. Our method is similar to a previously reported technique, except the jaw registrations are recorded optically, rather than with wax[15]. This has the potential to reduce clinical time and eliminate errors caused by physical manipulation and distortion of the inter-occlusal wax records[16,17]. The use of a computer to calculate the THA, rather than attempting to construct bisecting perpendicular lines on 1mm graph paper, using a pencil, may also enhance the accuracy of this technique. In the 1970s, Long[15] found this method to be prone to error and it consequently disappeared from the literature as quickly as it had appeared. In our method, the hinge about which the mandibular movement has occurred can be derived mathematically by tracking the movement of the mandibular teeth, using the maxillary teeth as a fixed point of reference.

We present the method and test its accuracy *in vitro* on dental study models mounted on an articulator. We define accuracy in two respects. Firstly, the repeatability of measurements, as described by the standard deviation of multiple repeated measures. Secondly, the absolute accuracy of the measurement, as compared to the true hinge axis location. We then consider our results in the context of existing methods to elucidate whether clinical studies are warranted.

**MATERIALS & METHODS**

A structured light 3D scanner was constructed using a DLP projector (Optoma PK201, Optoma Europe Ltd, Watford, UK) and two monochrome CMOS cameras (UEye UI-1240LE-M, IDS Imaging, Obersulm). Phase modulation patterns were encoded in the projector[18] and gamma compensation was applied to the projector-camera pairs[19]. The cameras were mounted on a rigid metal bar at an angle of 30º to each other, and a baseline separation of 900mm, such that their principle points were focussed on the same point in space. To ensure camera alignment, a calibration target of circles was printed using an Epson Stylus Photo 1400 (Epson UK Ltd, Hemel Hemstead), and mounted on an aluminium block which had been machined flat using a toolmakers block and a milling machine (Clarke CL500M, Clarke International, Epping). The relative alignment of the cameras was calculated using this target, and bespoke software utilising the OpenCV library (http://opencv.org). The projector was mounted equidistant between the two cameras. The field of view allowed a scanning area of 6x5cm at a working distance of 15cm. This meant one scan could typically capture six upper, and six lower teeth of the anterior labial segment. The projector served only to provide 'phase texture' to the scanned object, in order to reliably identify corresponding pixels in both camera images, for 3D calculations. Software was developed in-house to record and process 3D data using the PointCloudLibrary (http://pointclouds.org). The scanner was tested by scanning the aluminium calibration block, and measuring the deviation from true of a horizontal cross section.

Dental stone casts were arbitrarily mounted on an average value Freeplane articulator. With the teeth together in maximum intercuspation, 10 scans were taken with the aim of capturing from the mesial cusps of right first permanent molars, to just beyond the midline anteriorly. Between each scan the scanner was picked up and replaced to ensure slightly differing viewpoints and simulate the clinical situation. This procedure was repeated with 10 more scans aiming to capture the labial region from right canine to left canine, and a final set of 10 scans were taken capturing the mesial cusps of the left first permanent molars, to just beyond the midline anteriorly. The teeth were then separated by inserting a 7mm diameter wooden rod between the models posteriorly, behind the last standing molars. This provided about 10mm of vertical separation at the incisors. Without moving the models, the scanning process was repeated as before, to provide 10 more scans of the teeth apart from each of the three viewing positions. In total, 60 scans were taken (30 'teeth apart' and 30 'teeth together').

In order to determine the direct relationship between the hinge on the articulator and the stone casts, 14 more scans of the arches were captured, starting from the left hinge of the articulator, and working around the model to the right hinge. The stone models were then removed from the articulator and scanned in a dental model scanner (Lava Scan ST Scanner, 3M EPSE, St Paul, MN) which has an accuracy of 10µm according to testing standard VDI 2634/2. The scanned models were exported as .stl files into MeshLab software (http://meshlab.sourceforge.net/) along with the 14 scans previously taken of the articulated models. These scans were then aligned by 'wallpapering' our labial scans on to the models. This produced a dense point cloud, based on the highly accurate ST scans, but with more points on the buccal and labial surfaces (Figure 1). The upper model also contained the actual articulator hinge. Three points on the upper model were noted, upper right second molar palatal cusp tip, upper left second molar palatal cusp tip, and upper right central incisor mesio-incisal corner. Three points were similarly identified in the lower arch. These were the points from which all future measurements were taken. In fact, in the following experiment, our scans can be thought of as 'carriers' which are used to align the pre-existing models created in the ST scanner (in much the same way as traditional inter-occlusals records and stone models).

Each of the 60 scans were used as templates to position these 'wallpapered' models relative to each other. The alignment algorithm used was the Normal-Distributions Transform[20]. From each pair of scans (teeth apart and teeth together), an axis of rotation was calculated. This was achieved by aligning the three points in both upper scans to create a common coordinate system. Then the 3x4 transformation matrix was calculated that represented the movement of the three points in the lower model, from 'Closed' to 'Apart'. The upper left 3x3 sub-matrix of the transformation matrix was used to calculate the orientation of the axis of rotation, and the degree of rotation around the axis. There are an infinite number of spatial locations for this axis, each with a different translation vector applied following the rotation. In order to find the position of the axis corresponding to the hinge on the articulator, a point was tracked from the start position to the end position. A solution was found that constrained the translation vector to a direction coincident with the calculated axis. This provided a vector equivalent to a point on the axis, and also the magnitude of the translation vector along the axis (Figure 2). The latter vector should theoretically be zero. Finally, a standard horizontal reference plane was created using three points: the position of the hinge axis at the left and right TMJ (see below) and an arbitrary point located 43mm superior to the

upper right incisal edge. The real articulator axis was visible on the scans and the centre point of the 4mm diameter hinge cylinder was selected at the left and right extremes (131mm apart) to define the position of the true hinge (Figure 3).
The locations of these axes were then plotted in sagittal planes located at 57.5mm left and right of the midline to represent the position of the temporo-mandibular joints (TMJs). The repeatability and accuracy, of axis location was assessed, along with variation in orientation, and variation in degree of rotation.

**RESULTS**

The scan of the flat board deviated from true with a standard deviation of 14µm. The scanner sampled points every 50µm.

A total of 900 axes were calculated by combining the scans in all possible combinations (Figure 4).

The error radii of axis location for all the pairing combinations are shown in Table 1.

The mean radius of error for all 900 axes, regardless of viewpoint, and combining the left and right TMJs was 2.65 ± 1.01mm (standard deviation).

61.3% of the axes lay within 3mm of the true axis, and 99.2% of the axes lay within 5mm of the true axis. The maximum error radius was 5.57mm.

The mean calculated degree of rotation around the axis was 7.71 ± 0.09º. The range over the 900 axes was 0.43º (7.51 to 7.94º).

The mean angle between calculated axes and the true axis was 2.11 ± 0.90º. The range over the 900 axes was 4.26º (0.46 to 4.72º).

The mean translation along the axis was 0.24 ± 0.13mm. The range over the 900 axes was 0.62mm (0.00 to 0.62mm).

**DISCUSSION**

Our scanner used two cameras, not one, because the quality of their lenses was superior to that of our projector. This should lead to less image distortion, and more accurate 3D data. The precision of our calibration target could be questioned as the quality of ink jet printers is probably unreliable below 50 micrometers. This may, in fact, be the limiting factor in scanning accuracy and we will look at acquiring higher precision calibration targets. A 30° angle between cameras was chosen as a mathematically good compromise between depth accuracy, and X-Y accuracy.

The accuracy of our scanner has not been robustly investigated to industry standards. However, all hinge axis calculations, and measurements were performed using points from the models scanned in the Lava ST scanner, which has an accuracy of <10µm when tested against testing standard VDI 2634/2. Our scans are simply a positioning aid for these virtual models. We cautiously presume this positioning is accurate enough for clinical use, based on the accuracy with which the hinge axis is located, and the fact that our scans merged seamlessly with those of the ST scanner. However, further verification is required that our inter-occlusal records are sufficiently accurate and this will be the focus of future work. The practical benefit of our method is immediately applicable to digital workflows. It may also be possible articulate conventional stone models, using a mechanical linear stage set to a value determined by our system. This is a further area we plan to investigate in the future.

The most commonly used method for locating the THA is to locate an arbitrary point anatomically and record this with a facebow. This method has been shown to locate the THA with a mean radius of error of 4.7mm and a standard deviation of 2.9mm[21].

Electronic pantographs are more expensive, take longer to use, and consequently are generally restricted to use in highly specialized practice or as a research tool. The Cadiax Compact (GAMMA Co, Klosterneuberg, Austria) has been shown to reproduce the THA with a typical discrepancy of <0.2mm[22].

Our method lies somewhere between these two techniques, with a mean radius of error of 2.65 ± 1.01mm. However, workers have shown that the *radial* location of this error has a greater effect on introduced occlusal discrepancies than the radius of error[6,21]. Broadly speaking, errors in the posterior-superior and anterior-inferior quadrants have less influence on occlusal discrepancies. In our experiments, if the ‘Closed’ scan was taken from the labial view, the calculated axis tended to be

located in the favourable posterior-superior quadrant (Figure 4). The viewpoint of the 'Apart' view had less influence. One reason for this might be the behaviour of the alignment algorithm. When the teeth are closed, the lower arch is partially obscured by the overbite. Alignment relies on a feature-rich surface and it could be that the narrower lower incisor teeth provide more defined embrasures than the wider posterior teeth so the labial views have more useful points to align. The alignment of the 'Apart' views may show less variation because a sufficient area of the lower arch is always visible, regardless of viewpoint. Furthermore, the relatively flat labial segment may produce more dense scans with many points being visible to both cameras. Conversely, the 'Right' and 'Left' views may have less mutually visible points due to the curvature of the arch. The pattern of axis locations when a less favourable viewing angle has been used appears to be broadly linear horizontally, particularly on the side from which the scan took place. This might imply that alignment is successful superior-inferiorly, but that the lower model can 'slide' antero-posteriorly when insufficient data are captured. The effect of this linear error on the quality of the inter-occlusal records needs further investigation. Furthermore, the effect of using different dental models, with different tooth morphologies and arch forms requires investigation.

The orientation of the calculated axes was always close to that of the real axis (2.11 ± 0.90º). If analysis was restricted to labial 'Closed' scan sets (but any 'Apart' view) the deviation of the orientation of the axes improved to 1.12 ± 0.33º. Previous analyses of the occlusal effects of axis location errors tend to have simplified the problem to 2D, and considered the left and right TMJs in isolation[6,21]. However, the real situation is 3D, and each axis is defined by a pair of points (left and right TMJs). Future work should be directed at the effect of the skew in the axes in 3 dimensions.

The calculated degree of rotation about the different axes showed very little deviation (7.71 ± 0.09º), suggesting that our method calculates the relative orientations of the occlusal planes accurately. Small errors in our 'virtual' inter-occlusal records will be a cause of differences in degree of rotation about, and angulation of, our calculated axes. The magnitude and effect of these errors at the occlusal level requires further investigation. Our inter-occlusal records need to be far more accurate than the hinge axis location. It is the aim of future work to investigate the accuracy of our inter-occlusal records, but indirect evidence can be gained by looking at the predicted magnitude of occlusal errors for an axis located in the posterior-superior quadrant. Morneburg[21] shows that, with a 5mm radius

error, and an opening of 2mm, we can expect occlusal errors up to a maximum of 180µm, and generally less than 100µm, at the second molar region. At half this error radius (as our method produces) we can predict that our inter-occlusal records are accurate to below 100µm but further work is needed to verify this.

The magnitude of the translation along the axis should theoretically be zero. However, inaccuracies in scanning and alignment lead to slight inaccuracies in the angulation of the axis, and 'force' the computer to introduce a shift along the axis to compensate. If several scans have been taken, as would seem sensible clinically, the axis with the smallest translation should be the one most closely aligned to the true axis. This error checking mechanism, in relation to the actual occlusal discrepancies of the inter-occlusal records, will be the subject of future work.

In our system, the projector is set to a screen resolution of 640x480 (its maximum native resolution) and our cameras are 1.3 Mega pixels (1280x1024). These are low by today's standards, and illustrate how quickly cheap technology becomes available. An upgrade in hardware would only cost a few hundred pounds, and we could expect a 2 to 4 times increase in resolution. This is a key benefit of the use of digital technology in dentistry, and requires further investigation. Another benefit is the complete lack of any further distortions or warping of the data. Our errors are absolute. In general practice, many unknowns such as storage time and temperature of materials, incorrect handling of materials, loosening of screws on transfer jigs during postage/transportation or human error accumulate during the mounting of study casts, or the fabrication of prostheses. It seems reasonable to expect that, with a reduced number of variables in the procedure, a more consistent result will be achieved. A clinical comparison of traditional techniques and our new method is warranted.

Our clinical method would require the patient to be positioned in CR. This may decrease the repeatability of the method, although with minimal training, or using patient-guided techniques, this position is considered reproducible[23,24]. We would suggest the use of a leaf gauge to position the patient in CR, followed by the use of a thicker leaf gauge to provide the 'Apart' record.

**CONCLUSIONS**

Our new method for locating the THA is accurate and repeatable within clinically acceptable limits. The method works best when the first scan of the pair is captured viewing the full anterior labial segment. The accuracy of our inter-occlusal scans requires further investigation to determine if they are accurate enough at the level of the occlusion, and not just the THA, to justify clinical use.

## REFERENCES


1. Academy of Denture Prosthetics The Glossary of Prosthodontic Terms. *Journal of Prosthetic Dentistry* **94**, 10-92 (2005).

2. Soboļeva, U., Lauriņa, L. & Slaidiņa, A. Jaw tracking devices--historical review of methods development. Part II. *Stomatologija, Baltic Dental and Maxillofacial Journal* **7**, 67-71 (2005).

3. Lauritzen, A.G. & Wolford, L. Hinge Axis Location on an Experimental Basis. *Journal of Prosthetic Dentistry* **11**, 1059-1067 (1961).

4. Clark, D.M., Oyen, O.J. & Feil, P. The use of specific dental school-taught restorative techniques by practicing clinicians. *Journal of Dental Education* **65**, 760-5 (2001).

5. Morneburg, T.R. & Pröschel, P.A. Impact of arbitrary and mean transfer of dental casts to the articulator on centric occlusal errors. *Clinical Oral Investigations* **15**, 427-34 (2011).

6. Adrien, P. & Schouver, J. Methods for minimizing the errors in mandibular model mounting on an articulator. *Journal of Oral Rehabilitation* **24**, 929-935 (1997).

7. Choi, D.G., Bowley, J.F., Marx, D.B. & Lee, S. Reliability of an ear-bow arbitrary face-bow transfer instrument. *Journal of Prosthetic Dentistry* **82**, 150-156 (1999).

8. Shodadai, S.P., Türp, J.C., Gerds, T. & Strub, J.R. Is There a Benefit of Using an Arbitrary Facebow for the Fabrication of a Stabilization Appliance? *The International Journal of Prosthodontics* **14**, 517-522 (2001).

9. Euler, L. Formulae generales pro translatione quacunque corporum rigidorum. *Novi Comm. Acad. Sci. Petropol.* **20**, 189-207 (1775).

10. Gray, J.J. & Kline, M. Olinde Rodrigues' Paper of 1840 on Transformation Groups. *Archive for History of Exact Sciences* **21**, (1980).

11. Gal, J. a, Gallo, L.M., Palla, S., Murray, G. & Klineberg, I. Analysis of human mandibular mechanics based on screw theory and in vivo data. *Journal of Biomechanics* **37**, 1405-12 (2004).

12. Gallo, L.M., Airoldi, G.B., Airoldi, R.L. & Palla, S. Description of Mandibular Finite Helical Axis Pathways in Asymptomatic Subjects. *Journal of Dental Research* **76**, 704-713 (1997).

13. Grant, P.G. Biomechanical Significance of the Instantaneous Center of Rotation : The Human Temporomandibular Joint. *Journal of Biomechanics* **6**, 109-113 (1973).

14. Bennett, N. A Contribution to the Study of the Movements of the Mandible. *Proceedings of the Royal Society of Medicine, Section of Odontology* **April 27**, 79-95 (1908).

15. Long, J.H. Location of the terminal hinge axis by intraoral means. *The Journal of Prosthetic Dentistry* **23**, 11-24 (1970).

16. Lucia, V.O. Technique for recording centric relation. *Journal of Prosthetic Dentistry* **14**, 492 (1964).

17. Eriksson, A., Ockert-Eriksson, G., Lockowandt, P. & Eriksson, O. Clinical factors and clinical variation influencing the reproducibility of interocclusal recording methods. *British Dental Journal* **192**, 395-400; discussion 391 (2002).

18. Salvi, J., Fernandez, S., Pribanic, T. & Llado, X. A state of the art in structured light patterns for surface profilometry. *Pattern Recognition* **43**, 2666-2680 (2010).

19. Liu, K., Wang, Y., Lau, D.L., Hao, Q. & Hassebrook, L.G. Gamma model and its analysis for phase measuring profilometry. *Journal of the Optical Society of America. A, Optics, image science, and vision* **27**, 553-62 (2010).

20. Magnusson, M. The Three-Dimensional Normal-Distributions Transform — an Efficient Representation for Registration, Surface Analysis, and Loop Detection. (2009).

21. Morneburg, T.R. & Pröschel, P.A. Predicted incidence of occlusal errors in centric closing around arbitrary axes. *The International Journal of Prosthodontics* **15**, 358-64 (2002).

22. Tuppy, F., Celar, R., Celar, A., Piehslinger, E. & Jager, W. The Reproducibility of Condylar Hinge Axis Positions in Patients, by Different Operators, Using the Electronic Mandibular Position Indicator. *Journal of Orofacial Pain* **8**, 315-320 (1994).

23. McKee, J.R. Comparing condylar position repeatability for standardized versus nonstandardized methods of achieving centric relation. *The Journal of Prosthetic Dentistry* **77**, 280-4 (1997).

24. McKee, J.R. Comparing condylar positions achieved through bimanual manipulation to condylar positions achieved through masticatory muscle contraction against an anterior deprogrammer: a pilot study. *The Journal of Prosthetic Dentistry* **94**, 389-93 (2005).

**LEGENDS AND ILLUSTRATIONS**

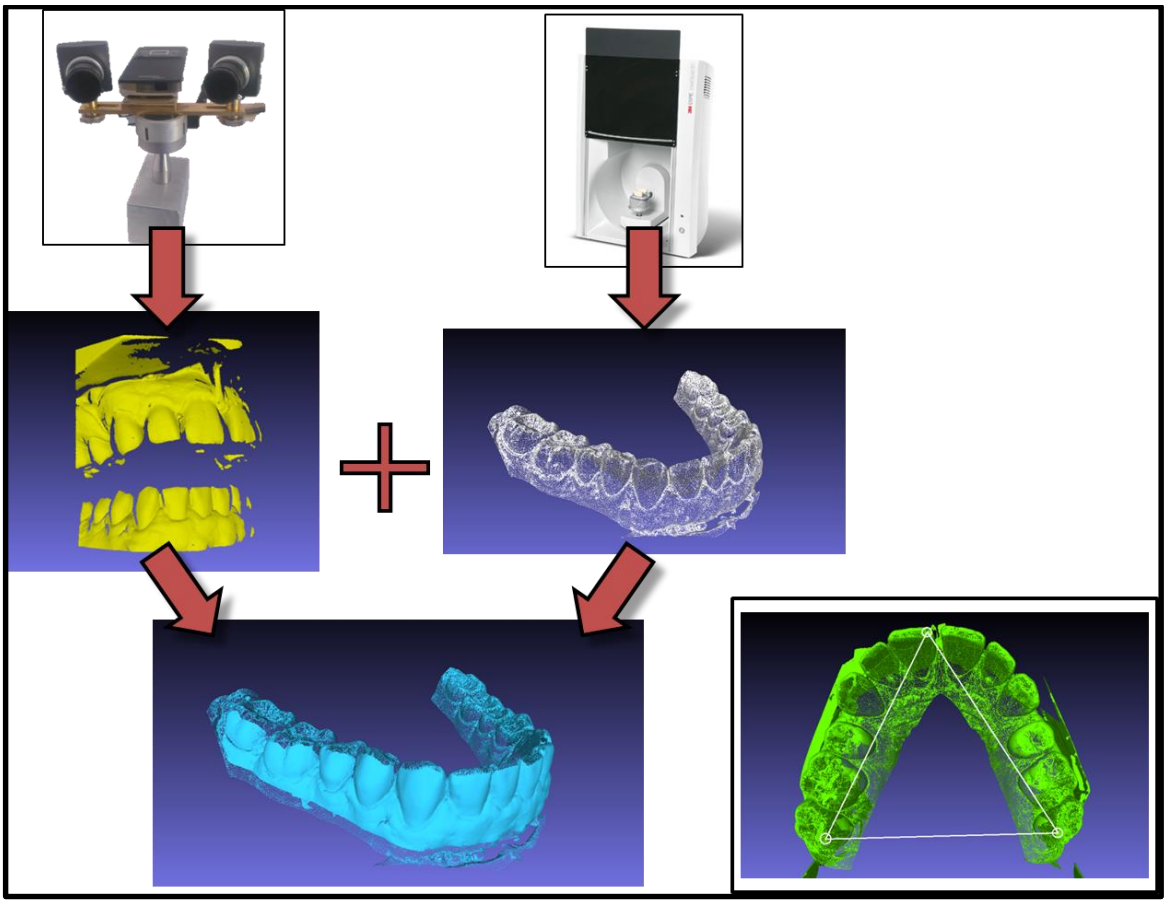

**Figure 138** Building the models. 14 buccal & labial scans are taken with our scanner starting from one hinge of the articulator and working around to the other (left). The upper and lower models are then scanned using the Lava ST scanner (right).All scans are merged to produce master models which have been 'wallpapered' buccally and labially with our dense point cloud scans. We define 3 points from the ST scan models in a tripod from which to take measurements (lower right).

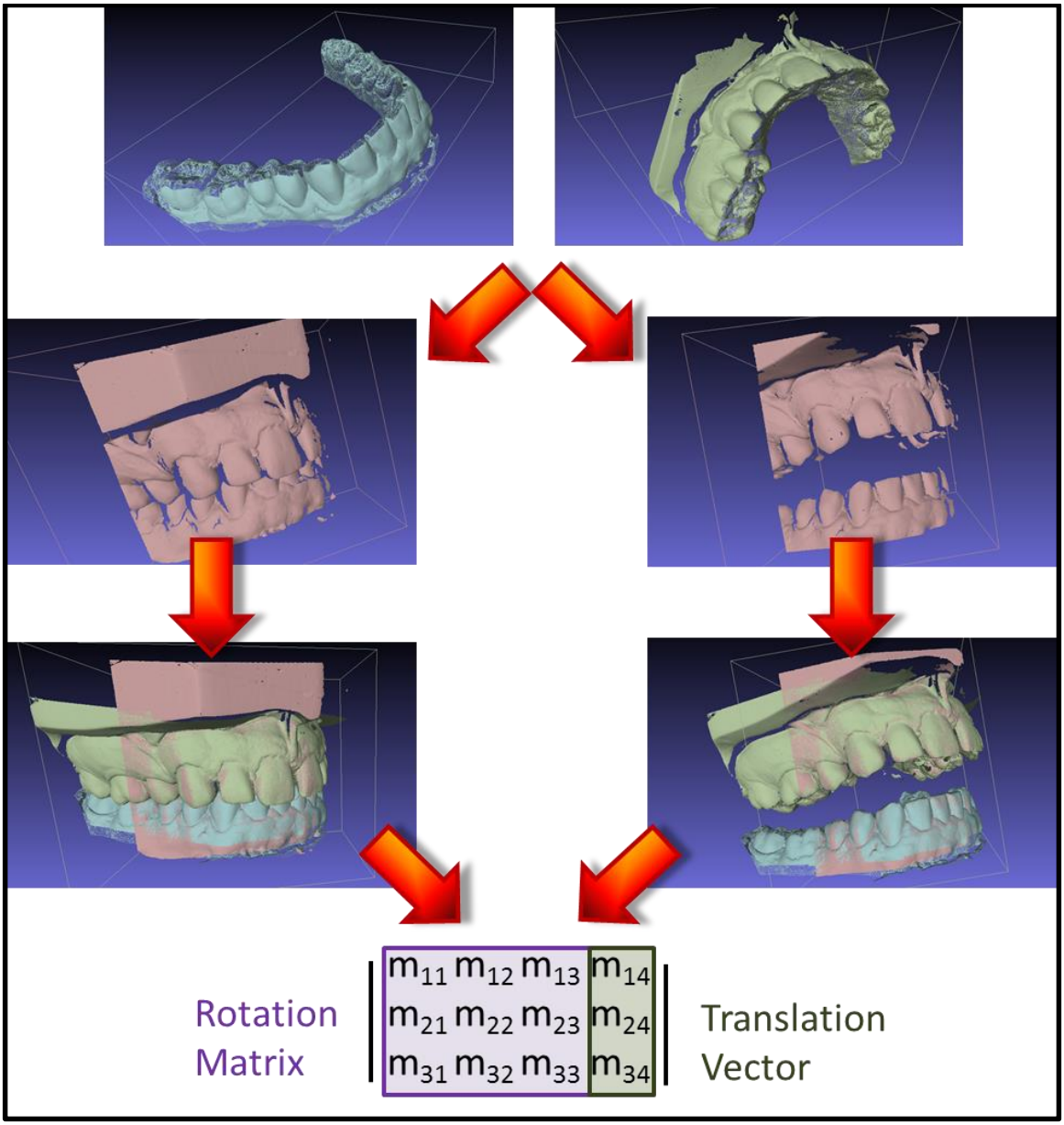


**Figure 139** Summary of the method. The models built in the preceding stage are aligned to each of the 'Closed' and 'Apart' scans. A 3x4 transformation matrix is then calculated for the movement of the lower arch. There are an infinite number of possible solutions for the translation part of this matrix. To find the solution that coincides with the THA, the matrix is further decomposed using vector mathematics under the constraint that any translation must occur along the direction of the axis of rotation.

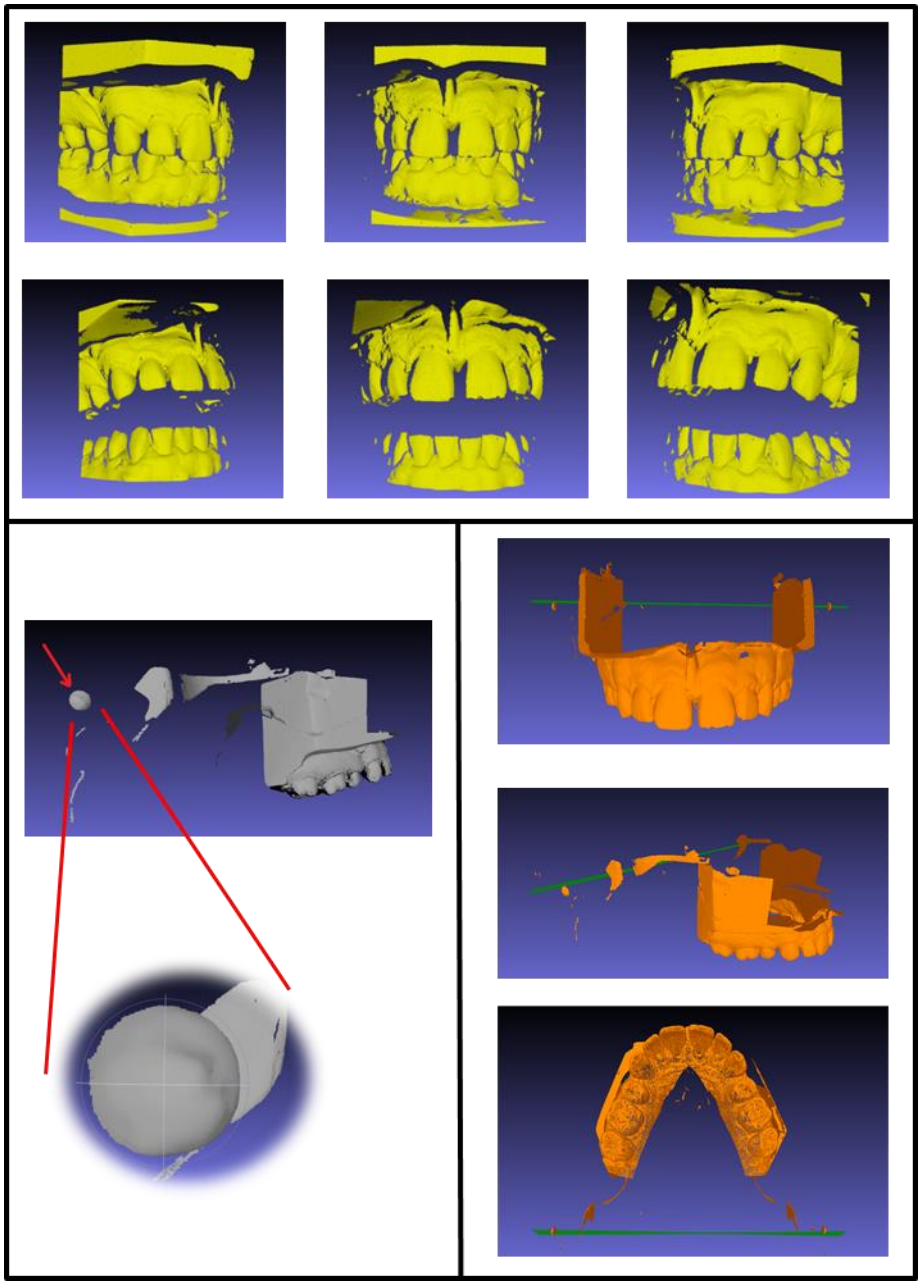

**Figure 140** Top: Examples of the different views. 10 scans were taken for each viewpoint. Lower Left : Identifying the true hinge axis. The ends of the articulator hinge are identified in the scan and the centre point is found (right hinge shown in picture). Lower Right : Example of the calculated axes. 100 axes are shown overlaid in green, representing all the axes calculated using the 'Labial Closed' to 'Labial Apart' scans.

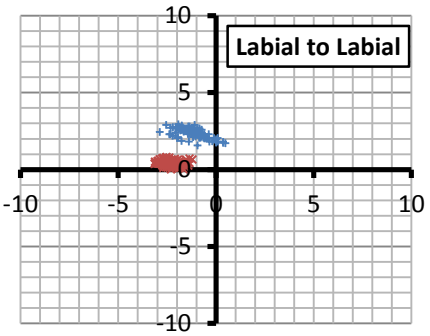


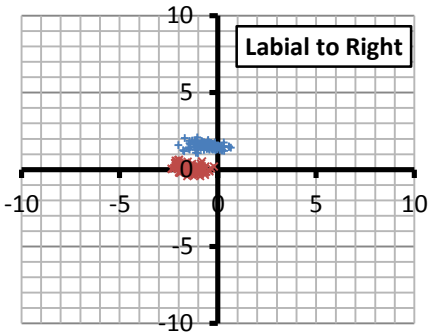


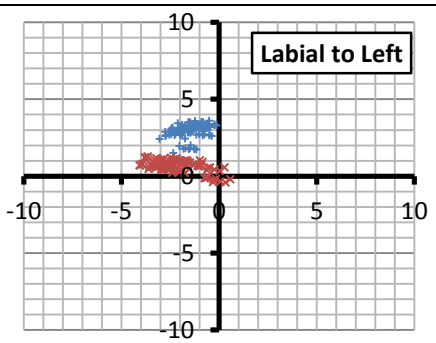


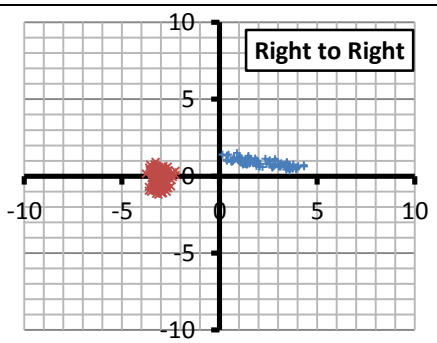


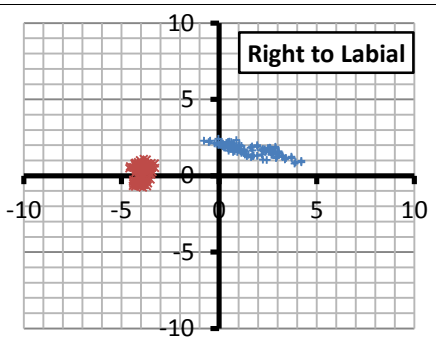


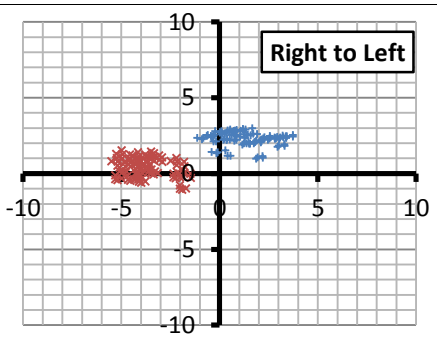


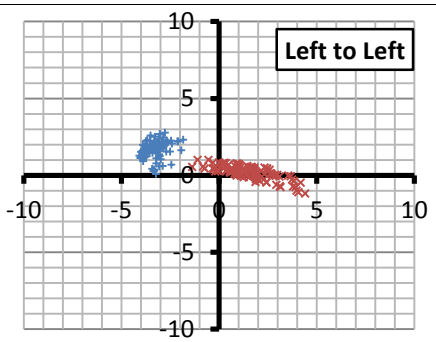


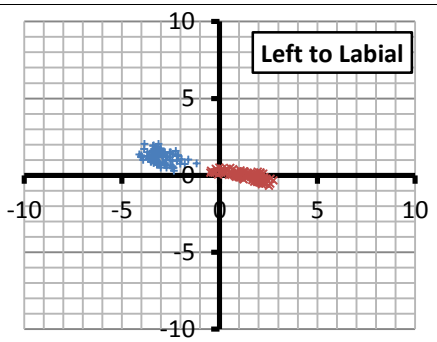


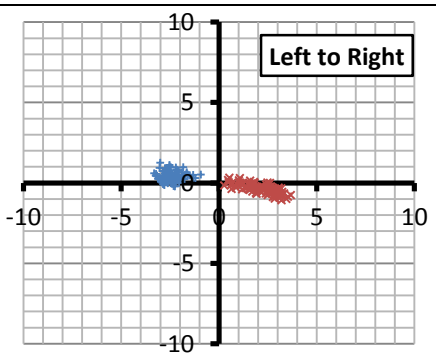


**Figure 4** Distribution and radius of axis location errors for all combinations of scan sets. Each chart shows 100 axes calculated from 10 'Closed' views and 10 'Apart' views.

The coordinates are in mm, with superior-inferior (Y) and anterior-posterior (X), with positive X pointing anteriorly.

BLUE Plus : Left TMJ

RED Cross : Right TMJ

**TABLES**

| Group | Left TMJ | | Right TMJ | | Combined | |
|---|---|---|---|---|---|---|
| | Mean | SD | Mean | SD | Mean | SD |
| Labial to Labial | 2.40 | 0.47 | 2.70 | 0.49 | 2.55 | 0.50 |
| Labial to Right | 1.49 | 0.50 | 1.72 | 0.30 | 1.61 | 0.42 |
| Labial to Left | 2.30 | 1.05 | 3.36 | 0.42 | 2.83 | 0.95 |
| Right to Right | 3.12 | 0.33 | 2.40 | 0.93 | 2.76 | 0.79 |
| Right to Labial | 4.00 | 0.28 | 2.58 | 0.65 | 3.29 | 0.87 |
| Right to Left | 3.82 | 1.05 | 2.87 | 0.68 | 3.34 | 1.00 |
| Left to Left | 1.80 | 1.04 | 3.73 | 0.41 | 2.77 | 1.25 |
| Left to Labial | 1.41 | 0.71 | 3.28 | 0.57 | 2.35 | 1.14 |
| Left to Right | 2.22 | 0.83 | 2.46 | 0.47 | 2.34 | 0.68 |
| All Combined | 2.51 | 1.17 | 2.79 | 0.81 | 2.65 | 1.01 |

**Table 1.** Mean error radius of axis location in the sagittal plane (all measurements in mm). Groups are described in terms of the sets of views used in calculating the axes. For example, ‘Labial to Right’ means that the 10 Labial views of the teeth together, and the 10 Right side views of the teeth apart, were used to calculate 100 axes.